

<http://researchcommons.waikato.ac.nz/>

## **Research Commons at the University of Waikato**

### **Copyright Statement:**

The digital copy of this thesis is protected by the Copyright Act 1994 (New Zealand).

The thesis may be consulted by you, provided you comply with the provisions of the Act and the following conditions of use:

- Any use you make of these documents or images must be for research or private study purposes only, and you may not make them available to any other person.
- Authors control the copyright of their thesis. You will recognise the author's right to be identified as the author of the thesis, and due acknowledgement will be made to the author where appropriate.
- You will obtain the author's permission before publishing any material from the thesis.

# Redox cycling of colloidal macro- and micro-nutrients in a monomictic lake

A thesis  
submitted in fulfilment  
of the requirements for the degree  
of  
**Doctor of Philosophy in  
Environmental Science**  
at  
**The University of Waikato**  
by  
**Huma Saeed**



THE UNIVERSITY OF  
**WAIKATO**  
*Te Whare Wānanga o Waikato*

2022

# Abstract

---

Lakes are more than just water bodies as they play an essential role in the cycling of nutrients and carbon, with impacts at the local and global scale. This study selected Lake Ngapouri, a small monomictic lake in the Waikiti Valley, Taupo Volcanic Zone, New Zealand, which receives a considerable amount of nutrients and organic carbon input from the surrounding pastures. The study was designed to investigate the cycling of nutrients and dissolved organic carbon in lake Ngapouri, with a focus on processes occurring at the colloidal size level under varying thermal and redox conditions.

To achieve the objectives of the study, a year-long sampling campaign was designed involving field and laboratory measurements of the lake's water column. The lake's physicochemical characteristics were determined via high-resolution depth profiles and paired with a detailed set of depth-resolved geochemical measurements. Analysis for reduced Fe (II) was used to control for oxidative loss during transportation and storage of samples, and generally demonstrated very good protocols and minimal sample alteration.

This work comprises a comparison of components in colloidal and dissolved size ranges, determined by ultrafiltration under a zero grade N<sub>2</sub> atmosphere, and in situ measurements by diffusive gradients in thin films (DGT). Colloids from the lake were additionally analyzed using transmission electron microscopy (TEM), atomic force microscopy (AFM), fluorescence spectroscopy, and a suite of complementary methods.

Results show considerable changes in the physicochemical properties of the lake over the hydrological year. Isothermal conditions prevailed through the water column during austral autumn and winter, with thermal stratification becoming established as the summer progressed. Dissolved oxygen concentration followed the thermal pattern, and thus vertically divided the water column into three distinct zones during summer. These zones are referred to as 1) Epilimnion (0-5m measuring from the surface) with uniform thermal and dissolved oxygen concentration, 2) transition zone with varying temperature and dissolved oxygen concentration referred to as metalimnion (6-13m), and 3) hypolimnion (15-20m) marked with cold water and reduced oxygen concentration in comparison to the upper two compartments. The pH of the water column stayed circumneutral during this study. The implications of the lake's variation in thermal and redox status on the cycling of macro and micronutrients are discussed in data chapters.

The third chapter of this thesis addresses the role of suspended iron hydroxides in phosphorus cycling. The spatial and temporal distribution of iron and phosphorus was clearly coupled and was strongly influenced by sediment releases of both elements in anaerobic bed sediments. Both iron and phosphorus were predominantly colloidal and displayed an increasing degree of lability (to DGT) as hypolimnetic anoxia deepened. The implications of this finding are that iron-based colloids can mediate phosphorus cycling even under anaerobic conditions, and might therefore influence iron and phosphorus bioavailability within the water column.

The fourth chapter of this thesis explores the evolution, seasonal production, and consumption of dissolved organic matter (DOM) in the water column of Lake Ngapouri. Both the quality and quantity of DOM influence the turnover of DOM in the lake system, and this influence was explored using the constituent molecules' fluorescent properties. The resulting excitation-emission matrices (EEM's) were analyzed using parallel factor analysis (PARAFAC), identifying two humic-like fluorophores and one protein-like fluorophore in both colloidal and dissolved size fractions. DOM in the lake showed marked seasonality with greater production and turnover during the summer season. This study shows that the concentration of humic-like DOM was ~3.5 times lower and less variable than protein-like DOM. The proteinaceous material in the low molecular weight fraction cycled actively in the anaerobic hypolimnetic water during summer, consistent with the contemporaneous dissimilatory reduction of manganese, iron, and sulphur.

Chapter 5 of this thesis examines the spatial and temporal distribution of trace elements (iron (Fe), manganese (Mn), zinc (Zn), copper(Cu), chromium (Cr), cobalt (Co), nickel (Ni), and cadmium (Cd)) in Lake Ngapouri, and the degree to which binding to colloidal surfaces and DOM influence trace element bioavailability. DGT-lability was thus used as a proxy the available metal for biological uptake. In general, the DGT-labile fraction was much lower than a total load of respective trace metal, indicating the significance of adsorption, precipitation, and complexation reactions for trace metal availability for biological uptake. Broadly, the study groups trace metals into two distinct categories: strongly redox cycled, and controlled by organic complexation. This work shows that colloidal association is often, but not always a predictor of lower bioavailability with important implications for our understanding of metal micronutrients in aquatic systems.



The contributions from this study are significant for studies of the bioavailability of macro and micronutrients which exhibit strong adsorption behavior. The redox state of lakes affects the formation, complexation character, and stability of various mineral colloids. Colloids clearly should be considered as an important intermediary phase with the potential to affect nutrient availability and with implications for lake restoration and management initiatives.

# Acknowledgements

---

So which of the favors of your Lord will you deny?

(AlQuran 55:13)

First of all, I am incredibly thankful to my chief supervisor Dr. Adam Hartland. When I started this journey, I did not think about publishing articles in reputed scientific journals, let alone as the first author. Your never-ending support, guidance, and patience enabled me to achieve this, Adam. I feel lucky to have had the opportunity to work with you.

I am thankful to my co-supervisor, Professor David Hamilton, for his constructive feedback and for pushing me to in-depth data analysis. Your guidance and comments have turned this thesis so much better.

Special thanks to Dr. Niklas Lehto; for DGT training and vital feedback on the manuscript. Your attention to detail and perfection in preparing DGT's is inspiring. I would not have asked for a better teacher than you. I am thankful to Dr. Mohammad Balousha and Mithun Sikdar for helping with particle characterization, Venessa Cottrell, and Dr. Berrie O'Brien for fluorometry and phytoplankton identification.

This study was impossible without incredible technical support. Thank you, Dean Sandwell and Warrick Powrie, for the field assistance. Your exceptional driving skills made water sampling possible during horrible weather. Thank you, Peter Jarman, Annie Barker, Jenny Stockdill, and Karla Watson, for your incredible behind the scene work in keeping labs running. An enormous thanks to the science librarian Cheryl Ward for her dedication and help.

Thank you to everyone at the Waikato Environmental Geochemistry group for the D3.12 banter. I would particularly acknowledge Andrew Pearson for lending his hands for water sampling and Chris Eager for MATLAB help. A huge thanks to my minion friend Jackson White for helping with Adobe Illustrator, Geoff Tait, Mahdijeh Salmanzadeh, and Dori Torres-Rojas, for listening to me and helping me to see the end of the tunnel.

The Environmental research institute scholarship, the University of Waikato, provided my funding. The project was supported by the Ministry of Business, innovation, and employment for enhancing the health and resilience of New Zealand lakes (UOWX1503).

To my parents, Khawar and Ahad Saeed, and aunt Shafqat, I can not thank you enough for your unconditional love and incredible constant support throughout my life. Thank you, Saima Saeed, for being on the other end of the line, bearing my tantrums, and believing that I am academically and physically capable of achieving this milestone. I am thankful to my parents-in-law for their encouragement and support.

To my little people, Abdullah, Tasweeb, and Elhuam, for all your love. Thank you for helping me with your little hands and big smiles. You are the best team I will ever be a part of.

Finally, Thank you, Imran, for so much else!

This Thesis is dedicated to my parents

# Table of Contents

---

Abstract .....	i
Acknowledgements .....	iv
Table of Contents .....	vi
List of Figures.....	ix
List of Tables .....	xii
Abbreviations.....	xiii
Chapter 1 Introduction .....	1
1.1 Thesis overview.....	1
1.2 Significance of the Present Research.....	1
1.3 Objectives .....	3
1.4 References .....	3
Chapter 2 Literature Review.....	4
2.1 Previous work and Regional setting .....	5
2.1.1 Origin of the lake .....	5
2.1.2 Physical properties of the lake .....	5
2.1.3 The New Zealand perspective .....	8
2.2 Factors controlling eutrophication in lakes .....	9
2.3 The limiting nutrient paradigm.....	10
2.4 Aquatic chemistry of phosphorus.....	11
2.4.1 Dissolved forms of phosphorus.....	12
2.5 Micronutrients .....	13
2.6 Micronutrients: occurrence and chemical speciation .....	16
2.6.1 Iron (Fe) .....	19
2.6.2 Manganese (Mn) .....	23
2.6.3 Zinc (Zn) .....	26
2.6.4 Copper (Cu).....	28
2.6.5 Chromium (Cr) .....	30
2.6.6 Cobalt (Co) .....	32
2.6.7 Nickel (Ni) .....	34
2.6.8 Cadmium (Cd) .....	36
2.7 Aquatic Chemistry; The Role of colloids .....	37
2.8 Aquatic chemistry: effect of inorganic colloids .....	39
2.9 Aquatic chemistry: effect of organic complexation.....	40

2.10	Aquatic chemistry: effect of inorganic-organic complexed colloids .....	42
2.11	Summary of the Review .....	42
2.12	References .....	44
Chapter 3 Regulation of phosphorus bioavailability by iron nanoparticles in a monomictic lake .....		60
Chapter 4 Anaerobic lake metabolism favours proteinaceous organic matter .....		87
	Highlights .....	88
4.1	Abstract .....	88
4.1	Introduction .....	90
4.2	Methods .....	93
4.2.1	Lake description and thermal regime .....	93
4.2.2	Cleaning protocol .....	93
4.2.3	Water sampling .....	93
4.2.4	Sample fractionation by ultrafiltration .....	94
4.2.5	DOC analysis .....	94
4.2.6	Estimation of Fe <sup>2+</sup> .....	95
4.2.7	Determination of DOM optical properties .....	95
4.2.8	Parallel factor analysis (PARAFAC) .....	96
4.2.9	Statistical analysis .....	97
4.2.10	Calculations .....	97
4.3	Results .....	98
4.3.1	DOM fluorescence characteristics .....	98
4.3.2	Physical characteristics of the lake .....	99
4.3.3	Seasonal changes in DOC and fluorescence .....	100
4.3.4	Anaerobic metabolism and the concentration of electron acceptors .....	103
4.3.5	Principal component analysis (PCA) of PARAFAC components, DOC and electron acceptors .....	106
4.4	Discussion .....	107
4.4.1	Seasonal variability in DOC .....	107
4.4.2	Coupling of DOM degradation and redox processes .....	110
4.5	Conclusion .....	113
4.6	Acknowledgments .....	113
4.7	References .....	114
4.8	Supplementary information .....	123
Chapter 5 When micronutrients are available (and when they are not): metal-colloid interactions in seasonally-stratified lakes .....		127

5.1	Abstract.....	128
5.2	Introduction .....	130
5.3	Materials and methods.....	132
5.3.1	Water sampling .....	132
5.3.2	Ultrafiltration.....	133
5.3.3	Assessing potential metal bioavailability with DGT .....	134
5.3.4	Trace metal, Chl-a and nutrient analysis .....	135
5.3.5	Equilibrium speciation modelling.....	136
5.4	Results.....	138
5.4.1	Thermal and redox stratification.....	138
5.4.2	Trace element concentrations: vertical and seasonal profiles .....	141
5.4.3	Precipitation and dissolution of mineral colloids: equilibrium speciation modelling.....	147
5.4.4	Surface complexation modelling of micronutrient binding to mineral colloids .....	150
5.5	Discussion .....	152
5.5.1	Particulate organic matter and dissolved organic ligands limit metal bioavailability.....	155
5.5.2	Implications for phytoplankton phenology and micronutrient dosing studies .....	156
5.6	Conclusion.....	156
5.1	Acknowledgments .....	157
5.7	Author contribution .....	157
5.8	References .....	157
5.2	Supplementary information .....	164
5.2.1	Fluorometric estimation of Chl-a .....	164
	Chapter 6 Summary and suggested future work .....	166
6.1	Conclusion.....	166
6.2	Suggested future work.....	168

# List of Figures

Figure 2.1: Literature review flow diagram and relevance to later research papers.....	4
Figure 2.2: Factors affecting primary productivity in lakes .....	9
Figure 2.3: Environmentally significant fractions of phosphorus .....	12
Figure 2.4: Overview of Fe cycle and its relation with other electron acceptors, adapted from Kappler <i>et al.</i> , 2021 (Kappler <i>et al.</i> , 2021) .....	22
Figure 2.5: A simplified Pourbaix Eh-pH diagram of aqueous iron speciation under standard conditions as adapted from Beverskog 1996 (Beverskog & Puigdomenech, 1996).....	22
Figure 2.6: The Manganese triangle for natural waters (Morgan, 2000). ....	25
Figure 2.7: A simplified Pourbaix Eh-pH diagram of aqueous manganese speciation under standard conditions adapted from Papazotos <i>et al.</i> , 2019 (Papazotos <i>et al.</i> , 2019).....	26
Figure 2.8: A simplified Pourbaix Eh-pH diagram of aqueous zinc speciation under standard conditions .....	28
Figure 2.9: A simplified Pourbaix Eh-pH diagram of aqueous copper speciation under standard conditions adapted from Woods <i>et al.</i> , 1987 (Woods <i>et al.</i> , 1987) ...	30
Figure 2.10: A simplified Pourbaix Eh-pH diagram of aqueous chromium speciation under standard conditions adapted from (Hagendorfer & Goessler, 2008).....	31
Figure 2.11: Aqueous geochemistry of chromium and its association with other redox couples in aqueous environment adapted from Richard and Bourg, 1991 (Richard & Bourg, 1991) .....	32
Figure 2.12: A simplified Pourbaix Eh-pH diagram of aqueous cobalt speciation under standard conditions adapted from Turner <i>et al.</i> , 1981 (Turner <i>et al.</i> , 1981) ....	34
Figure 2.13: A simplified Pourbaix Eh-pH diagram of aqueous cobalt speciation under standard conditions adapted from Beverskog and Puigdomenech (Beverskog & Puigdomenech, 1997) .....	35
Figure 2.14: A simplified Pourbaix Eh-pH diagram of aqueous cadmium speciation under standard conditions adapted from Ford <i>et al.</i> , 2007 (Ford <i>et al.</i> , 2007). 37	
Figure 2.15: Factors, chemical processes and pathways affecting the bioavailability of micronutrients in aquatic systems .....	39
Figure 4.1: Excitation emission matrix (EEM) plots of PARAFAC components C1 (a), corresponding to aromatic organic acids in the humic-like range, and C3 (b) showing protein-like components exhibiting fluorescence characteristic of tryptophan and tyrosine.....	98

Figure 4.2: Time series of physical parameters and dissolved organic carbon in both LMW (< 5 nm) and HMW (> 0.45  $\mu\text{m}$ ) fractions. (a) Air temperature and rainfall data retrieved from the National Climate database (CliFlo database) maintained by National Institute of Water and Atmospheric Science (NIWA), (b) water column temperature ( $^{\circ}\text{C}$ ), (c) HMW DOC concentration and (d) LMW DOC concentrations. Data in panel b were collected using a CTD. The DOC data are scaled to  $\log_{10}$  to allow clear depiction of key trends..... 101

Figure 4.3: Time series of fluorescent DOM fractions in the water column determined by PARAFAC modelling. (a) Humic-like C1 HMW fraction, (b) C1 LMW fraction, (c) protein-like C3 HMW fraction, (d) C3 LMW fraction. .... 102

Figure 4.4: (a) Relative Changes in PARAFAC components C1 and C3 (HMW) over the relative change in cumulative consumption of electron acceptors ( $\Sigma_e$ ) between 15 and 23 m depth (hypolimnion), (b) Relative change in PARAFAC components C1 and C3 (HMW) over the cumulative electron acceptor concentration (Sep. 2015 to October 2016). Values are averages for these depths ..... 105

Figure 4.5: Principal component analysis (PCA) loading plot for DOM fluorescence (PARAFAC components C1 and C3) and DOC concentrations as a function of size fraction (<0.45  $\mu\text{m}$  and <5 nm) and summed electron acceptors ( $\Sigma_e$ ). .... 106

Figure 5.1: Time vs Depth contour plots of physiochemical variables in Lake Ngapouri. (a) Temperature ( $^{\circ}\text{C}$ ), (b) dissolved oxygen ( $\text{mg L}^{-1}$ ), (c) Chl-a ( $\mu\text{g L}^{-1}$ ), (d) pH . 140

Figure 5.2: Time-depth distributions of three major mineral-forming trace elements (Fe (a-c), Mn (d-f), and Al (g-i)) in Lake Ngapouri..... 142

Figure 5.3: Time-depth distributions of Cd (a-c), Cr (d-f), and Co (g-i) in Lake Ngapouri. 144

Figure 5.4: Time-depth distributions of Zn (a-c), Ni (d-f), and Cu (g-i) in Lake Ngapouri.. 146

Figure 5.5: Time-depth distributions of modelled colloidal minerals in the water column of Lake Ngapouri. (a) iron(III) oxy-hydroxide ( $\text{Fe}(\text{OH})_3$ ), (b) boehmite<sub>(a)</sub> ( $\text{AlO}(\text{OH})$ ), (c) iron(II) sulphide<sub>(a)</sub> ( $\text{FeS}$ ), (d) cadmium sulphide ( $\text{CdS}$ ), (e) manganese hydrogen phosphate ( $\text{MnHPO}_4$ ), (f) pyrulosite ( $\text{MnO}_2$ ). The values are presented in  $\mu\text{g L}^{-1}$ , representing the simulated concentration of suspended mineral solids in the water column. .... 148

Figure 5.6: Surface complexation modelling of the interaction between Co, Cu, Zn, and Ni and suspended mineral particles in the lake surface water previously simulated with PHREEQC. The percent of <0.45  $\mu\text{m}$  available for DGT uptake (DGT-labile) is shown on the secondary Y-axis. Plots show (a) Co, (b) Cu, (c) Zn, and (d) Ni, respectively ..... 151

## Supplementary Figures

Figure S3.1: Depth profiles of physicochemical characteristics and different fractions of P and Fe in Lake Ngapouri from September 2015 to October 2016. The concentration values are in  $\mu\text{M L}^{-1}$  and depths are in meters. .... 77



Figure S3.2: pH of the water column of Lake Ngapouri between September 2015 and October 2016. Data are missing from January 2016 due to a faulty probe. Broken black lines show the timing of the onset (i) and end (iii) of stratified conditions in the lake as well as the approximate position of the thermocline (ii). Data from January 2016 are not included in the plot due to a probe malfunction in this month. ....	78
Figure S3.3: Temperature profile of Lake Ngapouri between September 2015 and October 2016 recorded using Hobo Tidbit temperature loggers programmed to collect data every 30 minutes. ....	79
Figure S3.4: DGT deployment in the field. DGT probes coated with dark precipitate are from close to the benthic nepheloid layer and provide evidence for the formation of metal sulphides at this depth. ....	79
Figure S3.5: Standard curve for the estimation of $\text{HPO}_4^{2-}$ by the molybdenum blue method. ....	81
Figure S3.6: Results of $C_{\text{DGT}}$ Fe values ( $\mu\text{M}$ ). The probes were deployed in pairs and $C_{\text{DGT}}\text{Fe}_{(b)}$ represents the results from the probes purged with zero grade $\text{N}_2$ overnight before deployment. These results highlight the remarkable reproducibility of fine-scale structure in the metal depth profiles measured by DGT. ....	84
Figure S3.7: Comparison of Fe(II) concentrations ( $\mu\text{M}$ ) determined by the Ferrozine method, “Fe <sub>(a)</sub> ”, “Fe <sub>(b)</sub> ” and “Fe <sub>(c)</sub> ” represent “in field measurements”, “after bringing to the lab <i>but</i> before ultrafiltration” and “after ultrafiltration through 100 KDa in the glove box”, respectively. ....	85
Figure S4.1: Excitation emission matrices (EEMs) of PARAFAC components 1-2 (plots a and b) corresponding to humic-like substances, and component 3 (c) protein-like components exhibiting fluorescence characteristic of tryptophan and tyrosine. Validation of the three component spectral model. ....	123
Figure S4.2: Time series of $\text{SUVA}_{254}$ in operationally defined fractions at $\log_{10}$ scale (a) shows $\text{SUVA}_{254}$ values in the LMW fraction (b) $\text{SUVA}_{254}$ in the HMW fraction (c) Fe(II) measured by the ferrozine method .....	124
Figure S4.3: Time series of the oxidising agents in Lake Ngapouri. (a) Dissolved Oxygen ( $\text{mg L}^{-1}$ ), (b) $\text{NO}_3^{-1}$ ( $\text{mg NO}_3^{-}\text{-N L}^{-1}$ ), $\text{NH}_4^{+}$ ( $\text{mg NH}_4^{+}\text{-N L}^{-1}$ ), Mn ( $\text{mg L}^{-1}$ ), Fe ( $\text{mg L}^{-1}$ ), $\text{SO}_4$ ( $\text{mg L}^{-1}$ ). ....	125

# List of Tables

Table 2.1: Physical characteristics of Lake Ngapouri: a review .....	6
Table 2.2: Trace metals, their common minerals and suggested role in metabolic pathways.....	15
Table 2.3: Suggested transport mechanisms for metal chemical species .....	17
Table 2.4 Trace metal speciation in freshwater exemplified by a hypothetical cobalt species distribution adapted from (Laxen & Harrison, 1981) .....	18
Table 4.1: PARAFAC component scores and corresponding emission wavelengths of maximum fluorescence ( $\lambda_{\max}$ ) and maximum fluorescence intensity ( $FI_{\max}$ ). Fluorophore designation determined from the literature. RU = Raman-normalised intensity units .....	100
Table 5.1: Trace metal ranking based on the median colloidal and DGT-labile concentrations in surface (2.5-10 m) and deep waters (15 and 20 m) across the hydrologic year.....	135
Table 5.2: Percentage association of trace elements with colloids and solutes in <0.45 $\mu\text{m}$ fraction (a) average surface water 2.5-5 m and (b) average hypolimnetic water from 15-20 m .....	149
Table 5.3: Suggested pathways for micronutrient cycling associated with redox reactions in a typical monomictic lake. ....	154
<b>Supplementary Tables</b>	
Table S3.1: Test deployment of DGT piston probes in 200 ppb $\text{HPO}_4^{2-}$ solution for a known time at room temperature (22°C). $\text{Sol}_{(i)}$ and $\text{Sol}_{(f)}$ represent the initial and final concentrations of P in the deployment solution, respectively. Conc. Is the concentration of P recovered in ferrihydrite elution solution. The initial and final pH of the immersion solution was 6.9 and 6.8 respectively. ....	82
Table S3.2: Test deployment of Chelex DGT probes in 200 ppb Cd solution for known time at 22°C. $\text{Sol}_{(i)}$ and $\text{Sol}_{(f)}$ represent the initial and final concentrations of Cd in the immersion solution. The immersion solution was stirred for at least 90 minutes before deployment.....	83
Table S4.1: Cumulative electron acceptors ( $\Sigma e^-$ ) and percentage $\text{SO}_4^{2-}$ reduction in Lake Ngapouri .....	126

## Abbreviations

AFM	Atomic force microscopy
TEM	Transmission electron microscopy
3D EEMs	Three dimensional excitataion emission matrix
PARAFAC	Parallel factor analysis
DOM	Dissolved organic matter
DOC	Dissolved organic carbon
DRP	Dissolved reactive pohosphorus
DGT	Diffusive gradients in thin films
FIA	Flow injection analyser
ICP-MS	Inductively coupled plasma mass spectrometry
Chl-a	Chlorophyll a

# Chapter 1

## Introduction

---

### 1.1 Thesis overview

The thesis is divided into six chapters. Chapter 1 is a general overview of the thesis, and describes the importance of this research for understanding macro and micronutrient cycling in lake systems.

Chapter 2 is a review of published literature. Chapters 3-5 are research chapters and have been published, submitted for publication, or prepared for publication in peer-reviewed scientific journals.

Chapter 3, entitled 'Regulation of phosphorus bioavailability by iron nanoparticles in a monomictic lake, has been published in *Scientific Reports* and can be accessed via <https://www.nature.com/articles/s41598-018-36103-x>. The article provides an insight into the colloidal control of Fe-bearing nanoparticles on the cycling of phosphorus in lake Ngapouri (Saeed *et al.*, 2018).

Chapter 4, entitled 'Anaerobic lake metabolism favors proteinaceous organic matter', is in preparation for publication. The article is based on the qualitative and quantitative analysis of dissolved organic matter and unravels the cycling of different size fractions in a monomictic lake.

Chapter 5, entitled 'When micronutrients are available (and when they are not): on the variable importance of metal-colloid interactions in seasonally-stratified lakes', is prepared for publication in *Biogeochemistry* and highlights the importance of colloidal association in the lability of different micronutrients.

Chapter 6 summarizes the highlights of the present study and sets the direction for future research required for a better understanding of nutrient cycling.

### 1.2 Significance of the Present Research

External input of nutrients is considered essential for supporting primary productivity in freshwater systems. However, the oversupply of nutrients leads to eutrophication, resulting in high primary productivity. This, as a result, influences the geochemical cycling

rate at the ecosystem level. Over past few decades, different nutrient reduction strategies have been adopted to reduce the nutrient input to lakes (Burns *et al.*, 2005; Smith *et al.*, 2016). However, evidence from these practices has questioned the relationship between external nutrient input and eutrophication, highlighting the significance of coupled internal nutrient cycling and primary productivity in freshwater systems (Soendergaard *et al.*, 2003; Soendergaard *et al.*, 2005; Kagalou *et al.*, 2008; Wu *et al.*, 2017).

Studies related to chemical speciation, mobility, and lability of nutrients are limited by the inclusion of colloids in the total dissolved fraction. Conventionally, particulate and dissolved fractions are separated by filtration through 0.45  $\mu\text{m}$  pore size. Colloids, a class of particles in a size range of 1 nm to 1  $\mu\text{m}$ , largely pass through these filter membranes and thus are an important constituent of the operationally defined total dissolved fraction (Lead & Wilkinson, 2006). Consequently, colloids provide surfaces in a broad size range with varying reactivities. Information on the role of colloids in aquatic settings is increasing rapidly; however, their role in the biogeochemical cycling of nutrients in freshwater systems is not fully understood. The present study addresses this gap and investigates the coupling of nutrients and trace metals as part of internal biogeochemical cycles, on a colloidal scale, in a freshwater shallow monomictic lake.

The present study used an ultrafiltration approach for the size fractionation of dissolved solids to quantify the colloidal concentration. The colloids were characterized using transmission electron and atomic force microscopy. DGT (diffusive gradients in thin films) was used to define the labile concentration, and was used as a proxy for the bioavailable load of nutrients. In addition, dissolved organic matter (DOM) in both size fractions was also characterized and quantified. The cycling of different fractions of DOM was compared with the consumption of electron acceptors. A suite of trace elements was also quantified in both size fractions and the results were evaluated using the chemical speciation models PHREEQC and Visual Minteq. The findings from the present study highlight the importance of colloidal scale interactions in an aquatic system, and provide insight to the cycling of different fractions of dissolved organic matter under varying redox conditions. The results can be extended to any aquatic system with comparable concentrations of nutrients and redox behavior. However, we suggest a careful evaluation of DOM composition when making a comparison in that domain.

### 1.3 Objectives

The overarching aim of this research was to understand the controls on the cycling and bioavailability of nutrients that exhibit binding/surface complexation behavior and characterize the biogeochemical cycling of these nutrients with organic matter in Lake Ngapouri.

Accordingly, data was collected at various spatial and temporal points to understand nutrient cycling in the lake system.

### 1.4 References

- Burns, N., McIntosh, J., & Scholes, P. (2005). Strategies for Managing the Lakes of the Rotorua District, New Zealand. *Lake and Reservoir Management*, 21(1), 61-72.
- Kagalou, I., Papastergiadou, E., & Leonardos, I. (2008). Long term changes in the eutrophication process in a shallow Mediterranean lake ecosystem of W. Greece: Response after the reduction of external load. *Journal of Environmental Management*, 87(3), 497-506.
- Lead, J., & Wilkinson, K. (2006). Aquatic Colloids and Nanoparticles: Current Knowledge and Future Trends. *Environmental Chemistry - ENVIRON CHEM*, 3.
- Saeed, H., Hartland, A., Lehto, N., Baalousha, M., Sikder, M., Sandwell, D., Mucalo, M., & Hamilton, D. P. (2018). Regulation of phosphorus bioavailability by iron nanoparticles in a monomictic lake. *Scientific reports*, 8(1), 1-14.
- Smith, V. H., Wood, S. A., McBride, C. G., Atalah, J., Hamilton, D. P., & Abell, J. (2016). Phosphorus and nitrogen loading restraints are essential for successful eutrophication control of Lake Rotorua, New Zealand. *Inland Waters*, 6(2), 273-283.
- Soendergaard, M., Jensen, J. P., & Jeppesen, E. (2005). Seasonal response of nutrients to reduced phosphorus loading in 12 Danish lakes. *Freshwater Biology*, 50(10), 1605-1615.
- Søndergaard, M., Jensen, J. P., & Jeppesen, E. (2003). Role of sediment and internal loading of phosphorus in shallow lakes. *Hydrobiologia*, 506(1), 135-145.
- Wu, Z., Liu, Y., Liang, Z., Wu, S., & Guo, H. (2017). Internal cycling, not external loading, decides the nutrient limitation in eutrophic lake: A dynamic model with temporal Bayesian hierarchical inference. *Water Research*, 116, 231-240.

# Chapter 2

## Literature Review

The literature on different aspects of nutrient cycling in freshwater lakes is enormous. This chapter overviews some relevant literature, and Figure 2.1 shows a flow of the literature survey and its relevance to the research data chapters.

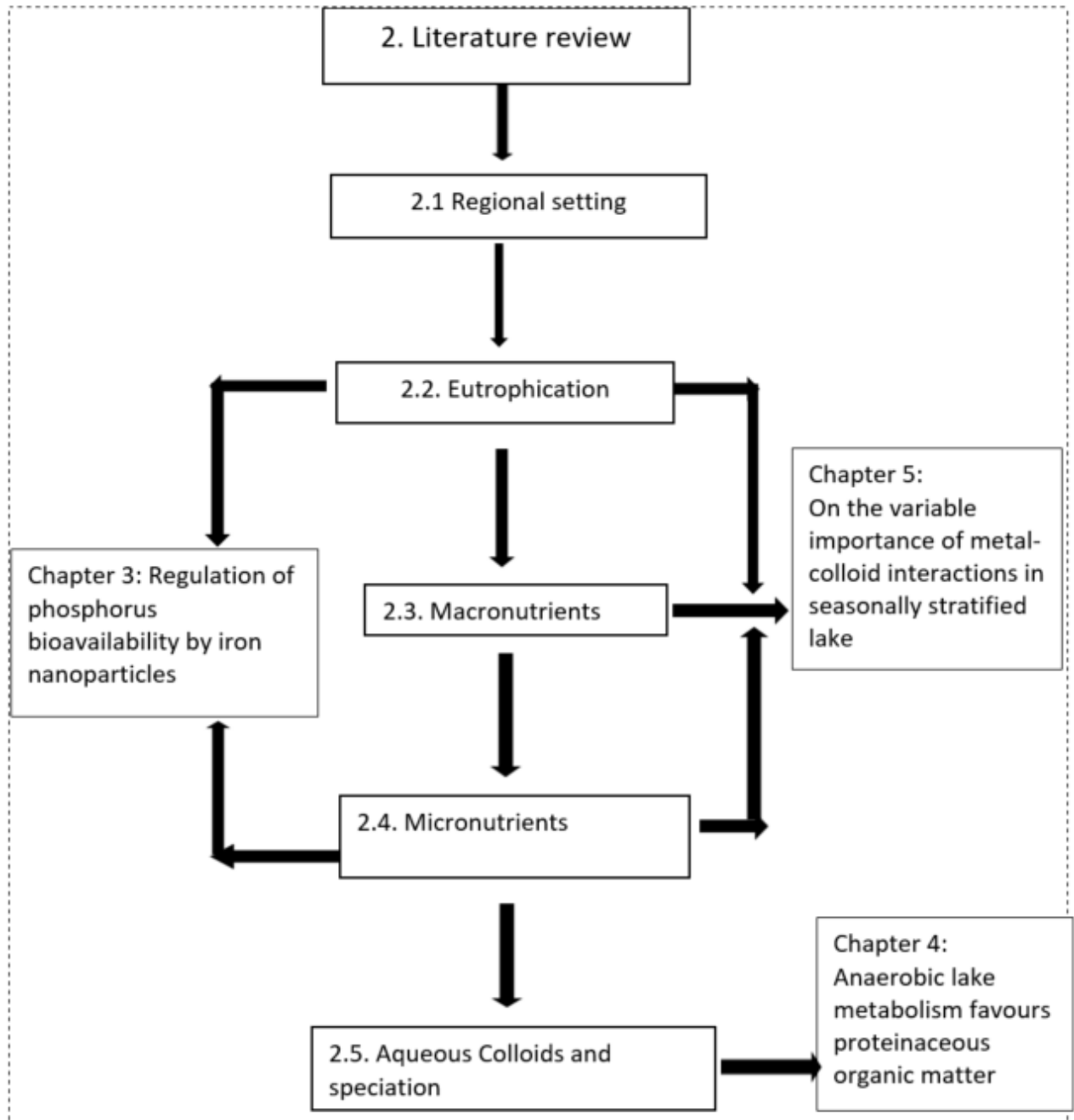


Figure 2.1: Literature review flow diagram and relevance to later research papers

## **2.1 Previous work and Regional setting**

### **2.1.1 Origin of the lake**

Lake Ngapouri was formed around one thousand years ago by hydrothermal eruptions (Cross, 1963; Fish, 1970) and is located 451 m above the sea level (Jolly, 1968) in the Waioatapu thermal area, south of Haroharo caldera, approximately 24 km from the city of Rotorua, in the Taupō volcanic zone (TVNZ), New Zealand.

Ngapouri is a small, monomictic, warm lake (Hutchinson classification) (Hutchinson, 1957) with a 0.19 km<sup>2</sup> lake area and a land catchment area of 4.81 km<sup>2</sup>. With a maximum depth of ~ 24 m, the lake has been mainly fed by small streams and run off from its 4.45 km<sup>2</sup> agricultural catchment since 1956, when most of the forest cover was removed from the surroundings for conversion to pasture (Jolly, 1968). In contrast to the other lakes in the region, the lake sediment is influenced by Taupō pumice and clay originating from its crater. In contrast, other lakes in the area typically have light pumice soils originating from various ash showers (Cross, 1963).

### **2.1.2 Physical properties of the lake**

The lake is highly eutrophic, and establishes a marked thermocline in summer (starting from October), followed by turnover in winter, beginning in May (Forsyth, 1986). During summer, the thermocline divides the water column into three distinct vertical compartments, a) epilimnion; upper 5 m of the lake water, b) transition zone from 6 to 13 m, also known as the metalimnion, and an area extending from 15 m to the lake sediment referred to as hypolimnion. Oxygen distribution follows the thermal stratification and a suboxic transition zone separates the oxygenated surface water from the anoxic deep water. Gradients of nutrients and trace metals also characterize this redoxcline.



**Table 2.1: Physical characteristics of Lake Ngapouri: a review**

Survey period	Water Temperature (°C)		DO (mg/L)	pH	Phytoplankton taxa (dominant/ studied)	Thermal structure	References
	Surface	Deep	Surface	Surface			
4/1956	16.5	11.4	6.4	6.9		A	(Jolly, 1968)
12/1965	20.5	9.9	-	-	-	B	(Irwin, 1968)
03/1961-03/1966	17-19	9.5-11	11.6-12.1	-	-	A	(Fish, 1970)
04/1970-04/1971	-	-	-	-	<i>Asterionella formosa</i> , <i>Melosira distans</i> , Dinobryon	-	(Flint, 1977)
04/1970-05/1971	8.4-22.9	8.2-16.8	11.3	7.2-7.6	Diatoms	A	(McColl, 1972)
12/1971-05/1972	9-12	-	9-16.5	-	-	A	(Forsyth, 1986)
11/2007-11/2008	20	11	-	6.7	-	C	(Pearson <i>et al.</i> , 2016)
03/2014	20		7.5	6.5	-	C	(Hartland, Andersen, & Hamilton, 2015)
09/2015-10/2016	9 - 23	8.4	7-15.8	6.5-9.2	<i>Asterionella formosa</i> , Microcystis, Diatoms-	C	(Saeed <i>et al.</i> , 2018)

A; irregular/ absence of stable thermal stratification

B; weak thermal stratification

C; stable thermal stratification

Previous studies have investigated a wide range of physical, chemical and biological properties of Lake Ngapouri such as seasonal temperature, oxygen regimes, and phytoplankton assemblages. Table 2.1 summarises the relevant available data for Lake Ngapouri. Studies that have reported the invertebrate population (Pearson *et al.*, 2016), (Chapman *et al.*, 1985), and food web dynamics (Rowe, 1984) of Lake Ngapouri were considered beyond the scope of review. The values denoted as ‘-’ in the table where the specific parameter(s) were not studied/reported. In addition, the value ranges, where provided, are the maximum and minimum values of that particular parameter supplied by the authors.

In Table 2.1, the first column shows the duration of time the lake was surveyed. Again, there is variability in the time of sampling events. A small number of studies have investigated the lake water column over a period ranging from months to years, while other studies, *e.g.*, Jolly 1968, have reported on one-off sampling events. The lake’s thermal structure has been categorized based on the stability of the thermocline. In Table 2.1, ‘A’ refers to the irregular or lack of stable thermal stratification, and ‘B’ and ‘C’ denote a weak and stable thermocline during stratification (Irwin, 1968).

### **Eutrophication in the global context**

Inorganic nutrients are a prerequisite for algal productivity in natural waters. The progression of freshwater ecosystems from low to excess productivity resulting from anthropogenic nutrient loading is a global phenomenon. There is a general lack of precision about the term eutrophication, as there is no ‘concentration range’ associated with it. However, an acceptable definition in ecology states eutrophication as an excessive growth of phytoplankton due to an over-enrichment of one or more nutrients in receiving water bodies through natural or artificial processes (Weber, 1907; Harper, 1992). Although eutrophication is a natural process of aging for water systems (Greeson, 1969), the term is however, broadly, used to denote an accelerated deterioration arising from anthropogenic activities. Hence, the term “cultural eutrophication” is also common (Rast & Thornton, 1996).

Eutrophication is considered a critical risk to water quality and the ecological integrity of freshwater systems (Khan & Ansari, 2005). The causes and effects of eutrophication are very complex and diverge for different ecosystems (Smith & Schindler, 2009). Furthermore, the behavior of receiving water systems in response to nutrient inputs also varies

seasonally and inter-annually (Khan & Mohammad, 2014). Eutrophication control procedures used around the globe generally fall into the following categories: reducing the inlet nutrient load (Daniel *et al.*, 1994; Qin *et al.*, 2006), altering nutrient ratios (Downing *et al.*), artificial mixing (Huisman *et al.*, 2004), use of flocculants (Welch & Cooke, 1999; Cooke *et al.*, 2016), and biomanipulation (Robertson *et al.*, 2000). However, the majority of these practices have proven to be expensive and impractical for large water bodies leaving external nutrient input management as the prominent practice. Yet, minimal or no improvements are typically observed even after many years of stripping the inlet load of nutrients in closed water systems (Soendergaard *et al.*, 2003; Wu *et al.*, 2017b; Wang *et al.*, 2019) with small outlets, such as lakes.

By the late 1980s, Roleoff and co-workers recognized that surface water quality declines even in natural reserves where there was no significant increase in the inlet nutrient load. They referred it to as “Internal eutrophication” in peatlands, and related it to potential processes controlling the cycling of nutrients (Roelofs & Cals, 1989). Initially, the idea was received with great scepticism but gradually became accepted by the late 1990s.

The present study is mainly related to the internal cycling of nutrients and ignores catchment management and nutrient inlet loading. Instead, of concern here is unraveling the processes governing nutrients that cycle between solid, colloidal and dissolved phases.

### **2.1.3 The New Zealand perspective**

New Zealand has more than 50,000 lakes, of which 4000 have an area larger than 1ha (Environment, 2007). Computer models estimate that 46% of the large NZ lakes have low to extremely poor water quality (Environment, 2020) with the loading of total phosphorus (TP) and total nitrogen (TN) in areas of high intensity pastoral, exotic forestry, and urban land use (Abell *et al.*, 2010a) being the leading causes. However, agricultural run-off is clearly the primary source of nutrient input to the water bodies (Hamilton, 2005).

In New Zealand, the land-use practices have changed between 1840 – 2005 with distinct effects on the receiving water bodies (O'Connor, 1982; Langer, 1990; Suren & McMurtrie, 2005; MacLeod & Moller, 2006). Cultural eutrophication is the leading cause of the impairment of freshwater in New Zealand. The view that New Zealand lakes are more likely to be nitrogen-limited compared to lakes in other developed countries was predominant around three decades ago based on a comparison made by White (White, 1983). However

dual control of nitrogen and phosphorus is recommended now to deal with eutrophication in New Zealand lakes. In particular, more effort is needed to reduce the phosphorus input to the receiving water bodies (Abell *et al.*, 2010b).

## 2.2 Factors controlling eutrophication in lakes

Many physical and chemical factors determine the growth of phytoplankton and macrophytes in lakes. The physical parameters include but are not limited to the composition of the catchment area (*e.g.*, geological structure and soil properties), weather conditions (*e.g.*, light, temperature, precipitation, wind, and depth of water basin), water flow, biological dynamics (*e.g.*, community composition, the ability of different biota to harness nutrients), sorption, sedimentation, and flocculation. The chemical controls relate to the nutrient loads, internal cycling, and the chemical reactions (*e.g.*, hydrolysis, redox, and complexation reactions) in the aquatic environment. See, for example (Kimmel 1984). While the physical factors are important determinants of productivity, the present review primarily focuses on chemical aspects (Figure 2.2).

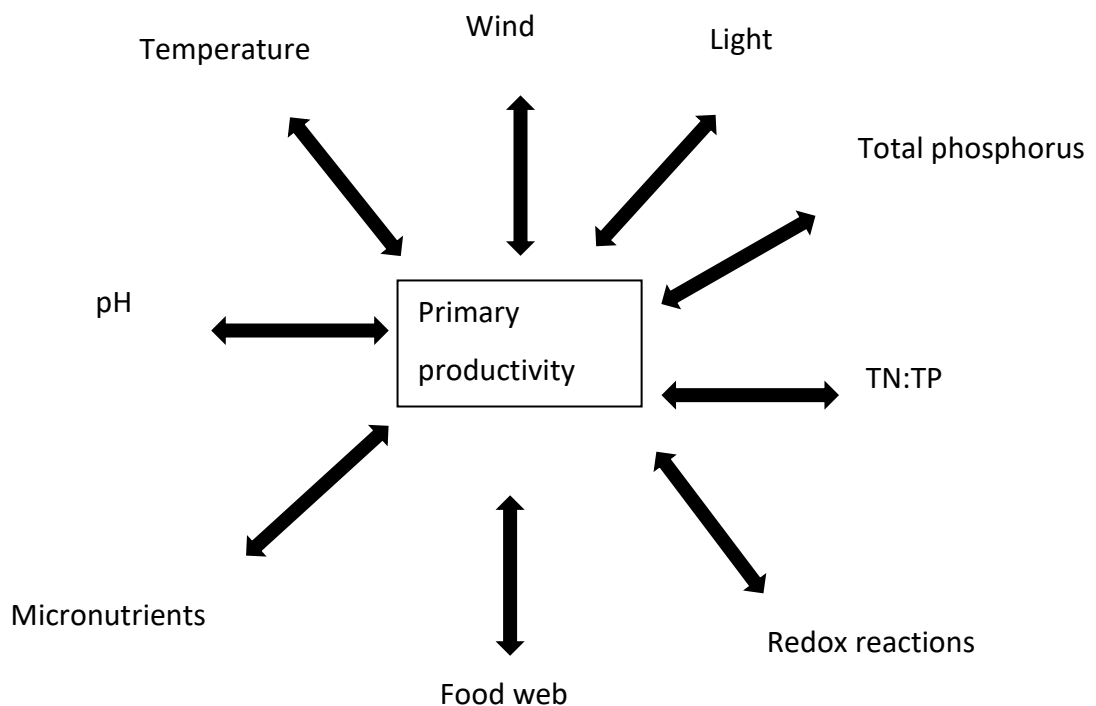


Figure 2.2: Factors affecting primary productivity in lakes

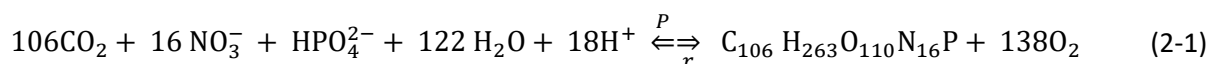
## 2.3 The limiting nutrient paradigm

A variety of nutrients are required to maintain phytoplankton growth in lakes. Some nutrients, *e.g.*, phosphorus (P), nitrogen (N), and potassium (K), are required in larger quantities to sustain a variety of cell physiological functions and are termed *macronutrients* (Edmondson, 1970; Lee *et al.*, 1978; Portielje & Van der Molen, 1999). While, the other class of nutrients, such as iron (Fe), copper (Cu), zinc (Zn), and other divalent metal cations, are required in small quantities but are essential in maintaining cellular functions and are referred to as *micronutrients*.

A proper balance of nutrients is required for the growth of phytoplankton. Ecological stoichiometry (broadly known as biological stoichiometry) is an approach that relates the physiology of organisms and ecosystem-level processes such as nutrient recycling, biogeochemical cycles, and limiting nutrients, to the relative ambient concentrations of nutrient species (Sterner & Elser, 2002; Scharler *et al.*, 2015). The approach analyses the limitations and significance of the mass balance of nutrients on ecological interactions and the stoichiometry of primary production determined by the ratio of elements in the cell's cytoplasm. The Redfield ratio is the fundamental concept relating to the productivity in aquatic systems. It is used as a reference value to understand the relationship between biogeochemical cycling and nutrient limitations in any aquatic system. The ratio is derived from the relative abundance of (carbon) C: N: O (106: 16: 1) in marine algae and is used to approximate the nutrient requirements of phytoplankton and varies for land plants (Sterner & Elser, 2002).

Although marine and freshwater phytoplankton have similar nutrient requirements, the sources of nutrients can vary broadly in both environments. Lakes often act as sources of carbon (not sinks) relative to global carbon cycling, and hence lake systems are often not carbon limited (Kling *et al.*, 1991). Instead, phytoplankton growth can depend on the availability of phosphorus and/or nitrogen (Carpenter *et al.*, 1998; Mosello *et al.*, 2011). Based on the Redfield ratio, phytoplankton growth is limited by phosphorus availability if more than 16 moles of N are present for every mole of P; otherwise, phytoplankton growth is deemed to be N-limited (Tett *et al.*, 1985). However, it is important to note that there are microbial community assemblages, *e.g.*, cyanobacteria, that can fix atmospheric nitrogen when N: P ratios are below 16:1; thereby increasing the N content of the water bodies (Schindler *et al.*, 2008).

Thus, the long-standing debate of N vs. P limitation for phytoplankton growth is more in favor of P for freshwater ecosystems (Schindler, 1977). P does not have any atmospheric forms and is primarily transported to lakes by surface water. Hence, It is rightfully argued that P acts as the primary limiting nutrient for most inland waters, which determines the biological productivity of the aquatic system. The general reaction is as follows,



Where  $p$  is photosynthesis, and  $r$  refers to respiration. For simplicity, if more P becomes available, more biomass is produced, and after death, the decomposition of biomass (detritus) will consume the corresponding amount of dissolved oxygen from the water.

## 2.4 Aquatic chemistry of phosphorus

Phosphorus has several vital biogeochemical roles, but unlike C and N, it does not have a rapid global cycle (Hutchinson, 1957). P is considered growth limiting in terrestrial and aquatic environments given the slow rate of natural mobilization, the low solubility of phosphate minerals, and rapid transformation to insoluble forms (Ruttenberg, 2003). Human activities have increased the release of P to waterways through point and non-point (*diffuse*) sources. A significant amount of P ends up in the water channels from sewers and treated wastewater. On the other hand, agricultural run-off, effluent from animal sheds, and recycling of crop residues and manures are important non-point sources of P loading to waterways and are difficult to control.

Once present, P takes a long time to flush out of aquatic systems, particularly from lakes, a phenomenon that can be attributed to the variety of biogeochemical cycles that impact the element's chemical form. While it is widely understood that excess P is an environmental problem, the specific chemical structure, or '*speciation*' of P is of crucial importance (Gerdes & Kunst, 1998; Huang *et al.*, 2005). Determination of an element's total concentration does not directly give insight into the likely environmental impacts without knowing its chemical speciation. Instead, it is more meaningful to determine the individual concentrations of the various chemical forms of an element that make up its total concentration in a given matrix. This is because the chemical structure of a substance critically determines its bioavailability and toxicity (Boström *et al.*, 1988; Hirose, 1990).

P is introduced to the aquatic system in several chemical forms. It has been described as being present in the aqueous phase (dissolved/soluble) and the solid phase (particulate). A dynamic equilibrium exists between dissolved/soluble and particulate fractions that affect the speciation and hence the availability of P to biota



Particulate and dissolved forms undergo microbial decomposition (mineralization), leading to phosphorus being transferred to the dissolved reactive phosphorus pool (DRP) (Lean, 1973). Although unfiltered water samples are analyzed for some particular purposes, the present study focuses on the dissolved concentrations of P (Chapter 3) and its interaction at the colloidal level, so this section of the review will focus on the operationally defined “dissolved P” fraction only. Figure 2.3 shows the general componenets of the particulate P fraction.

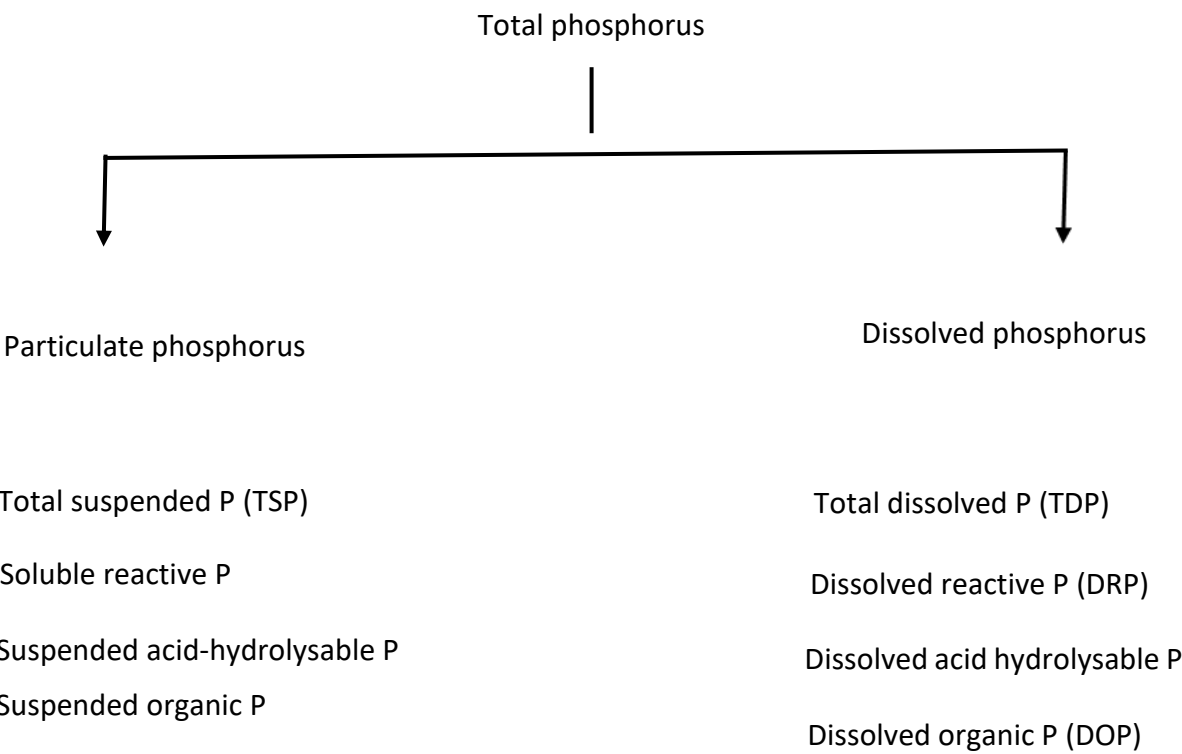


**Figure 2.3: Environmentally significant fractions of phosphorus**

### 2.4.1 Dissolved forms of phosphorus

The separation of dissolved and particulate fractions of P is conventionally based on filtration through 0.45 μm filter membranes and usually ignores the P-bearing particles

present at the colloidal size range in the dissolved fraction. Colloids are defined as the particles or molecules with at least one dimension in the size range of 1 nm and 1  $\mu$ m and vary in their chemical form and reactivity (Lead & ilkinson, 2006). Within the dissolved fraction, P may exist as dissolved inorganic reactive P (DRP), dissolved condensed P (DCP), dissolved organic P (DOP), and dissolved acid hydrolysable P (Holtan *et al.*, 1988).

DRP is also known as soluble reactive P or filterable reactive P and is used to quantify the monomeric inorganic P, the most frequent forms being orthophosphates ( $\text{H}_2\text{PO}_4^-$  and  $\text{HPO}_4^{2-}$ ) under the pH conditions typically found in natural waters (Krempin *et al.*, 1981). Orthophosphates are readily available for assimilation by biota and are also removed from the water column through inorganic colloidal interactions, *e.g.*, with iron (Fe), aluminum (Al), and calcium (Ca) through chemical precipitation (Lijklema, 1980; de Vicente *et al.*, 2008).

DCP (also known as meta, pyro, or polyphosphates) consists of two or more orthophosphate groups linked together that make good complexing agents; they are therefore found in many detergents. DCP provides a suitable substrate for microbial activity and converts to DRP, resulting in a short environmental half-life (Wazer, 1950; Jin *et al.*, 2019). Orthophosphates (DRP) and polyphosphates (DCP) are collectively known as total inorganic P or acid hydrolysable P.

DOP is the class of compounds containing P-O-C bonds (*e.g.*, orthophosphates attached to sugar) and is formed primarily by biological processes (Bentzen *et al.*, 1992; Hernández *et al.*, 2002), *e.g.*, plant and animal tissues, animal waste, and pesticides (Lean, 1973). TDP is the sum of the above mentioned dissolved fractions and measures all forms of P in a filtered water sample (Equations. 2-3 and 2-4).

$$\text{Total Dissolved P} = \text{TIP} + \text{Organic P} \quad (2-3)$$

$$\text{Total Dissolved P} = \text{Ortho } \text{PO}_4^{3-} + \text{Poly } \text{PO}_4^{3-} + \text{Organic P} \quad (2-4)$$

## 2.5 Micronutrients

Micronutrients are certain trace metals required in trace amounts but influence the productivity and species composition of aquatic biota. Trace metals (referred to as TM in



this review), *e.g.*, iron (Fe), manganese (Mn), zinc (Zn), copper (Cu), cobalt (Co), and nickel (Ni), have known metabolic functions (Sunda, 1989; Hänsch & Mendel, 2009) and are arranged in descending order of significance for phytoplankton in Table 2.2. To summarise, TM's act as co-factors of enzymes involved in electron transport or catalysis of redox reactions in biological systems. In addition, there is another class of trace elements that have no known metabolic functions and instead act as biological inhibitors such as cadmium (Cd), lead (Pb), silver (Ag), and mercury (Hg) (Sunda, 1989; Dogan *et al.*, 2009). This review will focus on nutrient TM's.

The importance of trace elements in aquatic systems can not be assessed clearly without considering the processes that control a trace elements' biological availability (Hirose, 1990). There are over twenty different definitions of bioavailability in the literature of various fields, but environmental scientists define the term as the accessibility of a chemical for assimilation (and possible toxicity) to biota (National Research Council, 2003).

The interactions between trace metals, including biological inhibitors and plankton, are essential determinants of the ecology of aquatic systems. Several exchanges need to be considered at the molecular, cellular, community, and environmental levels when trying to unravel the relationship between TM's and biological productivity. First is the chemistry of TM's, the second is the process of metal uptake at the cellular level, third is the reactions of TM's at different metabolic sites, *e.g.*, photosynthesis, respiration, and growth, which will then determine the total community composition of an aquatic system (Tilman *et al.*, 1982). The following section reviews the abundance in nature and chemical speciation of TM's in the freshwater systems.

**Table 2.2: Trace metals, their common minerals and suggested role in metabolic pathways**

Element	Common minerals	Biological role	Biogeochemical role	References
Fe	magnetite (Fe <sub>2</sub> O <sub>3</sub> ), siderite (FeCO <sub>3</sub> ), goethite (Fe <sub>2</sub> O <sub>3</sub> .H <sub>2</sub> O) pyrite (FeS), chalcopyrite (CuFeS <sub>2</sub> )	Oxygen and electron transport, part of enzyme photosynthetic transport chain, part of photosystem I and II. In <u>nitrogenase</u> , cytochrome b, c and f, component of superoxide dismutase	Photosynthesis, carbon fixation, and limitation in N-fixation, redox sensitive	(GR & S., 2015; Raven, Evans, & Korb, 1999; Schoffman, Lis, Shaked, & Keren, 2016), (Cotton, Wilkinson, Murillo, Bochmann, & Grimes, 1988)
Mn	<u>rhodochrosite (MnCO<sub>3</sub>)</u> , <u>rhodonite (CaMn<sub>3</sub>Mn[Si<sub>5</sub>O<sub>15</sub>])</u> <u>bixbyite (Mn,Fe)<sub>2</sub>O<sub>3</sub></u> , <u>pyrolusite (MnO<sub>2</sub>)</u>	Component of superoxide dismutase (to destroy undesirable <u>superoxides</u> ), component of O <sub>2</sub> evolving enzyme during photosynthesis	Redox sensitive	(Sunda, 1989)
Cr	chromite (FeCr <sub>2</sub> O <sub>4</sub> ), crocoite PbCrO <sub>4</sub> , chrome ochre Cr <sub>2</sub> O <sub>3</sub> .	Participate in glucose metabolism	Redox sensitive (Cr(III) and Cr(VI))	(Sunda, 1989)
Co	<u>spherochalcite (CoCO<sub>3</sub>)</u> , <u>heterogenite (HCoO<sub>2</sub>)</u>	Synthesis of Vitamin B <sub>12</sub>	Co limiting for productivity with Fe and Zn	(Sunda, 1989)
Zn	calamine (Zn <sub>2</sub> SiO <sub>4</sub> H <sub>2</sub> O) smithsonite (ZnCO <sub>3</sub> ), <u>sphalerite (ZnS)</u> , <u>zincite (ZnO)</u>	Structural role in DNA, part of enzymes e.g. carbonic anhydrase, alkaline phosphatase, , growth inhibitor at high conc.	Micronutrients and is used as proxy of Si in aquatic systems	(Sunda, 1989)
Ni	<u>pentlandite ((Fe,Ni)<sub>9</sub>S<sub>8</sub>)</u> , <u>millerite (NiS)</u> , <u>gersdorffite ((NiAsS)</u> ,	Component of superoxide dismutase, growth inhibitor at high conc.		(Sunda, 1989)
Cu	<u>bornite (Cu<sub>5</sub>FeS<sub>4</sub>)</u> , <u>tetrahedrite (3Cu<sub>2</sub>S Sb<sub>2</sub>S<sub>3</sub>)</u> , chalcocite (Cu <sub>2</sub> S), cuprite (Cu <sub>2</sub> O), Chalcopyrite (CuFeS <sub>2</sub> )	Can effect electron transport, component of enzymes e.g. nitrite reductase and cytochrome c oxidase, growth inhibitor at high conc.	Growth limiting at low levels but can be toxic above threshold.	(Kabata-Pendias, 2010; Sunda, 1989)

## 2.6 Micronutrients: occurrence and chemical speciation

Lakes are three-phased systems, and the interactions between these three phases determine the form of a chemical species. Liquid, *i.e.*, water, is the principal phase amongst these three. It interacts with atmospheric gases at one interface and with the solids (minerals, sediments) on the other. In addition, suspended solid surfaces also exist in the water such as living and dead plant and animal materials and inorganic solids. The mineral/inorganic and organic particles may occur as dissolved, colloidal, or suspended forms determined by the water column's physical and chemical properties.

The concept of chemical speciation dates back to 1954, when Goldberg coined the term speciation to improve the understanding of the geochemical cycling of TM's (Goldberg, 1954). IUPAC defines chemical speciation as an element's specific form, isotopic composition, oxidation/electronic state, and molecular structure. The process involves identifying particular chemical species or binding conditions and should not be confused with fractionation, which aims to classify an analyte or a group of analytes in a sample based on their physical properties such as size (Templeton *et al.*, 2000). In comparison, total concentration refers to the sum of all chemical species present in a sample for target TM.

The total concentration of a TM in any two different aquatic systems may be similar, but the chemical forms may differ. It is noteworthy that dissolved TM includes all metal species that can pass through a 0.45 µm pore size filter and essentially captures most colloidal particles. TM total concentrations typically remain very low in freshwaters, particularly that of free metal ion(s); considered the most labile fraction for biological uptake (Pesavento *et al.*, 2009). Conversely, the same TM's may pose a toxicity threat to aquatic biota when present as free ions above threshold limits (Painter *et al.*, 1994; Chau & Kulikovskyy-Cordeiro, 1995). Table 2.3 summarises some suggested transport mechanisms for metal chemical species.

The significance of chemical speciation in determining the mobility, availability, and toxicity of trace elements as micronutrients to phytoplankton cannot be overemphasized. Trace metals can exist as free hydrated ions, as inorganic complexes, complexes with organic ligands, or bound within various particles (Dzombak & Morel, 1990)


**Table 2.3: Suggested transport mechanisms for metal chemical species**

<b>Metal Chemical forms</b>	<b>Transport mechanisms</b>	<b>References</b>
Free ion/hydrous species	Convection, Dispersion, Diffusion	(Bridges & Zalups, 2005)
Complexed (in solution), <i>e.g.</i> , dissolved ligands	Dispersion, Diffusion	(Davison, 1993)
Precipitated/co-precipitated, <i>e.g.</i> , colloids	Solid particles, aggregation, sediment/settle out of water column	(Davison, 1993)
Adsorbed to inorganic/organic surfaces	Solid particles, aggregation, sediment/settle out of water column	(Davison, 1993)

The term ‘free ion activity’ reflects the chemical reactivity of TM ions when the system is at equilibrium. This reactivity determines the reaction with cellular/biotic surfaces and should be taken into account in bioavailability studies. This concept is often referred in the context of the ‘free ion activity model’ in the literature and was subsequently generalized to the biotic ligand model (BLM) (Di Toro *et al.*, 2001). In the BLM contextual framework, the metal interacts with a biotic ligand, and thus the toxicity of a given TM is directly proportional to the ligand-metal concentration.

Organic complexation and inorganic phases affect TM chemical speciation in aquatic systems and is a widely studied topic (Midorikawa & Tanoue, 1994). The degree of complexation depends on various factors, *e.g.*, concentration and chemical reactivity of TM’s and complexing ligands (Tessier & Turner, 1995). Considerable progress has been made in the development and parameterization of different models to predict trace element behaviour and fate in natural waters (Huber *et al.*, 2002; Luoma & Rainbow, 2005; Gustafsson, 2007; Parkhurst & Appelo, 2013). These techniques have demonstrated that TM bioavailability and biological activity are dependent on their free ion activity. Table 2.4 summarizes suggested pathways affecting the transport of different chemical species in the water column, the references are for example only. Fe, Mn, Co, and Cu can occur in more than one oxidation state and are thus also affected by the aquatic system's redox chemistry, particularly Fe and Mn (Batley *et al.*, 2004).

**Table 2.4 Trace metal speciation in freshwater exemplified by a hypothetical cobalt species distribution adapted from (Laxen & Harrison, 1981)**

							
Soluble				Colloidal		Particulate	
Metal Species	free metal ions	inorganic ion pairs/ organic chelates	organic complexes	metal bound to HMW organic matter	metals adsorbed to colloids	metals adsorbed to or incorporated in remains of living organisms	mineral solids, precipitates, coprecipitates
Possible examples	Co <sup>2+</sup>	Co(CO <sub>3</sub> ) <sub>2</sub>	Co-Fulvic acids	Co-Humic acids	Co-MnO <sub>2</sub>	Co-organic solids	Co-clay
	Pb <sup>2+</sup>	PbHCO <sub>3</sub> <sup>+</sup> Pb-EDTA	Pb-Fulvic acids	Pb-Humic acids	Pb-Fe(OH) <sub>3</sub>	Pb-organic solids	Pb-clay

### 2.6.1 Iron (Fe)

Fe is the second most widespread metal in nature, the fourth most abundant element (making up 6.3% of the Earth's crust, Table 2-2) (Taylor, 1964) and is the most frequently used transition metal in industry. It is an essential nutrient for its functional involvement in multiple metabolic pathways (Table 2-2) (Botebol *et al.*, 2015; Schoffman *et al.*, 2016) and plays a vital role in numerous physiological functions.

Iron enters surface waters from a variety of sources such as weathering of rocks, soil around watersheds, industrial effluent, and atmospheric deposition (Winchester & Nifong, 1971; Harris, 1992; Shi *et al.*, 2005). Generally, Fe concentration in surface freshwater remains low, (Molot & Dillon, 2003) which combined with the fact that Fe is required for various cellular functions (Table 2-2) (Botebol *et al.*, 2015; Schoffman *et al.*, 2016) leads to Fe being an important limiting micronutrient in a variety of aquatic environments.

As such, Fe exhibits two redox states in aquatic settings:  $\text{Fe}^{2+}$  as a soluble ion under anoxia and therefore more bioavailable, and,  $\text{Fe}^{3+}$  as poorly soluble ion which forms a stable solid under oxic conditions, under which the half life of  $\text{Fe}^{2+}$  can be measured in seconds (Stumm & Morgan, 1996; Molot & Dillon, 2003). Despite Fe having only two redox states, the biogeochemical cycling of Fe is of importance because it involves a complex interplay of biotic and abiotic transformations (Figure 2.4) (Emmenegger *et al.*, 1998; Rose & Waite, 2003). Iron is hugely effected by a range of competing processes including the chemical composition of receiving water bodies, redox recations, precipitation-dissolution, pH, ion exchange, organic-inorganic complexation-dissociation and adsorption-desorption reactions (Davison, 1993). Hence, these interactions dictate the speciation, lability and reactivity of Fe in the aquatic settings.

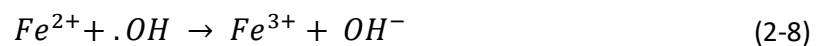
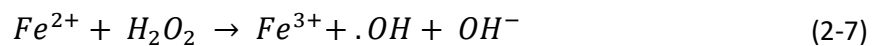
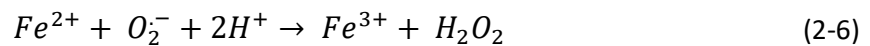
Despite the availability of a wide array of analytical methods, it is extremely challenging to identify the individual contribution of abiotic and biotic factors in Fe biogeochemical cycling. While, biotic and abiotic interactions occur in parallel, this part of the review describes the net changes in Fe geochemistry and briefly considers the effect of abiotic factors.

Fe budgets and cycling in surface fresh and marine water have been heavily studied, such as Tortell *et al.*, Shaked *et al.*, and the studies cited therein (Tortell *et al.*, 1999; Shaked *et al.*, 2004) and a few studies have focused on redox reactions at the oxic/anoxic boundaries

in the water column or on the sediment-water interface. The oxic/anoxic boundary provides fluctuating redox conditions depending on the concentration of dissolved oxygen which then affect the solubility of  $Fe^{2+}$  and  $Fe^{3+}$ . The redox potential of  $Fe^{2+}/Fe^{3+}$  couple broadly lies close to the redox couples of nitrogen, manganese and sulfur species (Figure 2.4). As a result, any redox reactions involving Fe are often tightly coupled with the cycling of above-mentioned elements.

In the photic, oxic zones of water bodies,  $Fe^{2+}$ , is thermodynamically unstable and oxidises to  $Fe^{3+}$  through chemical or biological pathways (Davison, 1993) (Figure 2.4). In the presence of oxygen or oxidizing agents,  $Fe^{2+}$  readily converts to  $Fe^{3+}$  coupled to the reduction of electron acceptors (*e.g.*,  $O_2$ ) and exhibits two stable and metastable oxidative forms (i)  $Fe^{3+}$  oxide (ii)  $Fe^{3+}$  hydroxides. These oxidative forms are insoluble and are not directly available for biological uptake. The biological pathway of  $Fe^{2+} \rightarrow Fe^{3+}$  conversion may involve photoferrotrophs, which use  $Fe^{2+}$  as an electron donor to fix carbon to organic matter, a process known as 'ancient photosynthesis' or photoferrotrophy (Camacho *et al.*, 2017). However, complexation with organic ligands and the activity of  $Fe^{2+}$  oxidizing bacteria determine the pathways and rate of these reactions.

In the literature, two distinct pathways have been reported for abiotic oxidation of  $Fe^{2+}$  to  $Fe^{3+}$ : homogenous and heterogenous oxidation. Homogenous oxidation involves a stepwise reaction of hydrated  $Fe^{2+}$  with  $O_2$  (Equations 2-5 to 2-8)



Heterogenous oxidation, on the other hand, involves the oxidation of  $\text{Fe}^{2+}$  sorbed on the surface of  $\text{Fe}^{3+}$  (oxyhydr)oxides.

Figure 2.5 illustrates the Eh (redox potential)-pH relationship of Fe in water. Theoretically, in areas above and below the dotted line, water itself will be present as oxidized and reduced forms, respectively, meaning that the space between dotted lines represents the possible speciation of Fe in aquatic environments.

To summarise, the diagram suggests  $\text{Fe}^{2+}$  is the dominant species across a range of redox potentials when pH is acidic and will precipitate as  $\text{Fe}(\text{OH})_2$  and  $\text{Fe}(\text{OH})_3$  under alkaline conditions depending on the redox activity of the system. However, a few studies suggest that  $\text{Fe}^{3+}$  reduction can also occur in oxygenated, high pH surface lake water (Aldrich *et al.*, 2001; Emmenegger *et al.*, 2001; Hopwood *et al.*, 2020). As a result, a small increase in  $\text{Fe}^{2+}$  concentrations can readily be assimilated by biota (Peng *et al.*, 2019).

In addition to dynamics at the oxic-anoxic interface, light can also play an important role in Fe cycling.  $\text{Fe}^{3+}$  has a high reactivity towards organic ligands forming organic ferric chelates.  $\text{Fe}^{3+}$  oxides and  $\text{Fe}^{3+}$  chelates can release  $\text{Fe}^{2+}$  into surface water via photoreduction and into deepwater under anoxic conditions (Davison, 1993; Hopwood *et al.*, 2020, Figure 2.4). The process is, however, tightly linked the biotic factors such as the activity of Fe oxidising bacteria. In surface water,  $\text{Fe}^{2+}$  is rapidly re-oxidized to  $\text{Fe}^{3+}$  by  $\text{O}_2$  and as a result, the concentration of labile  $\text{Fe}^{2+}$  remains low in surface water. However, in hypolimnetic waters, which are devoid of oxygen,  $\text{Fe}^{2+}$  remains the dominant species and total Fe concentrations can increase to orders of magnitude higher levels than in surface waters.



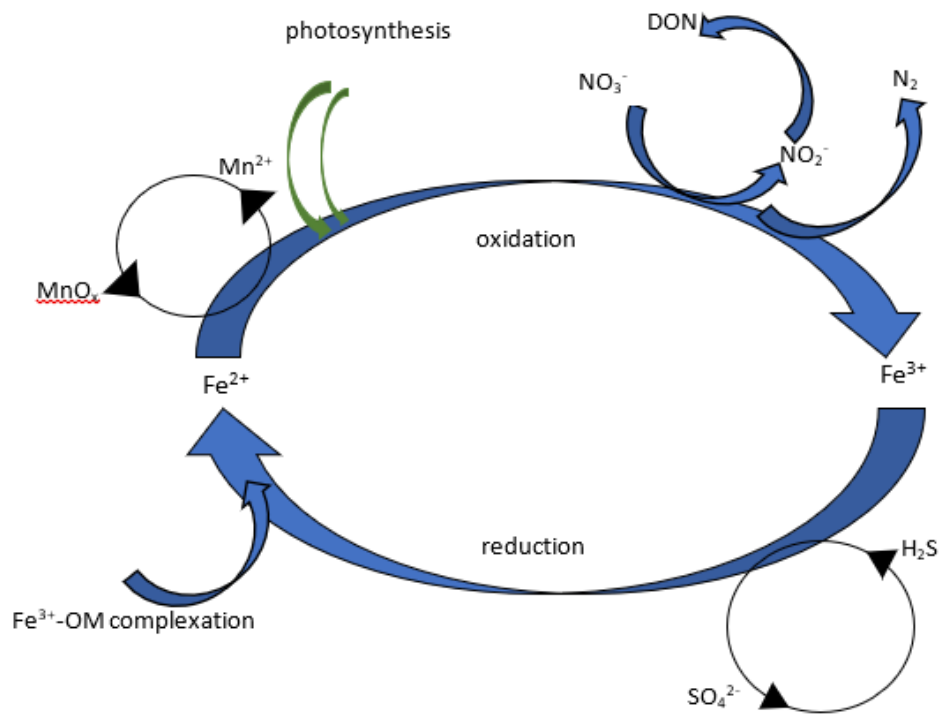


Figure 2.4: Overview of Fe cycle and its relation with other electron acceptors, adapted from Kappler *et al.*, 2021 (Kappler *et al.*, 2021)

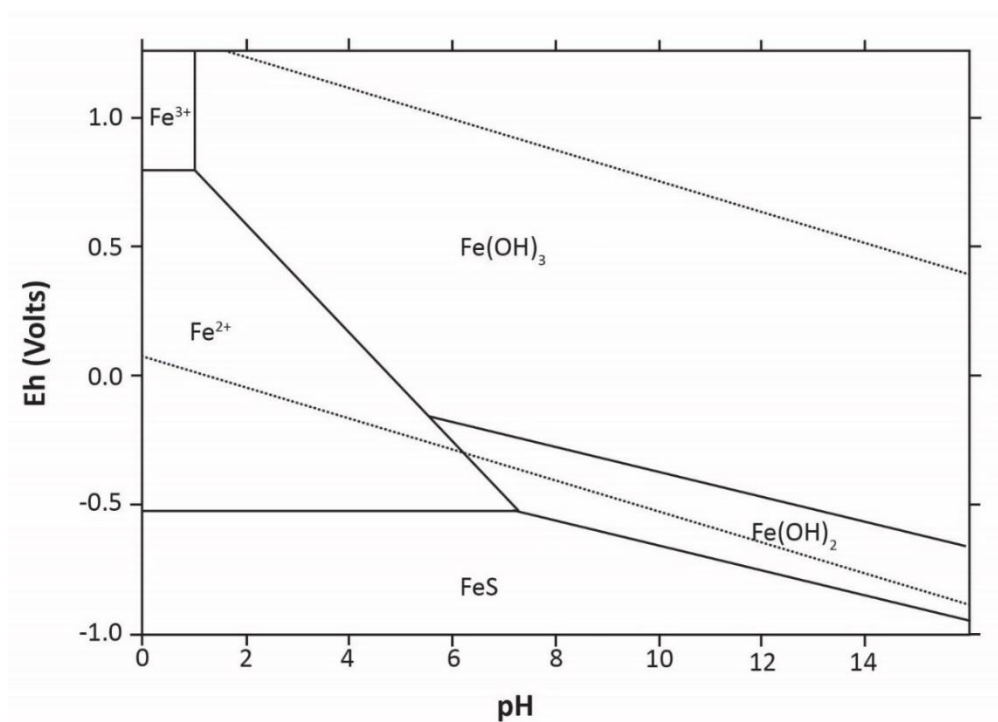


Figure 2.5: A simplified Pourbaix Eh-pH diagram of aqueous iron speciation under standard conditions as adapted from Beverskog 1996 (Beverskog & Puigdomenech, 1996).

### 2.6.2 Manganese (Mn)

Mn is the most abundant transition metal after Fe and forms 0.11% of the earth's crust (Taylor, 1964) and is commonly found in Fe ores. Mn is an essential element for being involved in more than twenty enzymatic reactions and metabolic pathways (Table 2.2), and thus is present in all body tissues.

Being prevalent in Earth's crust, Mn appears in the form of oxides, carbonates, and silicates in rocks and thus makes its way to the aquatic system via myriad ways, such as the weathering of volcanic rocks, fossil fuel combustion, wet and dry deposition (Willey *et al.*, 2009) from the atmosphere, and glacial releases (De Vitre & Davison, 2018).

Manganese may occur in all oxidation states between 0 and +7, but generally exhibits three oxidation states in aquatic settings:  $Mn^{2+}$ ,  $Mn^{3+}$ ,  $Mn^{4+}$ . Each oxidation state showcases different coordination chemistry and exhibits a wide range of strengths as a Lewis acid. Thus, various oxidation states have different ecological and biogeochemical impacts and the distribution is broadly affected by biotic and abiotic factors (Davison, 1993).

Like Fe, the cycling of Mn is linked with the cycling of  $O_2$ , Fe and S (Figure 2.4).  $O_2$  is the dominant electron acceptor in lake surface water and the linkage between Mn and  $O_2$  can be exemplified by Equation 2-9.



$Mn^{2+}$  is a weak reductant and is the most soluble reduced form in aquatic environments. In addition, it acts as an antioxidant in microbial cells. Under an oxygen-saturated, alkaline environment,  $Mn^{2+}$  forms thermodynamically stable  $Mn^{4+}$  (oxy) hydroxide minerals which are insoluble in oxic water, and tend to settle out of the water column to the sediments (Tipping *et al.*, 1984; Post, 1999).  $Mn^{3+}$  is a very unstable intermediate and acts both as oxidant and reductant in water and exhibits high affinity with metal oxides and organic complexes (Klewicki & Morgan, 1998).  $Mn^{7+}$  is another very soluble, powerful oxidant but is not known as being important for Mn species in aquatic settings due to negligible concentrations. Mn speciation and distribution are broadly affected by the thermodynamic and kinetic connection among the three main oxidation states and are summarized by Morgan as the Manganese triangle (Figure 2.6 (Morgan, 2000)).

Like Fe, oxidation of  $\text{Mn}^{2+}$  can be a biotic or abiotic process and both cycles are tightly linked in aquatic settings. Thus it is experimentally challenging to differentiate between the two processes. Oxidation of  $\text{Mn}^{2+}$  is far slower than the oxidation of  $\text{Fe}^{2+}$  at the pH range of natural freshwater, making  $\text{Mn}^{2+}$  energetically more stable than  $\text{Fe}^{2+}$  (Sulzberger *et al.*, 1989). The oxidation process is thermodynamically favorable under aerobic conditions (*i.e.*, in the presence of molecular oxygen) (Sung, 1981), but kinetically limited in the absence of an abiotic or biotic catalyst (Diem & Stumm, 1984).

Abiotic oxidation of  $\text{Mn}^{2+}$  can be catalyzed through organic complexation (Nico *et al.*, 2002), at mineral oxide surfaces (Diem & Stumm, 1984), and by photo-reduction of Mn-oxides (Sherman, 2005). Biotic oxidation of  $\text{Mn}^{2+}$  can take place directly or indirectly. Direct Biotic oxidation of  $\text{Mn}^{2+}$  can be catalysed by a wide range of taxonomical groups of bacteria and fungi, *e.g.*, *Leptothrix discophora* (Boogerd & De Vrind, 1987), *Acremonium* sp. (Miyata *et al.*, 2006; Butterfield *et al.*, 2013) and involve particular enzymes such as multicopper oxidase (Dick *et al.*, 2008) or heme peroxidase (Anderson *et al.*, 2009). In comparison, indirect biotic oxidation involves photosynthesis induced microclimates with high pH (Chaput *et al.*, 2019) or biologically produced free radical ( $\text{O}_2^-$ ).

The balance between oxidation and reduction of different species of Mn determines the lability or mobility of Mn in water systems. Davison (1993) describes the abiotic mineralization in oxic conditions and microbial reduction in anoxic water/sediment as key factors for speciation and distribution of Mn in freshwaters (Davison, 1993). This conceptual model stems from the patterns of the vertical distribution of Mn, molecular oxygen, and redox gradients (seasonal or permanent stratification) in the water column suggested earlier (Mortimer, 1971; Burns & Nriagu, 1976; Hongve, 1997).

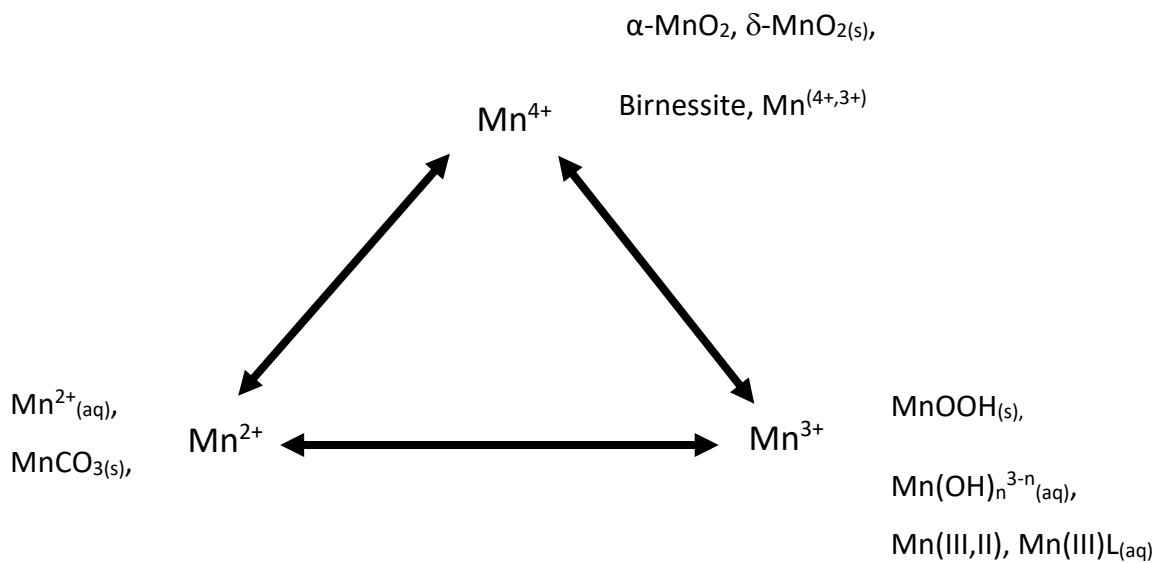


**Figure 2.6: The Manganese triangle for natural waters (Morgan, 2000).**

Where L represents ligands such as  $OH^-$ ,  $Cl^-$ ,  $SO_4^{2-}$ , humic acids, and citrates. Divalent Mn salts are more stable, and the  $Mn^{4+}$  oxidation state predominates in nature.

Like oxidation of  $Mn^{2+}$ , the reductive dissolution of  $MnO_x$  species can also be carried out via biotic and abiotic pathways. The abiotic pathways involve chemical and photoreduction, while bacterial reduction is the dominant biotic process. The oxide species, i.e.,  $Mn^{(3+,4+)}$  have very high sorption affinity to phosphorus and other trace metals such as Co and Pb. These oxides can also facilitate anaerobic degradation of organic matter by acting as terminal electron acceptors for microbes (Myers & Nealson, 1988; Novotnik *et al.*, 2019).

A convenient means for evaluating Mn chemistry's significant features is to look at the graphic relationship between Eh and pH. Figure 2.7 shows the ranges of stability and predominance for different Mn mineral species. To sum up, Mn will be present as  $MnO_x$  above the upper dotted line in the Figure 2.7, where Eh is higher than 1.0 volt, and as  $Mn^{2+}$  below the lower dotted line in the same figure. Acidic pH and low redox potential favor  $Mn^{2+}$  ions, while at high pH, the hydroxide form is predominant. Positive Eh and alkaline pH favor the formation of Mn oxide(s) (Tipping *et al.*, 1984; Davison, 1993).

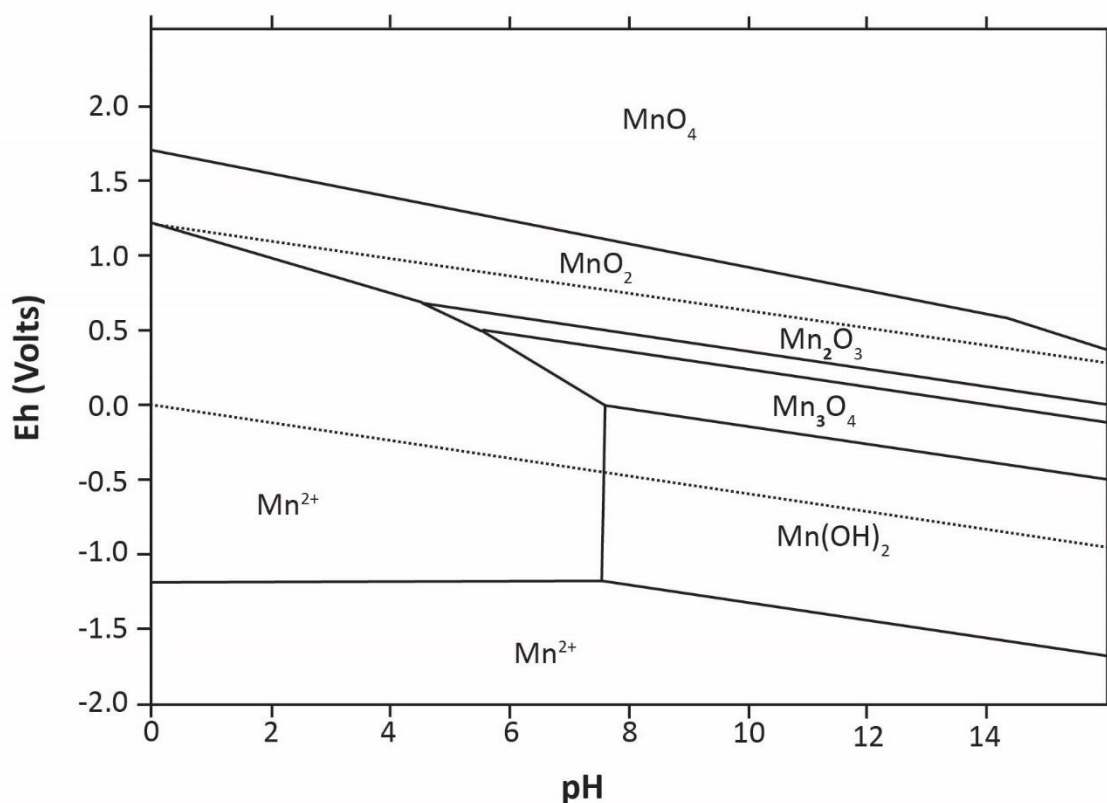


**Figure 2.7: A simplified Pourbaix Eh-pH diagram of aqueous manganese speciation under standard conditions adapted from Papazotos *et al.*, 2019 (Papazotos *et al.*, 2019).**

### 2.6.3 Zinc (Zn)

Zinc is a ubiquitous transition metal and one of the most significant micronutrients for all biota, due to its involvement in multiple biotic pathways (Table 2.2 and studies cited therein). In addition, Zn is a vital inorganic component in various compounds *e.g.*, see Zn minerals in Table 2.2. Zn is of particular interest in lake micronutrient cycling, because it is involved in both biotic (*e.g.*, organic complexation) and abiotic (*e.g.*, adsorption, dissolution) processes (Taylor, 1964)

It occurs mainly in the form of sulfides, carbonates, and silicate ores and its common minerals are listed in Table 2.2. Zn is widely used in the manufacture of alloys, pharmaceuticals, cosmetics, and wood preservatives and thus can enter waterways via a multitude of anthropogenic routes (Porter, 1991). The metal can bio-accumulate and bio-magnify, resulting in higher metal levels in organisms than the surrounding waters (Mummert, 1987).

The mobility of Zn within and between terrestrial and aquatic systems depends on transport processes and substantially depends on Zn's geochemistry. It is essential to understand Zn's aqueous speciation and the solubility of Zn-bearing minerals in order to predict its behavior. There are many Zn species in aqueous settings, but only a brief description of the species relevant for their transport in freshwater is given here (Figure 2.8).

Zn is generally found in the divalent form ( $\text{Zn}^{2+}$ ) in water, and its chemical speciation is affected by redox, organic complexation, and pH. In surface waters, where oxygen and carbon dioxide concentrations are high,  $\text{Zn}^{2+}$  readily dissolves in water forming  $\text{Zn}(\text{HCO}_3)^+$ . It can exist as a range of hydrolysis products depending upon the environmental conditions. (Masliy, 2000; Sherman, 2001; Bruce, 2009).

In general, Zn can be easily transported and solubilized in an acidic environment ( $\text{pH} < 7$ ) and forms complexes with organic and inorganic compounds, *e.g.*, approximately 60% of the available Zn ions are bound to humic substances when the pH is 5.8, but this bound fraction is reduced to near-zero when the pH drops below this value (Beverkog & Puigdomenech, 1997).

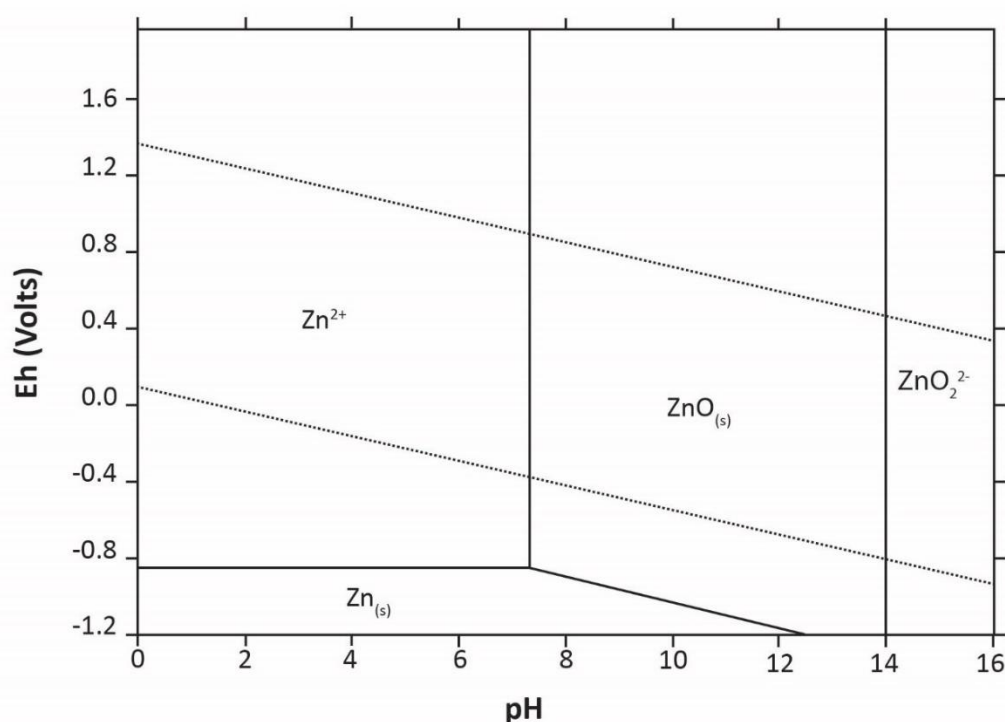


**Figure 2.8: A simplified Pourbaix Eh-pH diagram of aqueous zinc speciation under standard conditions**

Zn compounds are readily soluble under acidic conditions. The released ions from highly mobile minerals (*e.g.*, in the presence of sulfides) or organo-mineral complexes through sorption reactions. The sorption reactions are, however, dependent on the pH of the water body (McPhail *et al.*, 2003). Zn salts hydrolyze when the pH is in the range of 7-7.5 but immediately precipitate amphoteric  $\text{Zn}(\text{OH})_2^0$  if the pH is allowed to exceed eight, which tends to dissolve if the pH increases any further forming  $\text{Zn}(\text{OH})_4^0$  (Helgeson *et al.*, 1978).

#### 2.6.4 Copper (Cu)

Cu is an abundant transition metal found in a variety of rocks and minerals. In recent years, Cu and Cu-based nanoparticles have been used for various industrial processes, electrical equipment and as antimicrobial agents. Thus, Cu enters water systems from myriad paths such as metal plating, mining and Cu processing, effluents from smelters, corrosion from pipes (made from Cu, bronze, or brass) (Dorsey & Ingerman, 2004). Engineered nanoparticles form a relatively new class of Cu products with various applications including

drug delivery and thus raise a concern due to their toxicity and life cycle characteristics (Conway *et al.*, 2015).

In addition to the wide variety of uses of Cu on an industrial scale, it is an essential nutrient for primary productivity (Table 2.2). Cu containing enzymes function as redox catalysts or as dioxygen carriers and thus play a key role in several metabolic pathways (Table 2.2) (Montenegro *et al.*, 2015; Kumar *et al.*, 2020). Like other transition metals, Cu exhibits numerous oxidation states ( $\text{Cu}^0$ ,  $\text{Cu}^+$ ,  $\text{Cu}^{2+}$ ) of which  $\text{Cu}^+$  and  $\text{Cu}^{2+}$  predominate in aquatic environments.

$\text{Cu}^+$  is found primarily under anaerobic conditions and readily oxidizes to  $\text{Cu}^{2+}$  where  $\text{O}_2$  is present. In its ionic form ( $\text{Cu}^+$  and  $\text{Cu}^{2+}$ ) the metal is chemically active and may react with other inorganic and organic ligands/complexes. For instance,  $\text{Cu}^+$  complexes may be formed through photochemical processes and may persist for several hours in natural waters (Moffett & Zika, 1987). On the other hand,  $\text{Cu}^{2+}$  is stable, and forms complexes with inorganic ( $\text{CuCO}_3$ ,  $\text{Cu}(\text{OH})^+$ ,  $\text{Cu}(\text{OH})_2$ ) and organic ligands (dissolved organic matter) (Buck, Ross, Russell Flegal, & Bruland, 2007). Consequently, the element is found in soluble, colloidal and particulate forms (Harrison, 1985). The sum of these complexes dictates the total dissolved concentration of Cu (Equation 2-10) (Stumm & Wollast, 1990; Bruce, 2009)

$$\text{Cu}_T = [\text{Cu}^{2+}] + [\text{Cu}(\text{OH})^+] + 2[\text{Cu}_2(\text{OH})_2^{2+}] \quad (2-10)$$

Broadly speaking, the concentration of Cu is largely controlled through complexation in aquatic environments.

In freshwater,  $\text{OH}^-$  and  $\text{CO}_3^{2-}$  ions are particularly important for inorganic Cu complexation. The predominant hydroxide and carbonate-Cu species depend on the  $\text{OH}^-$  ion (pH) and  $\text{CO}_3^{2-}$  (hardness) of the water body (Figure 2.9). While the inorganic controls on Cu speciation are pertinent, organic complexation typically dominates due to the high stability of Cu-organic complexes (Hartland *et al.*, 2019). However, opinion is divided on the role of molecular weight of organic molecules on Cu-complexation (Cardwell *et al.*, 1985; Qin *et al.*, 2004; Gouvêa *et al.*, 2005; Wang *et al.*, 2010).



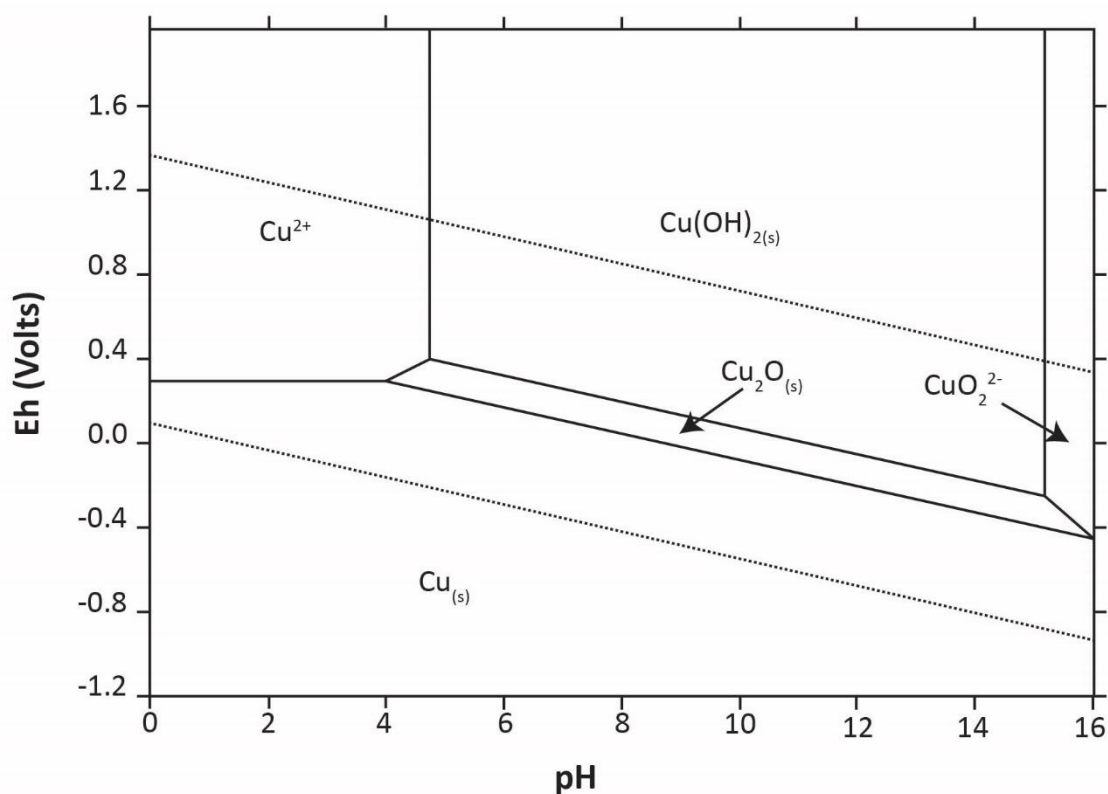


**Figure 2.9: A simplified Pourbaix Eh-pH diagram of aqueous copper speciation under standard conditions adapted from Woods *et al.*, 1987 (Woods *et al.*, 1987)**

### 2.6.5 Chromium (Cr)

Cr is the 24<sup>th</sup> most abundant element making up to 0.014% of the Earth's crust (Emsley, 2001) and is naturally found in rocks, soils, and volcanic dust. Chromium is contained in effluent from industries such as steelworks, chromium electroplating, and leather tanning effluents are loaded with Cr, making it essential to understand the behaviour of the trace metal in receiving water bodies. Cr is an essential nutrient involved in a range of metabolic pathways such as glucose metabolism and synthesis of nucleic acids in phytoplankton (Table 2.2).

Like all transition metals, Cr can exist in various oxidation states (0 to +6) in water. The total concentration of Cr in natural water does not generally exceed a few micrograms per liter (Świetlik, 1998). The most common oxidation states in natural waters are  $\text{Cr}^{+2}$ ,  $\text{Cr}^{+3}$ , and  $\text{Cr}^{+6}$ . Other oxidation states are mostly present below the detection limit of analytical speciation techniques. Thus, Cr speciation studies have been a long-standing analytical challenge as it exhibits complex, interchangeable reactions between different redox states.

For example,  $\text{Cr}^{3+}$  behaves as a typical 'Hard' lewis acid, and readily forms complexes with a variety of ligands, both natural and synthetic. Beside, the nature and behavior of various forms of Cr can be different in fresh, marine, and surface water.

The distribution of compounds containing  $\text{Cr}^{3+}$  and  $\text{Cr}^{6+}$  widely depends on the pH, Eh, the kinetics of redox reactions, and total Cr concentration (Elderfield & Letters, 1970). In general,  $\text{Cr}^{3+}$  and  $\text{Cr}^{6+}$  predominate under reducing and oxidizing conditions, respectively (Guertin *et al.*, 2004), with  $\text{Cr}^{6+}$  salts being more soluble than  $\text{Cr}^{3+}$  salts in surface water.  $\text{Cr}^{3+}$  acts as a micronutrient, while  $\text{Cr}^{6+}$  may be toxic (Langard & Costa, 2007).

A simplified Pourbaix diagram for aqueous Cr speciation is shown (Figure 2.10).  $\text{Cr}^{3+}$  exists as polymeric aqueous complex  $\text{Cr}(\text{H}_2\text{O})_6^{3+}$  below pH 4 (shown as  $\text{Cr}^{3+}$  on Pourbaix diagrams for simplicity as adapted from (Hagendorfer & Goessler, 2008) and hydrolyses to  $\text{Cr}(\text{OH})_2^+$  species in the pH range 4 to 7 in the absence of complexation agents. Cr precipitates as  $\text{Cr}(\text{OH})_3$  in the pH range 7-11.5, which redissolves if the pH is allowed to increase beyond 11.5 (Richard & Bourg, 1991).

Under oxidizing conditions, aqueous Cr is present as  $\text{Cr}^{6+}$  and the prevalent polymeric species are  $\text{HCrO}_4^-$  and  $\text{CrO}_4^{2-}$  depending on the pH (Figure 2.10) (Rakhunde *et al.*, 2012).

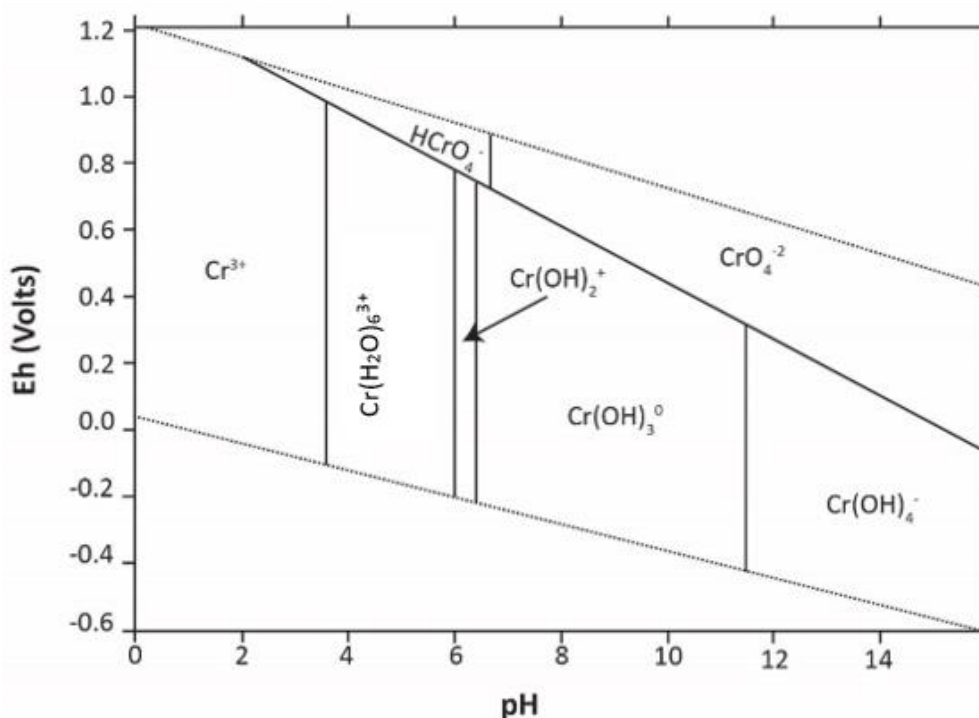


**Figure 2.10: A simplified Pourbaix Eh-pH diagram of aqueous chromium speciation under standard conditions adapted from (Hagendorfer & Goessler, 2008)**

The redox transformation of  $\text{Cr}^{3+}$  to  $\text{Cr}^{6+}$  or vice versa can only take place in the presence of another redox couple. Consequently, Cr cycling between these two redox states is closely related to other redox couples such as  $\text{H}_2\text{O}/\text{O}_2$  (Rue *et al.*, 1997; Fu *et al.*, 2021),  $\text{Mn}^{2+}/\text{Mn}^{4+}$  (Weaver & Hochella Jr, 2003),  $\text{NO}_2/\text{NO}_3$  (Schroeder & Lee, 1975; Moos *et al.*, 2020),  $\text{Fe}^{2+}/\text{Fe}^{3+}$  (Gorny *et al.*, 2016) in aqueous environments (Figure 2.11).

In addition to the redox, pH and temperature conditions, the effect of complexing agents and the concentration of complexing agents such as organic matter is important (Figure 2.11). As a result, the Cr cycle is strongly controlled by the local aquatic environment and the establishment of equilibrium between  $\text{Cr}^{3+}$  and  $\text{Cr}^{6+}$  is a slow-moving process (Rai *et al.*, 1989).

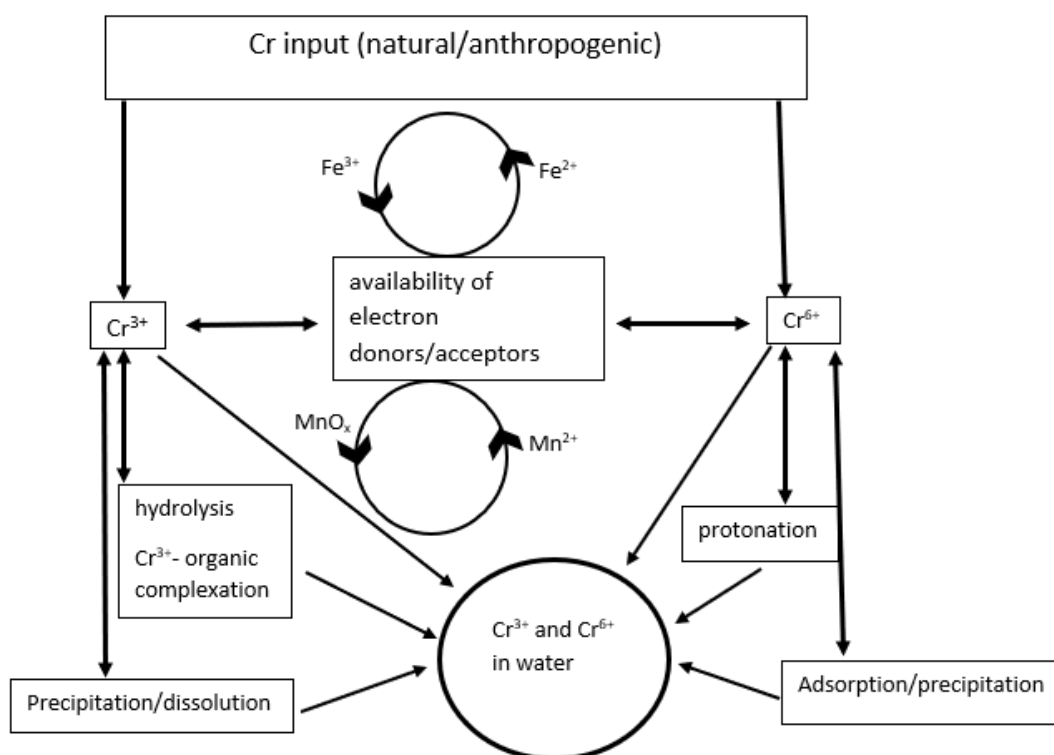


**Figure 2.11: Aqueous geochemistry of chromium and its association with other redox couples in aqueous environment adapted from Richard and Bourg, 1991 (Richard & Bourg, 1991)**

### 2.6.6 Cobalt (Co)

The average abundance of Co in the Earth's crust is approximately 25 ppm and hence is classified as one of the least abundant elements on earth (constituting 0.003% of the total crust (Hamilton, 1994). The metal mostly partitions into Fe- and Ni-rich phases and common minerals from which the element is refined into metal are listed in Table 2.2. Co has been recognised as a critical raw material (Commission, 2020) for its increasing demand

in multiple industries such as healthcare (Barceloux & Barceloux, 1999), renewable energy (Barton *et al.*, 2014), data storage and rechargeable batteries (Cobalt, 2020). Essentially, weathering of rocks and effluent from any of the above mentioned industrial activities release Co into waterways. Co is an essential nutrient and is involved in multiple biological pathways including the synthesis of vitamin B12 (Table 2.2).

Like other transition metals, the total dissolved concentration of Co in aquatic environments varies markedly depending upon the source of Co (weathering of the Earth's crust versus anthropogenic), physicochemical properties of the catchment area, and the partitioning processes in the receiving water. It is therefore essential to comprehend Co's aqueous speciation and how different chemical forms interconvert.

Co can exist in the  $\text{Co}^{2+}$  and  $\text{Co}^{3+}$  oxidation states, the former being the dominant, stable valence state in the pH and Eh range of most natural waters. It is rightly stated that Co chemistry is predominately controlled by  $\text{Co}^{2+}$  oxidation state in water. Which in turn is largely due to redox potential, affecting the  $\text{Co}^{2+}/\text{Co}^{3+}$  couple (Ansoborlo, 2005).  $\text{Co}^{3+}$  is a strong oxidizing agent, is not thermodynamically stable, and has extremely low solubility ( $K_{\text{sp}} \text{Co}(\text{OH})_3 = 10^{-44.5}$ ) (Smith & Martell, 1976) and so decomposes under Eh-pH conditions typical of freshwaters. Hence,  $\text{Co}^{3+}$  oxidation state is only detectable if bound to strong complexation agents (Duckworth *et al.*, 2009).

The Eh-pH diagram shows that under oxidizing and moderately reducing conditions, the dominant species predicted at pH values less than 8 is non-complexed free  $\text{Co}^{2+}$  ions. At pH values between 8 and 14, Co exists as hydrolytic species  $\text{Co}(\text{OH})_4^{2-}$  and  $\text{Co}(\text{OH})_2^0$ . Under reducing conditions, in the presence of dissolved sulphides,  $\text{Co}^{2+}$  forms bisulfide species such as  $\text{CoHS}^+$  and  $\text{Co}(\text{HS})_2^0$  (Figure 2.12).

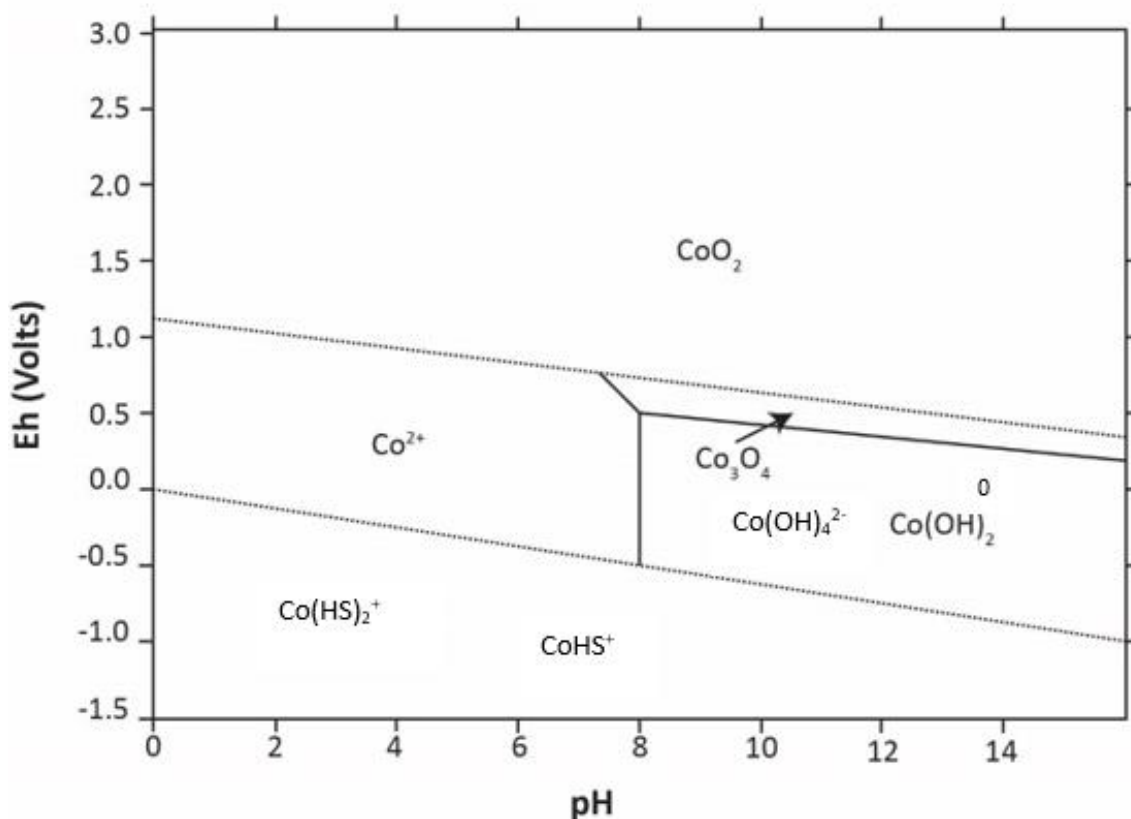


**Figure 2.12: A simplified Pourbaix Eh-pH diagram of aqueous cobalt speciation under standard conditions adapted from Turner *et al.*, 1981 (Turner *et al.*, 1981)**

Studies on the sorption behaviour of Co suggest that the adsorption of Co is largely controlled by the presence of iron and manganese oxides and clay minerals, see for example the following references and related citations (Means *et al.*, 1978; Sparks, 2003; Reddy & DeLaune, 2008).

### 2.6.7 Nickel (Ni)

The average abundance of Ni is approximately 80 ppm in earth's crust (representing 0.009%) and is a member of the so called 'Fe, Co and Ni' group (Greenwood & Earnshaw, 2012). As such, Ni is closely related to Co in its chemical and biochemical behaviour. It enters aquatic systems through natural sources such as the weathering of minerals, rocks,

and via anthropogenic activities such as coal combustion, ignition of waste (Coman *et al.*, 2013) and Ni-Cd batteries (Cempel & Nickel, 2006). More than 90% of aquatic Ni is associated with sedimentary particulate matter, and generally has a low background concentration in freshwater systems (Hart, 1982). Table 2.2 highlights a few metabolic pathways that categorize Ni as an essential micronutrient for primary productivity in lakes. However, concentrations above the threshold are considered toxic.

Ni can exist in any one of the oxidation states from 0 to +4. Although  $\text{Ni}^+$  and  $\text{Ni}^{+2}$  oxidation states can exist under certain conditions, however,  $\text{Ni}^{2+}$  is dominant inorganic species in the Eh-pH range of aquatic settings (Figure 2.13). The predominant Ni species in acidic region is  $\text{Ni}^{2+}$ , and  $\text{Ni}(\text{OH})^+$  is a metastable form (Figure 2.13), and competition between  $\text{Ni}^{2+}$  and  $\text{H}^+$  causes Ni dissociation from the oxyhydroxides of Fe and Mn (Theis & Richter, 1980). Under alkaline conditions,  $\text{Ni}(\text{OH})_2$  and  $\text{Ni}(\text{OH})_3^-$  become the dominant species (Figure 2.13). Under hypoxic to anoxic conditions, the metal forms insoluble sulfides.

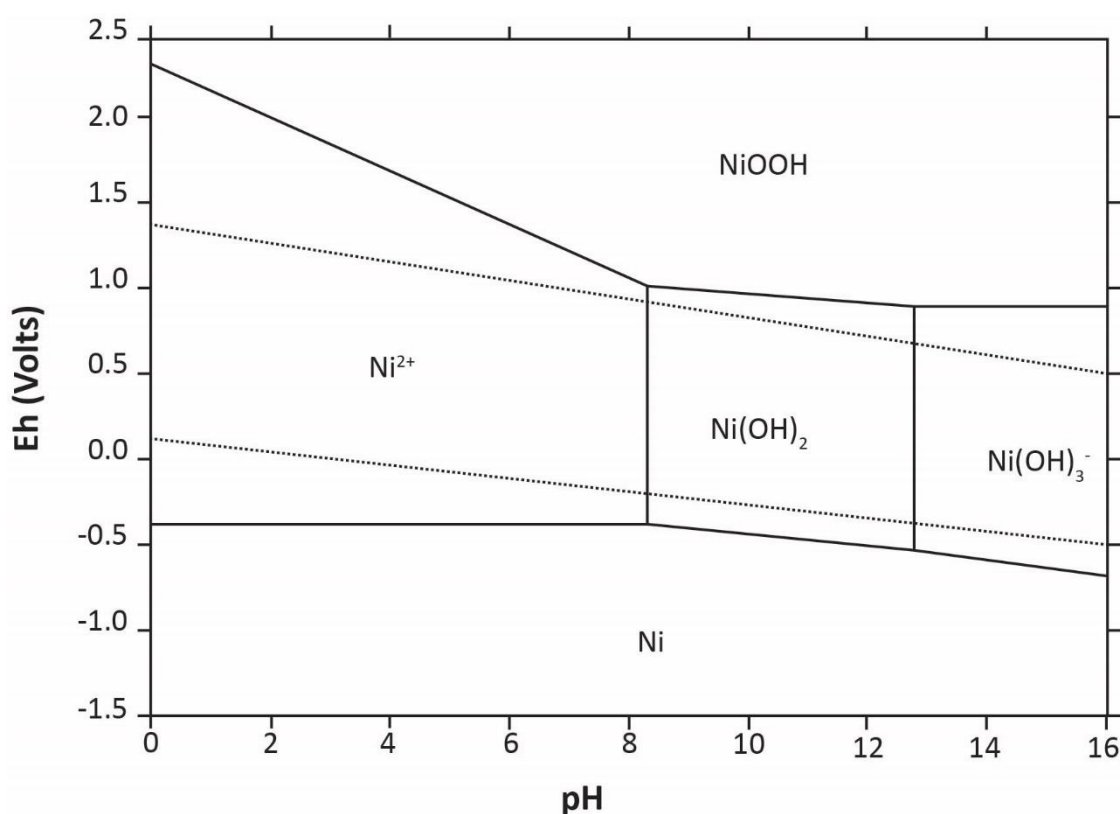


**Figure 2.13: A simplified Pourbaix Eh-pH diagram of aqueous cobalt speciation under standard conditions adapted from Beverskog and Puigdomenech (Beverskog & Puigdomenech, 1997)**

### 2.6.8 Cadmium (Cd)

Cd is biotoxic (McLaughlin & Singh, 1999), non-essential element and is present in low background concentration (crustal average 0.2 ppm) (Chuanwei *et al.*, 2015) in the geosphere. The metal is found in the sulfidic ores of zinc, lead and copper and the principle economic ore is sphalerite (ZnS) with a Cd content 0.02-1.8% by weight. The initial concern about Cd toxicity to humans arose in 1935 when people living in the vicinity of metal mines and smelters complained about the pain in bones, a disease now known as Itai-Itai (Shigematsu, 1984).

Natural sources of Cd to the environment include weathering of rocks (phosphate rocks in particular), volcanic activity, and aerosols from sea spray. Cd does not corrode easily and finds its applications in various industries such as metal plating, coating, batteries, certain dyes, pesticides, as well as being a contaminant in phosphate fertilizers. Therefore, Cd's anthropogenic sources to surface water span from point to non-point sources and include industrial discharge, agricultural run-off, and leaching from electrical dump sites.

The total dissolved concentration of Cd generally does not exceed  $0.5 \mu\text{g L}^{-1}$  in freshwater (Pan *et al.*, 2010). The two states of cadmium oxidation are;  $\text{Cd}^0$  (metallic form, rare and insoluble in water) and,  $\text{Cd}^{+2}$  which is considered to be predominant and soluble oxidation stater in water (Figure 2.14). Nevertheless, other forms of Cd such as those bound to various inorganic and organic ligands may be present depending on the pH and the concentration of inorganic and organic ligands in the water body.

Cd may start to precipitate as  $\text{Cd}(\text{CO}_3)_2$  as early as at pH 6 and  $\text{Cd}(\text{OH})_2$  becomes the dominant phase in highly alkaline conditions (Figure 2.14) (Simpson, 1981). However, under low redox potential or anoxic conditions, Cd may be present as soluble CdS (Figure 2.14). The adsorption of Cd to particulate material increases with increasing pH in freshwater.

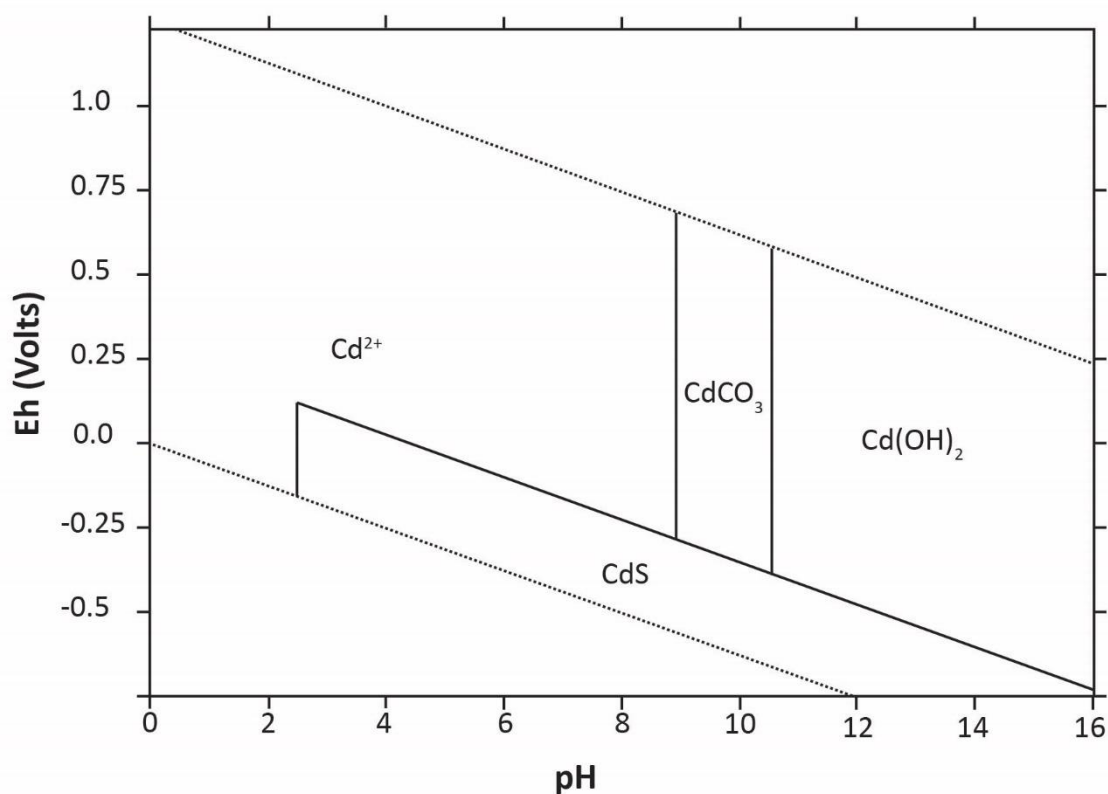


**Figure 2.14: A simplified Pourbaix Eh-pH diagram of aqueous cadmium speciation under standard conditions adapted from Ford *et al.*, 2007 (Ford *et al.*, 2007)**

## 2.7 Aquatic Chemistry; The Role of colloids

The mobility of nutrients in the water column depends mainly on interactions between transport processes and various other phenomena such as sorption and colloidal association. Table 2.3 summarises the effect of geochemical speciation on the transport and mobility of micronutrients, but as a general rule, adsorption delays and solubility increases the transport and mobility of trace metals. It is widely accepted that within the 0.45 $\mu\text{m}$  filterable phase, the free (hydrated) form of metal poses a higher risk to the receiving water body than the same metal in complexation with organic matter or associated with colloids, because these form stable associations and are hence less toxic (Morel & Morel-Laurens, 1983).

Colloids systems may be defined as systems with two physical components i.e., dispersing medium (water in case of lakes) and a disperse phase (usually solid) The disperse phase contains solids/particles/macromolecules in the size range of 1 nm to 1- $\mu\text{m}$  (Buffle &



Leppard, 1995; Gibson *et al.*, 2007). These particles are small in size but provide a large surface area and may be important for chemical reactions specially concerning the cycling of trace elements (Lead & Wilkinson, 2006).

In lakes, environmental colloidal particles originate either from autochthonous (indigenous primary or secondary production) or allochthonous (traveled from the terrestrial origin) sources depending upon the degree of human input, meteorological conditions of the area, hydrological characteristics, and sediment resuspension. Broadly, literature groups environmental colloids into three main categories, 1) inorganic colloidal particles, also referred to as inorganic mineral phases, 2) organic colloidal particles, and 3) organic-inorganic colloidal particles for example see (Buffle & Leppard, 1995). Figure 2.15 illustrates these processes and is colour coordinated, the text in green indicates that the fraction is generally bioavailable while the red colour shows that the trace metal is in complexation with inorganic or organic colloids and general is not available for biological uptake. Stability and aggregation broadly control the behavior of environmental colloids in an aquatic setting, which themselves are largely dependent on different parameters such as ionic strength, pH, and natural organic matter. Therefore, characterizing the nature and behavior of colloids in aquatic settings is an interdisciplinary problem. The following section reviews the chemical speciation of TM's in the context of colloids.

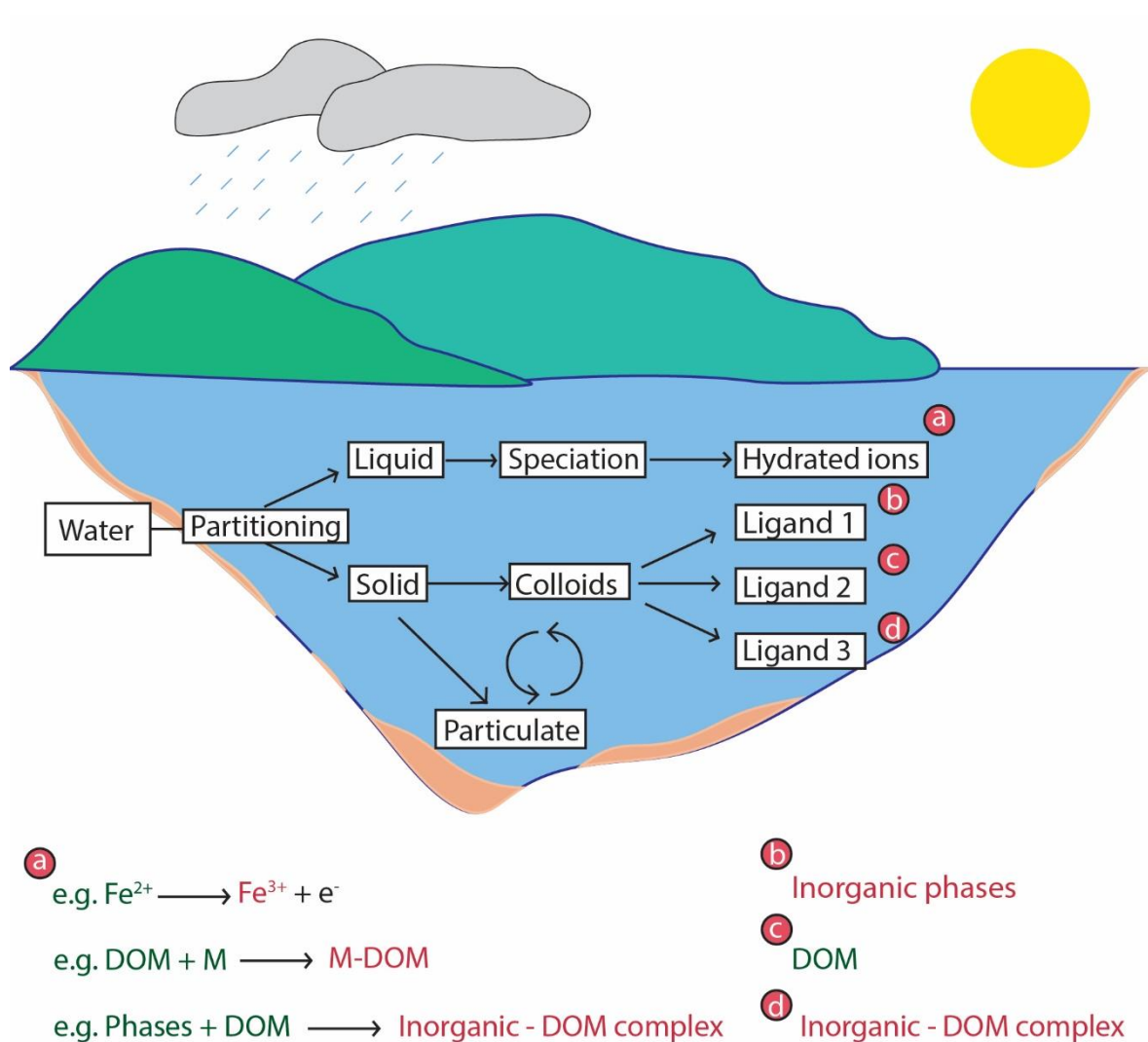


Figure 2.15: Factors, chemical processes and pathways affecting the bioavailability of micronutrients in aquatic systems

## 2.8 Aquatic chemistry: effect of inorganic colloids

Fe and Mn being sensitive to redox potential changes, precipitate out of solution as oxides, oxyhydroxides, and hydroxides under oxic conditions. If large enough, these particles may gravitate out of the water column to the sediment where anoxic conditions favor the formation of reduced soluble ions, which are circulated back to the upper water column through physical disturbance, bioturbation, or upwelling. However, if present in small size, these mineral phases remain unaffected by gravity and remain suspended in the water column as colloids. These minerals' formation sequester available Fe and Mn out of the water column in either case. To circumvent the reduction in these metals' bioavailability,

several aquatic microorganisms produce biotic compounds that bind to the mineral phases of Fe and Mn to free up the metal for biological uptake.

Considering a general reaction for trace metals (van Leeuwen, 1999)



Where TM is the trace metal and L is the inorganic ligand, a generalised equilibrium constant can be written as 2-12 and can be rearranged to determine the bound and free forms of any trace metal based on K.

$$K = \frac{[TML]}{[TM][L]} \quad (2-12)$$

For example, Cd can be complexed in solution by several inorganic ligands such as bisulphates, carbonic acid, chloride and hydroxides. However, it is well established that the stability constants of metal-organic complexes are generally several orders higher than inorganic complexes.

## 2.9 Aquatic chemistry: effect of organic complexation

Natural Organic Matter (NOM), meaning the material containing both carbon and hydrogen that is of biological origin, may be present as particulate, colloidal, or dissolved forms in aquatic systems. The distinction between dissolved organic matter and particulate organic matter is arbitrary and is merely based on filtration through a 0.45 µm filter (Aiken *et al.*, 2011). The fraction that passes through the 0.45 µm filter is called Dissolved Organic Matter (DOM), and the fraction retained by the same pore size is known as Particulate Organic Matter (POM). POM is a critical phase in water systems and is also essential in trace metal ion chemistry and can control the occurrence of trace metals. This review, however, focuses on DOM.

DOM is a poorly defined complex mixture of organic substances of varying size and nature in water systems (Leenheer & Croué, 2003) and can be an essential source of organic ligands that can form complexes with trace metals. DOM comprises of a complex heterogeneous continuum ( $10^{-8}$ - $10^{-4}$  cm) (Thurman, 2012) of low to high molecular weight substances with different characteristics (Hedges *et al.*, 1994). DOM may originate from autochthonous or allochthonous sources. Autochthonous organic substances are produced

within lakes due to primary and secondary productivity, such as microorganisms, algae, macrophytes (Nagata, 2002; Hansell & Carlson, 2014) and is mainly composed of the low molecular weight fulvic acids, carbohydrates, amino acids, proteins, lipids, organic acids. Allochthonous DOM, on the other hand, travels from terrestrial origins to water bodies and is mainly composed of substances from leachate of the soil organic matter and terrestrial plant material. High molecular weight compounds such as humic substances may form up to 90% of the allochthonous DOM. Thus, the quantity, quality, and reactivity of DOM vary spatially and temporally and is primarily dependent on the nature and proximity to source material and exposure to environmental processing (Aiken *et al.*, 2011). There is a consensus about the role of DOM in aquatic food web processes and nutrient dynamics. Potentially 40-50% of photosynthetically fixed carbon is cycled back in aquatic systems as dissolved organic carbon (DOC) by microbial actions.

Most of the DOM components, for instance, fulvic and humic substances from both autochthonous and allochthonous origin, proteins, aromatic amino acids such as tyrosine, tryptophan, and phenylalanine, show fluorescence as well as complexation properties. Their ability to fluoresce in a discrete wavelength range makes their identification relatively easy in water samples. DOC may constitute up to 90% of DOM and is often used as a proxy for the quantification of DOM. DOM's complexation properties originate from various functional groups in the molecular structure that can complex with the aquatic trace metals (Jørgensen, 2011).

DOM provides different organic ligands to complex aquatic trace metals such as allochthonous fulvic acids (Shin *et al.*, 2001; Wu *et al.*, 2002a, 2002b; Haitzer *et al.*, 2003; Sonke & Salters, 2006; Liu *et al.*, 2008), autochthonous fulvic acids (Xue & Sigg, 1993; Esteves da Silva *et al.*, 1996), allochthonous humic acids (Sonke & Salters, 2006; Shcherbina *et al.*, 2007; Liu & Cai, 2010; Reiller & Brevet, 2010; Mikutta *et al.*, 2011), amino acids such as tryptophans (Wu & Tanoue, 2001; Spencer *et al.*, 2007; Liying *et al.*, 2009). In addition, living organisms such as algae can uptake or complex trace metals directly or in the presence of humic acids that can enhance the uptake considerably (Xue & Sigg, 1993; Koukal *et al.*, 2003). Some higher aquatic organisms such as fish can also complex trace metals on the gill surfaces (Playle *et al.*, 1993).

Several factors such as concentration, reactivity and molecular size of organic matter effect the formation of metal-organic matter complexes (Leenheer & Croué, 2003). Besides,

occurrence of trace metals, pH, ionic strength and competing ions are also important determinants of the metal-DOM complexation (Pokrovsky *et al.*, 2012). A wide range of aquatic metals that can form metal-organic ligand complexes have been studied previously in different environments (Pokrovsky & Shirokova, 2013; Manasypov *et al.*, 2015). This part of the review will only briefly look at the complexation behaviour of the trace metals studied in the present work.

As a general rule for metal-DOM complexation, trace metals with high binding strengths such as Fe, Zn, Cu, Ni, Co and Cr are distributed in the high molecular size fraction and the ones with low binding strengths such as uranium (U), thorium (Th) and Cd are mostly distributed in the low molecular size fraction of the DOM (Irving & Williams, 1953; Wu *et al.*, 2004).

Bivalent heavy metals such as Ni, Zn and Cd show strong interactions with humic acids and may form covalent bonds with certain functional groups of the humic acids but not with fulvic acids suggesting that the above mentioned metals can form stable complexes with the high molecular weight humic acids (Laxen, 1985). The process has been reported to decrease the toxicity, mobility and hence bioavailability of these two metals in the presence of humic acids.

## **2.10 Aquatic chemistry: effect of inorganic-organic complexed colloids**

In freshwater bodies, dissolved organic matter in different forms, such as fulvic and humic substances, is essential for controlling trace metals' chemical speciation and behavior (Tipping *et al.*, 2002). For example,  $\text{Fe}^{3+}$ -DOM complexes are ubiquitous in rivers and lakes, and their persistence and proportion compared to the other forms are dependent mainly on the temperature and pH. Fe may undergo the ligand to metal charge transfer in such organic complexes, an electron sharing process that creates energy difference between them. This difference in energy generates a cleavage between the two resulting in the release of reduced  $\text{Fe}^{2+}$  form, which can either convert back to  $\text{Fe}^{3+}$  or uptaken by biota.

## **2.11 Summary of the Review**

The nature and concentration of trace metals and organic compounds result from a complex set of processes such as abundance in the earth's crust, weathering of rocks and minerals, leaching from the soil, degradation of terrestrial and aquatic biomass, formation

of mineral species in the water bodies, adsorption reactions to these inorganic and organic phases, coagulation and sedimentation of the particles in water bodies. The composition and concentrations of these components, therefore, vary in different aquatic systems. suspended particles play an important role in controlling the nature and concentration of trace metals in traditionally dissolved fraction. Some of these trace metals are eliminated from the water column through complexation with inorganic and organic surfaces, however the ones at small size level such as colloids remain suspended in the water column and provide surfaces for reactions in the water column. Major difficulty in trying to compare the literature data is the variability in the size fractionation and operational definitions of colloids.

## 2.12 References

- Abell, J. M., Özkundakci, D., & Hamilton, D. P. (2010a). Nitrogen and Phosphorus Limitation of Phytoplankton Growth in New Zealand Lakes: Implications for Eutrophication Control. *Ecosystems*, 13(7), 966-977.
- Abell, J. M., Özkundakci, D., & Hamilton, D. P. J. E. (2010b). Nitrogen and phosphorus limitation of phytoplankton growth in New Zealand lakes: implications for eutrophication control. 13(7), 966-977.
- Aiken, G. R., Hsu-Kim, H., & Ryan, J. N. (2011). Influence of Dissolved Organic Matter on the Environmental Fate of Metals, Nanoparticles, and Colloids. *Environmental Science & Technology*, 45(8), 3196-3201.
- Aldrich, A., van den Berg, C. M. G., Thies, H., & Nickus, U. (2001). The redox speciation of iron in two lakes. *Marine and Freshwater Research*, 52, 885-890.
- Anderson, C., Johnson, H., Caputo, N., Davis, R., Torpey, J., & Tebo, B. M. (2009). Mn (II) oxidation is catalyzed by heme peroxidases in “*Aurantimonas manganoxydans*” strain SI85-9A1 and *Erythrobacter* sp. strain SD-21. *Applied and Environmental Microbiology*, 75(12), 4130-4138.
- Ansoborlo, E. (2005). *Thermodynamics proposes, kinetics decides, speciation dares: speciation of actinides in biological media*. Paris-11 Univ.
- Barceloux, D. G., & Barceloux, D. (1999). Cobalt. *Journal of Toxicology: Clinical Toxicology*, 37(2), 201-216.
- Barton, I. F., Yang, H., & Barton, M. D. (2014). The mineralogy, geochemistry, and metallurgy of cobalt in the rhombohedral carbonates. *The Canadian Mineralogist*, 52(4), 653-670.
- Batley, G. E., Apte, S. C., & Stauber, J. L. (2004). Speciation and bioavailability of trace metals in water: progress since 1982. *Australian Journal of Chemistry*, 57(10), 903-919.
- Bentzen, E., Taylor, W., & Millard, E. (1992). The importance of dissolved organic phosphorus to phosphorus uptake by limnetic plankton. *Limnology and Oceanography*, 37(2), 217-231.
- Beverkog, B., & Puigdomenech, I. (1996). Revised pourbaix diagrams for iron at 25–300 °C. *Corrosion Science*, 38(12), 2121-2135.
- Beverkog, B., & Puigdomenech, I. (1997). Revised Pourbaix diagrams for nickel at 25–300 °C. *Corrosion Science*, 39(5), 969-980.
- Beverkog, B., & Puigdomenech, I. (1997). Revised pourbaix diagrams for zinc at 25–300 °C. *Corrosion Science*, 39(1), 107-114.
- Boogerd, F., & De Vrind, J. (1987). Manganese oxidation by *Leptothrix discophora*. *Journal of bacteriology*, 169(2), 489-494.

- Boström, B., Persson, G., & Broberg, B. (1988). Bioavailability of different phosphorus forms in freshwater systems. In *Phosphorus in Freshwater Ecosystems* (pp. 133-155). Springer.
- Botebol, H., Lesuisse, E., Šuták, R., Six, C., Lozano, J.-C., Schatt, P., Vergé, V., Kirilovsky, A., Morrissey, J., & Léger, T. J. P. o. t. N. A. o. S. (2015). Central role for ferritin in the day/night regulation of iron homeostasis in marine phytoplankton. *112*(47), 14652-14657.
- Bridges, C. C., & Zalups, R. K. (2005). Molecular and ionic mimicry and the transport of toxic metals. *Toxicology and applied pharmacology*, *204*(3), 274-308.
- Bruce, H. (2009). Coordination Chemistry (Complexation in Solution), *Geology & Geophysics*.
- Bruland, K. W., Rue, E. L., Donat, J. R., Skrabal, S. A., & Moffett, J. W. J. A. C. A. (2000). Intercomparison of voltammetric techniques to determine the chemical speciation of dissolved copper in a coastal seawater sample. *405*(1-2), 99-113.
- Buffle, J., & Leppard, G. G. (1995). Characterization of aquatic colloids and macromolecules. 1. Structure and behavior of colloidal material. *Environmental science & technology*, *29*(9), 2169-2175.
- Burns, N., McIntosh, J., & Scholes, P. (2005). Strategies for Managing the Lakes of the Rotorua District, New Zealand. *Lake and Reservoir Management*, *21*(1), 61-72.
- Burns, N., & Nriagu, J. (1976). Forms of iron and manganese in Lake Erie waters. *Journal of the Fisheries Board of Canada*, *33*(3), 463-470.
- Butterfield, C. N., Soldatova, A. V., Lee, S.-W., Spiro, T. G., & Tebo, B. M. (2013). Mn (II, III) oxidation and MnO<sub>2</sub> mineralization by an expressed bacterial multicopper oxidase. *Proceedings of the National Academy of Sciences*, *110*(29), 11731-11735.
- Camacho, A., Walter, X. A., Picazo, A., & Zopfi, J. (2017). Photoferrotrophy: Remains of an Ancient Photosynthesis in Modern Environments. *Frontiers in microbiology*, *8*, 323-323.
- Cardwell, R. D., Purdy, R., & Bahner, R. C. (1985). *Aquatic toxicology and hazard assessment, seventh symposium: a symposium*. ASTM International.
- Carpenter, S. R., Caraco, N. F., Correll, D. L., Howarth, R. W., Sharpley, A. N., & Smith, V. H. (1998). Nonpoint pollution of surface waters with phosphorus and nitrogen. *Ecological applications*, *8*(3), 559-568.
- Cempel, M., & Nikel, G. (2006). Nickel: a review of its sources and environmental toxicology. *Polish Journal of Environmental Studies*, *15*(3).
- Chapman, M., Green, J., & Jolly, V. (1985). Relationships between zooplankton abundance and trophic state in seven New Zealand lakes. *Hydrobiologia*, *123*(2), 119-136.



- Chaput, D. L., Fowler, A. J., Seo, O., Duhn, K., Hansel, C. M., & Santelli, C. M. (2019). Mn oxide formation by phototrophs: Spatial and temporal patterns, with evidence of an enzymatic superoxide-mediated pathway. *Scientific reports*, 9(1), 1-14.
- Chau, Y., & Kulikovskiy-Cordeiro, O. (1995). Occurrence of nickel in the Canadian environment. *Environmental Reviews*, 3(1), 95-120.
- Chuanwei, Z., Hanjie, W., Yuxu, Z., Yizhang, L., & Rongfei, W. (2015). Isotopic Geochemistry of Cadmium: A Review. *Acta Geologica Sinica - English Edition*, 89(6), 2048-2057.
- Cobalt Institute (Compiler) (2020). *Cobalt is used in a wide variety of applications*. <https://www.cobaltinstitute.org/about-cobalt/cobalt-life-cycle/cobalt-use/>.
- Coman, V., Robotin, B., & Ilea, P. (2013). Nickel recovery/removal from industrial wastes: A review. *Resources, Conservation and Recycling*, 73, 229-238.
- Conway, J. R., Adeleye, A. S., Gardea-Torresdey, J., & Keller, A. A. (2015). Aggregation, Dissolution, and Transformation of Copper Nanoparticles in Natural Waters. *Environmental Science & Technology*, 49(5), 2749-2756.
- Cooke, G. D., Welch, E. B., Peterson, S., & Nichols, S. A. (2016). *Restoration and management of lakes and reservoirs*. CRC press.
- Cross, D. (1963). Soils and geology of some hydrothermal eruptions in the Waiotapu district. *New Zealand Journal of Geology and Geophysics*, 6(1), 70-87.
- Daniel, T., Sharpley, A., Edwards, D., Wedepohl, R., & Lemunyon, J. (1994). Minimizing surface water eutrophication from agriculture by phosphorus management.
- Davison, W. (1993). Iron and manganese in lakes. *Earth-Science Reviews*, 34(2), 119-163.
- de Vicente, I., Huang, P., Andersen, F. Ø., & Jensen, H. S. (2008). Phosphate Adsorption by Fresh and Aged Aluminum Hydroxide. Consequences for Lake Restoration. *Environmental Science & Technology*, 42(17), 6650-6655.
- De Vitre, R. R., & Davison, W. J. R. E. P. V. (2018). Manganese particles in freshwaters. 317.
- Di Toro, D. M., Allen, H. E., Bergman, H. L., Meyer, J. S., Paquin, P. R., & Santore, R. C. (2001). Biotic ligand model of the acute toxicity of metals. 1. Technical basis. *Environmental Toxicology and Chemistry: An International Journal*, 20(10), 2383-2396.
- Dick, G. J., Torpey, J. W., Beveridge, T. J., & Tebo, B. M. (2008). Direct identification of a bacterial manganese (II) oxidase, the multicopper oxidase MnxG, from spores of several different marine Bacillus species. *Applied and Environmental Microbiology*, 74(5), 1527-1534.
- Diem, D., & Stumm, W. (1984). Is dissolved Mn<sup>2+</sup> being oxidized by O<sub>2</sub> in absence of Mn-bacteria or surface catalysts? *Geochimica et Cosmochimica Acta*, 48(7), 1571-1573.
- Dogan, M., Saygideger, S. D., & Colak, U. (2009). Effect of lead toxicity on aquatic macrophyte Elodea canadensis Michx. *Bulletin of environmental contamination and toxicology*, 83(2), 249-254.

- Dorsey, A., & Ingerman, L. (2004). Toxicological profile for copper.
- Duckworth, O. W., Bargar, J. R., Jarzecki, A. A., Oyerinde, O., Spiro, T. G., & Sposito, G. (2009). The exceptionally stable cobalt(III)–desferrioxamine B complex. *Marine Chemistry*, 113(1), 114-122.
- Dzombak, D. A., & Morel, F. M. (1990). *Surface complexation modeling: hydrous ferric oxide*. John Wiley & Sons.
- Edmondson, W. (1970). VOLLENWEIDER, RA 1968. Water management research. Scientific fundamentals of the eutrophication of lakes and flowing waters with particular reference to nitrogen and phosphorus as factors in eutrophication. Organization for Economic Co-operation and Development. Directorate for Scientific Affairs. Paris. *Limnology and Oceanography*, 15(1), 169-170.
- Elderfield, H. J. E., & Letters, P. S. (1970). Chromium speciation in sea water. 9(1), 10-16.
- Emmenegger, L., King, D. W., Sigg, L., Sulzberger, B. J. E. S., & Technology. (1998). Oxidation kinetics of Fe (II) in a eutrophic Swiss lake. 32(19), 2990-2996.
- Emmenegger, L., Schönenberger, R., Sigg, L., & Sulzberger, B. (2001). Light-induced redox cycling of iron in circumneutral lakes. 46(1), 49-61.
- Emsley, J. (2001). Chromium. In *Nature's Building blocks : An A-Z guide to the element* (pp. 495-498). Oxford, England Oxford University press
- Environment, M. f. t. (Compiler) (2007). *Lake water quality in New Zealand: status in 2006 and recent trends 1990–2006, vol 74., New Zealand*. . Wellington.
- Environment, M. f. t. (Compiler) (2020). *Our freshwater 2020 summary*.
- Esteves da Silva, J. C., Machado, A. A., Ramos, M. A., Arce, F., Rey, F. J. E. s., & technology. (1996). Quantitative study of Be (II) complexation by soil fulvic acids by molecular fluorescence spectroscopy. 30(11), 3155-3160.
- European Commission. (2020). *Critical Raw Materials Resilience: Charting a Path towards Greater Security and Sustainability*. . COM 474 Final. 2020. <https://eur-lex.europa.eu/legal-content/EN/TXT/?uri=CELEX:52020DC0474>.
- Fish, G. R. (1970). A limnological study of four lakes near Rotorua. *New Zealand Journal of Marine and Freshwater Research*, 4(2), 165-194.
- Flint, E. (1977). Phytoplankton in seven monomictic lakes near Rotorua, New Zealand. *New Zealand journal of botany*, 15(2), 197-208.
- Ford, R. G., Wilkin, R. T., & Puls, R. W. (2007). *Monitored natural attenuation of inorganic contaminants in ground water*. (Vol. 2). Naional Risk Management Research Laboratory, US Environmental Protection Agency.
- Forsyth, D. J. (1986). Distribution and production of Chironomus in eutrophic Lake Ngapouri. *New Zealand Journal of Marine and Freshwater Research*, 20(1), 47-54.

- Fu, Y., Wang, L., Peng, W., Fan, Q., Li, Q., Dong, Y., Liu, Y., Boczkaj, G., & Wang, Z. (2021). Enabling simultaneous redox transformation of toxic chromium (VI) and arsenic (III) in aqueous media—a review. *Journal of Hazardous Materials*, 417, 126041.
- Geology, L. (Compiler). *Reading: Abundance of elements in Earth's crust*
- Gerdes, P., & Kunst, S. (1998). Bioavailability of phosphorus as a tool for efficient P reduction schemes. *Water Science and Technology*, 37(3), 241-247.
- Gibson, C., Turner, I. J., Roberts, C. J., Lead, J. J. E. s., & technology. (2007). Quantifying the dimensions of nanoscale organic surface layers in natural waters. 41(4), 1339-1344.
- Goldberg, E. D. (1954). Marine geochemistry 1. Chemical scavengers of the sea. *The Journal of Geology*, 62(3), 249-265.
- Gorny, J., Billon, G., Noiriél, C., Dumoulin, D., Lesven, L., & Madé, B. (2016). Chromium behavior in aquatic environments: a review. *Environmental Reviews*, 24(4), 503-516.
- Gouvêa, S., Vieira, A., & Lombardi, A. (2005). Copper and cadmium complexation by high molecular weight materials of dominant microalgae and of water from a eutrophic reservoir. *Chemosphere*, 60(9), 1332-1339.
- Greenwood, N. N., & Earnshaw, A. (2012). *Chemistry of the Elements*. Elsevier.
- Greeson, P. E. (1969). Lake Eutrophication- A Natural process 5(4), 16-30.
- Guertin, J., Jacobs, J. A., & Avakian, C. P. (2004). *Chromium (VI) handbook*. CRC press.
- Gustafsson, J. P. (2007). Visual minteq. <http://www.lwr.kth.se/English/OurSoftware/vminteq/index.htm>.
- Hagendorfer, H., & Goessler, W. J. T. (2008). Separation of chromium (III) and chromium (VI) by ion chromatography and an inductively coupled plasma mass spectrometer as element-selective detector. 76(3), 656-661.
- Haitzer, M., Aiken, G. R., Ryan, J. N. J. E. s., & technology. (2003). Binding of mercury (II) to aquatic humic substances: Influence of pH and source of humic substances. 37(11), 2436-2441.
- Hamilton, D. (2005). Land use impacts on nutrient export in the Central Volcanic Plateau, North Island.
- Hamilton, E. I. (1994). The geobiochemistry of cobalt. *Science of The Total Environment*, 150(1), 7-39.
- Hänsch, R., & Mendel, R. R. (2009). Physiological functions of mineral micronutrients (Cu, Zn, Mn, Fe, Ni, Mo, B, Cl). *Current opinion in plant biology*, 12(3), 259-266.
- Hansell, D. A., & Carlson, C. A. (2014). *Biogeochemistry of marine dissolved organic matter*. Academic Press.

- Harper, D. M. (1992). *Eutrophication of Fresh Waters*. Springer.
- Harris, J. E. (1992). Weathering of rock, corrosion of stone and rusting of iron. *Meccanica*, 27(3), 233-250.
- Hart, B. T. (Compiler) (1982). *Australian water quality criteria for heavy metals*: Australian Government Publishing Service.
- Hartland, A., & Zitoun, R. (2018). Transition metal availability to speleothems controlled by organic binding ligands. *Geochemical Perspective Letters*, 8, 22-25.
- Hartland, A., Zitoun, R., Middag, R., Sander, S., Laferriere, A., Saeed, H., De Luca, S., & Ross, P. M. (2019). Aqueous copper bioavailability linked to shipwreck-contaminated reef sediments. *Scientific Reports*, 9(1), 9573.
- Hedges, J. I., Cowie, G. L., Richey, J. E., Quay, P. D., Benner, R., Strom, M., & Forsberg, B. R. (1994). Origins and processing of organic matter in the Amazon River as indicated by carbohydrates and amino acids. *Limnology and Oceanography*, 39(4), 743-761.
- Helgeson, H., Delany, J., Nesbitt, H. W., & Bird, D. (1978). Summary and Critique of the Thermodynamic Properties of Rock Forming Minerals. *Am J Sci*, 278–A.
- Hernández, I., Niell, F. X., & Whitton, B. A. (2002). Phosphatase activity of benthic marine algae. An overview. *Journal of Applied Phycology*, 14(6), 475-487.
- Hirose, K. (1990). Chemical speciation of trace metals in seawater: Implication of particulate trace metals. *Marine Chemistry*, 28(4), 267-274.
- Holtan, H., Kamp-Nielsen, L., & Stuanes, A. O. (1988). Phosphorus in Soil, Water and Sediment: An Overview. In G. Persson & M. Jansson (Eds.), *Phosphorus in Freshwater Ecosystems* (pp. 19-34). Dordrecht: Springer Netherlands.
- Hongve, D. (1997). Cycling of iron, manganese, and phosphate in a meromictic lake. *Limnology and Oceanography*, 42(4), 635-647.
- Hopwood, M. J., Santana-González, C., Gallego-Urrea, J., Sanchez, N., Achterberg, E. P., Ardelan, M. V., Gledhill, M., González-Dávila, M., Hoffmann, L., Leiknes, Ø., Santana-Casiano, J. M., Tsagaraki, T. M., & Turner, D. (2020). Fe(II) stability in coastal seawater during experiments in Patagonia, Svalbard, and Gran Canaria. *Biogeosciences*, 17(5), 1327-1342.
- Huang, Q.-H., Wang, Z.-J., Wang, D.-H., Wang, C.-X., Ma, M., & Jin, X.-C. (2005). Origins and mobility of phosphorus forms in the sediments of Lakes Taihu and Chaohu, China. *Journal of Environmental Science and Health*, 40(1), 91-102.
- Huber, C., Filella, M., & Town, R. M. (2002). Computer modelling of trace metal ion speciation: practical implementation of a linear continuous function for complexation by natural organic matter. *Computers & geosciences*, 28(5), 587-596.
- Hutchinson, G. E. (1957). A Treatise on. *Limnology*, 1, 243.

- Irving, H., & Williams, R. J. P. (1953). 637. The stability of transition-metal complexes. *Journal of the Chemical Society (Resumed)*(0), 3192-3210.
- Irwin, J. (1968). Observations of temperatures in some Rotorua district lakes. *New Zealand journal of marine and freshwater research*, 2(4), 591-605.
- Jin, X., Rong, N., Zhang, W. Q., Meng, X., & Shan, B. Q. (2019). Bioavailability of organic phosphorus in an eutrophic lake: Insights from an in-situ experiment. *Ecological Indicators*, 107, 6.
- Jolly, V. H. (1968). The comparative limnology of some New Zealand lakes: 1. Physical and chemical. *New Zealand journal of marine and freshwater research*, 2(2), 214-259.
- Jørgensen, L., Stedmon, C. A., Kragh, T., Markager, S., Middelboe, M., & Søndergaard, M. (2011). Global trends in the fluorescence characteristics and distribution of marine dissolved organic matter. *Marine Chemistry*, 126(1), 139-148.
- Kagalou, I., Papastergiadou, E., & Leonardos, I. (2008). Long term changes in the eutrophication process in a shallow Mediterranean lake ecosystem of W. Greece: Response after the reduction of external load. *Journal of environmental management*, 87(3), 497-506.
- Kappler, A., Bryce, C., Mansor, M., Lueder, U., Byrne, J. M., & Swanner, E. D. (2021). An evolving view on biogeochemical cycling of iron. *Nature Reviews Microbiology*, 19(6), 360-374.
- Khan, F. A., & Ansari, A. A. (2005). Eutrophication: An ecological vision. *The Botanical Review*, 71(4), 449-482.
- Khan, M. N., & Mohammad, F. (2014). Eutrophication: challenges and solutions. In *Eutrophication: Causes, consequences and control* (pp. 1-15). Springer.
- Klewicki, J. K., & Morgan, J. J. (1998). Kinetic Behavior of Mn(III) Complexes of Pyrophosphate, EDTA, and Citrate. *Environmental Science & Technology*, 32(19), 2916-2922.
- Kling, G. W., Kipphut, G. W., & Miller, M. C. (1991). Arctic lakes and streams as gas conduits to the atmosphere: implications for tundra carbon budgets. *Science*, 251(4991), 298-301.
- Koukal, B., Gueguen, C., Pardos, M., & Dominik, J. J. C. (2003). Influence of humic substances on the toxic effects of cadmium and zinc to the green alga *Pseudokirchneriella subcapitata*. 53(8), 953-961.
- Krempin, D. W., McGrath, S. M., SooHoo, J. B., & Sullivan, C. W. (1981). Orthophosphate uptake by phytoplankton and bacterioplankton from the Los Angeles Harbor and Southern California coastal waters. *Marine Biology*, 64(1), 23-33.
- Kumar, V., Pandita, S., Sidhu, G. P. S., Sharma, A., Khanna, K., Kaur, P., Bali, A. S., & Setia, R. J. C. (2020). Copper bioavailability, uptake, toxicity and tolerance in plants: A comprehensive review. 127810.

- Langard, S., & Costa, M. A. X. (2007). Chapter 24 - Chromium. In G. F. Nordberg, *et al.* (Eds.), *Handbook on the Toxicology of Metals (Third Edition)* (pp. 487-510). Burlington: Academic Press.
- Langer, R. H. M. (1990). *Pastures, their ecology and management*. Oxford University Press.
- Laxen, D. P. (1985). Trace metal adsorption/coprecipitation on hydrous ferric oxide under realistic conditions: the role of humic substances. *Water Research*, 19(10), 1229-1236.
- Laxen, D. P., & Harrison, R. M. (1981). A scheme for the physico-chemical speciation of trace metals in freshwater samples. *Science of the Total Environment*, 19(1), 59-82.
- Lead, J., & Wilkinson, K. (2006). Aquatic Colloids and Nanoparticles: Current Knowledge and Future Trends. *Environmental Chemistry - ENVIRON CHEM*, 3.
- Lean, D. (1973). Phosphorus dynamics in lake water. *Science*, 179(4074), 678-680.
- Lee, G. F., Rast, W., & Jones, R. A. (1978). Water Report: Eutrophication of water bodies: Insights for an age old problem. *Environmental Science & Technology*, 12(8), 900-908.
- Leenheer, J. A., & Croué, J.-P. (Compiler) (2003). *Peer reviewed: characterizing aquatic dissolved organic matter*: ACS Publications.
- Lijklema, L. (1980). Interaction of orthophosphate with iron(III) and aluminum hydroxides. *Environmental Science & Technology*, 14(5), 537-541.
- Liu, G., & Cai, Y. J. C. (2010). Complexation of arsenite with dissolved organic matter: Conditional distribution coefficients and apparent stability constants. 81(7), 890-896.
- Liu, J.-F., Zhao, Z.-S., & Jiang, G.-B. (2008). Coating Fe<sub>3</sub>O<sub>4</sub> magnetic nanoparticles with humic acid for high efficient removal of heavy metals in water. *Environmental Science & Technology*, 42(18), 6949-6954.
- Liyang, W., Fengchang, W., Zhang, R., Wen, L., & Haiqing, L. J. J. o. E. S. (2009). Characterization of dissolved organic matter fractions from Lake Hongfeng, Southwestern China Plateau. 21(5), 581-588.
- Luoma, S. N., & Rainbow, P. S. (2005). Why is metal bioaccumulation so variable? Biodynamics as a unifying concept. *Environmental Science & Technology*, 39(7), 1921-1931.
- MacLeod, C. J., & Moller, H. (2006). Intensification and diversification of New Zealand agriculture since 1960: An evaluation of current indicators of land use change. *Agriculture, Ecosystems & Environment*, 115(1), 201-218.
- Manasypov, R. M., Loiko, S. V., Kritskov, I., Shirokova, L. S., Shevchenko, V. P., Kirpotin, S. N., Kulizhsky, S. P., Kolesnichenko, L. G., Zemtsov, V. A., & Vorobyev, S. N. (2015). Seasonal dynamics of organic carbon and metals in thermokarst lakes from the discontinuous permafrost zone of western Siberia.

- Masliy, A. N., Shapnik, M.S. and Kuznetsov, A.M. (2000). Quantum-chemical investigation of electrochemical processes. Part I. Investigation of the mechanism of Zn(II) complex electroreduction from alkaline water solutions. Quantumchemical simulation, chemistry and computational simulation  
*Butlerov Communication*, 3, 1 – 6.
- McColl, R. H. S. (1972). Chemistry and trophic status of seven New Zealand lakes. *New Zealand Journal of Marine and Freshwater Research*, 6(4), 399-447.
- McLaughlin, M. J., & Singh, B. R. (1999). Cadmium in Soils and Plants. In M. J. McLaughlin & B. R. Singh (Eds.), *Cadmium in Soils and Plants* (pp. 1-9). Dordrecht: Springer Netherlands.
- McPhail, D., Summerhayes, E., Welch, S., Brugger, J., & Roach, I. J. A. i. r. (2003). The geochemistry and mobility of zinc in the regolith. 287-291.
- Means, J. L., Crerar, D. A., Borcsik, M. P., & Duguid, J. O. (1978). Adsorption of Co and selected actinides by Mn and Fe oxides in soils and sediments. *Geochimica et Cosmochimica Acta*, 42(12), 1763-1773.
- Memmert, U. (1987). Bioaccumulation of zinc in two freshwater organisms (*Daphnia magna*, crustacea and *Brachydanio rerio*, pisces). *Water Research*, 21(1), 99-106.
- Midorikawa, T., & Tanoue, E. (1994). Detection of a strong ligand for copper in sea water and determination of its stability constant. *Analytica chimica acta*, 284(3), 605-619.
- Mikutta, C., Kretzschmar, R. J. E. s., & technology. (2011). Spectroscopic evidence for ternary complex formation between arsenate and ferric iron complexes of humic substances. 45(22), 9550-9557.
- Miyata, N., Tani, Y., Maruo, K., Tsuno, H., Sakata, M., & Iwahori, K. (2006). Manganese (IV) oxide production by *Acremonium* sp. strain KR21-2 and extracellular Mn (II) oxidase activity. *Applied and Environmental Microbiology*, 72(10), 6467-6473.
- Moffett, J. W., & Zika, R. G. (1987). Photochemistry of Copper Complexes in Sea Water. In *Photochemistry of Environmental Aquatic Systems* (Chapter 9, pp. 116-130). American Chemical Society.
- Molot, L. A., & Dillon, P. J. (2003). Variation in iron, aluminum and dissolved organic carbon mass transfer coefficients in lakes. *Water Research*, 37(8), 1759-1768.
- Montenegro, A. C., Ferreyroa, G. V., Parolo, M. E., Tudino, M. B., Lavado, R. S., Molina, F. V. J. W., Air,, & Pollution, S. (2015). Copper speciation in soil: time evolution and effect of clay amendment. 226(9), 293.
- Moore, M. R. (1997). *Copper : report of an international meeting, 20-21 June 1996, Brisbane / edited by Michael R. Moore ... [et al.]*. National Environmental Health Forum monographs. Metal series ; no. 3. [Adelaide]: South Australian Health Commission for the National Environmental Health Forum.

- Moos, S. B., Boyle, E. A., Altabet, M. A., & Bourbonnais, A. (2020). Investigating the cycling of chromium in the oxygen deficient waters of the Eastern Tropical North Pacific Ocean and the Santa Barbara Basin using stable isotopes. *Marine Chemistry*, 221, 103756.
- Morel, F., & Morel-Laurens, N. (1983). Trace metals and plankton in the oceans: facts and speculations. In *Trace metals in sea water* (pp. 841-869). Springer.
- Morgan, J. J. (2000). Manganese in natural waters and earth's crust: Its availability to organisms. In *Metal ions in biological systems* (Vol. 37, pp. 1-34).
- Mortimer, C. H. (1971). Chemical exchanges between sediments and water in the great lakes-speculations on probable regulatory mechanisms 1. *Limnology and Oceanography*, 16(2), 387-404.
- Mosello, R., de Bernadi, R., & Ravera, O. (2011). Richard A. Vollenweider: contribution to our knowledge of Italian lakes. *Aquatic Ecosystem Health & Management*, 14(2), 174-178.
- Myers, C. R., & Nealson, K. H. J. S. (1988). Bacterial manganese reduction and growth with manganese oxide as the sole electron acceptor. *240*(4857), 1319-1321.
- Nagata, T. (2000). Production mechanisms of dissolved organic matter. *Microbial ecology of the oceans*. 121-152.
- National Research Council, U. (2003). *Bioavailability of contaminants in soils and sediments: processes, tools, and applications*. National Academies Press.
- Nico, P. S., Anastasio, C., & Zasoski, R. J. (2002). Rapid photo-oxidation of Mn (II) mediated by humic substances. *Geochimica et Cosmochimica Acta*, 66(23), 4047-4056.
- Novotnik, B., Zorz, J., Bryant, S., & Strous, M. J. F. i. m. (2019). The effect of dissimilatory manganese reduction on lactate fermentation and microbial community assembly. *10*, 1007.
- O'Connor, K. (1982). The implications of past exploitation and current developments to the conservation of South Island tussock grasslands. *New Zealand journal of ecology*, 5, 97-107.
- Painter, S., Cameron, E. M., Allan, R., & Rouse, J. (1994). Reconnaissance geochemistry and its environmental relevance. *Journal of Geochemical Exploration*, 51(3), 213-246.
- Pan, J., Plant, J. A., Voulvoulis, N., Oates, C. J., & Ihlenfeld, C. (2010). Cadmium levels in Europe: implications for human health. *Environ Geochem Health*, 32(1), 1-12.
- Papazotos, P., Vasileiou, E., & Perraki, M. (2019). *Chromium-manganese redox couple resulting in elevated Cr6+ concentration in groundwater of the Psachna basin, Central Euboea, Greece*. Presented at the 15th International Congress of the Geological Society of Greece.
- Parkhurst, D. L., & Appelo, C. A. J. (2013). *Description of input and examples for PHREEQC version 3: a computer program for speciation, batch-reaction, one-dimensional*



*transport, and inverse geochemical calculations*. Reston, VA. 519p.  
<http://pubs.er.usgs.gov/publication/tm6A43>.

- Pearson, L. K., Hendy, C. H., & Hamilton, D. P. (2016). Dynamics of silicon in lakes of the Taupo Volcanic Zone, New Zealand, and implications for diatom growth. *Inland Waters*, 6(2), 185-198.
- Peng, C., Bryce, C., Sundman, A., & Kappler, A. (2019). Cryptic Cycling of Complexes Containing Fe(III) and Organic Matter by Phototrophic Fe(II)-Oxidizing Bacteria. 85(8), e02826-18.
- Pesavento, M., Alberti, G., & Biesuz, R. (2009). Analytical methods for determination of free metal ion concentration, labile species fraction and metal complexation capacity of environmental waters: a review. *Analytica Chimica Acta*, 631(2), 129-141.
- Playle, R. C., Dixon, D. G., Burnison, K. J. C. J. o. F., & Sciences, A. (1993). Copper and cadmium binding to fish gills: estimates of metal–gill stability constants and modelling of metal accumulation. 50(12), 2678-2687.
- Pokrovsky, O., Shirokova, L., Zabelina, S., Vorobieva, T. Y., Moreva, O. Y., Klimov, S., Chupakov, A., Shorina, N., Kokryatskaya, N., & Audry, S. (2012). Size fractionation of trace elements in a seasonally stratified boreal lake: control of organic matter and iron colloids. *Aquatic Geochemistry*, 18(2), 115-139.
- Pokrovsky, O. S., & Shirokova, L. S. (2013). Diurnal variations of dissolved and colloidal organic carbon and trace metals in a boreal lake during summer bloom. *Water research*, 47(2), 922-932.
- Porter, F. C. (1991). *Zinc handbook: properties, processing, and use in design*. Crc Press.
- Portielje, R., & Van der Molen, D. (1999). Relationships between eutrophication variables: from nutrient loading to transparency. In *Shallow Lakes' 98* (pp. 375-387). Springer.
- Post, J. E. (1999). Manganese oxide minerals: Crystal structures and economic and environmental significance. *Proceedings of the National Academy of Sciences*, 96(7), 3447-3454.
- Qin, F., Shan, X.-q., & Wei, B. (2004). Effects of low-molecular-weight organic acids and residence time on desorption of Cu, Cd, and Pb from soils. *Chemosphere*, 57(4), 253-263.
- Qin, B., Yang, L., Chen, F., Zhu, G., Zhang, L., & Chen, Y. (2006). Mechanism and control of lake eutrophication. *Chinese Science Bulletin*, 51(19), 2401-2412.
- Rai, D., Eary, L. E., & Zachara, J. M. (1989). Environmental chemistry of chromium. *Science of The Total Environment*, 86(1), 15-23.
- Rakhunde, R., Deshpande, L., & Juneja, H. D. (2012). Chemical Speciation of Chromium in Water: A Review. *Critical Reviews in Environmental Science and Technology*, 42(7), 776-810.

- Rast, W., & Thornton, J. A. (1996). Trends in eutrophication research and control. *Hydrological processes*, 10(2), 295-313.
- Reddy, K. R., & DeLaune, R. D. (2008). *Biogeochemistry of wetlands: science and applications*. CRC press.
- Reiller, P. E., & Brevet, J. (2010). Bi-exponential decay of Eu (III) complexed by Suwannee River humic substances: spectroscopic evidence of two different excited species. *J Spectrochimica Acta Part A: Molecular Biomolecular Spectroscopy*, 75(2), 629-636.
- Richard, F. C., & Bourg, A. C. M. (1991). Aqueous geochemistry of chromium: A review. *Water Research*, 25(7), 807-816.
- Robertson, D. M., Goddard, G. L., Helsel, D. R., & MacKinnon, K. L. (2000). Rehabilitation of Delavan Lake, Wisconsin. *Lake and Reservoir Management*, 16(3), 155-176.
- Roelofs, J., & Cals, M. (1989). Effecten van de inlaat van gebiedsvreemd water op de waterkwaliteit en vegetatie-ontwikkeling in laag-en hoogveenplassen. In *Proceedings Symposium Gebiedsvreemd water: Omvang en effecten op ecosystemen* (pp. 72-86).
- Rose, A. L., & Waite, T. D. J. M. c. (2003). Kinetics of iron complexation by dissolved natural organic matter in coastal waters. *84*(1-2), 85-103.
- Rowe, D. K. (1984). Factors affecting the foods and feeding patterns of lake-dwelling rainbow trout (*Salmo gairdnerii*) in the North Island of New Zealand. *New Zealand journal of marine and freshwater research*, 18(2), 129-141.
- Rue, E. L., Smith, G. J., Cutter, G. A., & Bruland, K. W. (1997). The response of trace element redox couples to suboxic conditions in the water column. *Deep Sea Research Part I: Oceanographic Research Papers*, 44(1), 113-134.
- Ruttenberg, K. (2003). The global phosphorus cycle. *TrGeo*, 8, 682.
- Saeed, H., Hartland, A., Lehto, N., Baalousha, M., Sikder, M., Sandwell, D., Mucalo, M., & Hamilton, D. P. (2018). Regulation of phosphorus bioavailability by iron nanoparticles in a monomictic lake. *Scientific Reports*, 8(1), 1-14.
- Scharler, U. M., Ulanowicz, R. E., Fogel, M. L., Wooller, M. J., Jacobson-Meyers, M. E., Lovelock, C. E., Feller, I. C., Frischer, M., Lee, R., McKee, K. L., Romero, I. C., Schmit, J. P., & Shearer, C. (2015). Variable nutrient stoichiometry (carbon:nitrogen:phosphorus) across trophic levels determines community and ecosystem properties in an oligotrophic mangrove system. *Oecologia*, 179(3), 863-876.
- Schindler, D. W. (1977). Evolution of phosphorus limitation in lakes. *Science*, 195(4275), 260-2.
- Schindler, D. W., Hecky, R. E., Findlay, D. L., Stainton, M. P., Parker, B. R., Paterson, M. J., Beaty, K. G., Lyng, M., & Kasian, S. E. M. (2008). Eutrophication of lakes cannot be controlled by reducing nitrogen input: Results of a 37-year whole-ecosystem experiment. *105*(32), 11254-11258.

- Schoffman, H., Lis, H., Shaked, Y., & Keren, N. J. F. i. p. s. (2016). Iron–nutrient interactions within phytoplankton. *7*, 1223.
- Schroeder, D. C., & Lee, G. F. (1975). Potential transformations of chromium in natural waters. *Water, Air, and Soil Pollution*, *4*(3), 355-365.
- Shaked, Y., Erel, Y., & Sukenik, A. J. G. e. C. A. (2004). The biogeochemical cycle of iron and associated elements in Lake Kinneret. *68*(7), 1439-1451.
- Shcherbina, N. S., Perminova, I. V., Kalmykov, S. N., Kovalenko, A. N., Haire, R. G., Novikov, A. P. J. E. s., & technology. (2007). Redox and complexation interactions of neptunium (V) with quinonoid-enriched humic derivatives. *41*(20), 7010-7015.
- Sherman, D. (2001). Quantum Chemistry and Classical Simulations of Metal Complexes in Aqueous Solutions. *Reviews in Mineralogy and Geochemistry*, *42*, 273-317.
- Sherman, D. M. (2005). Electronic structures of iron (III) and manganese (IV)(hydr) oxide minerals: Thermodynamics of photochemical reductive dissolution in aquatic environments. *Geochimica et Cosmochimica Acta*, *69*(13), 3249-3255.
- Shi, Z., Shao, L., Jones, T. P., & Lu, S. J. J. o. G. R. A. (2005). Microscopy and mineralogy of airborne particles collected during severe dust storm episodes in Beijing, China. *110*(D1).
- Shigematsu, I. (1984). The epidemiological approach to cadmium pollution in Japan. *Ann Acad Med Singap*, *13*(2), 231-6.
- Shin, H.-S., Hong, K.-H., Lee, M.-H., Cho, Y.-H., & Lee, C.-W. J. T. (2001). Fluorescence quenching of three molecular weight fractions of a soil fulvic acid by UO<sub>2</sub> (II). *53*(4), 791-799.
- Simpson, W. R. (1981). A critical review of Cadmium in the Marine environment. *Progress in Oceanography*, *10*(1), 1-70.
- Smith, R. M., & Martell, A. E. (1976). *Critical stability constants: inorganic complexes*. (Vol. 4). Springer.
- Smith, V. H., & Schindler, D. W. (2009). Eutrophication science: where do we go from here? *Trends in ecology & evolution*, *24*(4), 201-207.
- Smith, V. H., Wood, S. A., McBride, C. G., Atalah, J., Hamilton, D. P., & Abell, J. (2016). Phosphorus and nitrogen loading restraints are essential for successful eutrophication control of Lake Rotorua, New Zealand. *Inland Waters*, *6*(2), 273-283.
- Soendergaard, M., Jensen, J. P., & Jeppesen, E. (2005). Seasonal response of nutrients to reduced phosphorus loading in 12 Danish lakes. *Freshwater Biology*, *50*(10), 1605-1615.
- Sondergaard, M., Jensen, J. P., & Jeppesen, E. (2003). Role of sediment and internal loading of phosphorus in shallow lakes [recurso electrónico].

- Sonke, J. E., & Salters, V. J. J. G. e. C. A. (2006). Lanthanide–humic substances complexation. I. Experimental evidence for a lanthanide contraction effect. *70*(6), 1495-1506.
- Sparks, D. L. (2003). *Environmental soil chemistry*. Elsevier.
- Spencer, R. G., Baker, A., Ahad, J. M., Cowie, G. L., Ganeshram, R., Upstill-Goddard, R. C., & Uher, G. J. S. o. t. T. E. (2007). Discriminatory classification of natural and anthropogenic waters in two UK estuaries. *373*(1), 305-323.
- Sterner, R. W., & Elser, J. J. (2002). *Ecological stoichiometry: the biology of elements from molecules to the biosphere*. Princeton university press.
- Stumm, W., & Wollast, R. (1990). Coordination chemistry of weathering: Kinetics of the surface-controlled dissolution of oxide minerals. *Reviews of Geophysics*, *28*(1), 53-69.
- Stumm, W. a., & Morgan, J. J. (1996). *Aquatic Chemistry (3rd edition)*. Wiley Interscience, New York.
- Sulzberger, B., Suter, D., Siffert, C., Banwart, S., & Stumm, W. J. M. C. (1989). Dissolution of Fe (III)(hydr) oxides in natural waters; laboratory assessment on the kinetics controlled by surface coordination. *28*(1-3), 127-144.
- Sunda, W. G. (1989). Trace metal interactions with marine phytoplankton. *Biological Oceanography*, *6*(5-6), 411-442.
- Sung, W., J. J. Morgan. (1981). Oxidative re- moval of Mn(II) from solution by the  $\alpha$ -FeOOH (lepidocrocite) surface. *Geochimica et Cosmochimica Acta*, *45*, 2377-2383.
- Suren, A. M., & McMurtrie, S. (2005). Assessing the effectiveness of enhancement activities in urban streams: II. Responses of invertebrate communities. *River research and Applications*, *21*(4), 439-453.
- Świetlik, R. (1998). Speciation analysis of chromium in waters. *Polish Journal of Environmental Studies*, *7*(5), 257-266.
- Taylor, S. R. (1964). Abundance of chemical elements in the continental crust: a new table. *Geochimica et Cosmochimica Acta*, *28*(8), 1273-1285.
- Templeton, D. M., Ariese, F., Cornelis, R., Danielsson, L.-G., Muntau, H., van Leeuwen, H. P., & Lobinski, R. (2000). Guidelines for terms related to chemical speciation and fractionation of elements. Definitions, structural aspects, and methodological approaches (IUPAC Recommendations 2000). *Pure and applied chemistry*, *72*(8), 1453-1470.
- Tessier, A., & Turner, D. R. (1995). *Metal speciation and bioavailability in aquatic systems*. Wiley Chichester.
- Tett, P., Heaney, S., & Droop, M. (1985). The Redfield ratio and phytoplankton growth rate. *Journal of the Marine Biological Association of the United Kingdom*. Plymouth, *65*(2), 487-504.

- Theis, T. L., & Richter, R. O. (1980). Adsorption Reactions of Nickel Species at Oxide Surfaces. In *Particulates in Water* (Chapter 4, pp. 73-96). AMERICAN CHEMICAL SOCIETY.
- Thurman, E. M. (2012). *Organic geochemistry of natural waters*. (Vol. 2). Springer Science & Business Media.
- Tilman, D., Kilham, S. S., & Kilham, P. (1982). Phytoplankton community ecology: the role of limiting nutrients. *Annual review of Ecology and Systematics*, 13(1), 349-372.
- Tipping, E., Rey-Castro, C., Bryan, S. E., & Hamilton-Taylor, J. (2002). Al (III) and Fe (III) binding by humic substances in freshwaters, and implications for trace metal speciation. *Geochimica et Cosmochimica Acta*, 66(18), 3211-3224.
- Tipping, E., Thompson, D., & Davison, W. (1984). Oxidation products of Mn (II) in lake waters. *Chemical Geology*, 44(4), 359-383.
- Turner, D., Whitfield, M., & Dickson, A. (1981). The equilibrium speciation of dissolved components in freshwater and sea water at 25 C and 1 atm pressure. *Geochimica et Cosmochimica Acta*, 45(6), 855-881
- Tortell, P. D., Maldonado, M. T., Granger, J., & Price, N. M. J. F. M. E. (1999). Marine bacteria and biogeochemical cycling of iron in the oceans. 29(1), 1-11.
- van Leeuwen, H. P. (1999). Metal Speciation Dynamics and Bioavailability: Inert and Labile Complexes. *Environmental Science & Technology*, 33(21), 3743-3748.
- Wang, M., Xu, X., Wu, Z., Zhang, X., Sun, P., Wen, Y., Wang, Z., Lu, X., Zhang, W., Wang, X. J. E. S., & Technology. (2019). Seasonal Pattern of Nutrient Limitation in a Eutrophic Lake and Quantitative Analysis of the Impacts from Internal Nutrient Cycling. 53(23), 13675-13686.
- Wang, X., Chen, X., Liu, S., & Ge, X. (2010). Effect of molecular weight of dissolved organic matter on toxicity and bioavailability of copper to lettuce. *Journal of Environmental Sciences*, 22(12), 1960-1965.
- Wazer, J. R. V. (1950). Structure and properties of the condensed phosphates. III. Solubility fractionation and other solubility studies. *Journal of the American Chemical Society*, 72(2), 647-655.
- Weaver, R. M., & Hochella Jr, M. F. (2003). The reactivity of seven Mn-oxides with Cr<sup>3+</sup> aq: A comparative analysis of a complex, environmentally important redox reaction. *American Mineralogist*, 88(11-12), 2016-2027
- Weber, K. (1907). *Aufbau und vegetation der Moore Norddeutschlands*.
- Welch, E. B., & Cooke, G. D. (1999). Effectiveness and Longevity of Phosphorus Inactivation with Alum. *Lake and Reservoir Management*, 15(1), 5-27.
- White, E. (1983). Lake eutrophication in New Zealand—a comparison with other countries of the organisation for economic co-operation and development. *New Zealand journal of marine and freshwater research*, 17(4), 437-444.

- Willey, J. D., Inscore, M. T., Kieber, R. J., & Skrabal, S. A. J. J. o. a. c. (2009). Manganese in coastal rainwater: speciation, photochemistry and deposition to seawater. *62*(1), 31-43.
- Winchester, J. W., & Nifong, G. D. (1971). Water pollution in Lake Michigan by trace elements from pollution aerosol fallout. *Water, Air, and Soil Pollution*, *1*(1), 50-64.
- Woods, R., Yoon, R., & Young, C. (1987). Eh-pH diagrams for stable and metastable phases in the copper-sulfur-water system. *International journal of mineral processing*, *20*(1-2), 109-120.
- hait, F., Evans, D., Dillon, P., & Schiff, S. J. J. o. A. A. S. (2004). Molecular size distribution characteristics of the metal-DOM complexes in stream waters by high-performance size-exclusion chromatography (HPSEC) and high-resolution inductively coupled plasma mass spectrometry (ICP-MS). *19*(8), 979-983.
- Wu, F. C., Evans, R. D., & Dillon, P. J. (2002). High-performance liquid chromatographic fractionation and characterization of fulvic acid. *Analytica Chimica Acta*, *464*(1), 47-55.
- Wu, F., Evans, R., & Dillon, P. J. A. C. A. (2002b). Fractionation and characterization of fulvic acid by immobilized metal ion affinity chromatography. *452*(1), 85-93.
- Wu, F., & Tanoue, E. J. O. G. (2001). Molecular mass distribution and fluorescence characteristics of dissolved organic ligands for copper (II) in Lake Biwa, Japan. *32*(1), 11-20.
- Wu, Z., Liu, Y., Liang, Z., Wu, S., & Guo, H. (2017a). Internal cycling, not external loading, decides the nutrient limitation in eutrophic lake: A dynamic model with temporal Bayesian hierarchical inference. *Water Research*, *116*, 231-240.
- Wu, Z., Liu, Y., Liang, Z., Wu, S., & Guo, H. J. W. r. (2017b). Internal cycling, not external loading, decides the nutrient limitation in eutrophic lake: A dynamic model with temporal Bayesian hierarchical inference. *116*, 231-240.
- Xue, H., & Sigg, L. (1993). Free cupric ion concentration and Cu (II) speciation in a eutrophic lake. *Limnology and Oceanography*, *38*(6), 1200-1213.

## Chapter 3

# Regulation of phosphorus bioavailability by iron nanoparticles in a monomictic lake

---

Published as

Saeed, H., Hartland, A., Lehto, N. J., Baalousha, M., Sikder, M., Sandwell, D., Mucalo, M., & Hamilton, D. P. (2018). Regulation of phosphorus bioavailability by iron nanoparticles in a monomictic lake. *Scientific Reports*, 8(1), 17736.

# SCIENTIFIC REPORTS

OPEN

## Regulation of phosphorus bioavailability by iron nanoparticles in a monomictic lake

H. Saeed<sup>1</sup>, A. Hartland<sup>1</sup>, N. J. Lehto<sup>2</sup>, M. Baalousha<sup>3</sup>, M. Sikder<sup>3</sup>, D. Sandwell<sup>1</sup>, M. Mucalo<sup>4</sup> & D. P. Hamilton<sup>5</sup>

Dissolved reactive phosphorous (DRP) in lake systems is conventionally considered to predominate over other dissolved P species, however, this view neglects an important set of interactions that occurs between P and reactive iron hydroxide surfaces. This study addresses the coupling of P with dispersed iron nanoparticles in lakes, an interaction that may fundamentally alter the bioavailability of P to phytoplankton. We used diffusive gradients in thin films (DGT) and ultrafiltration to study Fe-P coupling in the water column of a monomictic lake over a hydrological year. Fe and P were predominantly colloidal (particle diameters  $> \sim 5 \text{ nm} < \sim 20 \text{ nm}$ ) in both oxic epilimnetic and anaerobic hypolimnetic waters, but they were both DGT-labile under sub-oxic conditions, consistent with diffusion and dissolution of Fe-and-P-bearing colloids within the DGT diffusive gel. During peak stratification, increases in Fe and P bioavailability were spatially and temporally coincident with Fe nanoparticle dissolution and the formation of a deep chlorophyll maximum at 5–8 m depth. These results provide a window into the coupling and decoupling of P with mobile iron colloids, with implications for our understanding of the behaviour of nutrients and their influence on phytoplankton community dynamics.

Phosphorus (P) and nitrogen (N) play a central role in the biological productivity of aquatic systems<sup>1–3</sup>. In freshwaters, dissolved inorganic N and P act as limiting nutrients depending on their molar ratios<sup>4</sup>, but it is usually P that limits the productivity of terrestrial aquatic systems.

Excess P availability occurs primarily through human actions<sup>2,5</sup>, with the widespread use of P fertiliser, poor riparian buffering and uncontrolled sedimentation being major drivers<sup>5,6</sup>. Despite regulation of anthropogenic P inputs, the biogeochemical cycling of P between lake water columns and sediments typically maintains high P availability to phytoplankton<sup>7</sup>.

Phosphorus is present in a range of inorganic and organic species across the dissolved, colloidal and particulate size ranges<sup>8</sup>. Organic P constitutes a major part of the dissolved P pool<sup>9</sup>, while particulate ( $> 1 \mu\text{m}$ ) and colloidal (1–1000 nm) fractions (from plant, animal and bacterial sources) can be present as poly-phosphates adsorbed to metal oxides, hydroxides and clays<sup>10–12</sup>.

Bioavailable P is usually the sum of the P species that are immediately available for biological uptake, or species that are easily transformed into available form(s) by naturally occurring processes<sup>13–15</sup>. Thus, the bioavailable P fraction is a moving target subject to biological, chemical and physical processes that vary through time in lakes and which requires cautious monitoring to be meaningfully estimated.

During lake stratification events, organic matter (OM) is supplied to the hypolimnion through settling of suspended particulates, or bioturbation in the upper few mm of the sediment<sup>13,16</sup> or turbulent mixing across the thermocline<sup>17,18</sup>. To-date, two distinct phenomena have been proposed to explain the observed P fluxes from benthic sediments, (1) elevated pH (resulting from algal photosynthesis) favours the desorption of  $\text{PO}_4^{3-}$  from sediment solids<sup>19,20</sup> and (2) reductive dissolution of Iron(III) species at the onset of anaerobic conditions<sup>17</sup>. The

<sup>1</sup>Environmental Research institute, School of Science, Faculty of Science and Engineering, University of Waikato, Hamilton, Waikato, New Zealand. <sup>2</sup>Department of Soil and Physical Sciences, Faculty of Agriculture and Life Sciences, Lincoln University, Lincoln, New Zealand. <sup>3</sup>Center for Environmental Nanoscience and Risk, Department of Environmental Health Sciences, University of South Carolina, Columbia, SC, United States. <sup>4</sup>Chemistry, Faculty of Science and Engineering, University of Waikato, Hamilton, Waikato, New Zealand. <sup>5</sup>Australian Rivers Institute, Griffith University, Griffith, Australia. Correspondence and requests for materials should be addressed to A.H. (email: [adam.hartland@waikato.ac.nz](mailto:adam.hartland@waikato.ac.nz))



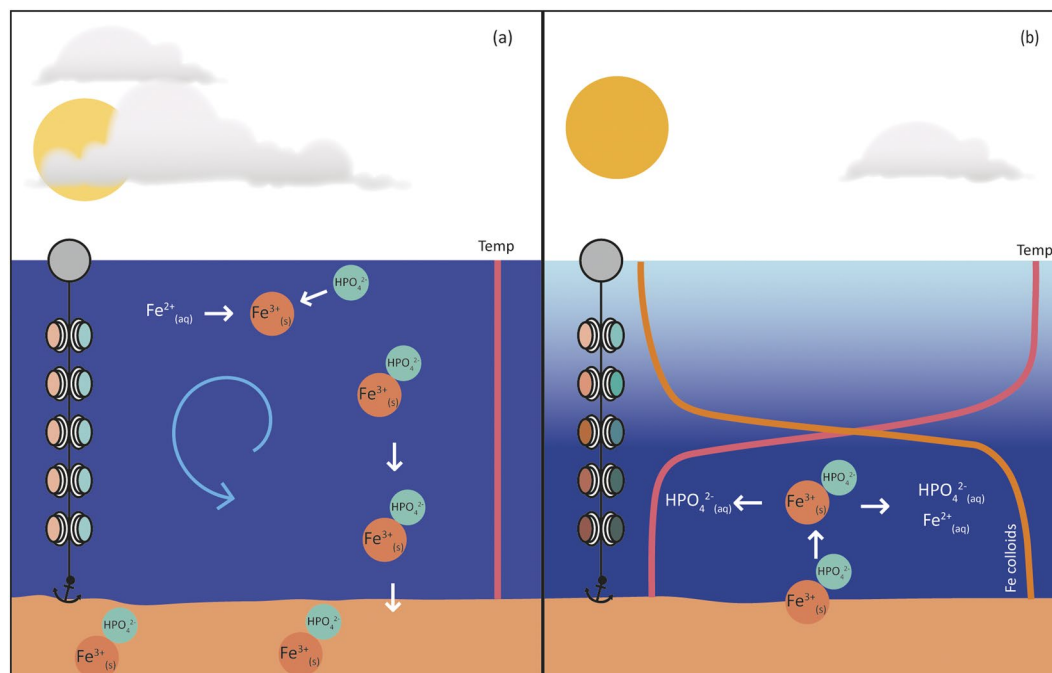


**Figure 1.** Conceptual figure summarising the biogeochemical cycling of iron (Fe) and phosphorus (P) in Lake Ngapouri, with DGT probes arrayed through the water column to detect changes in labile Fe and P concentration. In (a) oxidation of  $\text{Fe}^{2+}$  and co-precipitation of  $\text{Fe}^{3+}$  and P (and/or P adsorption on Fe hydroxide colloids) occurs during isothermal winter conditions, leading to Fe and P sedimentation and uniformly low dissolved Fe and P concentrations through the water column. In (b) the release of Fe colloids in the deep hypolimnion during summer stratified conditions is depicted (right and left arrows show products of reductive dissolution of Fe colloids and P desorption, respectively).

mineralisation of OM consumes oxygen and creates steep redox gradients between iron species present in sediments and water column. These gradients are expected to affect the distribution and bioavailability of P because of well-documented interactions between dissolved inorganic phosphorus (DIP) and Fe hydroxide surfaces<sup>21,22</sup>.

Iron oxide colloids often form by hydrolysis and oxidation of Fe(II) at oxic/anoxic boundaries in lakes<sup>17,23</sup>. Differences in the surface properties of ferrous ( $\text{Fe}(\text{OH})_2$ ) and ferric ( $\text{Fe}(\text{OH})_3$ ) colloids are likely to be significant for P binding<sup>24</sup>. The size, structure, and reactivity of this hydrolysis product can vary, e.g., because of natural organic matter coatings<sup>25,26</sup>. Previous studies of other freshwater ecosystems have reported mobile Fe colloids to be in the size range of 0.05 to 0.5  $\mu\text{m}$ <sup>27–31</sup>. Such Fe colloids have been shown to be stable in sub-oxic conditions<sup>32,33</sup> and can therefore potentially survive for extended periods under anaerobic conditions, with concomitant effects on solution chemistry. Hence, aquatic colloids can be rich in both P-binding surfaces and organic matter (the latter containing a significant amount of organic P)<sup>34</sup>.

Distinct from gravitoids (large particles  $>10\mu\text{m}$ <sup>27</sup>, colloids (1–1000 nm) and nanoparticles (1–100 nm) remain suspended for extended periods and thus provide surface sites for adsorption or other chemical reactions within the water column<sup>10</sup>. When present within the lake water column, these dispersed surfaces have the potential to significantly modify P bioavailability to phytoplankton (Fig. 1). While the coupled release of Fe and P has been previously demonstrated in lake sediments<sup>35,36</sup> the significance of Fe colloids for P bioavailability has yet to be elucidated in these systems.

The dearth of studies on the interaction between P and colloids in lakes can be explained by inherent difficulties associated with probing colloidal interactions in such sub-oxic (reduced) domains. This study seeks to address the lack of information on colloidal Fe-P interactions under reduced conditions, and the absence of highly spatially- and temporally-resolved data on P speciation in lake systems in general, by combining sensitive and representative measures of *in-situ* water column chemistry based on diffusive gradients in thin films (DGT) and ultrafiltration methods.

The use of diffusive gradients in thin films (DGT) has gained recognition as an alternative approach for rapid evaluation of labile metal/nutrient content in water and sediments. DGT solution probes are small plastic devices containing a filter membrane, ion permeable hydrogel and a binding agent incorporated in a basal gel layer. When immersed in solution, the solutes pass through the hydrogel of known thickness ( $\Delta g$ ), also referred as diffusive layer/gel, and accumulate at the binding gel layer. Dissolved species concentrations are then determined by using Fick's first law of diffusion from measured mass (M) over deployment time (t)<sup>37</sup>. These devices formed the principle means by which the biogeochemical dynamics of Fe and P in Lake Ngapouri were deduced. For further information on the use of DGT for evaluating bioavailability we refer readers to Zhang & Davison<sup>38,39</sup> and Zhang *et al.*<sup>40</sup>.

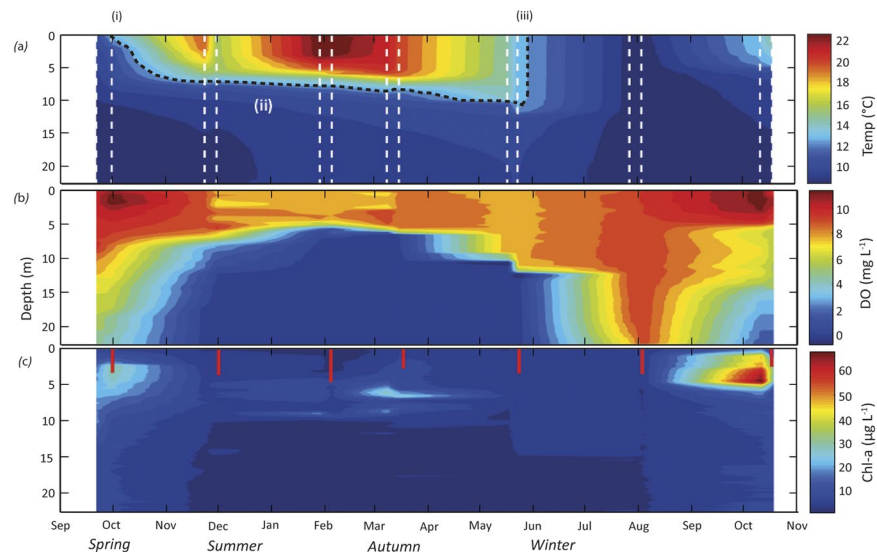


**Figure 2.** Physicochemical characteristics of the water column of Lake Ngapouri between September 2015 and October 2016. **(a)** Temperature, **(b)** dissolved oxygen (DO), and **(c)** chlorophyll fluorescence data were extracted from CTD casts conducted before and after each DGT deployment. Data points are interpolated using the MATLAB contour function. Vertical lines in **(a)** (broken white) and **(c)** (solid red) show the time of sampling and Secchi depth respectively. The broken black line in **(a)** shows the timing of the onset (i) and end (iii) of stratified conditions in the lake as well as the approximate position of the thermocline (ii) to aid visual identification of these features.

## Results and Discussion

### Physicochemical characteristics of Lake Ngapouri.

Stratification in Lake Ngapouri began in November 2015 (Fig. 2) and the lake water became markedly clearer at this point compared with the preceding winter mixed period. High turbidity during the winter may have been caused by the resuspension of sediment or a predominance of diatomaceous algae (Fig. 2), whereas increased clarity during summer can be plausibly explained by coagulation and sedimentation of the suspended particles<sup>41</sup>.

The surface water temperature of Lake Ngapouri ranged between 9 °C and 23 °C over the study period. The annual temperature cycle of the lake was characterised by two distinct phases: isothermal conditions and thermal stratification (Fig. 2).

CTD (Conductivity, Temperature, Depth profiler) casts indicate that isothermal conditions continued until September, and that a thermocline started to establish at the start of November 2015. Thermal stratification established as the summer progressed (Fig. 2).

The exact depth of the CTD casts varied due to changes in water levels over the course of this study. Therefore, the time series presented here was reduced to the minimum depth recorded in the sampling period (22 m from surface) for consistency. Since profiles for chlorophyll fluorescence were determined by CTD casts and no CTD data were collected at night time we were not able to determine the direct effect of non-photochemical quenching<sup>42</sup>. Chlorophyll fluorescence data indicate periods of high phytoplankton biomass during the winter mixed period in September 2015 and October 2016, and a peak just above the thermocline (ca. 5–8 m) during March–May 2015. This deep chlorophyll maximum (DCM) was quite similar to that observed in nearby Lake Okaro, a lake of similar trophic status with an anaerobic hypolimnion<sup>43</sup>. No response in chlorophyll fluorescence was observed after the diurnal mixing event in November 2015.

Once established, the thermocline was very stable and progressively deepened from 5 to 13 m from November 2015 to March 2016, respectively. The DO concentration markedly decreased below 5 m depth in November 2015 and established a completely anaerobic hypolimnion extending from 15 m depth to the bottom of the lake over the same interval. The epilimnion deepened to about 10 m by May 2016 and the lake experienced complete seasonal mixing in July 2016.

The lake water pH was almost uniform during winter mixed conditions, but started to decrease in deeper waters of the lake during early stratification. The onset of stratification coincided with elevated chlorophyll fluorescence near the lake surface, which coincided with higher pH conditions (exceeding pH 9 in October 2016; Fig. S2, supplementary information).

### Colloidal size distributions, morphology and chemistry through time.

**AFM Results.** Particle size distributions (PSD) measured by atomic force microscopy (AFM) of colloids are shown in Fig. 3. It should be noted that AFM is biased toward small particles and does not necessarily cover the entire colloid size distribution range. Colloids were predominantly in the size range of 1 to 10 nm in both epilimnetic and hypolimnetic samples. In the epilimnion during January 2016, particles in the 2–3 nm size range constituted >45% of total particle numbers. Particles >10 nm did not form a major proportion of the PSD during this month (Fig. 3) which may be

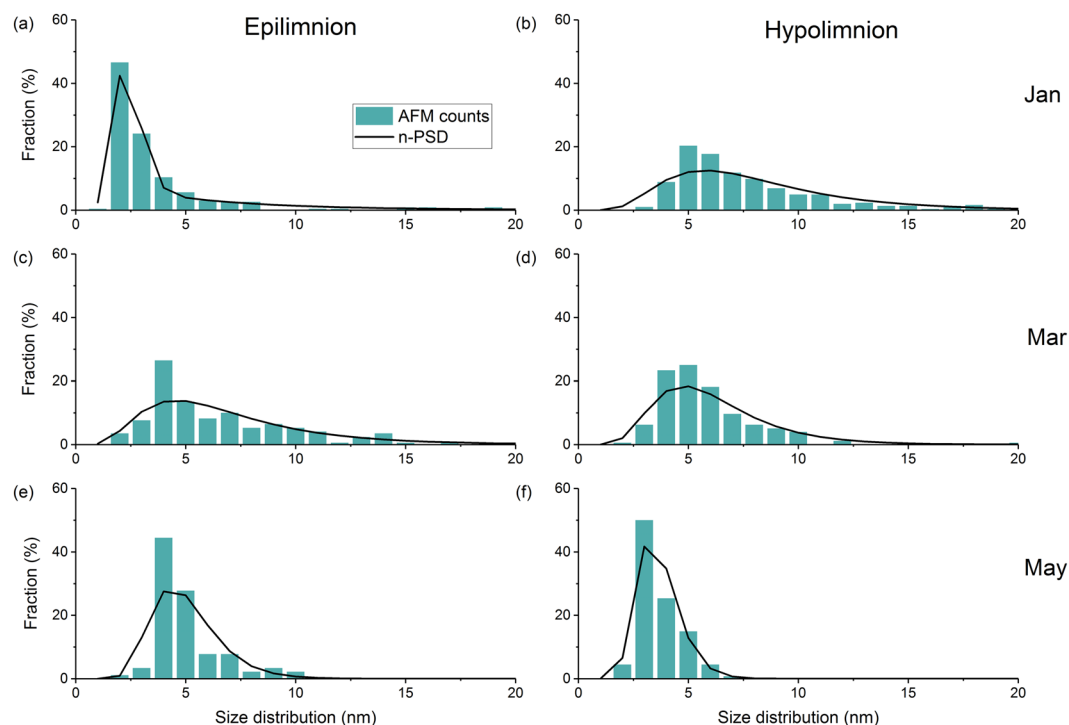


**Figure 3.** Atomic force microscopy (AFM) particle size distributions (PSD) from Lake Ngapouri samples collected between January and May 2016. First column are epilimnetic samples from (a) January, (c) March, (e) May and in the second column hypolimnetic samples from (b) January, (d) March, and (f) May 2016, respectively. Fraction (%) gives the percentage of total particles detected by AFM image analysis.

related to particle settling and gravitoids sedimentation under the prevailing stratification. On the other hand, in the hypolimnion during the same month colloid sizes shifted toward larger particle sizes (between 3 and 18 nm) with particles between 4–6 nm constituting the most significant fraction at ~40% of all measured particles (Fig. 3).

In the epilimnion during March 2016, particles were in the size range of 2–14 nm, with the greatest density between 4–5 nm (Fig. 3c). In the hypolimnion, particles remained distributed within a narrow size range, with those in the 4–7 nm range making up ~50% of the total particle number (Fig. 3e). In May, the epilimnion PSD centred on 3–9 nm, with these particles constituting more than 50% of the total particle number (Fig. 3a). This PSD was comparable to the hypolimnion PSD in January and March. The consistent size distributions between months in the hypolimnion might be explained by: (1) resuspension of the particles from the bed sediments during this stagnant phase, or (2) the recycling of nanoparticles by cycles of reduction and precipitation within the water column<sup>44</sup>. Generally, a trend was observed toward decreased particle size in the deeper anaerobic water during stratification. This could be consistent with the reductive dissolution of larger colloids and precipitation of fresh nano-scale Fe (II)/Fe (III) hydroxides, although this cannot be substantiated without higher spatial and temporal resolution data.

**TEM Results.** The Transmission Electron Microscope (TEM) analysis confirmed that Fe-bearing particles were the most prevalent class of nanoparticles detected in Lake Ngapouri. Figure 4 shows a representative TEM micrograph and EDX (Energy-dispersive x-ray analysis) spectrum, which show peaks for Fe, O with contributions from Si; all major elements commonly associated with colloidal species in freshwaters. Evidence was also found for the presence of Fe monosulfides in the hypolimnion as would be expected at the interface of Fe-reducing and S-reducing zones in the water column and sediments.

**Iron depth distributions through time.** Water sample aliquots collected after ultrafiltration in a zero-grade N<sub>2</sub> atmosphere were used to measure the fraction of Fe and P associated with colloidal particles. This analysis provides an approximation of the concentration of Fe and P in the colloidal range which excludes particles >0.45 μm and nanoparticles <~5 nm diameter (based on 100 KDa ultrafiltration).

Time series of Fe depth distributions in Lake Ngapouri (Fig. 5) reveal the dominant influence of stratification on Fe cycling. The Fe concentration started to build up in all fractions (dissolved, colloidal, C<sub>DGT</sub> and Ferrozine) over the period of early stratification and was maintained during summer. Fe < 0.45 μm was predominantly colloidal (Fig. 5b). Taken together with the AFM and TEM results, this implies that Fe was present in the hypolimnion either as simple inorganic colloids, e.g. Fe(III) hydroxides with particle sizes typically ≥5 nm, or in association with macromolecular organic colloids/aggregates. Analysis of the organic fraction of the dissolved and colloidal size range in the total organic carbon (TOC) measurement returned colloidal TOC concentrations in the 0.1–3.31 ppm range, constituting up to 100% of the organic carbon <0.45 μm (i.e., dissolved organic carbon (DOC)) in some cases.

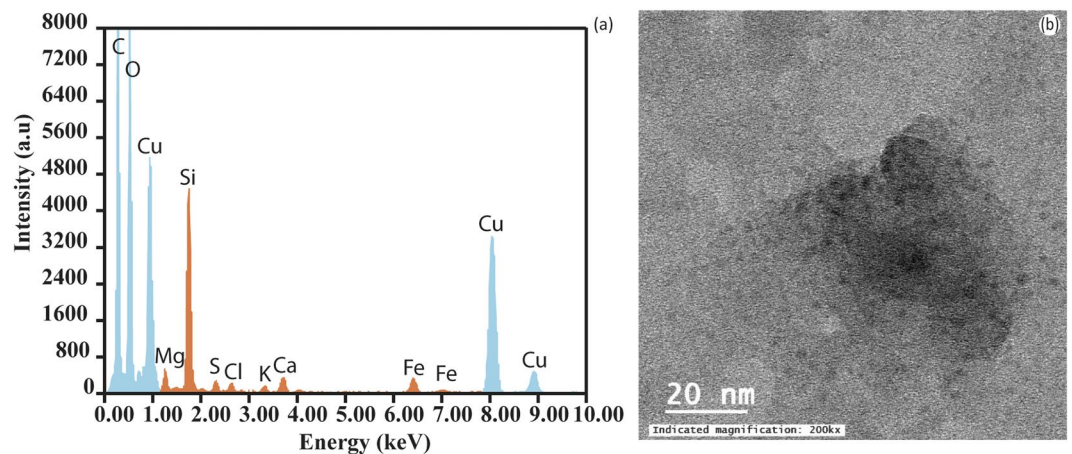


**Figure 4.** Representative TEM results from Lake Ngapouri showing abundant nano-scale colloids containing iron and silicon. (a) The accompanying EDX spectrum from the globular colloid photomicrograph shown in (b).

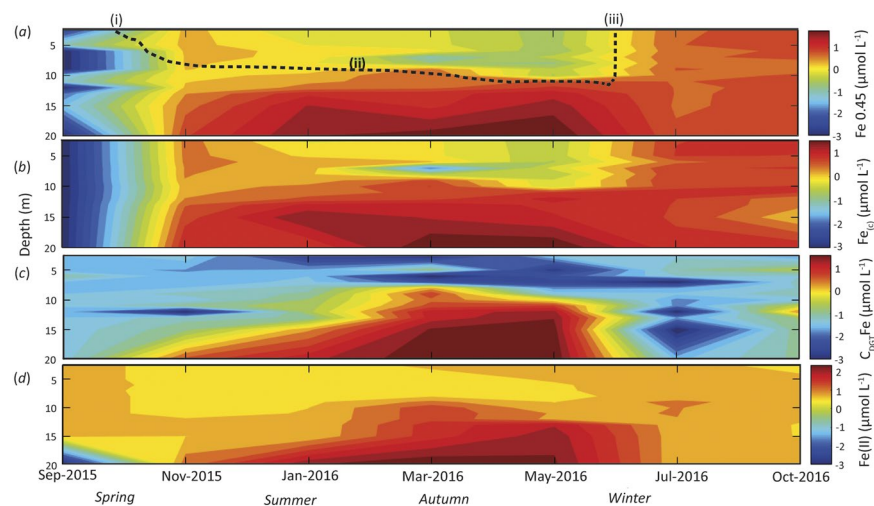


**Figure 5.** Time series of the depth-distribution of iron (Fe) at  $\log_{10}$  scale in operationally-defined water fractions from Lake Ngapouri, (a) Dissolved Fe ( $\mu\text{mol L}^{-1}$ ), (b) Colloidal Fe ( $\mu\text{mol L}^{-1}$ ), (c)  $C_{\text{DGT}}$  Fe ( $\mu\text{mol L}^{-1}$ ) and (d) Fe(II) by Ferrozine method ( $\mu\text{mol L}^{-1}$ ). Broken black line in (a) shows the timing of the onset (i) and end (iii) of stratified conditions in the lake as well as the approximate position of the thermocline (ii).

DGT is thought to measure (1) all hydrated free-ion species, (2) a vast majority of the colloidal and complexed species that may be released into free-ion species during the deployment and (3) colloidal species that can diffuse through the APA hydrogel and bind with the basal resin layer<sup>38,45</sup>. The diffusion coefficient of solutes in the hydrogel decreases with an increase in their hydrated radii. Although exact information on the porosity of APA diffusive gel is lacking, initial studies by Zhang and Davison<sup>37</sup> reported the pore size to be  $>5$  nm while Fatin-Rouge, *et al.*<sup>46</sup> gave indicative pore sizes in the 50–74 nm range, depending on the gel cooling rate during polymerization. Furthermore, particles  $>60$  nm were considered locally trapped and not evenly diffused through the gel<sup>46</sup>. However, Davison and Zhang<sup>38</sup> suggested that despite the probable existence of larger pore sizes, DGT devices can only measure particles  $<2$  nm size because of the slow diffusion rate of larger particles. In addition, the structure and composition of solutes are important determinants. Thus, DGT can be considered to be sensitive to nano-scale particles which are sufficiently labile to be measured by the DGT resin layer, or otherwise become embedded in the resin gel matrix<sup>39</sup>. The diffusion coefficients (D) of nanoparticles in the size range determined by AFM were calculated using Stokes law (Table 1). These D values were used to calculate the time to reach 95% of the steady state accumulation rate ( $T_{95\%}$ ) for colloids. D values from Zhang and Davison<sup>37</sup> were used to calculate  $T_{95\%}$  for dissolved Fe (Table 2). The  $T_{95\%}$  values are comparable for the colloids  $>1$  nm and demonstrate that over the course of a week (typical duration of deployment in this study), DGT is likely to have accurately recorded the concentration of DGT-labile colloidal species in the lake.

Direct measures of the initial increase in Fe concentration in the hypolimnion of Lake Ngapouri between November and January (Fig. 5) were not mirrored by an increase in  $C_{\text{DGT}}$  Fe, which appeared to lag colloidal Fe in the upper hypolimnion (Fig. 5c). Because DGT only measures the diffusible Fe concentration, it follows that Fe



Month	Compartment	Temp.(K)	Average particle radius (nm)	$1\sigma$	$\bar{D}$	Average colloid	Solute
						$D (\times 10^{-6} \text{ cm}^2 \text{ s}^{-1})$	$D (\times 10^{-6} \text{ cm}^2 \text{ s}^{-1})$
January	Epilimnion	295.15	0.61	3.47	2.86	4	5.63
March	Epilimnion	283.15	4.49	4.25	0.47	0.52	3.19
May	Epilimnion	294.15	6.45	5.43	0.41	0.37	5.47
January	Hypolimnion	283.15	4.8	4.93	0.51	0.49	3.19
March	Hypolimnion	287.15	2.25	1.53	0.34	1.05	4.45
May	Hypolimnion	283.15	1.58	0.98	0.31	1.47	3.19

**Table 1.** Calculation of the diffusion coefficient (D) of the nanoparticles in the size range determined by AFM assuming spherical morphology.  $1\sigma$  = 1 standard deviation ( $n$  = no. measurements);  $\bar{D}$  = dispersity.

Epilimnion			Hypolimnion		
Solute	Colloid	$T_{95\%}$ (hrs)	Solute	Colloid	$T_{95\%}$ (hrs)
$T_{95\%}$ (hrs)	particle radius (nm)		$T_{95\%}$ (hrs)	particle radius (nm)	
18	0.61	26	21	0.61	30
32	4.49	198	37	4.49	227
19	6.45	278	22	6.45	319
32	4.8	211	37	4.8	242
23	2.25	98	27	2.25	112
32	1.58	70	37	1.58	80

**Table 2.** Comparison of the time taken by DGT to reach 95% steady state accumulation rate for Fe using representative diffusion coefficients for colloids or solutes (i.e. hydrated  $\text{Fe}^{2+}$  ions) in the epilimnion and hypolimnion of Lake Ngapouri.  $T_{95\%}$  (hrs) = time taken by DGT to reach 95% steady state concentration.

released into the hypolimnion in the early period of stratification was non-DGT-labile. This supports the interpretation that Fe became more labile through time in the hypolimnion as reducing conditions intensified (Figs 2 and 5). Following March 2016, Fe concentrations measured by DGT showed improved agreement with the other Fe fractions. Indeed, in the latter months of stratification it appears that although Fe was predominantly colloidal (Fig. 5b), it was also DGT labile (Fig. 5c).

It is clear from Fig. 5 that the increase in Fe (II) started from the bottom of the lake, consistent with diffusion from the lake sediment/benthic nepheloid layer, which was characterised by lower DO concentrations than the overlying hypolimnetic water in the early period of stratification<sup>30</sup>. Dissolved Fe (II) first appeared in the lower-most sample in late November 2016 (Fig. 5), when the concentration of dissolved oxygen had fallen to  $0.1 \text{ mg L}^{-1}$  (Fig. 5b). From this point until the end of stratification Fe(II) was maintained at elevated levels.

Re-oxygenation of bottom waters occurred during winter in July 2016 (Fig. 2). The concentration of Fe decreased in all fractions (Fig. 5), consistent with the oxidation of Fe (II) species and the precipitation of Fe (III) hydroxides, most of which formed settleable gravitoids, and were removed from the water column. The measurements of dissolved Fe in July 2016 confirm that that while Fe was returned to the surface water by mixing, it was not DGT-labile (Fig. 5). Hence, the Fe data from July 2016 capture the suspension of Fe (III) colloids prior to aggregation and settling, a process which had continued to completion by October 2016.

Finally, the Fe(II) distribution (as determined by the Ferrozine method) was in broad agreement with the  $C_{\text{DGT}}$  data, but over-estimated Fe in all other fractions. It is important to note that Fe (III) can co-exist with Fe (II) at circumneutral pH values, and indeed thermodynamic disequilibrium between Fe(III)/Fe(II) species can be driven by microorganisms in some cases<sup>42,43</sup>. Although Viollier, *et al.*<sup>47</sup>, reported 3% higher absorption of Fe(II)-Ferozine complex in their system, the results of the present study are broadly in line with the findings of Anastacio, *et al.*<sup>48</sup> who overestimated Fe(II) as a result of photochemical reduction of Fe(III) complexes. To minimize the uncertainty in Fe(II) quantification here, the samples were pipetted to pre-prepared spectrophotometric cuvettes (containing Ferrozine) and treated for a short incubation time ( $<1 \text{ min}$ ), yet it was practically impossible to achieve the desired oxygen-free, dark conditions during measurements in an open boat. It is likely that the overestimation of Fe by the Ferrozine method was also due to interference by other divalent cations.

**Phosphorus depth distributions through time.** Mobile phosphorus has long been known to be intimately associated with particulate Fe in fluvial environments<sup>20,49</sup> and interactions of the two have recently been shown for colloids in streams and aquifers<sup>32</sup>. During this study, the colloidal fraction of P ( $P_{(\text{c})}$ ) was found to track the dissolved P concentration, demonstrating that  $P_{(\text{c})}$  was dominant over dissolved species. Given that Fe in Lake Ngapouri was predominantly colloidal (Fig. 6), one line of evidence for the interaction of Fe and P in the water column would be the colloidal association of both elements. Indeed, an analysis of P size-distributions through time also confirms that DRP in this system (Fig. 6b) is mostly in the colloidal size range. Increases in P in both dissolved and colloidal fractions also coincided with increases in the DGT-labile P concentration (Fig. 6d).

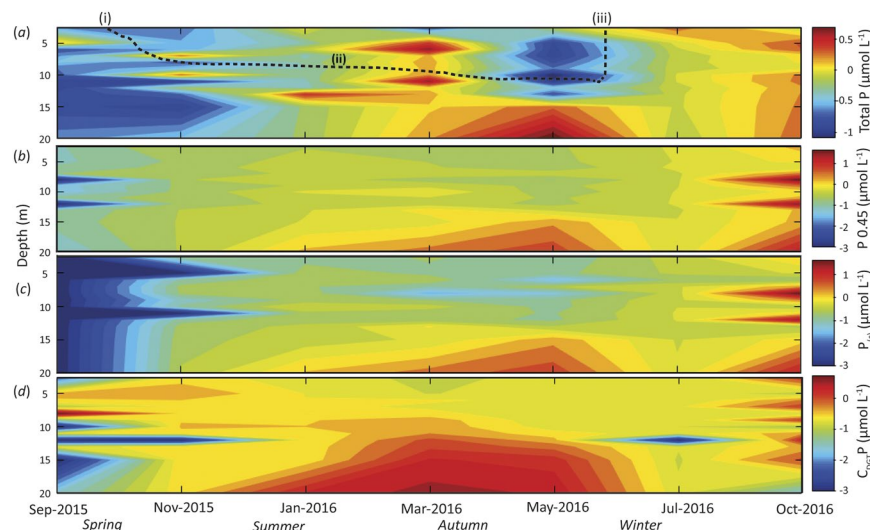


**Figure 6.** Time series of the depth-distribution of phosphorus (P) at  $\log_{10}$  scale in operationally-defined water fractions from Lake Ngapouri, **(a)** Total P ( $\mu\text{mol L}^{-1}$ ), **(b)** 0.45  $\mu\text{m}$  filtered fraction (dissolved P ( $\mu\text{mol L}^{-1}$ )), **(c)** colloidal P<sub>c</sub> ( $\mu\text{mol L}^{-1}$ ) and **(d)** C<sub>DGT</sub> P ( $\mu\text{mol L}^{-1}$ ). Broken black line in **(a)** shows the timing of the onset (i) and end (iii) of stratified conditions in the lake as well as the approximate position of the thermocline (ii).

DGT probes recorded three prominent instances of P release: discrete increases between 5–10 m depth during the onset of stratified conditions, and a sustained hypolimnetic increase in P through the summer period (Fig. 6c). It is notable that these increases in DGT-labile P were mirrored by high chlorophyll fluorescence and solvent-extracted chlorophyll *a* at the same or adjacent depths (Fig. 2).

**Coupling and decoupling of iron and phosphorus.** Generally, under winter mixed conditions, the highly oxic water column was characterised by low concentrations of Fe (from being undetectable up to 11.6  $\mu\text{mol L}^{-1}$  towards the bottom of the lake). Low dissolved Fe also coincided with low concentrations of C<sub>DGT</sub> Fe (often close to zero) (Fig. 5). Thus, under mixed oxic conditions in the lake, the Fe data support the classical interpretation that Fe was present as colloidal Fe(III) hydroxides<sup>50</sup> and was not DGT-labile because the Fe was held in the insoluble Fe(III) oxidation state.

During the summer-autumn stratified period the concentration of dissolved Fe (<0.45  $\mu\text{m}$ ) increased towards the bottom of the lake, reaching the highest value recorded in this study of 109  $\mu\text{mol L}^{-1}$  at 20 m depth in May 2016, which coincided with a higher concentration of hypolimnetic P in the same fraction (7.51  $\mu\text{mol L}^{-1}$ ). The same trend was observed in the P<sub>c</sub> fraction, possibly indicating the release of adsorbed or co-precipitated P from Fe(III) hydroxides as a result of Fe(III) reduction and hydrolysis of Fe(II).

Phosphorus determined by inductively coupled plasma mass spectrometry (ICP-MS) from the filtered samples (<0.45  $\mu\text{m}$ ) was highest at 8 m depth under completely mixed conditions in October 2016 (74  $\mu\text{mol L}^{-1}$ ). Notably, there was an increase in chlorophyll fluorescence at this depth during March 2016, which suggests that the higher value of P not associated with dissolution of Fe mineral phases, was instead driven by another process, such as the mineralisation of biomass.

The coupling and decoupling of Fe and P is directly evident in the C<sub>DGT</sub> data from the lake in the two seasons (Fig. 7). In the autumn (March–May), reductive dissolution of Fe colloids in the hypolimnion is implicated as the driver of elevated C<sub>DGT</sub> Fe and P values. Dissolution of Fe colloids reached its zenith in March, and over the following two months the P: Fe ratio measured by DGT declined, probably consistent with biological uptake of P over that interval. Conversely, during the winter/spring mixed periods, phytoplankton blooms can be seen to have been entirely decoupled from Fe hydroxide reduction (Figs 2 and 5). The decoupling of P and Fe during the oxic intervals is consistent with the sequestration of P by insoluble Fe hydroxides, destabilisation of this colloidal suspension and sedimentation of the resulting Fe gravitoids. It appears that recently-sequestered Fe and P particles were likely suspended into the water column of the re-stratifying lake in the spring period (see colloidal distributions of P and Fe in the water column over these periods (Figs 5 and 6)), which could have been aided by bioturbation<sup>51,52</sup>.

At the onset of thermal stratification, the concentration of Fe<sup>2+</sup> (inferred by the ferrozine assay) increased in the hypolimnion and gradually built up in summer through until March. In January 2015, Fe was predominantly colloidal in the hypolimnion, of which very little was DGT-labile. In addition, DGT-labile Fe was very closely related to Ferrozine Fe<sup>2+</sup>, implying that at this stage, Fe was present in a relatively inert form in the hypolimnion.

During stratification in deep lakes, when the upper layer of the euphotic zone is nutrient-depleted and phytoplankton in the lower level are more likely to be limited by light supply, a so-called ‘deep chlorophyll maximum’ (DCM) develops—typically situated around the thermocline. This phytoplankton distribution has been linked to upward diffusion of nutrients from the enriched hypolimnion waters<sup>42,52,53</sup>. In this study, when the stratification was still strongly maintained in March, the DCM was observed at 11 m in association with a strong depletion of

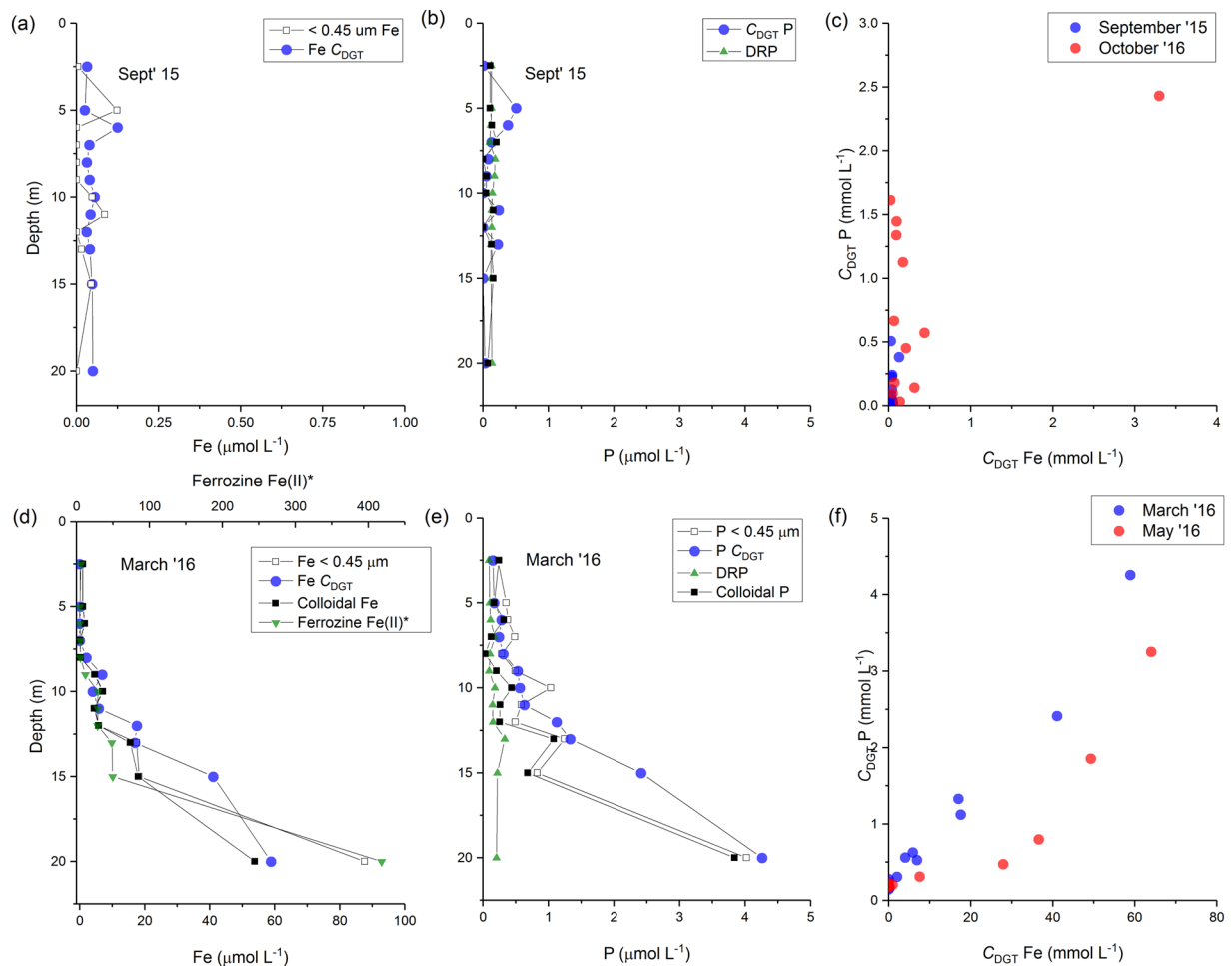


**Figure 7.** Depth distributions of iron (Fe), phosphorus (P) and cross-plots of DGT-labile Fe vs P in the winter mixed period (a–c) and summer-spring stratified period (d–f).

dissolved Fe, colloidal Fe and DGT-labile Fe, as well as some depletion in colloidal P (Fig. 8) at the same stratum, likely reflecting biological uptake of this important micronutrient. Interestingly, the depletion of P was only observed in the colloidal P fraction, which would be consistent with targeted dissolution of Fe colloids to release Fe (an important micronutrient for phytoplankton). In the hypolimnion in March 2015, the DGT-labile fraction of Fe exceeded the concentration of Fe in the  $< 0.45 \mu\text{m}$  fraction. This can be explained, but not demonstrated (due to a lack of particulate data), by the removal of Fe colloids as gravitoids<sup>27</sup>.

## Conclusion

This investigation suggests that colloidal Fe oxides are generated during mixing in monomictic lakes and possibly at the interface of oxic epilimnetic and hypolimnetic waters by cycles of microbial oxidation-reduction reactions. Our results also suggest that P was associated to these iron nanoparticles and that both Fe and P increased in concentration as reducing conditions deepened in the hypolimnion. These findings are in line with those of Gottselig, *et al.*<sup>54</sup> and Jiang, *et al.*<sup>55</sup> who demonstrated P associated with Fe oxide colloids in the size range of 1 to 20 nm in forest stream waters and agricultural soils, respectively, using coupled flow fractionation and ICP-MS, and Hartland *et al.*<sup>32</sup> who showed dominant P adsorption to iron nanoparticles in streams and shallow (reduced) aquifers.

Further to this, we suggest that freshly precipitated Fe (oxy) hydroxides are small enough to diffuse through the APA hydrogel used in DGT solution probes at a rate comparable to that of solutes (at least when integrating over several days). These colloids bind P and thereby reduce the P concentration in the  $< 100 \text{ kDa}$  fraction. Based on elevated chlorophyll values at the same or adjacent depths, we conclude that colloidal P (and also Fe) is available for biological uptake and that DGT-labile P provides an analogous measure of P bioavailability. This interpretation is consistent with the findings of Montalvo, *et al.*<sup>56</sup> who demonstrated that the colloidal P fraction was available for uptake by terrestrial plants. Our results confirm that iron nanoparticles play an important role in P transport and cycling in the lake systems, with important implications for phytoplankton community dynamics.

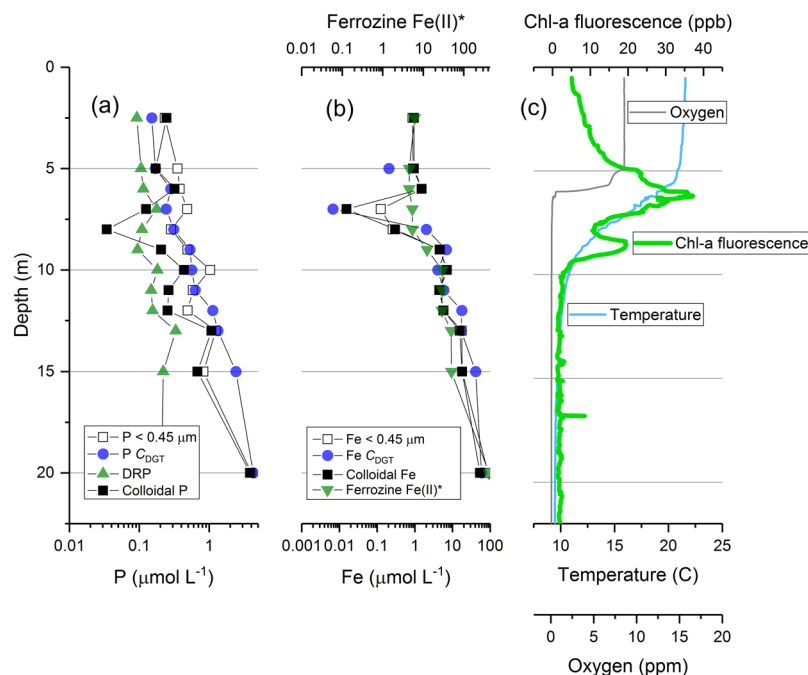


**Figure 8.** Depth distributions of (a) phosphorus and (b) iron fractions measured in Lake Ngapouri in March 2016. Panel (c) shows the corresponding CTD depth profiles for molecular oxygen, temperature and chlorophyll fluorescence.

## Materials and Methods

**Site description.** Lake Ngapouri is a small (0.19 km<sup>2</sup>) eutrophic lake located in Waikiti valley south of Rotorua, Bay of Plenty, New Zealand. It has a maximum depth of 24.5 m. A previous study reported increased concentrations of Fe, Mn, P and As in the anaerobic hypolimnion of the lake<sup>44</sup>. Being holomictic, monomictic and high in Fe, the lake was considered to be an ideal model system for examining P-Fe interactions.

**Field Methods.** *Water sampling.* Sampling of Lake Ngapouri took place every second month, from September 2015 to October 2016). Water samples were taken from 12 depths between 0 and 23 m, at the deepest point of the lake ~23 m depth). Figure 9 summarises the field-to-lab workflow.

A Van dorn water sampler (PVC Beta<sup>TM</sup> Horizontal bottle, Envco, Auckland, New Zealand) was used to collect representative water samples from the discrete depth intervals. Vertical profiles of water column chemistry were constructed by sampling every meter (relative to the lake bottom) through the thermocline, as well as at two sampling points in the epilimnion and two in the hypolimnion. A conductivity, temperature and depth profiler (CTD; SBE 19 plus V2 SeaCAT profiler, Sea-Bird Electronics Inc., Washington) equipped with sensors for pH, dissolved oxygen, photosynthetically active radiation (Licor Inc.) and chlorophyll fluorescence (Chelsea Instruments Ltd.) was used to determine the physiochemical character of the lake prior to and after each DGT deployment. Secchi depth was also measured to determine water clarity.

*Filtration and preservation (in field).* Samples of 15 ml lake water were filtered on site by using 0.45 µm syringe filters (Sartorius Stedim, Germany) in acid-washed bottles and were acidified on-site with ultrapure HNO<sub>3</sub> to achieve 2% acidity in preparation for ICP-MS analysis (acid was prepared using low-temperature distillation in a Savillex (Eden Prairie, MN, USA) DST-1000 acid purification system). Overloading of filters was avoided as it can affect the pore size and may cause variable removal of particulates and colloids. To maintain the integrity of the collected water samples for major cation analysis, the screw-capped bottles were sealed using laboratory film and maximum care was taken to leave no head space in the bottles, to avoid oxidation. The bottles were then covered with aluminium foil and transferred in the dark at <5 °C to avoid photolysis. Additional samples were collected in pre-cleaned (acid/deionised water) syringes to determine the size distribution of the components of interest in the water column. Syringes were capped to avoid diffusion of O<sub>2</sub> into the samples, and were then sealed with laboratory film and stored in the dark at or below 4 °C until analysis. As a measure of the extent of oxidative loss of Fe, the Ferrozine method (Hach, Colorado, USA) was used in the field to determine the dissolved Fe(II) concentration<sup>47</sup>. This analysis was conducted by taking an aliquot immediately from the Van dorn sampler which was directly transferred to a spectrophotometric cuvette already containing Ferrozine. This allowed immediate complex formation and thus minimised the potential for oxidative loss. The Ferrozine method was also used to measure the extent of post-sampling oxidation of the samples during handling in the laboratory and during separation of colloids by ultra-filtration.

Samples for Chl-*a* estimation were collected from each depth by filtering 50 mL of the water sample through 0.45 µm GF/C filters (Whatman, Maidstone, United Kingdom). The filters were then folded in half (sample side



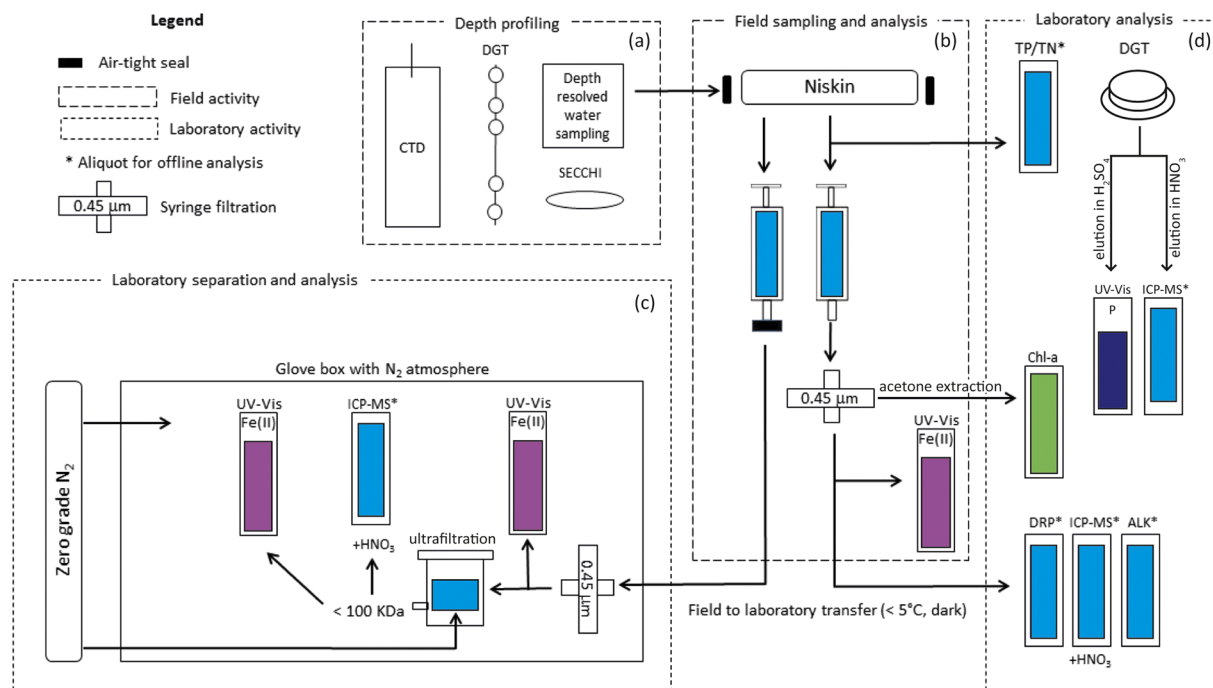


**Figure 9.** Water sampling and laboratory analysis workflow. Part (a) shows the range of in-field methods employed, (b) shows the water sample collection workflow including on-site filtration. Minimally-perturbed samples were collected in syringes and were capped for transport to the lab. Fe (II) was estimated on-site using Ferrozine analysis. Part (c) illustrates particle separation using stirred-cell ultrafiltration performed in a zero-grade N<sub>2</sub> environment to avoid oxidative loss of Fe(II). Finally, part (d) shows the laboratory analysis procedure including the elution and subsequent analysis of DGT binding gels. \*Denotes a water sample taken for off-line analysis.

inward), individually wrapped in aluminium foil, kept in a container pre-wrapped with aluminium foil as extra precaution, and kept on ice until return to the laboratory, where the samples were frozen in dark and analysed using acetone extraction method within one week of collection.

**Diffusive gradients in thin films.** To determine the concentration of labile trace elements and P in the lake water column, Chelex 100 (Bio Rad Laboratories Pty, Rosedale, Auckland, NZ) and ferrihydrite DGT devices were used in this study and prepared in-house after Zhang, *et al.*<sup>45</sup> and Zhang and Davison<sup>57</sup> respectively. The precision and accuracy of C<sub>DGT</sub> values determined using DGT solution probes was confirmed before deployment in the lake and were found to be accurate to within 5% for Cd and P (Supplementary information, Tables S1 and S2). The assembled probes were transferred to airtight containers, immersed in 0.01 M NaNO<sub>3</sub> and purged with zero grade N<sub>2</sub> overnight to ensure removal of dissolved oxygen. This procedure was carried out in a pre-N<sub>2</sub>-purged glove box as an extra precaution. The dissolved oxygen level in the 1 M NaNO<sub>3</sub> solution containing the DGT probes was below the level of detection of a DO probe (<1 mg L<sup>-1</sup>). The probes were then transferred to the field in airtight containers and the DO content was measured before deployment, and never exceeded 1 mg L<sup>-1</sup>.

Duplicate Chelex and ferrihydrite probes were strung onto a nylon rope at the required depth intervals, secured using cable ties, and immersed into the lake with minimum delay (Fig. S4). Probes were co-located with temperature loggers (UTBI-001, TidbiT v2 Temp Loggers (Onset Computer Corp., Cape Cod, MA, USA)) which, in addition to CTD data, were used to calculate the average temperature at each respective depth. During each deployment, a duplicate set of DGT probes which had not been purged with N<sub>2</sub> was deployed to examine variations caused by oxygen trapped in the hydrogels (Fig. S6). The results showed no difference in concentration of analyte species bound to resin gels (Fig. S6).

After typically 4–5 days, the probes were retrieved from the lake water column, rinsed with DI water (resistivity 18.2 MΩ) and kept in sealed, pre-cleaned individual plastic bags which were transferred to the lab at <5 °C in the dark and kept under the same conditions until analysis.

**Laboratory Methods.** The syringe samples were transferred to the N<sub>2</sub> purged glove box for ultrafiltration in a stirred-cell ultrafiltration system (Amicon<sup>®</sup>, model 8400) equipped with Millipore Ultracel 100 KDa (molecular weight cut-off (MWCO)) regenerated cellulose ultrafiltration discs (Millipore Corporation, Billerica, MA, U.S.A.) which provide size exclusion above approximately 5 nm. Ultrafiltration for separation of colloids has been a focus of potential artefact<sup>10,58</sup> and maximum care was taken to avoid these potential issues. The ultrafiltration unit was washed with 5% HNO<sub>3</sub> and rinsed three times with deionized (DI) water before each use. Everything else, except for Chl-*a* estimation, was cleaned by soaking in 10% HCl overnight, rinsing with DI water, soaking in 10% HNO<sub>3</sub>.

at least overnight and finally rinsing three times with DI water, and then air dried under a Class 100 laminar flow hood. Glassware was cleaned using Clean Aid and rinsed five times before Chl-*a* measurements. Prior to lake water filtration, the filter discs were washed with 50 mL of DI water and an aliquot was analysed as a blank for potential contamination from the filtration step. All blanks ranged between  $\pm 1 \mu\text{g L}^{-1}$  for P and  $\pm 1 \mu\text{g L}^{-1}$  for Fe.

Before ultrafiltration, the syringes were opened in the glove box and the Fe (II) content was again determined by complexation with Ferrozine<sup>47</sup> to determine any Fe(II) loss during transportation and storage. The sampling trip was repeated when there was oxidative loss  $>3\%$ . A 50 mL  $0.45 \mu\text{m}$  filtered sample was then ultra-filtered under minimum back pressure ( $<30 \text{ kPa}$ ) of zero grade  $\text{N}_2$  and aliquots were collected in pre-cleaned (as described earlier) conical tubes that were kept open in the purging  $\text{N}_2$  glove box overnight to remove oxygen in the tubes. The filter membranes were exhaustively cleaned with 50 mL of DI water between every sample to avoid cross contamination and metal sorption to filters<sup>59,60</sup>. Aliquots were collected frequently to determine if any contamination had occurred. The filtration process was quick (5 mL/min) and the  $\text{N}_2$  flow rate was adjusted accordingly to avoid rupturing of the filter discs. The filtered fraction collected for major cation analysis was acidified in the glove box by using the same protocol as described under the “Filtration and preservation in the field” heading. The screw capped bottles were then analysed by ICP-MS calibrated using NIST-traceable certified reference materials from Inorganic Ventures (Christiansburg, Virginia).

Filter fractions were categorised on the basis of their relative pore size. However, because there is no direct relationship between molecular weight and the size of nanoparticles<sup>60,61</sup> the size estimates based on filtration used in this study are approximate. The four fractions defined in this study are as follows: dissolved (corresponding to the sample filtered at  $0.45 \mu\text{m}$ ), colloidal (corresponding to the difference between  $0.45 \mu\text{m}$ –100 kDa permeates), and nominally dissolved (corresponding to the 100 kDa permeate).

DGT probes were disassembled within 24 hrs of collection from the field and retrieved resins (binding gels) were immediately transferred to 1 M  $\text{HNO}_3$  in the case of Chelex and 0.25 M  $\text{H}_2\text{SO}_4$  for ferrihydrite. The ferrihydrite eluent was analysed using the molybdenum blue method<sup>62</sup>. Eluents of Chelex gels were analysed by ICP-MS.

**Characterization of colloids.** Colloids from Lake Ngapouri were characterized by using transmission electron microscopy (TEM) and atomic force microscopy (AFM). TEM samples were prepared by placing  $\sim 30 \mu\text{L}$  of water sample on support films (Formvar/carbon coated 200-mesh copper, obtained from ProSciTech, QLD, Australia) and allowed to dry under a zero-grade  $\text{N}_2$  atmosphere. Freshly cleaved mica sheets (ProSciTech, QLD, Australia) were placed in 15 mL of water sample for 24 hr immediately after return to the laboratory and then allowed to dry under the same  $\text{N}_2$  atmosphere in screw-capped bottles (thereby avoiding deposition of settling particles). We recognize the possible salt crystallization on the surface of mica sheets during sample preparation steps<sup>61</sup> and so the results are interpreted accordingly.

**Instrumental method.** Both filter fractions, i.e. dissolved ( $<0.45 \mu\text{m}$ ) and nominally dissolved ( $<100 \text{ kDa}$ ) were analysed on a Perkin Elmer (Waltham MA) quadrupole ICP-MS calibrated using certified reference materials. Internal standards of known concentration were also analysed to determine instrumental drift during analysis. Blanks (DI water, 18.2 M $\Omega$ ) and procedural blanks (DI water transported to the field with samples) were also analysed following every sampling campaign and reported values of most trace elements were very low. The average concentration of Fe was  $0.168 \mu\text{mol L}^{-1}$  for the nominally dissolved fraction i.e.  $<100 \text{ kDa}$  and  $0.179 \mu\text{mol L}^{-1}$  for colloidal fraction, i.e.  $0.45 \mu\text{m}$ –100 kDa permeates.

**Flow injection analyser.** Dissolved reactive phosphorus (from  $0.45 \mu\text{m}$ ) was analysed using standard colorimetric methods (APHA, 1998)<sup>63</sup> on a Lachat QuickChem flow injection analyser (Zellweger Analytics Inc.). A range of standards was prepared in DI water to confirm the analytical detection limit, which was found to be  $0.004 \text{ mg L}^{-1}$ . DI water was used as a blank. The total phosphorus concentration was determined in unfiltered lake water sample by using the same method as described above but after persulphate digestion<sup>62</sup>.

**Atomic Force Microscopy.** AFM imaging was carried out by using an XE-100 atomic force microscope (Park systems Corporation, Suwon, Korea). The analyses were carried out in a true noncontact mode under ambient conditions using silicon cantilevers with a spring constant of  $42 \text{ N m}^{-1}$  (PPP-NCHR, Park Systems Corp.) and images were recorded in topography mode. Images were collected from 15 to 20 arbitrary areas on the film and were recorded in  $256 \times 256$  pixel resolution. Particles were then grouped at 5 nm intervals based on measured heights.

**Fluorometric estimation of Chl-*a*.** The frozen glass fibre filter was transferred to clean tubes in very dim light and Chl-*a* was extracted by adding 5 mL buffered acetone. The filter was then ground by using an IKA® T10 basic Ultra-Turrax homogenizer (Thermo Fisher Scientific, Auckland, New Zealand). Five mL of buffered acetone was then added to wash any left overs off the grinding tip. The samples were allowed to steep for  $\sim 24 \text{ hr}$ , shaking at least once during this time. After the steeping period, the samples were shaken and centrifuged for 10 min at 3300 rpm, then allowed to stand for  $\sim 30 \text{ mins}$  in the dark at room temperature before reading.

Before proceeding to measure Chl-*a*, glass cuvettes were visually checked for any scratches. 5 mL of buffered acetone was read as a blank, followed by addition of  $150 \mu\text{L}$  of 0.1 N HCl. Five mL of the sample was decanted off and read at the “High” setting, then diluted with buffered acetone when the reading was “Over”, with the dilution factor was subsequently taken into account in calculations.  $150 \mu\text{L}$  of 0.1 N HCl was then added, mixed by gently tapping the cuvette, and re-read after 90 seconds.

**Calculations.** The concentration of colloidal Fe and Colloidal P was calculated according to Equations 1 and 2 respectively:

$$Fe_{(c)} = Fe_{(d)} - Fe_{(100KDa)} \quad (1)$$

$$P_{(c)} = P_{(d)} - P_{(100KDa)} \quad (2)$$

where  $Fe_{(c)}$  represents the colloidal fraction and  $Fe_{(d)}$  is filtrate through 0.45  $\mu\text{m}$  filter membrane and  $Fe_{(100KDa)}$  is the permeate filtering through 100 KDa filter membranes.

**Calculating  $C_{DGT}$ .**  $C_{DGT}$  concentrations were calculated for each resin disc by the following steps:

First, the mass (M) of P and Fe was calculated in respective resin gels using Equation 3

$$M = Ce(V_{acid} + V_{gel})/f_e \quad (3)$$

where  $Ce$  is concentration of P or Fe in resin gel eluent,  $V_{acid}$  is the volume of acid added to the resin gels,  $V_{gel}$  is volume of the resin gel and  $f_e$  is the elution factor of P or Fe.

The DGT concentration was then calculated by Equation (4)

$$C_{DGT} = M\Delta g/(DtA) \quad (4)$$

where  $\Delta g$  is diffusive boundary layer (thickness of diffusive gel + thickness of the filter membrane),  $D$  = diffusion coefficient of the elements in gel as reported by Zhang and Davison<sup>37</sup>,  $t$  is deployment time (s) and  $A$  is exposure area ( $\text{cm}^2$ ). This equation was used for calculating  $C_{DGT}$  value in the solution probes by using geometric area of standard solution DGT holders. When DGTs are immersed in water, a thin layer of water which is in line with the exposed window of the device is usually inactive and transport of material through this layer, known as Diffusive Boundary Layer (DBL), is believed to happen through diffusion only. The effect of DBL was minimised during this study by deploying devices for longer periods of time. Moreover, a 0.8 mm thick layer of diffusive gel along with 0.14 mm thick filter membrane was used for simplicity.

**Calculating Chl-a.** The concentration of Chl-a was calculated by using the following equation:

$$Chl - a(\mu\text{g L}^{-1}) = F_s[(r/(r - 1))(R_1 - R_2)] [(V_e X d_f)/V_f]$$

where  $F_s$  is response factor of the fluorometer,  $R_1$  and  $R_2$  are readings before and after the acidification step, respectively,  $r$  is the acidification coefficient,  $d_f$  is dilution factor,  $V_e$  is extraction volume and  $V_f$  is the volume of water filtered.

The depth of the thermocline was determined by calculation of  $dT/dz$  where  $z$  is the depth of water column increasing downwards<sup>42</sup> and  $T$  is temperature. The water column was considered fully mixed when  $dT/dz$  was  $> -0.225^\circ\text{C m}^{-1}$ . Data from CTD profiles were averaged over 0.125 m intervals to minimize noise. The top 5 m of the water profile was not included in thermocline calculations to avoid temporary diurnal thermoclines formed under calm conditions during daytime.

## References

- Anderson, D. M., Glibert, P. M. & Burkholder, J. M. Harmful algal blooms and eutrophication: Nutrient sources, composition, and consequences. *Estuaries* **25**, 704–726, <https://doi.org/10.1007/bf02804901> (2002).
- Elser, J. & Bennett, E. A broken biogeochemical cycle. *Nature* **478**, 29–31, <https://doi.org/10.1038/478029a> (2011).
- Kpdonu, A. T. N. K., Hamilton, D. P., Hartland, A., Laughlin, D. C. & Lusk, C. H. Coupled use of sediment phosphorus speciation and pigment composition to infer phytoplankton phenology over 700 years in a deep oligotrophic lake. *Biogeochemistry* **129**, 181–196, <https://doi.org/10.1007/s10533-016-0227-3> (2016).
- Guildford, S. J. & Hecky, R. E. Total nitrogen, total phosphorus, and nutrient limitation in lakes and oceans: Is there a common relationship? *Limnology and Oceanography* **45**, 1213–1223, <https://doi.org/10.4319/lo.2000.45.6.1213> (2000).
- Downs, T. M., Schallenberg, M. & Burns, C. W. Responses of lake phytoplankton to micronutrient enrichment: a study in two New Zealand lakes and an analysis of published data. *Aquatic Sciences* **70**, 347–360, <https://doi.org/10.1007/s00027-008-8065-6> (2008).
- Parkyn, S. M., Davies-Colley, R. J., Halliday, N. J., Costley, K. J. & Croker, G. F. Planted Riparian Buffer Zones in New Zealand: Do They Live Up to Expectations? *Restoration Ecology* **11**, 436–447, <https://doi.org/10.1046/j.1526-100x.2003.rec0260.x> (2003).
- Wilson, T. A., Amirbahman, A., Norton, S. A. & Voytek, M. A. A record of phosphorus dynamics in oligotrophic lake sediment. *Journal of Paleolimnology* **44**, 279–294, <https://doi.org/10.1007/s10933-009-9403-y> (2010).
- Van Moorleghem, C., Six, L., Degryse, F., Smolders, E. & Merckx, R. Effect of Organic P Forms and P Present in Inorganic Colloids on the Determination of Dissolved P in Environmental Samples by the Diffusive Gradient in Thin Films Technique, Ion Chromatography, and Colorimetry. *Analytical Chemistry* **83**, 5317–5323, <https://doi.org/10.1021/ac200748e> (2011).
- Van Moorleghem, C., De Schutter, N., Smolders, E. & Merckx, R. The bioavailability of colloidal and dissolved organic phosphorus to the alga *Pseudokirchneriella subcapitata* in relation to analytical phosphorus measurements. *Hydrobiologia* **709**, 41–53, <https://doi.org/10.1007/s10750-013-1442-8> (2013).
- Buffle, J. & Leppard, G. G. Characterization of Aquatic Colloids and Macromolecules. 2. Key Role of Physical Structures on Analytical Results. *Environmental Science & Technology* **29**, 2176–2184, <https://doi.org/10.1021/es00009a005> (1995).
- Maher, W. & Woo, L. Procedures for the storage and digestion of natural waters for the determination of filterable reactive phosphorus, total filterable phosphorus and total phosphorus. *Analytica Chimica Acta* **375**, 5–47, [https://doi.org/10.1016/s0003-2670\(98\)00274-8](https://doi.org/10.1016/s0003-2670(98)00274-8) (1998).
- Olsen, S. *Recent trends in the determination of orthophosphate in water*. (NV Noord-Hollandsche Uitgevers Maatschappij, 1967).
- Boström, B., Andersen, J. M., Fleischer, S. & Jansson, M. Exchange of phosphorus across the sediment-water interface. *Hydrobiologia* **170**, 229–244, <https://doi.org/10.1007/bf00024907> (1988).
- DePinto, J. V., Young, T. C. & Martin, S. C. Algal-Available Phosphorus in Suspended Sediments from Lower Great Lakes Tributaries. *Journal of Great Lakes Research* **7**, 311–325, [https://doi.org/10.1016/s0380-1330\(81\)72059-8](https://doi.org/10.1016/s0380-1330(81)72059-8) (1981).
- Zhang, H., Boegman, L., Scavia, D. & Culver, D. A. Spatial distributions of external and internal phosphorus loads in Lake Erie and their impacts on phytoplankton and water quality. *Journal of Great Lakes Research* **42**, 1212–1227, <https://doi.org/10.1016/j.jglr.2016.09.005> (2016).

16. Søndergaard, M., Jensen, J. P. & Jeppesen, E. Role of sediment and internal loading of phosphorus in shallow lakes. *Hydrobiologia* **506**–509, 135–145, <https://doi.org/10.1023/b:hydr.0000008611.12704.dd> (2003).
17. Davison, W. Iron and manganese in lakes. *Earth-Science Reviews* **34**, 119–163, [https://doi.org/10.1016/0012-8252\(93\)90029-7](https://doi.org/10.1016/0012-8252(93)90029-7) (1993).
18. Imberger, J. & Hamblin, P. F. Dynamics of Lakes, Reservoirs, and Cooling Ponds. *Annual Review of Fluid Mechanics* **14**, 153–187, <https://doi.org/10.1146/annurev.fl.14.010182.001101> (1982).
19. Gao, Y., Cornwell, J. C., Stoecker, D. K. & Owens, M. S. Influence of cyanobacteria blooms on sediment biogeochemistry and nutrient fluxes. *Limnology and Oceanography* **59**, 959–971 (2014).
20. Gao, Y. *et al.* High-resolution imaging of labile phosphorus and its relationship with iron redox state in lake sediments. *Environmental Pollution* **219**, 466–474, <https://doi.org/10.1016/j.envpol.2016.05.053> (2016).
21. Amirbahman, A., Pearce, A. R., Bouchard, R. J., Norton, S. A. & Kahl, J. S. Relationship between hypolimnetic phosphorus and iron release from eleven lakes in Maine, USA. *Biogeochemistry* **65**, 369–386 (2003).
22. Hongve, D. Cycling of iron, manganese, and phosphate in a meromictic lake. *Limnology and Oceanography* **42**, 635–647, <https://doi.org/10.4319/lo.1997.42.4.0635> (1997).
23. Gunnars, A., Blomqvist, S., Johansson, P. & Andersson, C. Formation of Fe(III) oxyhydroxide colloids in freshwater and brackish seawater, with incorporation of phosphate and calcium. *Geochimica et Cosmochimica Acta* **66**, 745–758, [https://doi.org/10.1016/s0016-7037\(01\)00818-3](https://doi.org/10.1016/s0016-7037(01)00818-3) (2002).
24. Mai, T. H. N. *et al.* Adsorption and desorption of arsenic to aquifer sediment on the Red River floodplain at Nam Du, Vietnam. *Geochimica et Cosmochimica Acta* **142**, 587–600, <https://doi.org/10.1016/j.gca.2014.07.014> (2014).
25. Baalousha, M. & Lead, J. R. Characterization of Natural Aquatic Colloids (<5 nm) by Flow-Field Flow Fractionation and Atomic Force Microscopy. *Environmental Science & Technology* **41**, 1111–1117, <https://doi.org/10.1021/es061766n> (2007).
26. Baalousha, M., Manciulea, A., Cumberland, S., Kendall, K. & Lead, J. R. Aggregation and Surface Properties of Iron Oxide Nanoparticles: Influence of pH and Natural Organic Matter. *Environmental Toxicology and Chemistry* **27**, 1875, <https://doi.org/10.1897/07-559.1> (2008).
27. Gustafsson, C. & Gschwend, P. M. Aquatic colloids: Concepts, definitions, and current challenges. *Limnology and Oceanography* **42**, 519–528, <https://doi.org/10.4319/lo.1997.42.3.0519> (1997).
28. Leppard, G. G., Buffle, J., De Vitre, R. R. & Perret, D. Ultrastructure and physical characteristics of a distinctive colloidal iron particulate isolated from a small eutrophic lake. *Archiv fuer Hydrobiologie AHYBA* **4**, 113 (1988).
29. Pizarro, J. *et al.* Coagulation/sedimentation of submicron iron particles in a eutrophic lake. *Water Research* **29**, 617–632, [https://doi.org/10.1016/0043-1354\(94\)00167-6](https://doi.org/10.1016/0043-1354(94)00167-6) (1995).
30. Tipping, E., Woof, C. & Cooke, D. Iron oxide from a seasonally anoxic lake. *Geochimica et Cosmochimica Acta* **45**, 1411–1419, [https://doi.org/10.1016/0016-7037\(81\)90275-1](https://doi.org/10.1016/0016-7037(81)90275-1) (1981).
31. Laxen, D. P. H. & Chandler, I. M. Size distribution of iron and manganese species in freshwaters. *Geochimica et Cosmochimica Acta* **47**, 731–741, [https://doi.org/10.1016/0016-7037\(83\)90107-2](https://doi.org/10.1016/0016-7037(83)90107-2) (1983).
32. Hartland, A., Larsen, J. R., Andersen, M. S., Baalousha, M. & O'Carroll, D. Association of Arsenic and Phosphorus with Iron Nanoparticles between Streams and Aquifers: Implications for Arsenic Mobility. *Environmental Science & Technology* **49**, 14101–14109, <https://doi.org/10.1021/acs.est.5b03506> (2015).
33. Lapworth, D. J., Stolpe, B., Williams, P. J., Goody, D. C. & Lead, J. R. Characterization of Suboxic Groundwater Colloids Using a Multi-method Approach. *Environmental Science & Technology* **47**, 2554–2561, <https://doi.org/10.1021/es3045778> (2013).
34. Darch, T., Blackwell, M. S. A., Hawkins, J. M. B., Haygarth, P. M. & Chadwick, D. A Meta-Analysis of Organic and Inorganic Phosphorus in Organic Fertilizers, Soils, and Water: Implications for Water Quality. *Critical Reviews in Environmental Science and Technology* **44**, 2172–2202, <https://doi.org/10.1080/10643389.2013.790752> (2014).
35. Ding, S. *et al.* *In situ*, high-resolution evidence for iron-coupled mobilization of phosphorus in sediments. Vol. 6 (2016).
36. Rydin, E. *Potentially Mobile Phosphorus in Lake Erken Sediment*. Vol. 34 (2000).
37. Zhang, H. & Davison, W. Diffusional characteristics of hydrogels used in DGT and DET techniques. *Analytica Chimica Acta* **398**, 329–340, [https://doi.org/10.1016/s0003-2670\(99\)00458-4](https://doi.org/10.1016/s0003-2670(99)00458-4) (1999).
38. Davison, W. & Zhang, H. Progress in understanding the use of diffusive gradients in thin films (DGT) – back to basics. *Environmental Chemistry* **9**, 1–13, <https://doi.org/10.1071/EN11084> (2012).
39. Zhang, H. & Davison, W. Use of diffusive gradients in thin-films for studies of chemical speciation and bioavailability. *Environmental Chemistry* **12**, 85, <https://doi.org/10.1071/en14105> (2015).
40. Zhang, C., Ding, S., Xu, D., Tang, Y. & Wong, M. H. Bioavailability assessment of phosphorus and metals in soils and sediments: a review of diffusive gradients in thin films (DGT). *Environmental Monitoring and Assessment* **186**, 7367–7378, <https://doi.org/10.1007/s10661-014-3933-0> (2014).
41. Buffle, J., Wilkinson, K. J., Stoll, S., Filella, M. & Zhang, J. A Generalized Description of Aquatic Colloidal Interactions: The Three-colloidal Component Approach. *Environmental Science & Technology* **32**, 2887–2899, <https://doi.org/10.1021/es980217h> (1998).
42. Hamilton, D. P., O'Brien, K. R., Burford, M. A., Brookes, J. D. & McBride, C. G. Vertical distributions of chlorophyll in deep, warm monomictic lakes. *Aquatic Sciences* **72**, 295–307, <https://doi.org/10.1007/s00027-010-0131-1> (2010).
43. Özkundakci, D., Hamilton, D. & Gibbs, M. *Hypolimnetic phosphorus and nitrogen dynamics in a small, eutrophic lake with a seasonally anoxic hypolimnion*. Vol. 661 (2011).
44. Hartland, A., Andersen, M. S. & Hamilton, D. P. Phosphorus and arsenic distributions in a seasonally stratified, iron- and manganese-rich lake: microbiological and geochemical controls. *Environmental Chemistry* **12**, 708, <https://doi.org/10.1071/en14094> (2015).
45. Zhang, H. & Davison, W. Performance characteristics of diffusion gradients in thin films for the *in situ* measurement of trace metals in aqueous solution. *Analytical chemistry* **67**, 3391–3400 (1995).
46. Fatin-Rouge, N., Starchev, K. & Buffle, J. Size Effects on Diffusion Processes within Agarose Gels. *Biophysical Journal* **86**, 2710–2719, [https://doi.org/10.1016/s0006-3495\(04\)74325-8](https://doi.org/10.1016/s0006-3495(04)74325-8) (2004).
47. Viollier, E., Inglett, P. W., Hunter, K., Roychoudhury, A. N. & Van Cappellen, P. The ferrozine method revisited: Fe(II)/Fe(III) determination in natural waters. *Applied Geochemistry* **15**, 785–790, [https://doi.org/10.1016/s0883-2927\(99\)00097-9](https://doi.org/10.1016/s0883-2927(99)00097-9) (2000).
48. Anastácio, A. S., Harris, B., Yoo, H.-I., Fabris, J. D. & Stucki, J. W. Limitations of the ferrozine method for quantitative assay of mineral systems for ferrous and total iron. *Geochimica et Cosmochimica Acta* **72**, 5001–5008, <https://doi.org/10.1016/j.gca.2008.07.009> (2008).
49. Ting, D.-S. & Appan, A. General characteristics and fractions of phosphorus in aquatic sediments of two tropical reservoirs. *Water Science and Technology* **34**, 53–59, [https://doi.org/10.1016/S0273-1223\(96\)00724-X](https://doi.org/10.1016/S0273-1223(96)00724-X) (1996).
50. Hasselov, M. & von der Kammer, F. Iron Oxides as Geochemical Nanovectors for Metal Transport in Soil-River Systems. *Elements* **4**, 401–406, <https://doi.org/10.2113/gselements.4.6.401> (2008).
51. Hupfer, M., Ruübe, B. & Schmieder, P. Origin and diagenesis of polyphosphate in lake sediments: A <sup>31</sup>PuNMR study. *Limnology and Oceanography* **49**, 1–10, <https://doi.org/10.4319/lo.2004.49.1.0001> (2004).
52. Ståhl-Delbanco, A. & Hansson, L.-A. Effects of bioturbation on recruitment of algal cells from the “seed bank” of lake sediments. *Limnology and Oceanography* **47**, 1836–1843, <https://doi.org/10.4319/lo.2002.47.6.1836> (2002).
53. Mooij, W. M. *et al.* Challenges and opportunities for integrating lake ecosystem modelling approaches. *Aquatic Ecology* **44**, 633–667, <https://doi.org/10.1007/s10452-010-9339-3> (2010).



54. Gottselig, N. *et al.* Phosphorus Binding to Nanoparticles and Colloids in Forest Stream Waters. *Vadose Zone Journal* **16**, 0, <https://doi.org/10.2136/vzj2016.07.0064> (2017).
55. Jiang, X. *et al.* Phosphorus Containing Water Dispersible Nanoparticles in Arable Soil. *Journal of Environment Quality* **44**, 1772, <https://doi.org/10.2134/jeq.2015.02.0085> (2015).
56. Montalvo, D., Degryse, F. & McLaughlin, M. J. Natural Colloidal P and Its Contribution to Plant P Uptake. *Environmental Science & Technology* **49**, 3427–3434, <https://doi.org/10.1021/es504643f> (2015).
57. Zhang, H., Davison, W., Gadi, R. & Kobayashi, T. *In situ* measurement of dissolved phosphorus in natural waters using DGT. *Analytica Chimica Acta* **370**, 29–38, [https://doi.org/10.1016/S0003-2670\(98\)00250-5](https://doi.org/10.1016/S0003-2670(98)00250-5) (1998).
58. Buesseler, K. O. *et al.* An intercomparison of cross-flow filtration techniques used for sampling marine colloids: Overview and organic carbon results. *Marine Chemistry* **55**, 1–31, [https://doi.org/10.1016/S0304-4203\(96\)00046-1](https://doi.org/10.1016/S0304-4203(96)00046-1) (1996).
59. Wen, L.-S., Stordal, M. C., Tang, D., Gill, G. A. & Santschi, P. H. An ultraclean cross-flow ultrafiltration technique for the study of trace metal phase speciation in seawater. *Marine Chemistry* **55**, 129–152, [https://doi.org/10.1016/S0304-4203\(96\)00052-7](https://doi.org/10.1016/S0304-4203(96)00052-7) (1996).
60. Benoit, G. & Rozan, T. F. The influence of size distribution on the particle concentration effect and trace metal partitioning in rivers. *Geochimica et Cosmochimica Acta* **63**, 113–127, [https://doi.org/10.1016/S0016-7037\(98\)00276-2](https://doi.org/10.1016/S0016-7037(98)00276-2) (1999).
61. Baalousha, M. & Lead, J. R. Characterization of natural and manufactured nanoparticles by atomic force microscopy: Effect of analysis mode, environment and sample preparation. *Colloids and Surfaces A: Physicochemical and Engineering Aspects* **419**, 238–247, <https://doi.org/10.1016/j.colsurfa.2012.12.004> (2013).
62. Murphy, J. & Riley, J. P. A modified single solution method for the determination of phosphate in natural waters. *Analytica Chimica Acta* **27**, 31–36, [https://doi.org/10.1016/S0003-2670\(00\)88444-5](https://doi.org/10.1016/S0003-2670(00)88444-5) (1962).
63. APHA. (American Public Health Association Washington, 1998).

## Acknowledgements

We acknowledge the valuable contributions of Prof. Bill Perry in providing training in R, Jackson White for help with preparing graphical illustrations, and the assistance of Andrew Pearson and Chris Eager during field work. We are thankful to the University of Waikato technical staff for their assistance in completing the field work and laboratory analysis. This research was enabled in part by a Rutherford Discovery Fellowship award to AH (RDF-UOW1601) and funding through the Ministry of Business, Innovation and Employment for Enhancing the Health and Resilience of New Zealand Lakes (UOWX1503).

## Author Contributions

H.S. completed all laboratory and fieldwork, created Figures 2, 4, 5 and 6, and co-wrote the manuscript with A.H. who designed the study, co-wrote the manuscript, created Figures 1, 3, 7, 8 and 9 and obtained funding for the research. N.J.L. trained H.S. in manufacture of DGT probes and contributed to the writing of the manuscript. M.B. and M.S. completed TEM and AFM analyses respectively and D.S. assisted in fieldwork sampling design and execution. M.M. and D.H. co-supervised H.S. and contributed to the writing of the manuscript.

## Additional Information

**Supplementary information** accompanies this paper at <https://doi.org/10.1038/s41598-018-36103-x>.

**Competing Interests:** The authors declare no competing interests.

**Publisher's note:** Springer Nature remains neutral with regard to jurisdictional claims in published maps and institutional affiliations.



**Open Access** This article is licensed under a Creative Commons Attribution 4.0 International License, which permits use, sharing, adaptation, distribution and reproduction in any medium or format, as long as you give appropriate credit to the original author(s) and the source, provide a link to the Creative Commons license, and indicate if changes were made. The images or other third party material in this article are included in the article's Creative Commons license, unless indicated otherwise in a credit line to the material. If material is not included in the article's Creative Commons license and your intended use is not permitted by statutory regulation or exceeds the permitted use, you will need to obtain permission directly from the copyright holder. To view a copy of this license, visit <http://creativecommons.org/licenses/by/4.0/>.

© The Author(s) 2018

## Supplementary information

### Regulation of phosphorus bioavailability by iron nanoparticles in a monomictic lake

Saeed, H<sup>1</sup>; Hartland, A<sup>1\*</sup>; Lehto, N<sup>2</sup>; Baalousha, M<sup>3</sup>; Sikder, M<sup>3</sup>; Sandwell, D<sup>1</sup>; Mucalo, M<sup>4</sup>; Hamilton, DP<sup>5</sup>.

#### Addresses

<sup>1</sup>Environmental Research institute, School of Science, Faculty of Science and Engineering, University of Waikato, New Zealand

<sup>2</sup>Dept. of Soil and Physical Sciences, Faculty of Agriculture and Life Sciences, Lincoln University, New Zealand

<sup>3</sup>Center for Environmental Nanoscience and Risk, Department of Environmental Health Sciences, University of South Carolina, Columbia, SC, United States

<sup>4</sup>Chemistry, Faculty of Science and Engineering, University of Waikato, Hamilton, New Zealand

<sup>5</sup>Australian Rivers Institute, Griffith University, Australia

\*Corresponding author: [adam.hartland@waikato.ac.nz](mailto:adam.hartland@waikato.ac.nz)

#### Summary

**Figure S1.** Depth profiles of physicochemical characteristics, different fractions of P and Fe of lake Ngapouri from September 2015 to October 2016.

**Figure S2.** pH of the water column of Lake Ngapouri from September 2015 to October 2016.

**Figure S3.** Temperature profile of Lake Ngapouri based on temperature loggers programmed to collect data every 30 minutes.

**Figure S4.** DGT deployment in the field, probes with black precipitates are from near the bottom of the lake and show the accumulation of metal sulphides.

**Figure S5** Standard curve for the estimation of  $\text{HPO}_4^{2-}$  by the molybdenum blue method.

**Table S1** Test deployment of ferrihydrite DGT probes in 200ppb  $\text{HPO}_4^{2-}$  solution for known time at room temperature

**Table S2** Test deployment of chelex DGT probes in 200 ppb  $\text{HPO}_4^{2-}$  solution for known time at room temperature.

**Figure S6.** Results of Chelex DGT paired measurements during summer stratification.

**Figure S7.** Comparison of Fe (II) measurements by the Ferrozine method, “Fe”, “Fe\_b” and “Fe \_c” represents “in field measurements”, “after bringing to the lab *but* before ultrafiltration” and “after ultrafiltration through 100KDa in the glove box” respectively.

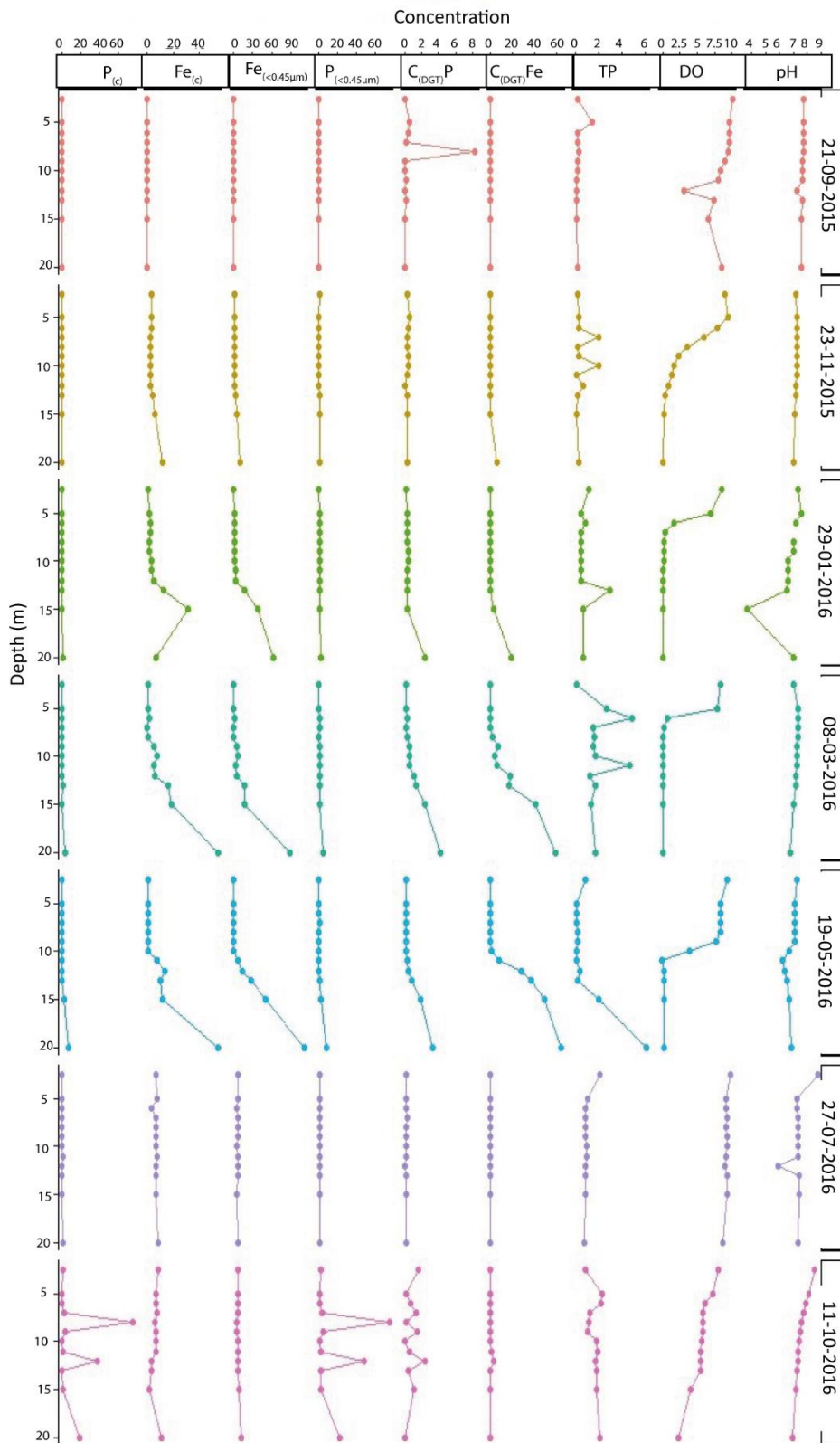


**Figure S3.1: Depth profiles of physicochemical characteristics and different fractions of P and Fe in Lake Ngapouri from September 2015 to October 2016. The concentration values are in  $\mu M L^{-1}$  and depths are in meters.**



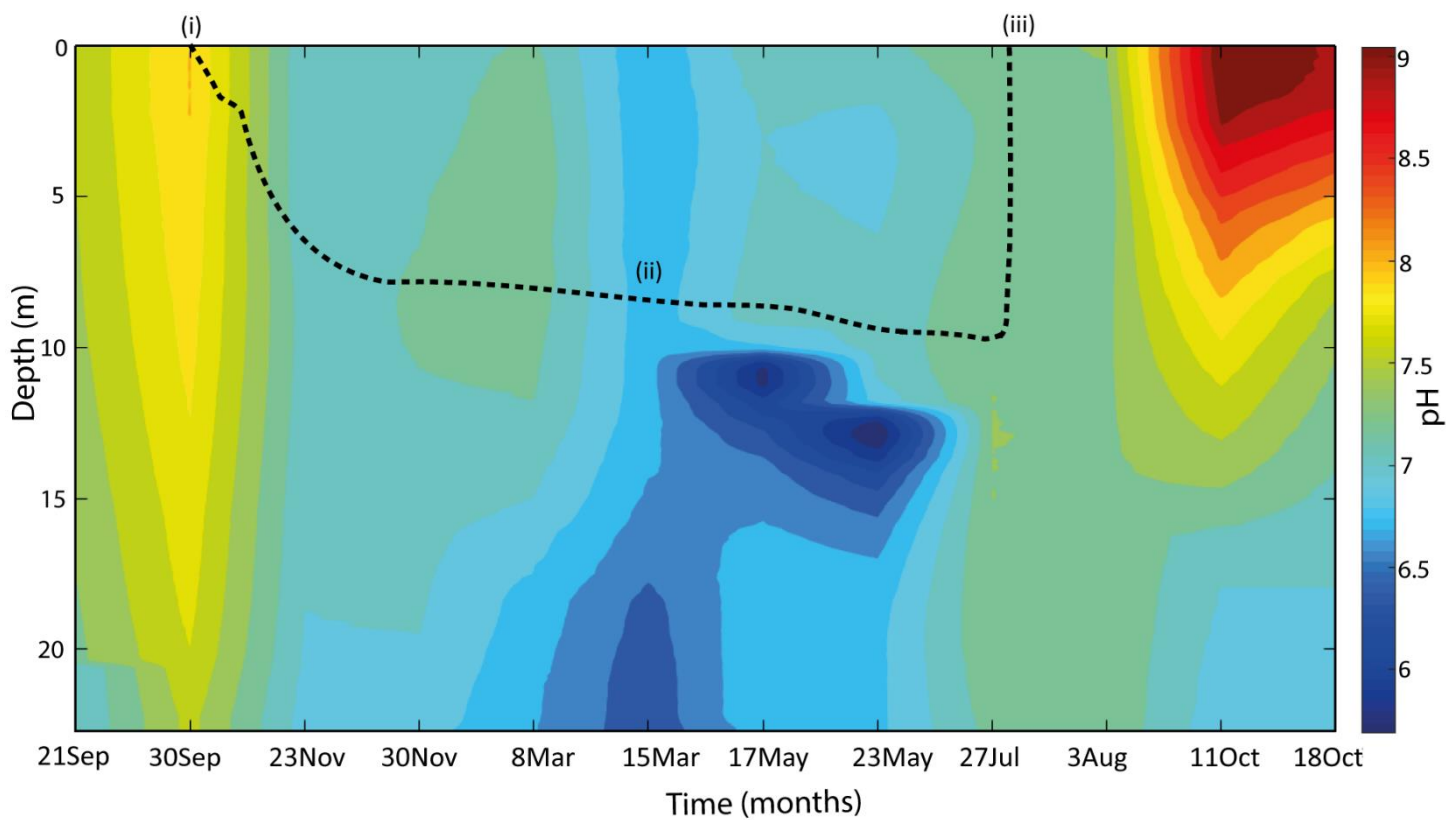


**Figure S3.2: pH of the water column of Lake Ngapouri between September 2015 and October 2016. Data are missing from January 2016 due to a faulty probe. Broken black lines show the timing of the onset (i) and end (iii) of stratified conditions in the lake as well as the approximate position of the thermocline (ii). Data from January 2016 are not included in the plot due to a probe malfunction in this month.**

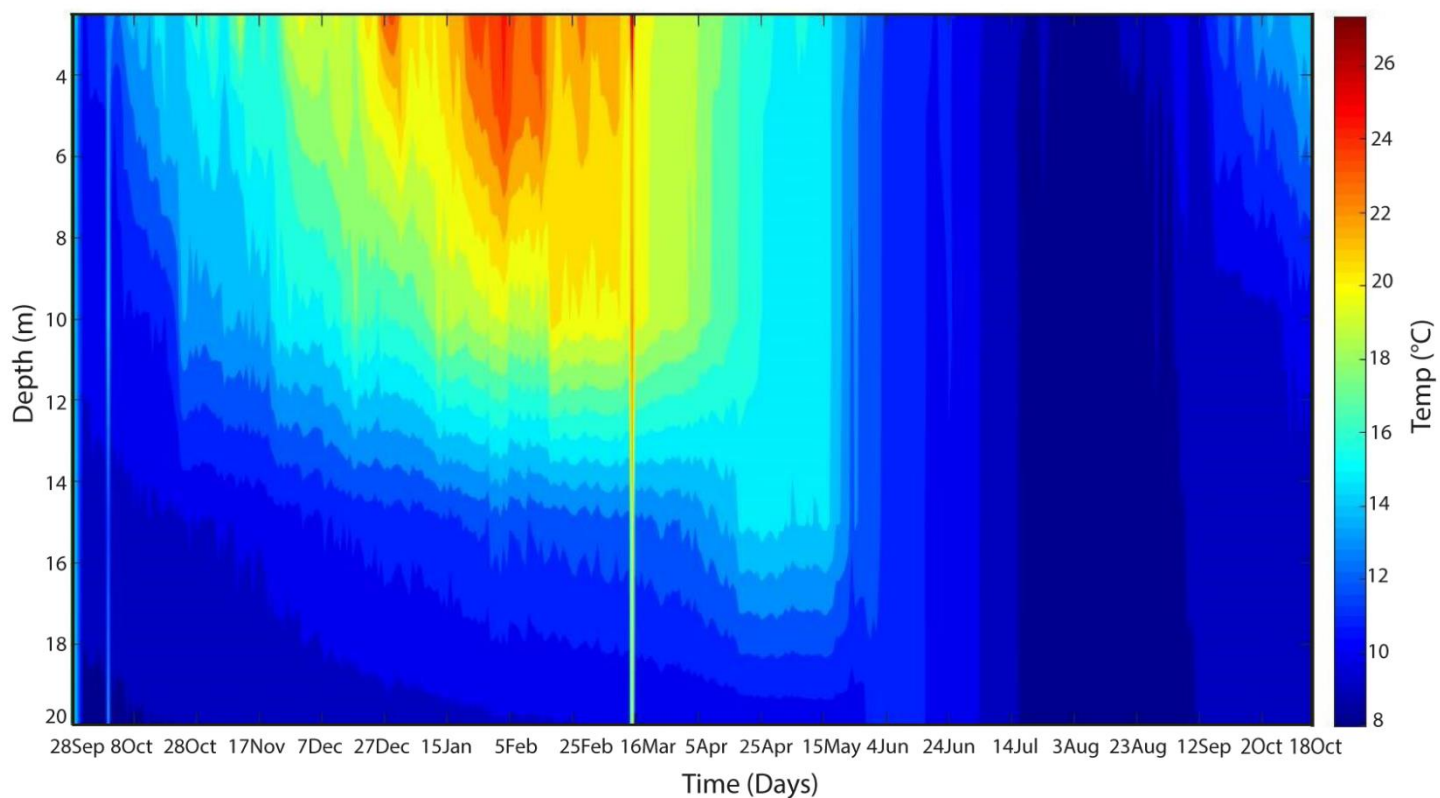


**Figure S3.3: Temperature profile of Lake Ngapouri between September 2015 and October 2016 recorded using Hobo Tidbit temperature loggers programmed to collect data every 30 minutes.**



**Figure S3.4: DGT deployment in the field. DGT probes coated with dark precipitate are from close to the benthic nepheloid layer and provide evidence for the formation of metal sulphides at this depth.**

### Test deployment of DGT probes in a standard solution

The gel solution was prepared by mixing 15% of acrylamide and 0.3% cross linker V/V (from DGT research ltd, Lancaster). A 10% ammonium persulphate (W/V), from now on referred to as “the initiator”, was prepared fresh by dissolving 0.1 g salt to 1 mL of deionised (DI) water. 70  $\mu$ L of initiator was added to 10 mL of gel solution followed by 20  $\mu$ L of TEMED catalyst and was immediately cast between two glass plates separated by sheet styrene spacers and allowed to polymerise at about  $\sim 42\text{--}44^{\circ}\text{C}$ .

The ferrihydrite solution probes were prepared after Zhang *et al* <sup>(1)</sup>. Briefly, to prepare the ferrihydrite slurry, 0.1 M  $\text{Fe}^{3+}$  was titrated with 1M NaOH while stirring vigorously until the pH reached to  $\sim 7$  (never allowed to exceed 7). Ferrihydrite was allowed to settle and the surface water was removed carefully by pipetting. The ferrihydrite slurry was then washed at least three times with deionised water and was stored in dark at  $4^{\circ}\text{C}$  until used. 2 g of this slurry was added to 10 mL of gel solution following the same casting procedure as described earlier.

To prepare chelex gel sheets, 4 g of hydrated Chelex 100 resin in the Na form (Bio-Rad, Australia) was added to 10 mL of gel solution followed by 60  $\mu$ L of initiator and 15  $\mu$ L TEMED, respectively, and cast and polymerised as described in previous paragraphs in this document. All gels were hydrated in deionised water for 24 hrs before use to obtain stable dimensions and remove unreacted reactants or impurities.

To test the precision and accuracy of the ferrihydrite piston probes the assembled probes were immersed in 200 ppb P solution (from here on referred to as the “immersion solution”) prepared by using  $\text{KH}_2\text{PO}_4$  (Merck, Darmstadt, Germany). 3 L of immersion solution was prepared fresh before each deployment and vigorously stirred for at least 90 minutes before immersion of the probes. The DGT probes placed in a holder and placed in the immersion solution and the stirring speed was adjusted to avoid the formation of a vortex. A 10 ml aliquot of immersion solution was collected at the start and end of the test was analysed by the molybdenum blue method for  $\text{PO}_4^{2-}$  concentration.

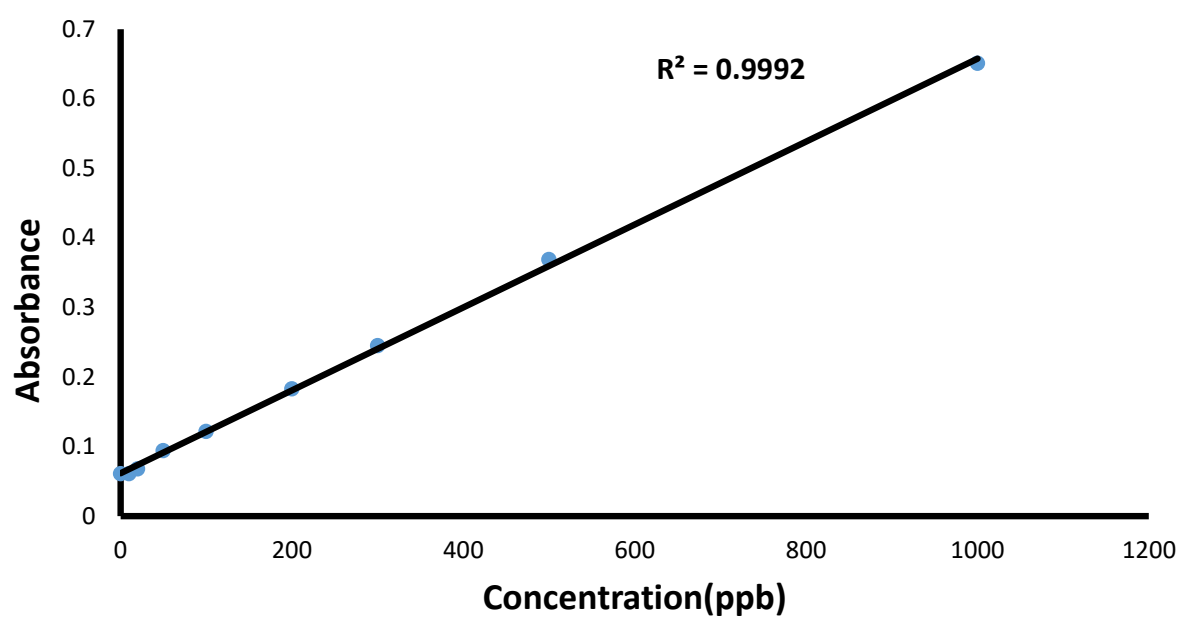


Figure S3.5: Standard curve for the estimation of  $\text{HPO}_4^{2-}$  by the molybdenum blue method.

**Table S3.1: Test deployment of DGT piston probes in 200 ppb  $\text{HPO}_4^{2-}$  solution for a known time at room temperature (22°C).  $\text{Sol}_{(i)}$  and  $\text{Sol}_{(f)}$  represent the initial and final concentrations of P in the deployment solution, respectively. Conc. Is the concentration of P recovered in ferrihydrite elution solution. The initial and final pH of the immersion solution was 6.9 and 6.8 respectively.**

Sample ID	Absorbance	Conc.(ppb)	$C_{\text{DGT}}$ P(ppb)	$t$ (sec)	Temp (°C)	Diffusion coefficient
blank 1	<b>0.008</b>	<b>0</b>				
blank 2	<b>0.01</b>	<b>0</b>				
blank 3	<b>0.009</b>	<b>0</b>				
Probe 1	<b>0.095</b>	<b>132.57</b>	<b>180.59</b>	<b>58500</b>	<b>22</b>	<b>5.57E-06</b>
Probe 2	<b>0.087</b>	<b>121.14</b>	<b>170.62</b>			
Probe 3	<b>0.096</b>	<b>134.00</b>	<b>154.65</b>			
Probe 4	<b>0.092</b>	<b>126.86</b>	<b>162.63</b>			
Probe 5	<b>0.092</b>	<b>126.86</b>	<b>162.63</b>			
Sol. (i)	<b>0.124</b>	<b>174</b>				
Sol. (f)	<b>0.117</b>	<b>164</b>				

Chelex DGT probes for trace metal uptake were tested by immersing five probes in a 200 ppb Cd solution prepared from  $\text{CdCl}_2$ . Probes were deployed for a known time and the temperature was recorded at the beginning and end of the experiment. Aliquots of the initial and final immersion solution was acidified and analysed by ICP-MS. Chelex gels were eluted in 1 M  $\text{HNO}_3$  overnight at room temperature and analysed by ICP-MS.

**Table S3.2: Test deployment of Chelex DGT probes in 200 ppb Cd solution for known time at 22°C. Sol<sub>(i)</sub> and Sol<sub>(f)</sub> represent the initial and final concentrations of Cd in the immersion solution. The immersion solution was stirred for at least 90 minutes before deployment**

Sample ID	Conc.(ppb)	C <sub>DGT</sub> Cd	t (sec)
blank 1	<b>0.22</b>		
blank 2	<b>0.21</b>		
blank 3	<b>0.23</b>		
Probe 1	<b>23.13</b>	<b>236.71</b>	<b>21300</b>
Probe 2	<b>23.89</b>	<b>244.56</b>	
Probe 3	<b>24.79</b>	<b>253.86</b>	
Probe 4	<b>23.83</b>	<b>243.94</b>	
Probe 5	<b>24.56</b>	<b>251.49</b>	
Sol. (i)	<b>260.34</b>		
Sol. (f)	<b>214.04</b>		

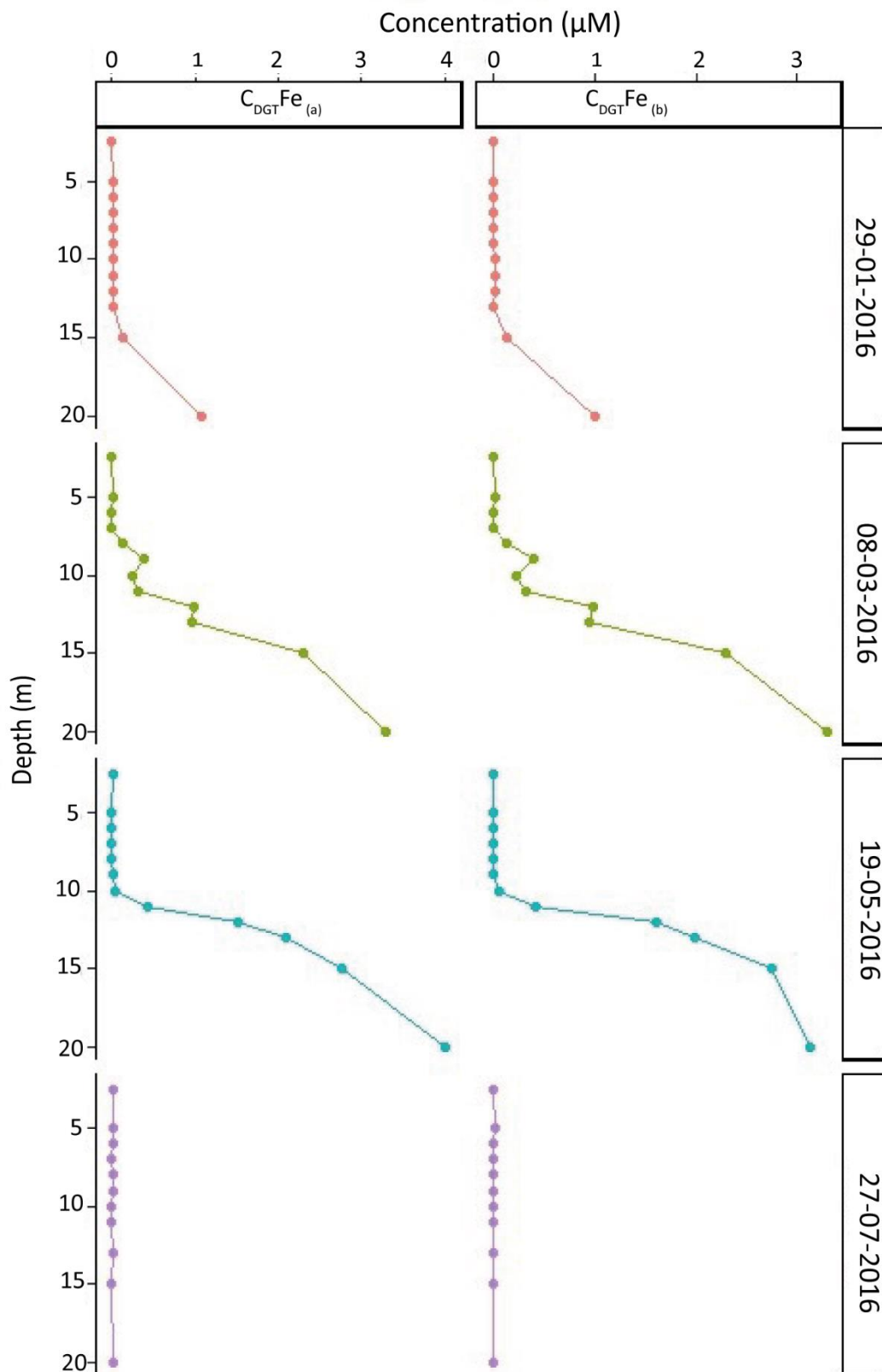
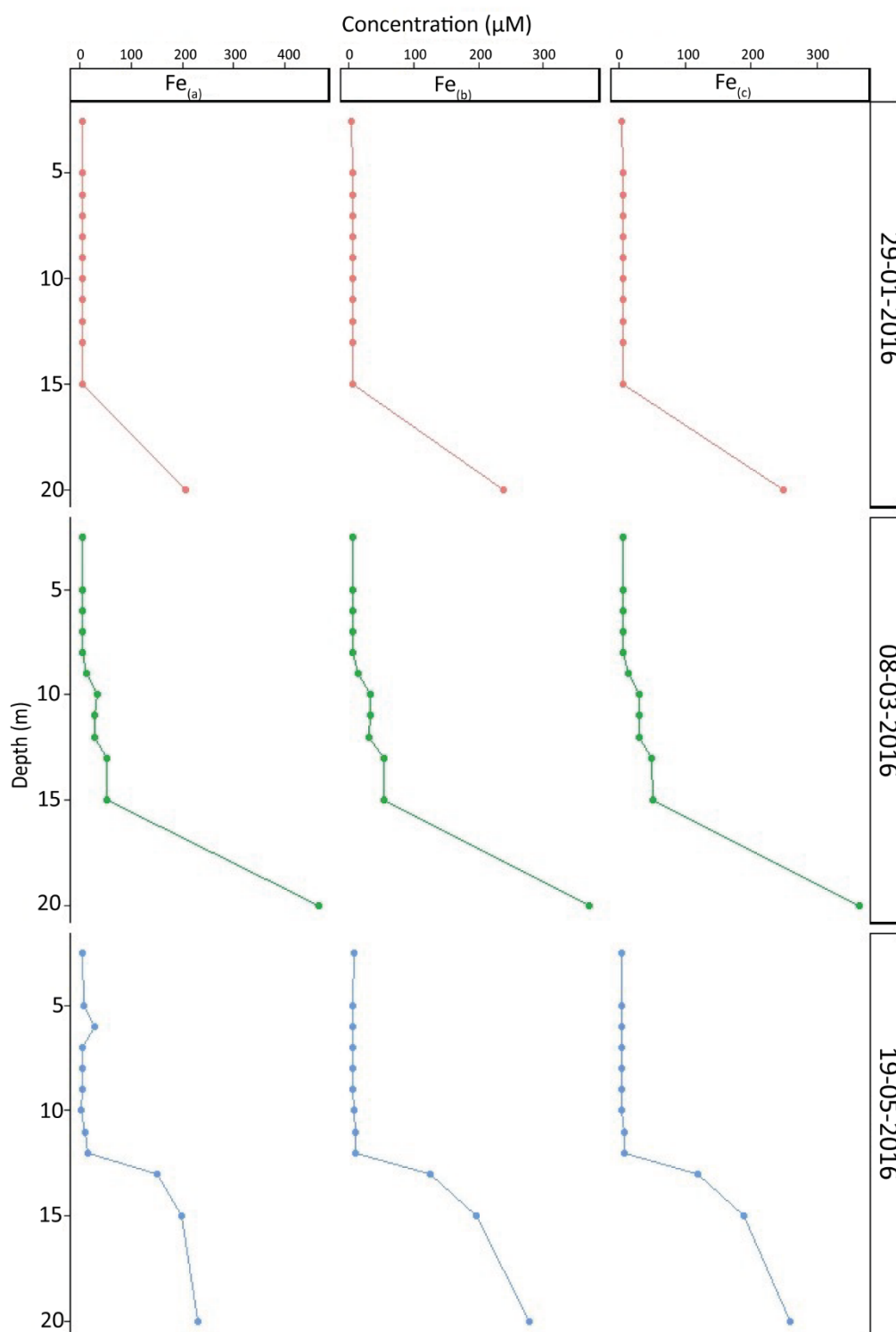


Figure S3.6: Results of  $C_{DGT} \text{ Fe}$  values ( $\mu\text{M}$ ). The probes were deployed in pairs and  $C_{DGT} \text{ Fe}_{(b)}$  represents the results from the probes purged with zero grade  $\text{N}_2$  overnight before deployment. These results highlight the remarkable reproducibility of fine-scale structure in the metal depth profiles measured by DGT.



**Figure S3.7: Comparison of Fe(II) concentrations (μM) determined by the Ferrozine method, “Fe<sub>(a)</sub>”, “Fe<sub>(b)</sub>” and “Fe<sub>(c)</sub>” represent “in field measurements”, “after bringing to the lab *but* before ultrafiltration” and “after ultrafiltration through 100 KDa in the glove box”, respectively.**



## References

1. Zhang H, Davison W, Gadi R, Kobayashi T. In situ measurement of dissolved phosphorus in natural waters using DGT. *Analytica Chimica Acta*. 1998;370(1):29-38.
2. Zhang H, Davison W. Diffusional characteristics of hydrogels used in DGT and DET techniques. *Analytica Chimica Acta*. 1999;398(2):329-40.

# Chapter 4

## Anaerobic lake metabolism favours proteinaceous organic matter

---

Saeed, H<sup>1</sup>✉, Pearson, A<sup>1</sup>, Hamilton, D, P<sup>2</sup>, Hartland, A<sup>1</sup>

<sup>1</sup>Environmental Research Institute, School of Science, The University of Waikato, Private Bag 3105, Hamilton, New Zealand

<sup>2</sup>Australian Rivers Institute, Griffith University, Australia

✉ Corresponding author

List of authors	Institution name	Email
Huma Saeed	Environmental Research Institute, School of Science, The University of Waikato, Private Bag 3105, Hamilton, New Zealand	<a href="mailto:hsaeed@waikato.ac.nz">hsaeed@waikato.ac.nz</a>
Andrew Pearson	Environmental Research Institute, School of Science, The University of Waikato, Private Bag 3105, Hamilton, New Zealand	Andrew.Pearson@esr.cri.nz
David P Hamilton	Australian Rivers Institute, Griffith University, Australia	<a href="mailto:david.p.hamilton@griffith.edu.au">david.p.hamilton@griffith.edu.au</a>
Adam Hartland	Environmental Research Institute, School of Science, The University of Waikato, Private Bag 3105, Hamilton, New Zealand	<a href="mailto:adam.hartland@waikato.ac.nz">adam.hartland@waikato.ac.nz</a>

## Highlights

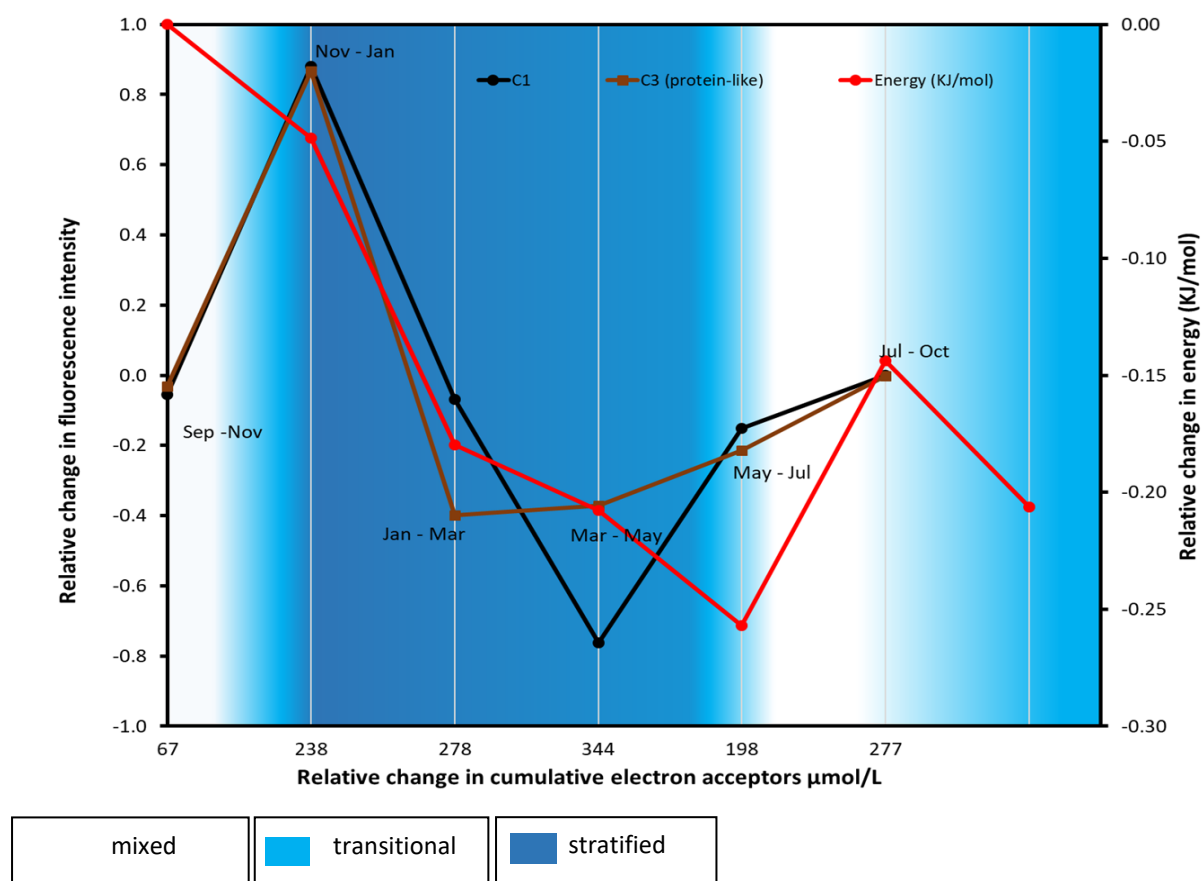
Three fluorophores were identified in two size fractions, comprising humic-like fluorophores and one protein-like fluorophore

The rate of consumption of both humic-like and protein-like fluorophores was similar under aerobic conditions

Protein like fluorophores were more actively degraded in the hypolimnion on the lake under anaerobic conditions

### 4.1 Abstract

The flux of dissolved organic matter (DOM) across the land-water continuum encompasses the production, turnover and storage of huge quantities of organic carbon. In particular, DOM metabolism links to the global carbon cycle by returning CO<sub>2</sub> and CH<sub>4</sub> to the atmosphere and likewise affects water quality and ecological processes locally via the consumption of dissolved oxygen, and a cascading chain of anaerobic redox reactions. Yet, the degree to which qualitative molecular differences in DOM fractions factor into DOM metabolism and associated water quality changes is difficult to ascertain. Therefore, this study addresses the relationship between DOM quality and electron-acceptor turnover in a lake water column, utilising spatially-resolved fluorescence to examine the interplay between DOM composition, concentration and redox processes. Turnover in biomass in Lake Ngapouri, Aotearoa New Zealand, exhibited a pronounced seasonality, with high levels of autochthonous DOM production in the summer. During summer, low molecular weight proteinaceous DOM was ~3.5 times more concentrated than humic DOM and was depleted more rapidly in the deoxygenated hypolimnion under conditions of dissimilatory N, Mn, Fe and S reduction, whereas humic-like DOM was more stable throughout the water column. Our results suggest that protein-rich DOM is more actively cycled under reducing conditions than condensed, aromatic (humic) fractions which are more likely to be preserved as carbon is cycled in lakes. Despite higher levels of primary productivity, eutrophic lake systems may not act as a larger C sink than oligotrophic lakes which have a higher proportion of allochthonous DOM input.



**Graphical Abstract** that shows the relative change in the fluorescence intensities of humic-like and protein-like fluorophores.

**Key words:** dissolved organic matter (DOM), anoxia, iron,  $\text{SUVA}_{254}$ , carbon turnover, lake metabolism, PARAFAC, ANNAMOX

## 4.1 Introduction

The study of dissolved organic matter (DOM) sources, dynamics and transformation mechanisms informs the functioning of ecosystems, from primary productivity, to terminal respiration, and therefore addresses pivotal questions for biologists, geochemists, environmental chemists and ecologists (Hood *et al.*, 2005). DOM is operationally defined as the class of organic compounds that can pass through a 0.45 µm filter membrane (Zsolnay 2003), comprising a complex mixture of heterogeneous low to high molecular weight organic substances and is commonly expressed by its carbon (C) content. Dissolved organic carbon (DOC), can be viewed as an intermediate between biogenic organic matter and the inorganic products of respiration (*i.e.*, CO<sub>2</sub>) generated by heterotrophic microorganisms. DOM/DOC is not conservative in lakes and undergoes transformations which may be affected by differences in the structure of DOM compounds, which may potentially confer a range of bioavailabilities to microbes, and hence individual molecules can be expected to degrade at different rates (Kellerman *et al.*, 2015).

DOM is ubiquitous and is one of the most active materials in natural aquatic environments, being the most common form of organic matter in most lakes (Tranvik *et al.*, 2009). The flux of DOM from terrestrial plants and soils (allochthonous DOM) into aquatic systems is important in terrestrial carbon budgets, representing the largest pool ( $0.6 \times 10^{18}$  g C) of reactive organic carbon at the global cycle ; (Hedges 1992). This pool not only fuels microbial growth but influences water quality in myriad ways. For example, DOM plays an important role in the attenuation of visible and ultraviolet light in lake surface waters (Rae *et al.*, 2001). Similarly, DOM can modify underwater heat transfer and alter lake stratification patterns, which can further affect oxygen availability in stratified waters (Read and Rose 2013). As such, DOM exerts strong controls over alkalinity (Eshleman and Hemond 1985), energy supply (Wetzel 1992), elemental cycling through biogeochemical reactions (Lawlor and Tipping 2003), as well as trace element speciation (Taillefert *et al.* 2000) and transport of metals (McKnight *et al.*, 1992). Indeed, DOM is an important aspect of water quality and several studies have suggested that assessments of water quality (*e.g.*, lake trophic state) should incorporate the nutrient-colour paradigm, which includes fluorescent DOM absorption (Webster *et al.*, 2008; Williamson *et al.*, 1999).

The reactivity and fate of DOM is related to its molecular composition, which is in part dependent on the hydrology of lakes and the prevailing climate (Kellerman *et al.*, 2014; Kellerman *et al.*, 2015). Despite the large amount of information available on DOC, very little is known about within-lake DOM cycling on time scales of ecological significance (Hanson *et al.*, 2011; Kothawala *et al.*, 2014).

Outside of the lake basin, the lateral movement of DOM at the landscape scale can be described via an aquatic continuum, whereby DOM can be transported from upland soils to the open sea, via lakes, rivers, streams and estuaries (Regnier *et al.*, 2013). Along the aquatic continuum, DOM is processed biogeochemically, exported to the atmosphere as CO<sub>2</sub> or CH<sub>4</sub> or stored within sediments (Regnier *et al.*, 2013).

Inland waters comprise 1.3-2.2% of earth's non-oceanic area (Meybeck 1995; Raymond *et al.*, 2013; Wetzel 1990); of which 91.3% is classified as lakes and 8.7% as reservoirs, not including wetlands, the latter being lost at an alarming rate every year (Davidson, 2014). Recent estimates of carbon emission from lakes globally indicate ~0.3-0.6 Pg C yr<sup>-1</sup> as CO<sub>2</sub> (Battin *et al.*, 2009; Downing *et al.*, 2006; Pace 2005; Raymond *et al.*, 2013) and ~0.12 Pg C yr<sup>-1</sup> as CH<sub>4</sub> (DelSontro *et al.*, 2018), with 0.02-0.07 Pg C yr<sup>-1</sup> (Tranvik *et al.*, 2009) to 0.06-0.25 Pg C yr<sup>-1</sup> (Mendonça *et al.*, 2017) stored in lake sediments. Aotearoa, New Zealand has 3820 lakes greater than 1 ha in surface area (Leathwick *et al.*, 2010) representing 1.3 % of New Zealand's total land area, whilst rivers have been estimated to export around twice the global average of DOM ( $4 \pm 1$  Mg C km<sup>-2</sup> yr<sup>-1</sup>, 1994-2006), equivalent to approximately 40% of New Zealand's fossil fuel emissions (Scott *et al.*, 2006). Despite considerable uncertainties, the great majority of allochthonous and autochthonous organic carbon generated from lakes is returned to the atmosphere. Given that only a fraction of lacustrine DOM is stored along the aquatic continuum, there is therefore substantial interest and debate about the role of allochthonous (terrestrial origin) carbon as an energy source (Kortelainen *et al.*, 2006) due to the dominance of humic substances in this DOM pool. Previous work indicates that humic substances are recalcitrant and generally <15% of humic-DOM is available for bacterial growth. However, humic matter can become an important substrate in peat lakes where the influx significantly exceeds autochthonous DOM production (Salonen and Hammar 1986).

Aerobic respiration and photochemical oxidation (Spencer *et al.*, 2009) are the main routes for mineralization of DOM in lakes, but DOM may also be exposed to fluctuating redox

conditions, particularly during thermal stratification. Indeed, the balance between decomposition of DOM and the supply of dissolved oxygen drives redox gradients in lakes (Lau *et al.*, 2017). Hence, DOM both contributes to the redox status of a waterbody, and is, in turn, affected by these changes (*e.g.*, by changes in heterotrophic rates associated with shifts between oxic- anoxic anaerobic- metabolism).

A portion of DOM absorbs light in the UV-visible range and can be reliably measured using optical methods, including fluorescence spectroscopy. (Henderson *et al.*, 2009 ; Fellman *et al.*, 2009; Murphy *et al.*, 2008; Lapworth *et al.*, 2008; Hudson *et al.*, 2007). ( ) Fluorescence is experimentally simple to use and can readily distinguish certain classes of organic matter (Baker and Lamont-Black 2001; Chen *et al.*, 2003; Rhymes *et al.*, 2015; Senesi *et al.*, 1991; Yamashita and Tanoue 2003). Recent developments in the technique allow for generation of high resolution 3D excitation emission matrices (EEMs) which further aid in discriminating sources and transformation processes (Baker and Lamont-Black 2001; Birdwell and Engel 2010; Chen *et al.*, 2003).

While oxygen consumption is a widely used tool in lake metabolism studies (Hartnett *et al.*, 1998; Kristensen 2000b), O<sub>2</sub> variations do not inform the rate and magnitude of mineralization of organic matter during thermal stratification, as DOM mineralization can be coupled with dissimilatory reduction of N, Mn, Fe and S. In this work, we examine the production and degradation of DOM in a monomictic lake using a combination of size-fractionation (ultrafiltration), fluorescence spectroscopy and geochemical analysis of dissolved electron acceptors. Using highly spatially resolved sampling, we ask how DOM production and degradation relates to changes in nutrient availability (via primary production) and electron acceptors (degradation coupled to anaerobic metabolism), and the implications for lake biogeochemistry and C cycling. The specific goals of the study were (1) to characterize the evolution of DOM in the lake water column, (2) understand DOM turnover processes and relevant environmental controls, and (3) trace the production and removal of DOM in various size fractions at the seasonal time scale.

## 4.2 Methods

### 4.2.1 Lake description and thermal regime

Lake Ngapouri is a small lake (0.19 km<sup>2</sup>) with a maximum depth of 24.5 m. It is situated in the Taupo volcanic zone of the North Island, Aotearoa New Zealand and exhibits stable thermal stratification for approximately nine months per year, interspersed with a period of mixing during the austral winter (July-September). The sampling campaign started in September 2015 (austral spring) just before the establishment of thermal stratification. For more site information see Hartland *et al.* 2015 and Saeed *et al.* 2018).

The pH, conductivity, temperature and dissolved oxygen concentration of the water column was measured every second month using a Sea-Bird Electronics 19 plus SEACAT conductivity, temperature, depth profiler (CTD; Sea-Bird Electronics Inc., Washington). In the present study, ambient air temperature and rain data were downloaded from three weather stations in the area maintained by the National Institute of Water and Atmospheric Sciences (NIWA).

The depth of the thermocline was calculated using a method described by Hamilton *et al.* (2010). Briefly, the water column was considered fully mixed for  $dT/dz > -0.225\text{ }^{\circ}\text{C m}^{-1}$ , where  $dT$  is the temperature gradient and  $dz$  is the depth of water column increasing downwards.

### 4.2.2 Cleaning protocol

Low-density polyethylene sampling bottles were rigorously cleaned prior to sample collection by soaking in trace element free detergent CITRANOX® (Merck, Auckland) overnight followed by a triplicate deionized (DI) water rinse followed by a 10 % reagent grade HCl bath (> 72 hrs), and 10 % reagent grade HNO<sub>3</sub> bath (> 72 h) and a final triple DI rinse. The bottles were then air dried in a clean room and placed in double plastic bags for transportation to the field. All sampling equipment including the ultrafiltration unit was cleaned using the same protocol.

### 4.2.3 Water sampling

The water samples were collected using a horizontally positioned Van Dorn sampler (PVC Beta™, Envco, Auckland) and transferred to the pre-cleaned bottles. Samples were collected from 2.5 m and at 1 m intervals from 5 to 15 m and from a depth of 20 m for analysis of major electron acceptors, DOM, NO<sub>3</sub><sup>-</sup> and NH<sub>4</sub><sup>+</sup> concentrations.



Dissolved fractions were separated on-site using 0.45 µm cellulose acetate syringe filters (Sartorius Stedim, Göttingen, Germany) (fraction henceforth referred to as high molecular weight (HMW)) during sixteen field campaigns from September 2015 to October 2016. Syringe filters were used to keep the filtration step quick and minimise changes associated with oxidation. Samples for iron (Fe) and manganese (Mn) analysis were preserved in-field using ultrapure HNO<sub>3</sub> to 2% final acid concentration.

Samples for DOM concentration and characterization were also filtered on site. Sample bottles were individually wrapped in aluminium foil to avoid photobleaching, then frozen prior to analysis for total organic carbon (TOC). Syringe-filtered water samples collected for NO<sub>3</sub><sup>-</sup> and NH<sub>4</sub><sup>+</sup> concentrations were frozen upon return to the lab and were kept frozen until analysis. Unfiltered water samples for further in-lab size fractionation were collected in airtight plastic syringes from the same depths and similarly protected from light-induced reactions.

All sample tubes and air-tight syringes were kept in plastic double bags and placed on ice in the dark for transportation to the laboratory. In the lab, samples were either preserved as previously mentioned above or processed as detailed in the following section(s).

#### **4.2.4 Sample fractionation by ultrafiltration**

Water samples held in gas tight syringes were transferred to a glove box pre-purged with zero grade N<sub>2</sub> (Saeed *et al.*, 2018) and equipped with a stirred cell ultrafiltration system (Amicon<sup>R</sup>, model 8400, Merck, North Shore City, New Zealand). Stirred-cell ultrafiltration was carried out under N<sub>2</sub> (5 Bar) using 100 kDa (~ 5 nm) (molecular weight cut-off (MWCO)) regenerated cellulose ultrafiltration discs (Millipore Corporation, Billerica, MA, USA) (Hartland *et al.*, 2011). This fraction is henceforth referred to as low molecular weight (LMW). To minimise contamination of the subsequent sample, 20 mL of DI water was ultrafiltered between samples. The filtered water samples for trace element analysis were preserved using ultrapure HNO<sub>3</sub> to 2 % final acid concentration.

#### **4.2.5 DOC analysis**

Water samples were thawed and brought to room temperature (22 °C) in a water bath immediately before analysis. Dissolved organic carbon (DOC) content was determined with

an OI Analytical TOC analyser (OI Analytical, USA) using a persulfate oxidation method (Bisutti *et al.*, 2004; Hartland *et al.*, 2012; Urbansky 2001). All glassware used during analysis was cleaned as described in the “cleaning protocol” section. Instrument performance and calibration was monitored using calibration standards (0, 5, 10, 20 and 50 ppm organic carbon) prepared gravimetrically from sodium hydrogen phthalate. The samples were analysed in triplicate.

#### **4.2.6 Estimation of Fe<sup>2+</sup>**

Fe<sup>2+</sup> concentration was determined on-shore within 30 minutes of sample collection using the Ferrozine method from water collected in gas-tight syringes, which was kept on ice in the dark to minimise oxidation (Saeed *et al.*, 2018). See Bonneville and Viollier *et al.*, and Saeed *et al.*, for detection limit, sensitivity and other method details (Bonneville *et al.*, 2004; Saeed *et al.*, 2018; Viollier *et al.*, 2000).

#### **4.2.7 Determination of DOM optical properties**

##### **4.2.7.1 Fluorescence excitation emission matrix (EEM) analysis**

The fluorescence spectra of filtered samples from both HMW and LMW fractions were determined at room temperature (22 °C) in pre-cleaned quartz cuvette (1 cm path length) using an Aqualog spectrometer (Horiba instruments, New Jersey, USA) equipped with a Xenon lamp, CCD detector and double grating monochromator. To obtain EEMs for each sample, the excitation wavelengths were incremented from 240-600 nm at 5 nm intervals at 0.5 s integration time. For each excitation wavelength, fluorescence emission was measured from 300-650 nm. To avoid photo bleaching, the samples were scanned from low to high-energy wavelengths (600 to 240 nm) to reduce sample exposure to high energy photons during the excitation process. DI water samples were run after every five samples as a blank. Collected spectra were blank-subtracted and corrected for inner filter effects before normalization to the peak intensity of Raman scattering in the water blank (Murphy *et al.*, 2013). Fluorescence data are thus reported in Raman-normalized units.

##### **4.2.7.2 DOC absorption measurements**

Absorbance at 254 nm (UV<sub>254</sub>) was acquired using a quartz cuvette (1 cm path length) in a CARY 100 scan UV-Visible spectrophotometer (Agilent Technologies, NZ). SUVA<sub>254</sub> values

were then calculated using the following equation, with values reported in units of L mg<sup>-1</sup> C<sup>-1</sup> m<sup>-1</sup>.

$$SUVA_{254} = \left( \frac{UV \text{ absorption at } 254 \text{ nm}}{DOC} \right) * 100 \quad (4-1)$$

#### . Inorganic analysis

The water samples from both filtered fractions were analysed for Fe, Mn and S concentrations using a Perkin Elmer (Waltham MA) quadrupole ICP-MS. Certified reference material and internal standards of known concentration were used to calibrate and determine the internal drift of the instrument. The samples were also analysed for nitrate-N (NO<sub>3</sub><sup>-</sup>-N) and ammonium-N (NH<sub>4</sub><sup>+</sup>-N) concentrations on a Lachat QuickChem Flow injection analyser (Zellweger Analytics Inc.). DI water was used as a blank and a range of standards were prepared in DI water to correct for internal drift in the instrument.

#### 4.2.8 Parallel factor analysis (PARAFAC)

PARAFAC was carried out in MATLAB R2016b using the N-way toolbox at default numerical settings (Bro 1997). PARAFAC is a multivariate modelling technique, which allows decomposition of the combined fluorescence signature of DOM into individual, distinct modelled components (Cory and McKnight 2005; Jaffé *et al.*, 2014; Murphy *et al.*, 2013). . See Stedmon *et al.*, (2003) for further details on this method. PARAFAC components provide information about the origin, composition and relative distribution of each component to the total DOM fluorescence signal, when considered in the context of a suitable reference sample set (Baker and Lamont-Black 2001; Borisover *et al.*, 2009).

To validate the appropriate number of PARAFAC components, a split validation method was used whereby the data were randomly split into two halves and a PARAFAC model was obtained for each half, independently. The excitation emission loadings were then compared to check similarity. The results showed a strong agreement between excitation and emission of the randomly divided dataset. A three-component model was developed to explain fluorescence variations between EEMs, and the modelled component spectra were collected.

#### 4.2.9 Statistical analysis

Principle component analysis (PCA) was carried out to identify the drivers of DOM turnover. The PCA analysis included output from PARAFAC modelling (components), DOC and electron acceptor concentrations from both size fractions. The significance of correlations between variables was determined using Pearson's Correlation analysis ( $p < 0.05$ ) in Origin 2016 (OriginLab Corporation, Northampton, MA, USA).

#### 4.2.10 Calculations

The summed consumption of electron acceptors was calculated using coefficients from the half-reactions for Fe, Mn and  $\text{SO}_4^{2-}$  reduction. (Hartland *et al.*, 2015; Stumm and Morgan 1996):

$$\Sigma_{e^-} = ((\Delta[\text{Fe}^{3+}] * 1) + (\Delta[\text{Mn}^{2+}] * 2) + (\Delta[-\text{SO}_4^{2-}] * 8)) \quad (4-2)$$

where each component represents the molar concentration consumed in the corresponding half reaction. While the products of  $\text{Fe}^{3+}$  and  $\text{Mn}^{4+}$  reduction were measured directly,  $\text{S}^{6+}$  reduction products were inferred on the basis of the loss of  $\text{SO}_4^{2-}$ .  $\text{NO}_3^-$  was not included in the calculation of  $\Sigma_{e^-}$  because of its low concentration. Electron acceptor concentrations were averaged for the calculation of changing hypolimnetic concentrations.

The relative change in component concentrations was calculated as:

$$[\Delta C] = C_{(i)} - C_{(f)} \quad (4-3)$$

where  $C_{(i)}$  and  $C_{(f)}$  is the initial and final concentration of any given analyte, with the final concentration at the end of the time step becoming the initial concentration for the subsequent time-step.

The HMW fraction of each analyte was calculated using the following equation:

$$C_{\text{HMW}} = C_{<0.45 \mu\text{m}} - C_{<5 \text{ nm}} \quad (4-4)$$

where  $C_{<0.45 \mu\text{m}}$  and  $C_{<5 \text{ nm}}$  is the concentration of a given analyte in water filtered through 0.45  $\mu\text{m}$  and 100 KDa (MWCO) pore sizes, respectively.

## 4.3 Results

### 4.3.1 DOM fluorescence characteristics

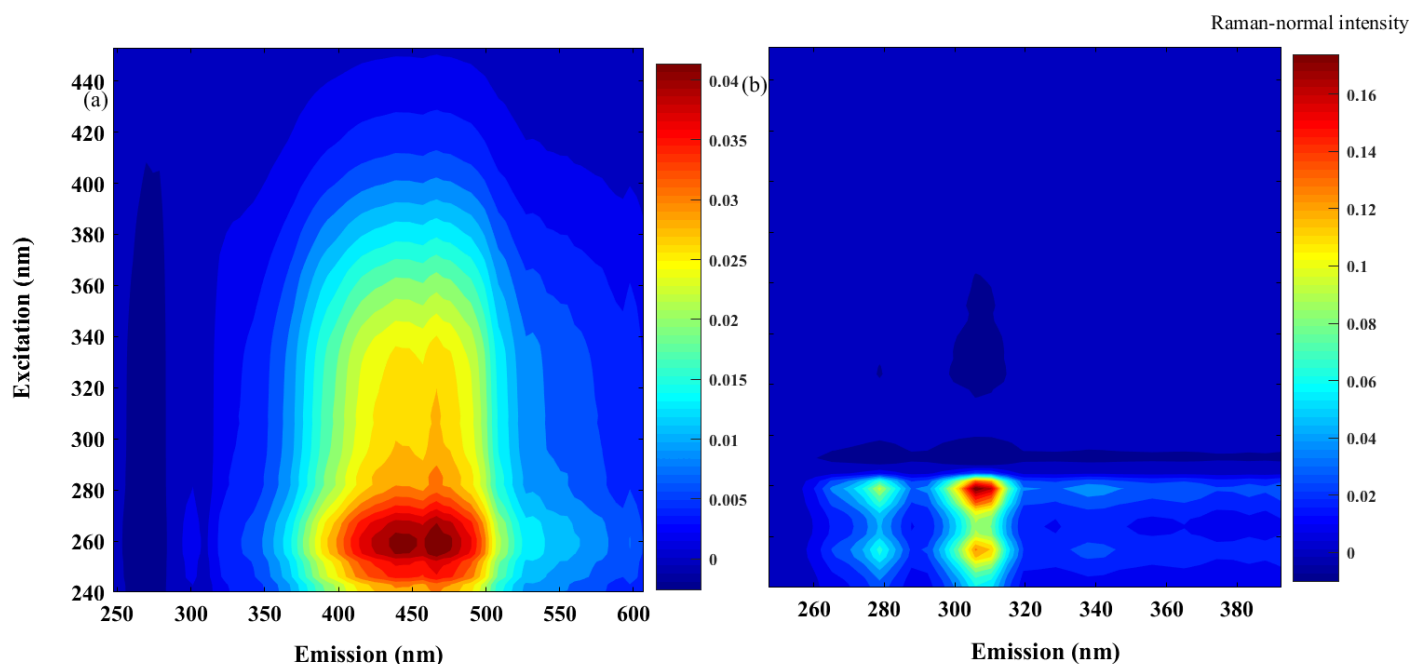


**Figure 4.1: Excitation emission matrix (EEM) plots of PARAFAC components C1 (a), corresponding to aromatic organic acids in the humic-like range, and C3 (b) showing protein-like components exhibiting fluorescence characteristic of tryptophan and tyrosine.**

In this study, three fluorescent components were validated using PARAFAC Fluorescence intensities of the three components are shown in Supplementary Information (Figure S1). PARAFAC component 1 (henceforth referred to as C1) had two distinct excitation maxima,  $\lambda_{\text{max}}$  at 258 and 261 nm, corresponding to an emission maximum of 467 nm (Figure 4.1a).

PARAFAC component 2 (C2) exhibited peak emission at 440 nm (excitation in the range 240-320 nm), overlapping with the fluorescence emission of C1. Hence, these two components represent similar fluorophores but with some differentiation based on  $\lambda_{\text{max}}$  (C2 being blue-shifted relative to C1). For clarity, we discuss C1 in the main text, but it should be recognised that both fluorophores *i.e.*, C1 and C2 are broadly equivalent and certainly responded spatio-temporally in an entirely consistent manner.

PARAFAC Component 3 (henceforth referred to as C3) was characterized by peaks at excitation of ~280 nm and emission at ~300 nm (Figure 4.1). C3 was clearly distinct from C1 and C2 both in spectral shape and wavelength range. Based on the relative fluorescence intensities of the PARAFAC components in the water samples, the concentration of C3 was ~4 times higher than C1 in Lake Ngapouri (Figure 4.1b). The range of these variables is shown in Figure 4.1.

#### **4.3.2 Physical characteristics of the lake**

Ambient air temperature and rainfall data for the local area during the study (Figure 4.2a) were typical of the temperate regional climate, with moderate variations in air temperature over the year and evenly-distributed rainfall. Surface water temperature (Figure 4.2b) ranged between 9 and 23°C during the study period. The water column was well mixed in winter, (no obvious vertical thermal gradient) and stratification began in early October, becoming established as summer progressed, and lasting until autumn (July). Stratification vertically divided the water column into three distinct zones, comprising an isothermal epilimnion (surface to 5 m), metalimnion (5 to 13 m (Figure 4.2b)), and cooler hypolimnion (15 to 20 m). The epilimnion stayed oxygenated throughout the study period (Figure S3a), with the thermocline deepening as summer progressed. Dissolved oxygen in the isolated waters of the hypolimnion rapidly dropped from 8.5 mg L<sup>-1</sup> to 0.07 mg L<sup>-1</sup> in March with the establishment of stratified conditions (Figure S4.3a).

**Table 4.1: PARAFAC component scores and corresponding emission wavelengths of maximum fluorescence ( $\lambda_{\max}$ ) and maximum fluorescence intensity ( $FI_{\max}$ ). Fluorophore designation determined from the literature. RU = Raman-normalised intensity units**

PARAFAC Component	$\lambda_{\max}$ (nm) (Ex/Em)	$FI_{\max}$ (RU)	Peak ID/type
1	261(258)/467	0.043	A, C <sub>2</sub> , M/ Humic-like <sup>1</sup>
2	240/440	0.103	A,C <sub>2</sub> , <sup>1,2,3,4</sup>
3	279/305 280/310	0.183 0.071	T, Tryptophan-like <sup>1</sup> B, Tyrosine-like <sup>1,5</sup>

<sup>1</sup>. (Coble 1996)

<sup>2</sup>. (Stedmon *et al.* 2003)

<sup>3</sup>. (Stedmon and Markager 2005; Williams *et al.* 2010)

<sup>4</sup>. (Yamashita and Jaffé 2008)

<sup>5</sup>. (Murphy *et al.* 2008)

### 4.3.3 Seasonal changes in DOC and fluorescence

Lake water samples revealed that variations in the concentration of DOC as a function of depth were less pronounced than seasonal changes in both size fractions (Figure 4.2c-d Sep 2015, and Jun-Oct 2016). At the onset of summer stratification, DOC concentrations increased in both fractions with increasing depth in the lake (Figure 4.2c-d) with vertical variations consistent with the development of thermal stratification. DOC showed considerable variability in both fractions around the region of the metalimnion, with clear peaks for LMW DOC between December and May. LMW DOC accumulated in the epilimnion during stratification, being redistributed through the water column during winter. Markedly reduced concentrations of LMW DOC were observed in the hypolimnion during peak stratification. In March 2016, when stratification had persisted for some months, there was a rapid loss of the LMW DOC fraction (Figure 4.2c) in the metalimnion and upper hypolimnion, accompanied by a transient increase in the HMW fraction (Figure 4.2d, Jan - Mar).

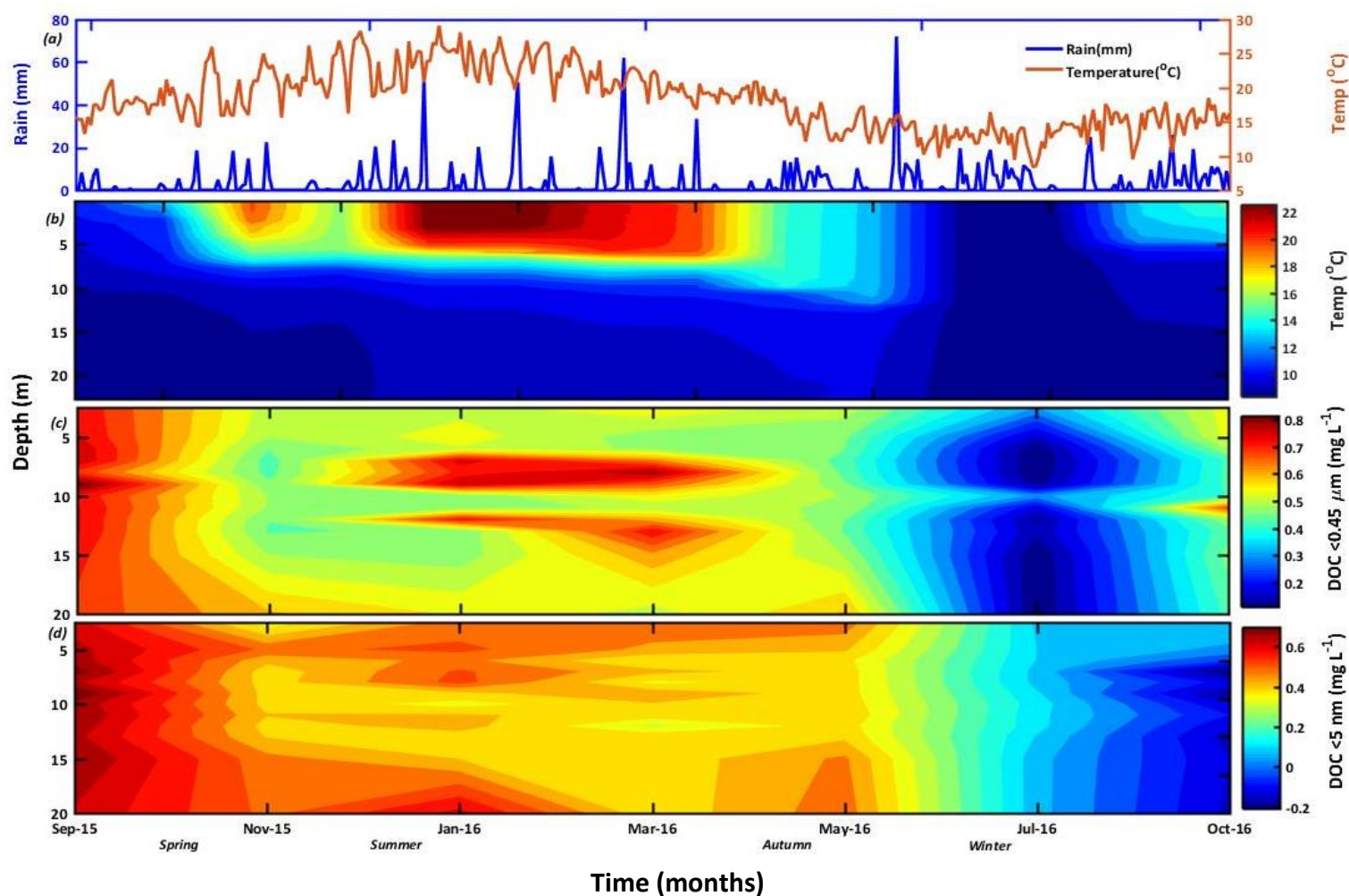


**Figure 4.2:** Time series of physical parameters and dissolved organic carbon in both LMW (< 5 nm) and HMW (> 0.45  $\mu\text{m}$ ) fractions. (a) Air temperature and rainfall data retrieved from the National Climate database (CliFlo database) maintained by National Institute of Water and Atmospheric Science (NIWA), (b) water column temperature ( $^{\circ}\text{C}$ ), (c) HMW DOC concentration and (d) LMW DOC concentrations. Data in panel b were collected using a CTD. The DOC data are scaled to  $\log_{10}$  to allow clear depiction of key trends.

SUVA<sub>254</sub> values were generally higher in the LMW fraction (Figure S4.2), with the SUVA<sub>254</sub> signal in both fractions increasing in the near benthic nepheloid layer during March (stable thermal stratification), coincident with relatively high Fe(II) concentrations (Figure S4.2). The highest value of Fe(II) (2.62  $\text{mg L}^{-1}$ ) coincided with the benthic nepheloid layer during March, coincident with the increased SUVA<sub>254</sub> signal. Indeed, both determinands were highly correlated, across all fractions ( $r^2 = 0.94$  to  $0.99$ ,  $p < 0.01$ ) Hypolimnetic concentrations of HMW Fe and LMW Fe ranged between 80 and 110  $\text{mg L}^{-1}$ . Fe(II) concentration was negligible



during winter isothermal conditions, while Fe  $<0.45 \mu\text{m}$  (mainly present as Fe(III), (Saeed *et al.*, 2018) was  $11.62 \text{ mg L}^{-1}$  at this time. Fe concentrations remained significantly correlated to  $\text{SUVA}_{254}$  ( $r^2 = 0.52$ ,  $p < 0.01$ ) during winter.

$\text{SUVA}_{254}$  values in the LMW fraction were higher than the HMW fraction and were unrelated to Fe concentrations in the same fraction or with the HMW Fe ( $p > 0.05$ ).

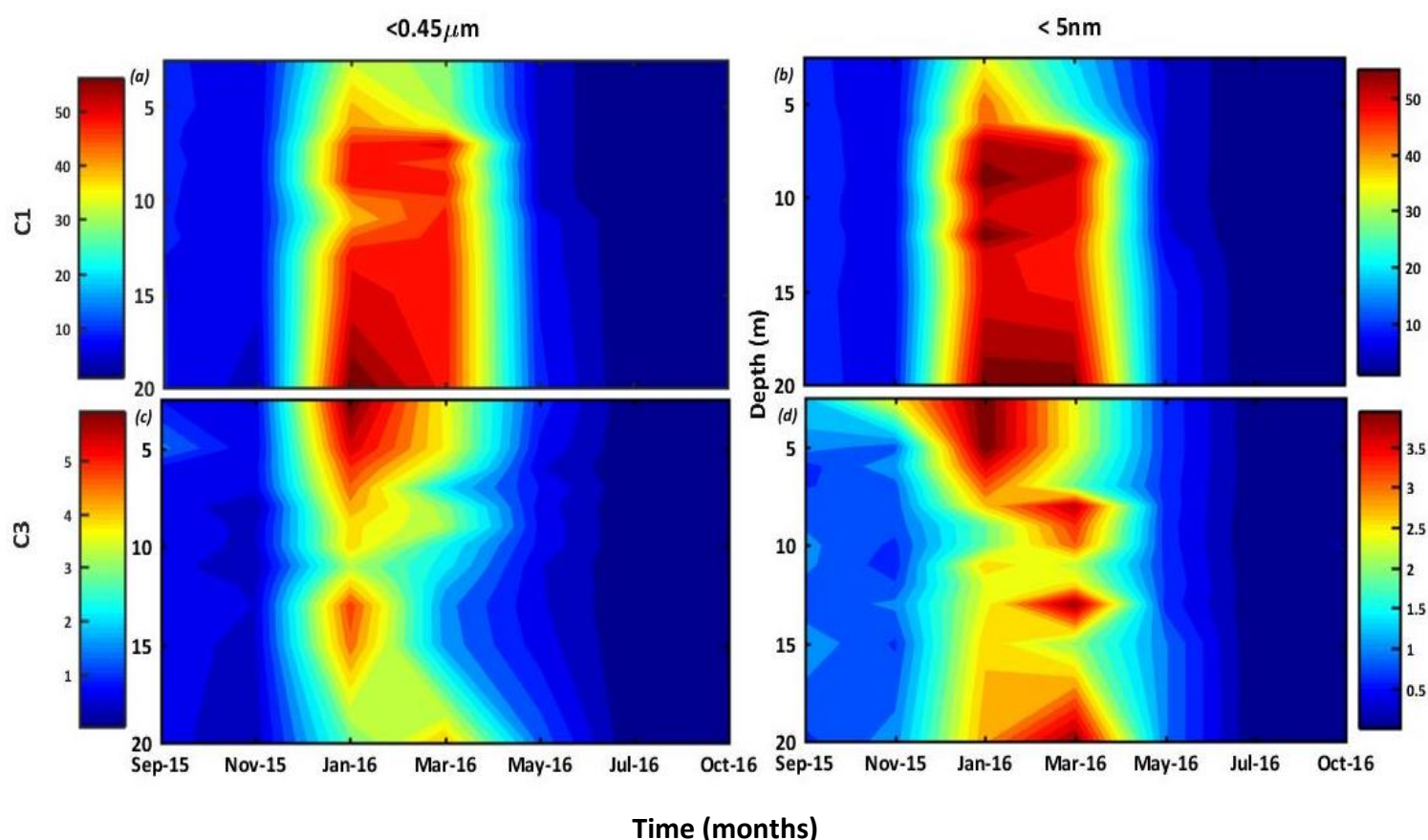


**Figure 4.3: Time series of fluorescent DOM fractions in the water column determined by PARAFAC modelling. (a) Humic-like C1 HMW fraction, (b) C1 LMW fraction, (c) protein-like C3 HMW fraction, (d) C3 LMW fraction.**

The fluorescence intensities of humic-like and protein-like substances ranged from 0.02 to 0.10 and 0.01 to 0.18 (Raman-normalised units). The  $\text{FI}_{(\text{max})}$  value for protein-like substances was markedly higher than that of humic-like fluorophores during the study period (Table 4.1), consistent with an ratio of autochthonous:allochthonous DOM of 4:1

The molecular weight and spatio temporal distributions of both fluorophores in the lake (Figure 4.3) suggest that HMW humic-like fluorescence (C1) (Figure 4.3a) was uniformly high in summer and rapidly reduced by winter mixing (Figure 4.3a). HMW protein-like substances

by contrast, showed broadly the same pattern of summer build-up (Figure 4.3c), but reflected mainly change in LMW molecules. In addition, both fluorophores in the LMW fraction tracked the distribution of the HMW fraction, indicating that both humic and proteinaceous material were sourced from within-lake production or were mobilised from bed sediments.

#### 4.3.4 Anaerobic metabolism and the concentration of electron acceptors

In the deoxygenated hypolimnion, the products of reduction of alternate electron acceptors (i.e. Mn(II), Fe(II), H<sub>2</sub>S) built up throughout the summer (Figure 4.4 a). Broadly, this process followed the most common order of electron acceptor consumption defined by the hierarchy of Gibbs free energy changes of reaction ( $\Delta G$ ), i.e., DO, NO<sub>3</sub><sup>-</sup>, Mn(IV), Fe(III), S(VI) (Stumm and Morgan 1996) (Figure S3).

In spring (November), the concentration of NO<sub>3</sub><sup>-</sup> increased in the surface mixed layer (Figure S4.3b) coinciding with depletion in NH<sub>4</sub><sup>+</sup> (Figure S4.3c). Simultaneously, NH<sub>4</sub><sup>+</sup> concentration increased near benthic nepheloid layer, but was lost again upon winter mixing (Figure S4.3c). Following loss of NO<sub>3</sub><sup>-</sup>, a chain of reactions occurred linking inorganic electron acceptors to organic biomass oxidation (equation on Figure S4.3). Firstly, Mn, then Fe, increased sequentially near the benthic nepheloid layer, with Fe concentrations quickly exceeding Mn. The vertical migration of Mn extended higher than Fe as redox conditions deepened in the hypolimnion (Figure S4.3 (d-e), possibly due to slower oxidation kinetics of Mn<sup>2+</sup>, or stronger biological assimilation of Fe. The seasonal variation of SO<sub>4</sub><sup>2-</sup> concentration suggests that SO<sub>4</sub><sup>2-</sup> reduction in the hypolimnion (Figure S4.3 (d)) followed in sequence from the reduction of Mn(IV) and Fe(III) (See Table S4.1).

Figure 4.4a shows the relative change of PARAFAC components C1 and C3 in HMW fraction over the relative change in the cumulative consumption of electron acceptors in the hypolimnion (Equation 4.2). This plot allows the removal of the DOM fluorescence components (C1 and C3) to be compared to the relative change of electron acceptors (i.e. the progression of anaerobic lake metabolism). The rate of change of C1 was similar to that of C3 when the water column was oxygenated (Figure 4.4 Sep-Nov), but during the summer, C3 concentrations quicker than C1 (Figure 4.4) and by a magnitude approximately 4x greater than C1. The rapid increase in the products of anaerobic reactions

(calculated as  $\Sigma_{e-}$ ) coincided with the depletion of HMW protein-like DOM and increases the C3 LMW fraction (Figure 4.3c-d).

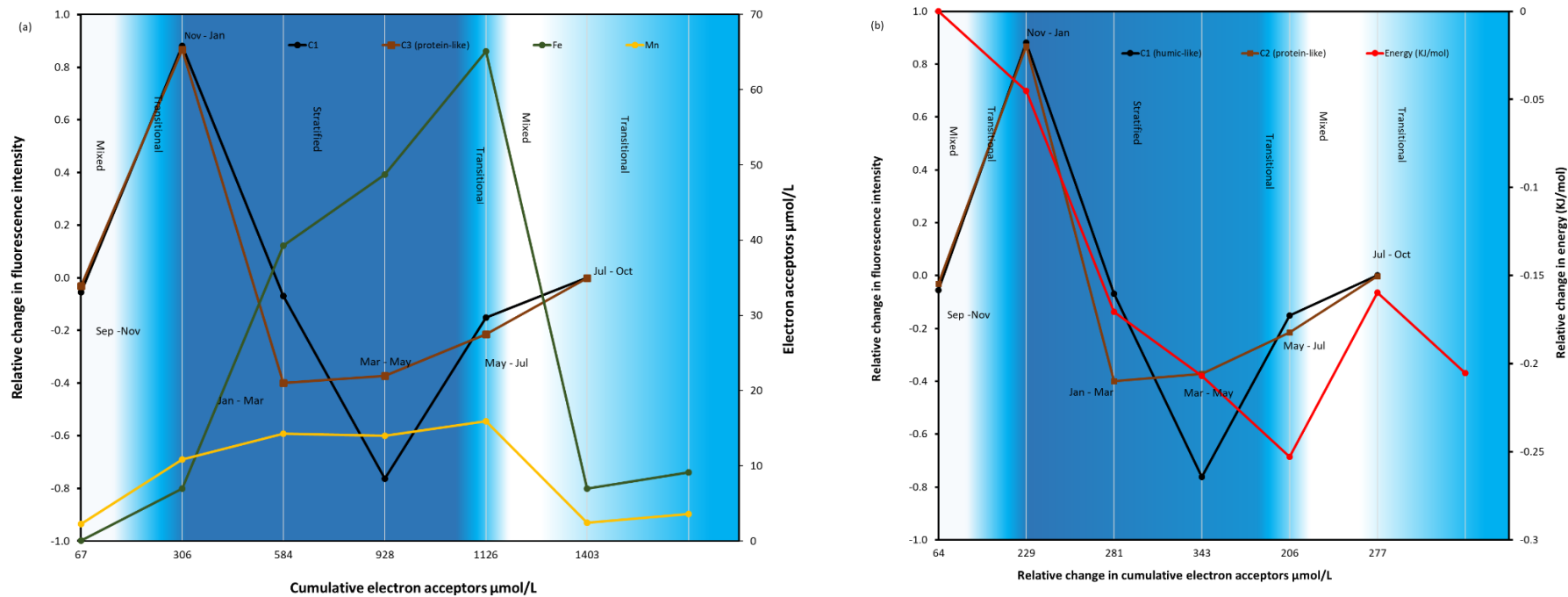


Figure 4.4: (a) Relative Changes in PARAFAC components C1 and C3 (HMW) over the relative change in cumulative consumption of electron acceptors ( $\Sigma e_-$ ) between 15 mand 23 m depth (hypolimnion), (b) Relative change in PARAFAC components C1 and C3 (HMW) over the cumulative electron acceptor concentration (Sep. 2015 to October 2016). Values are averages for these depths

### 4.3.5 Principal component analysis (PCA) of PARAFAC components, DOC and electron acceptors

Principal components analysis (PCA) was used to explore the relationship between DOM composition and concentration as a function of size fraction, time of the year and the amount of DOM oxidation that was coupled to reduction reactions (taken as the relative change in the summed electrons ( $\Sigma e^-$ ) consumed) (Figure 4.5). In PCA, the first four components explained 92% of the variability. The first and second components accounted for 43 % and 23 %, respectively; with PC1 differentiating the mixed and stratified periods, and PC2 separating the onset of stratification from peak summer stratification. DOC and C1 fluorescence in both fractions and HMW C3 showed positive scores on both axes and were loaded with January data. In contrast, samples from spring were located in the regions with lower PC1 scores and higher PC2 scores. Samples from mixed periods tended to load together in regions with lower PC1 and PC2 scores. LMW protein-like DOM (C3) and electron acceptors were grouped together along the PC1 axis and showed negative scores for PC2. Thus, the PCA showed DOC and humic-like DOM were decoupled from protein-like DOM and anaerobic reduction reactions ( $\Sigma e^-$ ) (Figure 4.5).

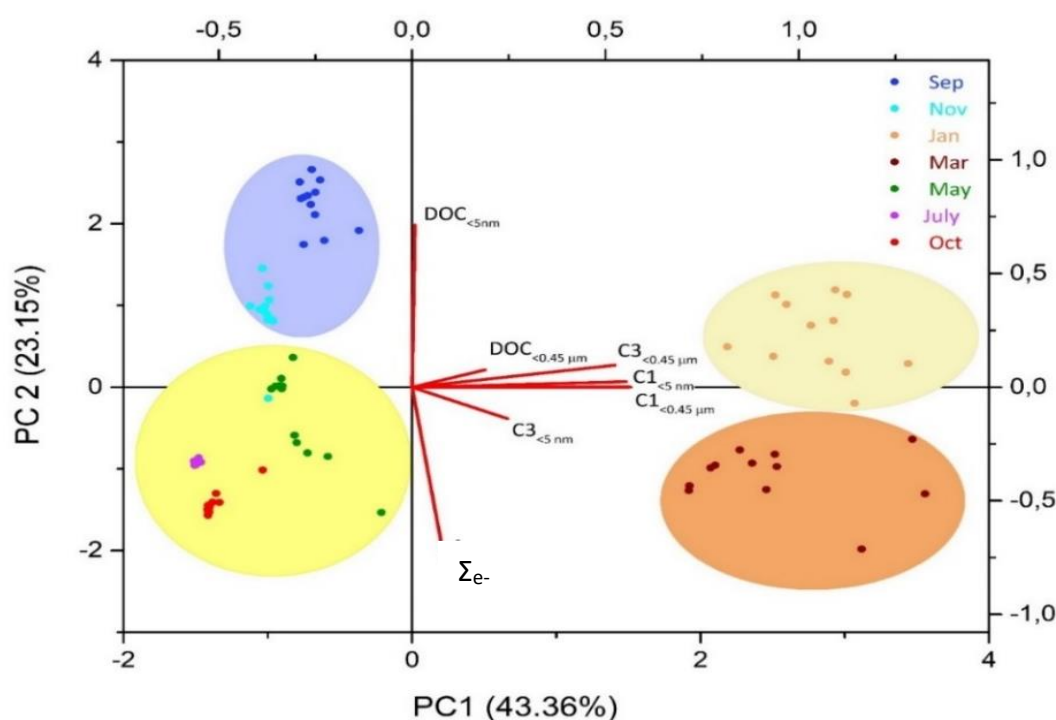


Figure 4.5: Principal component analysis (PCA) loading plot for DOM fluorescence (PARAFAC components C1 and C3) and DOC concentrations as a function of size fraction (<0.45  $\mu\text{m}$  and <5 nm) and summed electron acceptors ( $\Sigma e^-$ ).

## 4.4 Discussion

DOM 'quality' is defined by properties such as aromaticity, hydrophilicity and hydrophobicity, and differs widely depending on the origin of the DOM (Fellman *et al.*, 2009). The complexity and variability of processes determining the quality of DOM becomes magnified in dynamic systems like lakes, making assignment of sources difficult. Nevertheless, DOM fluorescence can shed light on microbial utilization/degradation potential of DOM when lakes stratify, because the hypolimnion can be conceptualised as a closed system. Using this conceptual framework, fluorescence characteristics of DOM were studied and a system-dependent relationship between DOM and fluorescence characteristics was established (Filella 2009; Zhang *et al.*, 2011; Zhang *et al.*, 2010). This study identified three fluorophores which defined the pool of DOM through a hydrological year, but these components appeared decoupled from other DOM measures such as SUVA<sub>254</sub> and DOC concentration. . The following section seeks to tease out the interrelationships between DOM analyses and other variables relating to lake metabolism.

### 4.4.1 Seasonal variability in DOC

Aquatic DOC is a dynamic component in inland waters, which continuously cycles through physical, chemical and biological processes. Physical processes involve wind and temperature driven circulation of surface water, and biological controls include, but are not limited to, viral lysis (Daly 1997), bacterial decomposition, exudation by phytoplankton (Jiao *et al.*, 2010) and grazing by zooplankton (Lampert and Taylor 1985). In this study, variations in DOC concentration in both high- and low-molecular weight fractions followed a seasonal structure with higher DOC concentrations during spring and summer, consistent with increases in lake productivity (higher chlorophyll-a) (Figure S4.5).

DOC turnover occurred most dynamically around the the metalimnion, a region already known to be particularly biogeochemically active (Saeed *et al.*, 2018). Summertime increases in LMW DOC above 7 m depth may be attributable either to biological processes (*e.g.*, exudation by phytoplankton) (Kinsey, 2008) and/or cellular photolysis in the water column (Bertilsson and Tranvik 2000; Lindell *et al.*, 2000). The latter process would be consistent with

our observations of generally lower epilimnetic HMW DOC concentrations compared to LMW DOC.

Persistent stratification is expected promote higher exposure of DOM to solar radiation in surface waters (Hansen *et al.*, 2016) and this process is known to convert high molecular weight DOC to highly bio-reactive LMW compounds in oceanic, riverine and lacustrine surface waters (Bushaw *et al.*, 1996; DeGrandpre *et al.*, 1996; Moran and Zepp 1997; Panneer Selvam *et al.*, 2019; Twardowski and Donaghay 2002). Previous studies (Bertilsson *et al.*, 1999; Bertilsson and Tranvik 2000) have reported a positive relationship between the photochemical degradation and biological uptake of DOC, and results from Lake Ngapouri are consistent with this reaction mechanism operating in the lakes' sunlit surface waters Seasonal variability in fluorescence characteristics

The spectral characteristics of the fluorophores observed in Lake Ngapouri were similar to those identified in other aquatic environments (summarised in Table 4.1). These assignments allow C1 and C2 to be identified as a humic-like and red-shifted humic-like fluorophores, respectively. The significant overlap between the two fluorophores is attributable to inter-molecular energy transfer and presence of high-molecular weight, conjugated compounds in these complex DOM mixtures (Hudson *et al.*, 2007; Senesi *et al.*, 1991; Wu *et al.*, 2003). The distribution of C1 in the lake water column was almost identical to that of C2 for both fractions, indicating that these components have a common source and similar biogeochemical interactions. The term 'humic-like' is a somewhat artificial distinction between extracted humic substances and natural organic matter (NOM) (Filella 2009), but is useful to distinguish the distinct behaviour of these compounds when compared to more labile components.

PARAFAC component C3 was designated the protein-like fluorophore (Chen *et al.*, 2003; Kulkarni *et al.*, 2017) and its behaviour was quite different from C1 and C2, being more actively cycled in the water column particularly during Jan-March (Figure 4.4). Changes in C3 with time and depth are the result of the degradation of submerged phytoplankton which can release large amounts of polysaccharides during growth and decomposition phases (Zhang *et al.*, 2009).

Protein-like fluorescence components are thought to be both produced and consumed by microorganisms (Hudson *et al.*, 2007), although the spectral position of fluorescence peaks do vary across different environments and reflect the unique mixture of compounds present, often with overlapping excitation and emission wavelengths. Spectral overlaps are influenced by DOM chemistry, matrix effects, proteins at various stages of degradation (*i.e.*, depolymerisation/metabolism), and even potential alteration in the structure of fluorophores during sampling and sample handling (Zsolnay 2003).

A strong linear relationship ( $r^2 = 0.98$ ) between the fluorescence intensities of C1 and C2 indicates that the separation (in fluorescence space) was artificial and related to compounds within the same pool of humic-like matter. The fluorescence intensity of C3 had a positive, significant linear relation with C1 and C2 ( $r^2 = 0.77$  and  $0.78$ , respectively), indicating that all three fluorophores were coupled (Lü *et al.*, 2018), and were likely produced during the rapid increase in phytoplankton biomass between Nov 2015 – Jan 2016 (Figure 4.4). We cannot however discount the possibility that the increase in humic-like fluorescence reflected allochthonous carbon inputs associated with high-intensity summer rainfall (Figure 4.3) and the associated runoff, as well as increased autochthonous production driven by a spring phytoplankton bloom in the epilimnion. Previous studies (Borisover *et al.*, 2009; Zhang *et al.*, 2011; Zhang *et al.*, 2010) have reported independent sources for humic and protein like fluorescence and that humic-like substances are controlled more strongly by hydrological processes, whereas protein-like fluorescence is tightly linked with autochthonous production (Lu *et al.* 2015; Spencer *et al.*, 2008). Terrestrial DOM is known to absorb significant amounts of solar radiation (Rae *et al.*, 2001) increasing photochemical oxidation rates. Indeed, this may be a factor in the observed dynamics of DOC in the HMW and LMW fractions as previously discussed (see *seasonal variability in DOC*).

It is interesting to note that the relationship between the PARAFAC components (C1, C2 and C3) and DOC was generally stronger in the LMW fraction ( $r^2 = 0.60$ ,  $p < 0.01$ ) than in  $<0.45 \mu\text{m}$  fraction ( $r^2 = 0.36$ ), likely because of lower inner filter effects. Indeed, it has been shown previously that quenching of fluorescence by colloidal DOM reduces the strength of correlations between DOC concentration and fluorescence intensity in humic-like DOM (Hartland *et al.*, 2010).



SUVA<sub>254</sub> values indicated higher DOM aromaticity during winter mixed conditions. However, both Fe(II) and Fe(III) can interfere with the SUVA<sub>254</sub> signal at the concentrations reported in this study and Fe(II) in particular can interfere with the signal at much lower concentrations. These results are in line with the findings of Weishaar *et al.*, (2003) who argued that Fe(II) strongly absorbs UV light at 254 nm, interfering with the SUVA<sub>254</sub> signal at concentrations as low as 0.05 mg L<sup>-1</sup>. In addition, the highest SUVA<sub>254</sub> signal coincided with winter mixed conditions, when Fe was likely to be present as Fe<sup>3+</sup> (Poulin *et al.*, 2014). Previous studies do not agree on the minimum concentration of Fe needed to affect these measurements. We therefore suggest that SUVA<sub>254</sub> should be used with caution for qualitative analysis of DOM in lakes with milli-molar Fe concentrations.

#### **4.4.2 Coupling of DOM degradation and redox processes**

The issue of how oxygen concentration affects the mineralization of organic matter in aquatic systems has received substantial attention and there is an ongoing debate (Bastviken *et al.* 2003) about how fluctuating redox conditions affect the degradation of organic matter (Hartnett *et al.*, 1998; Kristensen 2000b). Aquatic organic matter is likely to be exposed to, and drive changes in, gradients in dissolved oxygen. The coupling of DOM and oxidants in any given environment will depend on the energy yield available through the interaction of DOM substrate, microbes and electron acceptors. The basis of using the changes in hypolimnetic Fe, Mn and SO<sub>4</sub><sup>2-</sup> concentrations presupposes that reduction is the driver of increases in Fe and Mn, and losses in SO<sub>4</sub><sup>2-</sup>. Therefore, when Fe and Mn decrease in concentration these values were excluded from the calculation of cumulative electron consumption (*i.e.*, since losses of Fe and Mn, must relate to precipitation or adsorption reactions (Hartland *et al.*, 2015)). This is a minor concern in terms of this analysis because in practice, decreases in Fe and Mn only occurred in the winter and reflected precipitation of hydr(oxides) following re-oxygenation of the lake (Table S4.1).

Decomposition of DOM under anoxic conditions is strongly influenced by the quality of DOM (Gudasz *et al.*, 2012; Sobek *et al.*, 2009). For instance, low molecular weight, labile compounds are expected to be readily decomposed while recalcitrant, high molecular weight, more-complex molecules go through slow hydrolysis and fermentation (Bastviken *et al.*, 2003; Zehnder and Svensson 1986). There are two primary explanations in the literature for these different rates of mineralization under oxic and anoxic conditions. The first refers to the

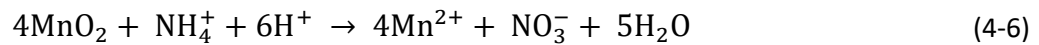
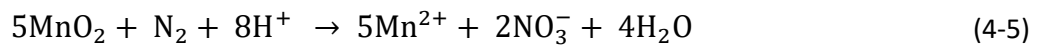
degree of adsorption of DOM to mineral particles (Mayer 1994; Rodger Harvey *et al.*, 1995), while the other concerns the selective degradation of DOM due to qualitative differences in the composition of DOM itself (Hedges 2002). While both schools of thought are likely more-or-less correct in different systems and settings, DOM degradation within the water column of Lake Ngapouri was more influenced by qualitative differences in DOM composition, as evidenced by differential rates of loss in the protein-like and humic-like DOM fractions (Figure 4.4).

Consumption of oxygen in the water column may not solely describe the mineralization of organic matter during thermal stratification (Hulth *et al.*, 1999; Kristensen 2000a). Both manganese and iron act as favoured electron acceptors for anaerobic respiration (Moran and Zepp 1997) with redox potentials near to  $\text{NO}_3^-$  reduction and higher than those for sulfate reduction. With each shift in electron acceptors, a physiological succession of bacteria and phytoplankton likely takes place. Nevertheless the sequence of redox reactions in our study was remarkably consistent with thermodynamic theory. While the sequence of reduction clearly followed the Gibbs free energy change of reaction (Stumm and Morgan 1996), on a mass basis,  $\text{SO}_4^{2-}$  reduction accounted for 68-100 % of all reduction reactions within the hypolimnion over any 2-month period.

Redox reactions involving DOM oxidation in monomictic lakes can be studied in an essentially 'closed' system – the hypolimnion – because the oxygen depletes quickly, leaving much of the labile organic matter available for anaerobic respiration. Oxygen concentrations in the hypolimnion varied widely between seasons, being depleted to near zero concentration between Feb-May (Figure 4.2b). Oxygen concentrations are the key variable determining speciation differences in the concentrations of oxidised dissolved nitrogen species ( $\text{NO}_x$ ), but the transformation pathways can be complex (Lin and Taillefert 2014; Pina-Ochoa and Álvarez-Cobelas 2006). In well aerated systems, ammonium oxidation is thought to produce most of the  $\text{NO}_3^-$  while in situations where the oxygen concentration is below  $0.2 \text{ mg L}^{-1}$ ,  $\text{NO}_2^-$ , when present, is used as the terminal electron acceptor by denitrifying bacteria to produce  $\text{N}_2$  (Christensen and Rowe 1984; Nishri and Hamilton 2010). However, both processes are active in the region of partial oxygen depletion (oxic-anoxic interfaces) and are largely controlled by the supply of oxygen through molecular and turbulent diffusion and the consumption of oxidants due to organic matter mineralization (Paerl and Pinckney 1996;

Seitzinger *et al.*, 2006). The apparent distribution of oxygen and  $\text{NO}_3^-$  was consistent with the production of  $\text{NO}_3^-$  where oxygen was  $> \sim 0.2 \text{ mg L}^{-1}$ , followed by rapid nitrate depletion in the anaerobic hypolimnion.

Nitrification can occur through two main pathways under anaerobic conditions, (1) ANAMMOX, which is mainly controlled by microbes, and (2) chemo nitrification which is an abiotic process governed by metal oxide availability (Luther *et al.*, 1997; Swathi *et al.*, 2017), predominantly  $\text{MnO}_x$  (Pearson *et al.*, 2012). There is growing evidence that the N and Mn cycles may be closely coupled in anaerobic sediments that are rich in organic carbon and Mn, where  $\text{NO}_3^-$  serves as an oxidant, Equation 4-5 (Hulth *et al.*, 1999; Pearson *et al.*, 2012; Swathi *et al.*, 2017). Nitrification also occurs in the absence of oxygen through  $\text{MnO}_x$  reduction according to Equation 4-6 (Lin and Taillefert 2014).



The coupled anaerobic reactions outlined above are however, yet to be demonstrated to occur in the anaerobic conditions present in hypolimnetic lake water (Lin and Taillefert 2014; Thamdrup and Dalsgaard 2000). Although thermodynamically favourable, the process tends not to occur through iron oxide and sulfate reduction, because the reduction half reactions are energetically less efficient than for reduction of manganese oxide ( $\Delta G \text{ MnO}_{2\text{red}} = -228 \text{ kJ mol}^{-1}$ ,  $\Delta G \text{ Fe}_{\text{red}} = -277 \text{ kJ mol}^{-1}$  and  $\Delta G \text{ SO}_4^{2-\text{red}} = -744 \text{ kJ mol}^{-1}$  (Stumm and Morgan 1996) (Figure 4.4a. On the balance of the data collected in this study, we suggest that nitrification coupled to  $\text{MnO}_2$  reduction occurred mostly at the onset of stratification (spring) periods in Lake Ngapouri, for example at depths between 15 and 20 m in November and January (Figure S4.3) when the concentration of DO was 0.09 and 0.07  $\text{mg L}^{-1}$  respectively. These findings are consistent with a previous study carried out in the same lake suggesting  $\text{NH}_4^+$  oxidation to  $\text{NO}_3^-$  in the anoxic zone took place in the abundant presence of  $\text{MnO}_2$  (Pearson *et al.*, 2012).

The data produced in this study show a clear depletion of low molecular weight DOM in the hypolimnion during summer. The LMW DOM appears to have been more strongly cycled than the HMW fraction associated with autochthonous (phytoplankton) production (Saeed *et al.*, 2018). In addition, the protein-like fraction of DOM appeared to be depleted faster than the humic-like fractions (C1 and C2), although the temporal resolution of the data are not sufficient to disentangle the rates of consumption of these fluorophores (Figure 4.5). Regardless of the differences in rate, proteins likely constituted the main substrates for anaerobic metabolism in the lake hypolimnion.

Data on the concentration of the inorganic electron acceptors involved in biomass oxidation show a clear chain of reactions linked to the energetics of these processes, i.e. the redox ladder (Stumm and Morgan 1996). This was manifest as the initial depletion of O<sub>2</sub> and NO<sub>3</sub><sup>-</sup>, followed by increases in Mn and latterly Fe (linked to dissimilatory reduction of Mn and Fe oxides), and finally reductions in SO<sub>4</sub><sup>2-</sup> (dissimilatory S reduction). It is clear from these results that all of these heterotrophic microbial processes were linked to consumption of DOM, likely with the LMW proteinaceous fraction being most actively cycled.

## **4.5 Conclusion**

DOM in Lake Ngapouri predominantly consisted of low molecular weight compounds, with the protein-bearing fraction being more actively cycled through the lake water column during spring and summer seasons. Our findings reinforce that metal oxides, particularly MnO<sub>x</sub>, can have a strong impact on mineralization of DOM, mainly in the hypolimnion during anaerobic conditions in the water column. Levels of SUVA<sub>254</sub> should be carefully evaluated before being reported in Fe rich lakes because Fe can potentially interfere with the absorption signal in varying concentrations.

## **4.6 Acknowledgments**

This work was funded by the Ministry of Business, Innovation and Employment for Enhancing the Health and Resilience of New Zealand Lakes (UOWX1503). We thank technical staff at School of science, university of Waikato for help during field campaigns and laboratory analysis. The authors declare no conflict of interest.

## 4.7 References

- Andersen, C. M., and R. Bro. 2003. Practical aspects of PARAFAC modeling of fluorescence excitation-emission data. *Journal of Chemometrics* **17**: 200-215.
- Baker, A., and J. Lamont-Black. 2001. Fluorescence of dissolved organic matter as a natural tracer of ground water. *Ground Water* **39**: 745-750.
- Bastviken, D., M. Olsson, and L. Tranvik. 2003. Simultaneous measurements of organic carbon mineralization and bacterial production in oxic and anoxic lake sediments. *Microbial ecology* **46**: 73-82.
- Battin, T. J., S. Luyssaert, L. A. Kaplan, A. K. Aufdenkampe, A. Richter, and L. J. Tranvik. 2009. The boundless carbon cycle. *Nature Geoscience* **2**: 598.
- Bertilsson, S., R. Stepanauskas, R. Cuadros-Hansson, W. Granéli, J. Wikner, and L. Tranvik. 1999. Photochemically induced changes in bioavailable carbon and nitrogen pools in a boreal watershed. *Aquatic Microbial Ecology* **19**: 47-56.
- Bertilsson, S., and L. J. Tranvik. 2000. Photochemical transformation of dissolved organic matter in lakes. *Limnology and Oceanography* **45**: 753-762.
- Birdwell, J. E., and A. S. Engel. 2010. Characterization of dissolved organic matter in cave and spring waters using UV-Vis absorbance and fluorescence spectroscopy. *Organic Geochemistry* **41**: 270-280.
- Bisutti, I., I. Hilke, and M. Raessler. 2004. Determination of total organic carbon—an overview of current methods. *TrAC Trends in Analytical Chemistry* **23**: 716-726.
- Bonneville, S., Van Cappellen, P., & Behrends, T. (2004). Microbial reduction of iron (III) oxyhydroxides: effects of mineral solubility and availability. *Chemical Geology*, 212(3-4), 255-268.
- Borisover, M., Y. Laor, A. Parparov, N. Bukhanovsky, and M. Lado. 2009. Spatial and seasonal patterns of fluorescent organic matter in Lake Kinneret (Sea of Galilee) and its catchment basin. *Water Research* **43**: 3104-3116.
- Bro, R. 1997. PARAFAC. Tutorial and applications. *Chemometrics and Intelligent Laboratory Systems* **38**: 149-171.
- Bushaw, K. L. and others 1996. Photochemical release of biologically available nitrogen from aquatic dissolved organic matter. *Nature* **381**: 404-407.
- Chen, W., P. Westerhoff, J. A. Leenheer, and K. Booksh. 2003. Fluorescence excitation-emission matrix regional integration to quantify spectra for dissolved organic matter. *Environmental Science and Technology* **37**: 5701-5710.
- Christensen, J. P., and G. T. Rowe. 1984. Nitrification and oxygen consumption in northwest Atlantic deep-sea sediments. *Journal of Marine Research* **42**: 1099-1116.

- Coble, P. G. 1996. Characterization of marine and terrestrial DOM in seawater using excitation-emission matrix spectroscopy. *Marine Chemistry* **51**: 325-346.
- Cory, R. M., and D. M. McKnight. 2005. Fluorescence spectroscopy reveals ubiquitous presence of oxidized and reduced quinones in dissolved organic matter. *Environmental Science and Technology* **39**: 8142-8149.
- Daly, K. 1997. Flux of particulate matter through copepods in the Northeast Water Polynya.
- Davidson, N. C. (2014). How much wetland has the world lost? Long-term and recent trends in global wetland area. *Marine and Freshwater Research*, 65(10), 934-941.
- DeGrandpre, M. D., A. Vodacek, R. K. Nelson, E. J. Bruce, and N. V. Blough. 1996. Seasonal seawater optical properties of the U.S. Middle Atlantic Bight. *Journal of Geophysical Research* **101**: 22727-22736.
- DelSontro, T., J. J. Beaulieu, and J. A. Downing. 2018. Greenhouse gas emissions from lakes and impoundments: Upscaling in the face of global change. *Limnology and Oceanography* **3**: 64-75.
- Downing, J. A. and others 2006. The global abundance and size distribution of lakes, ponds, and impoundments. *Limnology and Oceanography* **51**: 2388-2397.
- Eshleman, K., and H. Hemond. 1985. The role of organic acids in the acid-base status of surface waters at Bickford Watershed, Massachusetts. *Water Resources Research* **21**: 1503-1510.
- Fellman, J. B., E. Hood, R. T. Edwards, and D. V. D'Amore. 2009. Changes in the concentration, biodegradability, and fluorescent properties of dissolved organic matter during stormflows in coastal temperate watersheds. *Journal of Geophysical Research* **114**.
- Filella, M. 2009. Freshwaters: which NOM matters? *Environmental Chemistry Letters* **7**: 21-35.
- Gudasz, C., D. Bastviken, K. Premke, K. Steger, and L. J. Tranvik. 2012. Constrained microbial processing of allochthonous organic carbon in boreal lake sediments. *Limnology and Oceanography* **57**: 163-175.
- Hamilton, D. P., K. R. O'Brien, M. A. Burford, J. D. Brookes, and C. G. McBride. 2010. Vertical distributions of chlorophyll in deep, warm monomictic lakes. *Aquatic Sciences* **72**: 295-307.
- Hansen, A. M., T. E. C. Kraus, B. A. Pellerin, J. A. Fleck, B. D. Downing, and B. A. Bergamaschi. 2016. Optical properties of dissolved organic matter (DOM): Effects of biological and photolytic degradation. *Limnology and Oceanography* **61**: 1015-1032.

- Hanson, P. C., D. P. Hamilton, E. H. Stanley, N. Preston, O. C. Langman, and E. L. Kara. 2011. Fate of allochthonous dissolved organic carbon in lakes: a quantitative approach. *PLoS One* **6**: e21884.
- Hartland, A., M. S. Andersen, and D. P. Hamilton. 2015. Phosphorus and arsenic distributions in a seasonally stratified, iron-and manganese-rich lake: microbiological and geochemical controls. *Environmental Chemistry* **12**: 708-722.
- Hartland, A., A. Baker, W. Timms, Y. Shutova, and D. Yu. 2012. Measuring dissolved organic carbon  $\delta^{13}\text{C}$  in freshwaters using total organic carbon cavity ring-down spectroscopy (TOC-CRDS). *Environmental Chemistry Letters* **10**: 309-315.
- Hartland, A., I. J. Fairchild, J. R. Lead, and A. Baker. 2010. Fluorescent properties of organic carbon in cave dripwaters: Effects of filtration, temperature and pH. *Science of The Total Environment* **408**: 5940-5950.
- Hartland, A., I. J. Fairchild, J. R. Lead, H. Zhang, and M. Baalousha. 2011. Size, speciation and lability of NOM–metal complexes in hyperalkaline cave dripwater. *Geochimica et Cosmochimica Acta* **75**: 7533-7551.
- Hartnett, H. E., R. G. Keil, J. I. Hedges, and A. H. Devol. 1998. Influence of oxygen exposure time on organic carbon preservation in continental margin sediments. *Nature* **391**: 572-575.
- Hedges, J. I. 1992. Global biogeochemical cycles: progress and problems. *Marine Chemistry* **39**: 67-93.
- Hedges, J. I. 2002. Sedimentary Organic Matter Preservation and Atmospheric  $\text{O}_2$  Regulation, p. 105-123. In A. Gianguzza, E. Pelizzetti and S. Sammartano [eds.], *Chemistry of Marine Water and Sediments*. Springer Berlin Heidelberg.
- Henderson, R. K., A. Baker, K. Murphy, A. Hambly, R. Stuetz, and S. Khan. 2009. Fluorescence as a potential monitoring tool for recycled water systems: a review. *Water research* **43**: 863-881.
- Hood, E., M. W. Williams, and D. M. McKnight. 2005. Sources of dissolved organic matter (DOM) in a Rocky Mountain stream using chemical fractionation and stable isotopes. *Biogeochemistry* **74**: 231-255.
- Hudson, N., A. Baker, and D. Reynolds. 2007. Fluorescence analysis of dissolved organic matter in natural, waste and polluted waters—a review. *River Research and Applications* **23**: 631-649.
- Hulth, S., R. C. Aller, and F. Gilbert. 1999. Coupled anoxic nitrification/manganese reduction in marine sediments. *Geochimica et Cosmochimica Acta* **63**: 49-66.
- Jaffé, R., K. M. Cawley, and Y. Yamashita. 2014. Applications of excitation emission matrix fluorescence with parallel factor analysis (EEM-PARAFAC) in assessing environmental dynamics of natural dissolved organic matter (DOM) in aquatic environments: a

- review. Advances in the physicochemical characterization of dissolved organic matter: impact on natural and engineered systems **1160**: 27-73.
- Jiao, N. and others 2010. Microbial production of recalcitrant dissolved organic matter: long-term carbon storage in the global ocean. *Nature Reviews Microbiology* **8**: 593.
- Kellerman, A. M., T. Dittmar, D. N. Kothawala, and L. J. Tranvik. 2014. Chemodiversity of dissolved organic matter in lakes driven by climate and hydrology. *Nature Communications* **5**: 3804.
- Kellerman, A. M., D. N. Kothawala, T. Dittmar, and L. J. Tranvik. 2015. Persistence of dissolved organic matter in lakes related to its molecular characteristics. *Nature Geoscience* **8**: 454.
- Kortelainen, P., T. Mattsson, L. Finér, M. Ahtiainen, S. Saukkonen, and T. Sallantausta. 2006. Controls on the export of C, N, P and Fe from undisturbed boreal catchments, Finland. *Aquatic Sciences* **68**: 453-468.
- Kothawala, D. N., C. A. Stedmon, R. A. Müller, G. A. Weyhenmeyer, S. J. Köhler, and L. J. Tranvik. 2014. Controls of dissolved organic matter quality: evidence from a large-scale boreal lake survey. *Global Change Biology* **20**: 1101-1114.
- Kristensen, E. 2000a. Organic matter diagenesis at the oxic/anoxic interface in coastal marine sediments, with emphasis on the role of burrowing animals. *Hydrobiologia* **426**: 1-24.
- Kristensen, E. 2000b. Organic matter diagenesis at the oxic/anoxic interface in coastal marine sediments, with emphasis on the role of burrowing animals, p. 1-24. Life at interfaces and under extreme conditions. Springer.
- Kulkarni, H. V., N. Mladenov, K. H. Johannesson, and S. Datta. 2017. Contrasting dissolved organic matter quality in groundwater in Holocene and Pleistocene aquifers and implications for influencing arsenic mobility. *Applied Geochemistry* **77**: 194-205.
- Lampert, W., and B. E. Taylor. 1985. Zooplankton Grazing in a Eutrophic Lake: Implications of Diel Vertical Migration. *Ecology* **66**: 68-82.
- Lapworth, D. J., D. Gooddy, A. Butcher, and B. Morris. 2008. Tracing groundwater flow and sources of organic carbon in sandstone aquifers using fluorescence properties of dissolved organic matter (DOM). *Applied Geochemistry* **23**: 3384-3390.
- Lau, M. P., M. Hupfer, and H.-P. Grossart. 2017. Reduction-oxidation cycles of organic matter increase bacterial activity in the pelagic oxycline. *Environmental Microbiology Reports* **9**: 257-267.
- Lawlor, A., and E. Tipping. 2003. Metals in bulk deposition and surface waters at two upland locations in northern England. *Environmental Pollution* **121**: 153-167.
- Leathwick, J. and others 2010. Freshwater ecosystems of New Zealand (FENZ) geodatabase. Department of Conservation.) Available at [Verified 3 April 2017].



- Lin, H., and M. Taillefert. 2014. Key geochemical factors regulating Mn (IV)-catalyzed anaerobic nitrification in coastal marine sediments. *Geochimica et Cosmochimica Acta* **133**: 17-33.
- Lindell, M. J., H. W. Granéli, and S. Bertilsson. 2000. Seasonal photoreactivity of dissolved organic matter from lakes with contrasting humic content. *Canadian Journal of Fisheries and Aquatic Sciences* **57**: 875-885.
- Lü, W., X. Yao, B. Zhang, Y. Liu, and Y. Li. 2018. Fluorescent Characteristics and Environmental Significance of Particulate Organic Matter in Lake Taihu, China. *Huan jing ke xue-Huanjing kexue* **39**: 2056-2066.
- Lu, Y., J. W. Edmonds, Y. Yamashita, B. Zhou, A. Jaegge, and M. Baxley. 2015. Spatial variation in the origin and reactivity of dissolved organic matter in Oregon-Washington coastal waters. *Ocean Dynamics* **65**: 17-32.
- Luther, G. W., B. Sundby, B. L. Lewis, P. J. Brendel, and N. Silverberg. 1997. Interactions of manganese with the nitrogen cycle: Alternative pathways to dinitrogen. *Geochimica et Cosmochimica Acta* **61**: 4043-4052.
- Mayer, L. M. 1994. Relationships between mineral surfaces and organic carbon concentrations in soils and sediments. *Chemical Geology* **114**: 347-363.
- McKnight, D. M., K. E. Bencala, G. W. Zellweger, G. R. Aiken, G. L. Feder, and K. A. Thorn. 1992. Sorption of dissolved organic carbon by hydrous aluminum and iron oxides occurring at the confluence of Deer Creek with the Snake River, Summit County, Colorado. *Environmental Science & Technology* **26**: 1388-1396.
- Mendonça, R. and others 2017. Organic carbon burial in global lakes and reservoirs. *Nature communications* **8**: 1694.
- Meybeck, M. 1995. Global distribution of lakes, p. 1–35. Springer-Verlag.
- Moran, M. A., and R. G. Zepp. 1997. Role of photoreactions in the formation of biologically labile compounds from dissolved organic matter. *Limnology and Oceanography* **42**: 1307-1316.
- Murphy, K. R., C. A. Stedmon, D. Graeber, and R. Bro. 2013. Fluorescence spectroscopy and multi-way techniques. PARAFAC. *Analytical Methods* **5**: 6557-6566.
- Murphy, K. R., C. A. Stedmon, T. D. Waite, and G. M. Ruiz. 2008. Distinguishing between terrestrial and autochthonous organic matter sources in marine environments using fluorescence spectroscopy. *Marine Chemistry* **108**: 40-58.
- Nishri, A., and D. P. Hamilton. 2010. A mass balance evaluation of the ecological significance of historical nitrogen fluxes in Lake Kinneret. *Hydrobiologia* **655**: 109-119.
- Pace, M. L., and Y. T. Prairie. 2005. Respiration in lakes,. Oxford Univ. Press.

- Paerl, H. W., and J. Pinckney. 1996. A mini-review of microbial consortia: their roles in aquatic production and biogeochemical cycling. *Microbial Ecology* **31**: 225-247.
- Panneer Selvam, B., J.-F. Lapierre, A. R. A. Soares, D. Bastviken, J. Karlsson, and M. Berggren. 2019. Photo-reactivity of dissolved organic carbon in the freshwater continuum. *Aquatic Sciences* **81**: 57.
- Pearson, L. K., C. H. Hendy, D. P. Hamilton, and W. B. Silvester. 2012. Nitrogen-15 Isotope Enrichment in Benthic Boundary Layer Gases of a Stratified Eutrophic Iron and Manganese Rich Lake. *Aquatic Geochemistry* **18**: 1-19.
- Pina-Ochoa, E., and M. Álvarez-Cobelas. 2006. Denitrification in aquatic environments: a cross-system analysis. *Biogeochemistry* **81**: 111-130.
- Poulin, B. A., J. N. Ryan, and G. R. Aiken. 2014. Effects of Iron on Optical Properties of Dissolved Organic Matter. *Environmental Science & Technology* **48**: 10098-10106.
- Eshlemwetze, R., C. Howard-Williams, I. Hawes, A. M. Schwarz, and W. F. Vincent. 2001. Penetration of solar ultraviolet radiation into New Zealand lakes: influence of dissolved organic carbon and catchment vegetation. *Limnology* **2**: 79-89.
- Raymond, P. A. and others 2013. Global carbon dioxide emissions from inland waters. *Nature* **503**: 355.
- Read, J. S., and K. C. Rose. 2013. Physical responses of small temperate lakes to variation in dissolved organic carbon concentrations. *Limnology and Oceanography* **58**: 921-931.
- Regnier, P. and others 2013. Anthropogenic perturbation of the carbon fluxes from land to ocean. *Nature Geoscience* **6**: 597-607.
- Rhymes, J. and others 2015. Using chemical, microbial and fluorescence techniques to understand contaminant sources and pathways to wetlands in a conservation site. *Science of the Total Environment* **511**: 703-710.
- Rodger Harvey, H., J. H. Tuttle, and J. Tyler Bell. 1995. Kinetics of phytoplankton decay during simulated sedimentation: Changes in biochemical composition and microbial activity under oxic and anoxic conditions. *Geochimica et Cosmochimica Acta* **59**: 3367-3377.
- Saeed, H. and others 2018. Regulation of phosphorus bioavailability by iron nanoparticles in a monomictic lake. *Scientific Reports* **8**: 17736.
- Salonen, K., and T. Hammar. 1986. On the importance of dissolved organic matter in the nutrition of zooplankton in some lake waters. *Oecologia* **68**: 246-253.
- Scott, D. T. and others 2006. Localized erosion affects national carbon budget. *Geophysical Research Letters* **33**.
- Seitzinger, S. and others 2006. Denitrification across landscapes and waterscapes: a synthesis. *Ecological applications* **16**: 2064-2090.

- Senesi, N., T. M. Miano, M. R. Provenzano, and G. Brunetti. 1991. Characterization, differentiation, and classification of humic substances by fluorescence spectroscopy. *Soil Science* **152**: 259-271.
- Sobek, S. and others 2009. Organic carbon burial efficiency in lake sediments controlled by oxygen exposure time and sediment source. *Limnology and Oceanography* **54**: 2243-2254.
- Spencer, R. G. M., G. R. Aiken, K. D. Butler, M. M. Dornblaser, R. G. Striegl, and P. J. Hernes. 2009. Utilizing chromophoric dissolved organic matter measurements to derive export and reactivity of dissolved organic carbon exported to the Arctic Ocean: A case study of the Yukon River, Alaska. *Geophysical Research Letters* **36**.
- Spencer, R. G. M., G. R. Aiken, K. P. Wickland, R. G. Striegl, and P. J. Hernes. 2008. Seasonal and spatial variability in dissolved organic matter quantity and composition from the Yukon River basin, Alaska. *Global Biogeochemical Cycles* **22**.
- Stedmon, C. A., and S. Markager. 2005. Tracing the production and degradation of autochthonous fractions of dissolved organic matter by fluorescence analysis. *Limnology and Oceanography* **50**: 1415-1426.
- Stedmon, C. A., S. Markager, and R. Bro. 2003. Tracing dissolved organic matter in aquatic environments using a new approach to fluorescence spectroscopy. *Marine Chemistry* **82**: 239-254.
- Stumm, W., and J. J. Morgan. 1996. Aquatic chemistry : chemical equilibria and rates in natural waters. Wiley.
- Swathi, D., P. C. Sabumon, and S. M. Maliyekkal. 2017. Microbial mediated anoxic nitrification-denitrification in the presence of nanoscale oxides of manganese. *International Biodeterioration & Biodegradation* **119**: 499-510.
- Taillefert, M., C.-P. Lienemann, J.-F. Gaillard, and D. Perret. 2000. Speciation, reactivity, and cycling of Fe and Pb in a meromictic lake. *Geochimica et Cosmochimica Acta* **64**: 169-183.
- Thamdrup, B., and T. Dalsgaard. 2000. The fate of ammonium in anoxic manganese oxide-rich marine sediment. *Geochimica et Cosmochimica Acta* **64**: 4157-4164.
- Tranvik, L. J. and others 2009. Lakes and reservoirs as regulators of carbon cycling and climate. *Limnology and Oceanography* **54**: 2298-2314.
- Twardowski, M. S., and P. L. Donaghay. 2002. Photobleaching of aquatic dissolved materials: Absorption removal, spectral alteration, and their interrelationship. *Journal of Geophysical Research: Oceans* **107**: 6-1-6-12.
- Urbansky, E. T. 2001. Total organic carbon analyzers as tools for measuring carbonaceous matter in natural waters This is the work of a United States government employee

- engaged in his official duties. As such it is in the public domain and exempt from copyright. © US government. *Journal of Environmental Monitoring* **3**: 102-112.
- Viollier, E., Inglett, P. W., Hunter, K., Roychoudhury, A. N., & Van Cappellen, P. (2000). The ferrozine method revisited: Fe(II)/Fe(III) determination in natural waters. *Applied Geochemistry*, *15*(6), 785-790.
- Webster, K. E. and others 2008. An empirical evaluation of the nutrient-color paradigm for lakes. *Limnology and Oceanography* **53**: 1137-1148.
- Weishaar, J. L., G. R. Aiken, B. A. Bergamaschi, M. S. Fram, R. Fujii, and K. Mopper. 2003. Evaluation of Specific Ultraviolet Absorbance as an Indicator of the Chemical Composition and Reactivity of Dissolved Organic Carbon. *Environmental Science & Technology* **37**: 4702-4708.
- Wetzel, R. G. 1990. Land-water interfaces: Metabolic and limnological regulators. *SIL Proceedings, 1922-2010* **24**: 6-24.
- Wetzel, R. G. 1992. Gradient-dominated ecosystems: sources and regulatory functions of dissolved organic matter in freshwater ecosystems, p. 181-198. *Dissolved organic matter in lacustrine ecosystems*. Springer.
- Williams, C. J., Y. Yamashita, H. F. Wilson, R. Jaffé, and M. A. Xenopoulos. 2010. Unraveling the role of land use and microbial activity in shaping dissolved organic matter characteristics in stream ecosystems. *Limnology and Oceanography* **55**: 1159-1171.
- Williamson, C. E., D. P. Morris, M. L. Pace, and O. G. Olson. 1999. Dissolved organic carbon and nutrients as regulators of lake ecosystems: Resurrection of a more integrated paradigm. *Limnology and Oceanography* **44**: 795-803.
- Wu, F. C., R. D. Evans, and P. J. Dillon. 2003. Separation and Characterization of NOM by High-Performance Liquid Chromatography and On-Line Three-Dimensional Excitation Emission Matrix Fluorescence Detection. *Environmental Science & Technology* **37**: 3687-3693.
- Yamashita, Y., and R. Jaffé. 2008. Characterizing the Interactions between Trace Metals and Dissolved Organic Matter Using Excitation–Emission Matrix and Parallel Factor Analysis. *Environmental Science & Technology* **42**: 7374-7379.
- Yamashita, Y., and E. Tanoue. 2003. Chemical characterization of protein-like fluorophores in DOM in relation to aromatic amino acids. *Marine Chemistry* **82**: 255-271.
- Zehnder, A. J. B., and B. H. Svensson. 1986. Life without oxygen: what can and what cannot? *Experientia* **42**: 1197-1205.
- Zhang, Y. and others 2011. Characterizing chromophoric dissolved organic matter in Lake Tianmuhu and its catchment basin using excitation-emission matrix fluorescence and parallel factor analysis. *Water Research* **45**: 5110-5122.

- Zhang, Y., van Dijk, M. A., Liu, M., Zhu, G., & Qin, B. (2009). The contribution of phytoplankton degradation to chromophoric dissolved organic matter (CDOM) in eutrophic shallow lakes: Field and experimental evidence. *Water Research*, 43(18), 4685-4697.
- Zhang, Y. and others 2010. Characteristics and sources of chromophoric dissolved organic matter in lakes of the Yungui Plateau, China, differing in trophic state and altitude. *Limnology and Oceanography* **55**: 2645-2659.
- Zsolnay, Á. 2003. Dissolved organic matter: artefacts, definitions, and functions. *Geoderma* **113**: 187-209.

## 4.8 Supplementary information

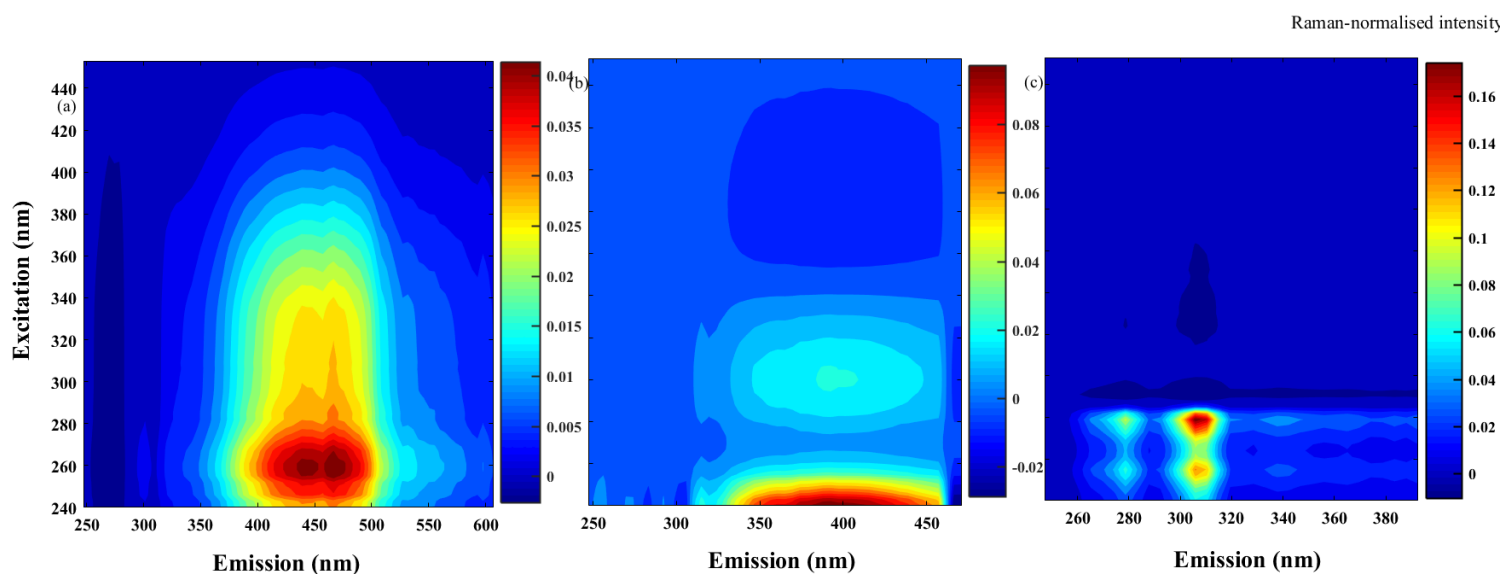


**Figure S4.1:** Excitation emission matrices (EEMs) of PARAFAC components 1-2 (plots a and b) corresponding to humic-like substances, and component 3 (c) protein-like components exhibiting fluorescence characteristic of tryptophan and tyrosine. Validation of the three component spectral model.

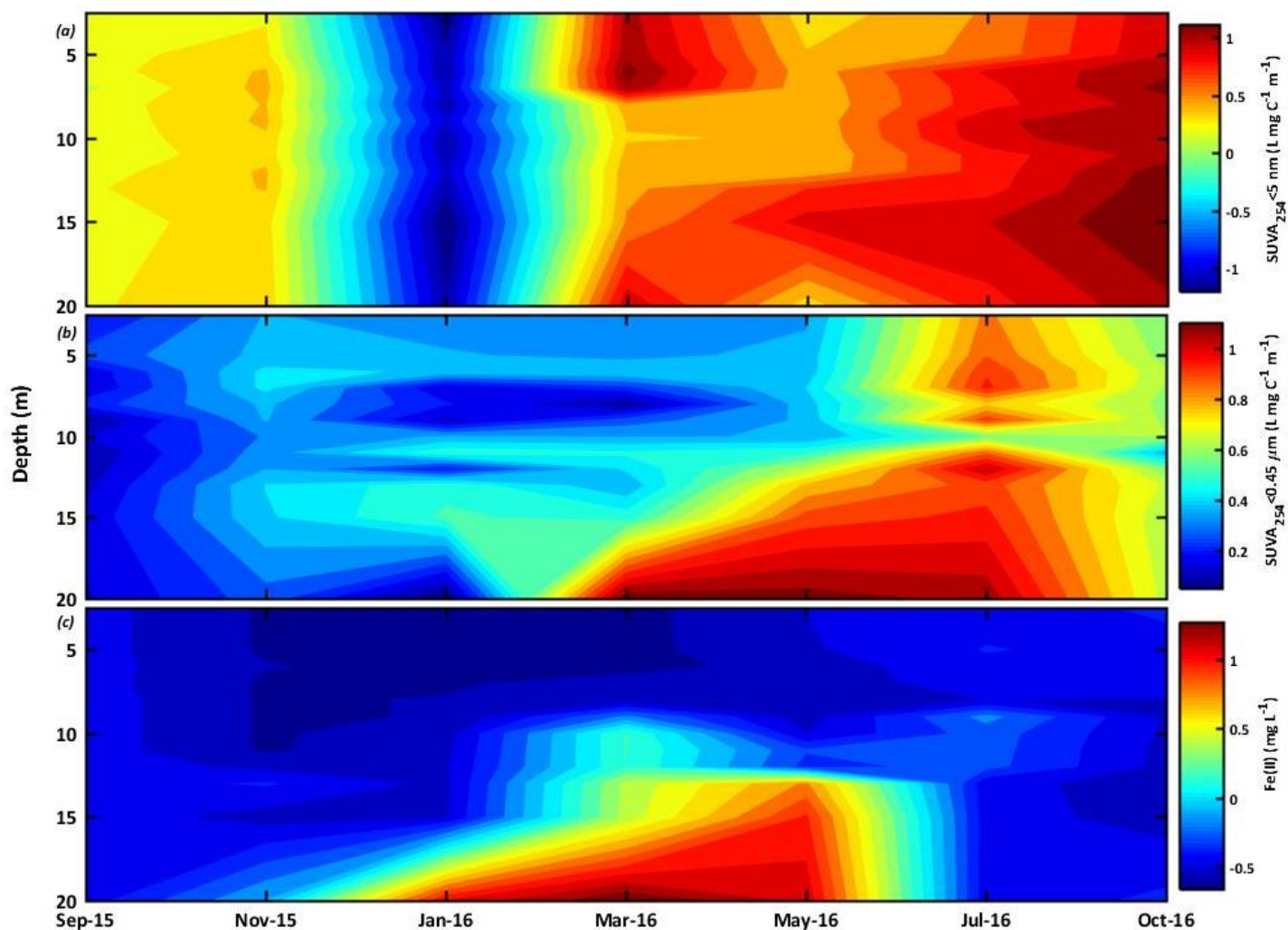


Figure S4.2: Time series of SUVA<sub>254</sub> in operationally defined fractions at log<sub>10</sub> scale (a) shows SUVA<sub>254</sub> values in the LMW fraction (b) SUVA<sub>254</sub> in the HMW fraction (c) Fe(II) measured by the ferrozine method

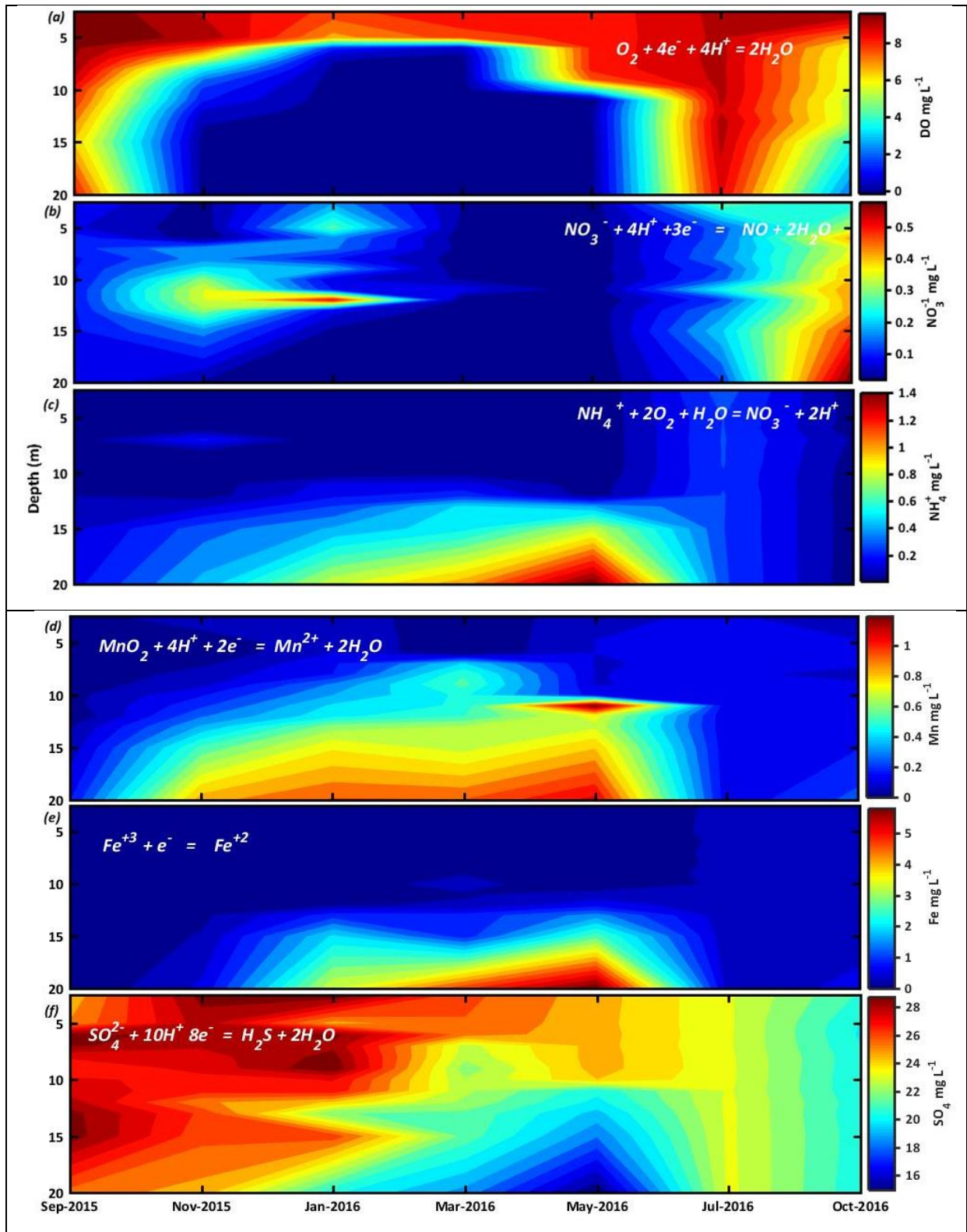


Figure S4.3: Time series of the oxidising agents in Lake Ngapouri. (a) Dissolved Oxygen ( $\text{mg L}^{-1}$ ), (b)  $\text{NO}_3^-$  ( $\text{mg NO}_3\text{-N L}^{-1}$ ),  $\text{NH}_4^+$  ( $\text{mg NH}_4^+\text{-N L}^{-1}$ ), Mn ( $\text{mg L}^{-1}$ ), Fe ( $\text{mg L}^{-1}$ ),  $\text{SO}_4$  ( $\text{mg L}^{-1}$ ).



**Table S4.1: Cumulative electron acceptors ( $\Sigma_{e^-}$ ) and percentage  $\text{SO}_4^{2-}$  reduction in Lake Ngapouri**

<b>Month</b>	<b>Month <math>\Sigma_{e^-}</math></b>	<b>% <math>\text{SO}_4^{2-}</math> reduction</b>
Sep-Nov	46.6	82.3
Nov-Jan	119.6	95.0
Jan-Mar	54.1	95.5
Mar-May	58.9	93.9
May-Jul	0.0	90.6
Jul-Oct	44.3	98.5

## Chapter 5

# **When micronutrients are available (and when they are not): metal-colloid interactions in seasonally-stratified lakes**

---

Saeed, H<sup>1</sup>, Hamilton, D, P<sup>2</sup>, Lehto, N<sup>3</sup>, Hartland, A<sup>1\*</sup>,

<sup>1</sup>Environmental Research Institute, School of Science, The University of Waikato, Private Bag, 3105, Hamilton, New Zealand

<sup>2</sup>Australian Rivers Institute, Griffith University, Australia

<sup>3</sup>Dept. of Soil and Physical Sciences, Faculty of Agriculture and Life Sciences, Lincoln University, New Zealand

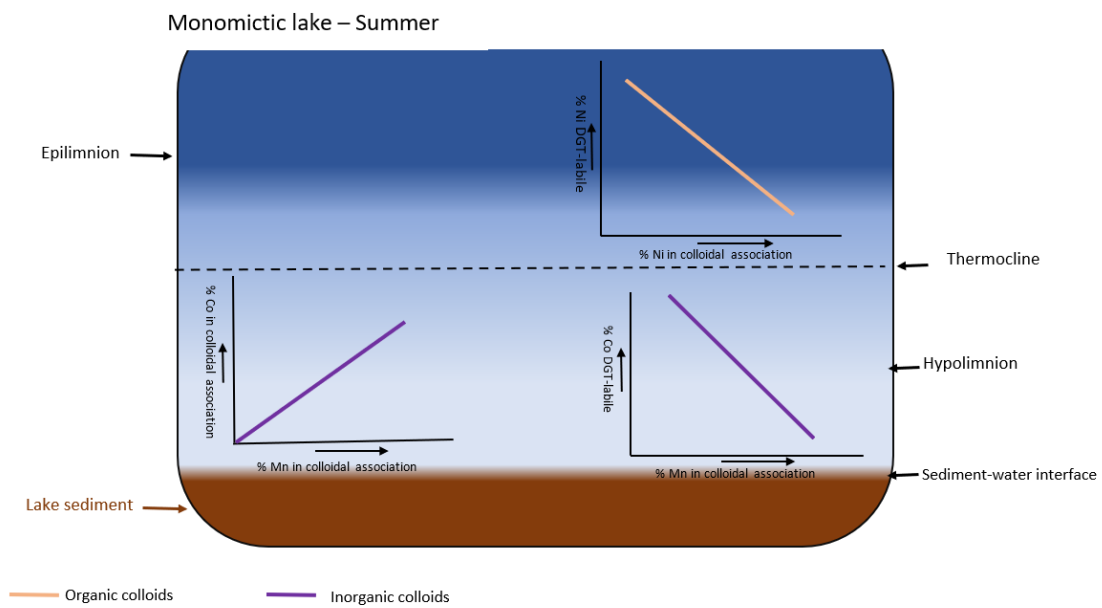
- Corresponding author

## 5.1 Abstract

Seasonal cycles in precipitation and dissolution of iron and manganese colloids alter trace metal (micronutrient) bioavailability in lakes, potentially impacting phytoplankton dynamics. We conducted a year-long study of the water column of Lake Ngapouri, Aotearoa, New Zealand to examine the role of colloids in regulating metal bioavailability. Diffusive gradients in thin films (DGT) probes were deployed in a vertical array every two months and analyzed for Fe, Mn, Cr, Co, Ni, Cu, Zn, and Cd alongside aquatic metal concentrations in colloidal (~5 nm to ~450 nm) and nominally dissolved (<5 nm) fractions.

Overall, DGT-labile trace metal concentrations were much lower than the dissolved and colloidal fractions, indicating the importance of complexation, adsorption, and precipitation in lowering the free ion activity of these metals. During stratification in summer, Fe, Mn, and Co lability increased in the hypolimnion, coincident with decreased Cr and Cd lability. Cr and Cd remained decoupled from Fe, Mn and Co in winter, with increases in Cr and Cd lability and complete loss of Fe, Mn, and Co under oxidizing conditions. In contrast to clear redox-driven cycles in Fe, Mn, Co, Cr, and Cd, the metals Cu, Ni, and Zn, displayed low lability and patchy distributions, independent of depth and season.

We ranked metals according to their median percentage associations with colloids and DGT-labilities. In surface waters (upper 10 m), Fe and Cr had the highest colloidal association and lowest DGT-lability, while Mn was both the least colloidal and most DGT-labile. Conversely, below 10 m, Cd was the most colloidal, and Cr and Ni were the least colloidal metals, yet Cd was the most DGT-labile, and Cr and Ni were the least DGT-labile elements. We conclude that colloidal interactions limit metal micronutrient availability in oxidising surface conditions, but metal-associated colloids (i.e., metal sulfides) are substantially more labile under anoxic conditions.



**Graphical abstract indicating that in the hypolimnion colloidal association is not a predictor of DGT-lability *i.e.*, DGT lability for Mn increased with colloidal association in hypolimnion suggesting that mineral colloids are more dynamic than organic complexes.**

**Keywords:** trace metals, speciation, colloids, eutrophic, redox, biogeochemical cycling, bioavailability, DGT

## 5.2 Introduction

Trace metals are an essential part of aquatic ecosystems (Hay, 1984; Morel *et al.*, 1991; Hongve, 1997; Kabata-Pendias, 2010; Rainbow, 2018). A subset of these metals, including iron (Fe), manganese (Mn), cobalt (Co), and nickel (Ni) (Morel and Price 2003) are essential for various metabolic pathways involving enzymes (Holm *et al.*, 1996; Pilon *et al.*, 2006), whereas other metals, such as Cd, are toxic for phytoplankton (Juneja *et al.*, 2013; Wong *et al.*, 1979). The chemical form, or speciation in which a trace metal ion determines its reactivity and the controls on its cycling in the environment. Because of this, changes in metal availability due to biogeochemical processes can affect primary productivity (Mildvan, 1970; Solomon & Hadt, 2011; Paerl *et al.*, 2015).

Bioactive metals can control primary productivity (Peers *et al.*, 2005; Kouba *et al.*, 2010; Facey *et al.*, 2019) in high-nutrient, low-chlorophyll (HNLC) in ocean surface waters (Valerie *et al.*, 2003; Korb & Whitehouse, 2004; Venables & Moore, 2010) as well as freshwater ecosystems (Horne, 1994; Evans & Prepas, 1997; North *et al.*, 2007). For these reasons there is now considerable interest in trace metal cycling in this context. Most notably, multi-factorial design experiments have been used to understand nutrient limitation in this context (Healey, 1979; Horne, 1994; Vrede & Tranvik, 2006; Dengg *et al.*, 2022), but previous studies have not necessarily made the explicit link to trace metal speciation, which is fundamental to considerations of micronutrient limitation and bioavailability.

Natural colloids and nanoparticles provide sites for critical geochemical processes in natural waters (Adams *et al.*, 1969; Pokrovsky *et al.*, 2012) and are fundamental for understanding trace metal behavior (Flemming & Trevors, 1989; Kimball *et al.*, 1995). The bioavailability (as well as the potential toxicity) of trace metals largely depend on free ion activity, which is inversely related to the degree of adsorption to solid surfaces and complexation with organic ligands (Davison, 1993). The ability of these phases to release ions (via desorption/dissociation) under varying physiochemical conditions, ultimately determines metal activity or lability. Where the rate of biological metal uptake is greater than the free ion's diffusion rate, lability can serve as an analog of bioavailability (Degryse *et al.*, 2009). This principle is largely supported by evidence from controlled dosing experiments (Havens *et al.*, 1999; Zhao *et al.*, 2016). However, the mechanisms and pathways that may limit or enhance

micronutrient availability to phytoplankton (Churchman & Lowe, 2012; Worms *et al.*, 2019), are yet to be studied in lakes.

Trace metal concentrations in lakes are governed by a range of dynamic reactions, and often, only a very small percentage of the total metal concentration is labile (Baeyens *et al.*, 2011). In seasonally stratified lakes, gradual changes in the redox state of hypolimnetic water cause spatial and temporal variations of redox-sensitive trace metals (Davison, 1993). Fe and Mn are very active in this regard, moving from insoluble oxides, to reduced and mobile forms ( $\text{Mn}^{2+}$ ,  $\text{Fe}^{2+}$ ) (Saeed *et al.*, 2018).

Other than Fe and Mn, there is limited data on the cycling of trace elements across the oxic-anoxic boundary (metalimnion) of lakes. The metalimnion, an interface between these geochemically distinct water masses, often coincides with higher primary productivity, and the zone referred to as the deep chlorophyll maximum (DCM) (Camacho González, 2006). Evidence from depth profiles of trace elements such as Hartland *et al.*, (2015) and Saeed *et al.*, (2018), point to active consumption of trace elements associated with DCM, which may in itself hint at a positive feedback that reinforces the development of DCM's (Hartland *et al.*, 2015).

Trace metal analysis of environmental samples is not a simple task due to the complexity of environmental matrices. In addition, detailed analyses of metal speciation can be confounded by the need to transfer samples to laboratories for analysis, which can further induce changes in the distribution of species before laboratory measurements can be conducted. Thus, an *in-situ* approach to trace metal speciation is needed to at least partially circumvent this issue (Hudson & Morel, 1990; Baeyens *et al.*, 2011; Achterberg & Braungardt, 1999; Sigg *et al.*, 2006; Cindrić *et al.*, 2020).

The aim of this study was to understand the role of colloids in the biogeochemical cycling of trace elements in the monomictic and eutrophic Lake Ngapouri, in order to better inform studies of micronutrient limitation in similar environments. To that end, we quantified trace elements in two size fractions to evaluate the partitioning of trace elements between colloidal and nominally-dissolved (<5 nm) size fractions. In addition, diffusive gradients in thin films (DGT) was used to quantify the *in-situ* availability of labile metals for phytoplankton uptake (Allan *et al.*, 2008; Montero *et al.*, 2012; Gao *et al.*, 2019). To enhance our interpretations,

geochemical modelling was used to predict organic complexation, mineral precipitation and dissolution in the water column, and to delineate the key geochemical processes driving elemental variations.

## **5.3 Materials and methods**

### **5.3.1 Water sampling**

Lake Ngapouri is a small crater lake (area 0.19 km<sup>2</sup>, mean depth 24 m) located in Aotearoa, New Zealand's central Northland. Seasonal anoxia in Lake Ngapouri's hypolimnetic waters as well as clear DCM, and high dissolved Fe and Mn concentrations, make the lake an interesting site for process-based research.

Water samples were collected using a Van Dorn sampler (PVC Beta<sup>TM</sup>, Envco, Auckland) which was deployed horizontally to collect water samples from 12 discrete depths, coincident with the deepest point of the lake. Samples were collected every second month from September 2015 to October 2016 at depths of 2.5 m, every meter between 5 and 13 m, and at 15 m and 20 m. Vertical profiles of the water column were measured for conductivity, temperature, pH, Chl-a fluorescence, and dissolved oxygen using a conductivity-temperature-depth profiler (CTD; Sea-Bird Electronics Inc., Washington) during every water sampling trip, with the exception of pH data for January 2016, which are missing due to a faulty probe. Water transparency was recorded using a Secchi disk during every sampling event (Preisendorfer, 1986).

Water samples were then immediately filtered in the field using 0.45 µm syringe filters (Sartorius Stedim, Germany) into pre-cleaned bottles and were preserved using ultrapure HNO<sub>3</sub> (distilled using a Savillex DST-1000, Teflon distillation unit, Savillex, MA, USA) to 2% final acid concentration for cation analysis using ICP-MS. Samples collected for major anions analysis were filtered in the field but not acidified. Water samples for size fractionation were collected in airtight syringes from identical depths. All samples were individually placed in doubled plastic bags, and transported to the laboratory on ice in the dark.

Samples for the estimation of Chl-a were collected by filtering 50 mL of the lake water through GF/C filter membranes (Whatman, Maidstone, United Kingdom) from each depth. The filters were folded in half, individually wrapped in aluminium foil and transported to the laboratory. The samples were then frozen in the laboratory under dark conditions and analysed within a week of collection (Welschmeyer, 1994).

All samplers, containers, and filtration devices except for Chl-a were rigorously cleaned by soaking in trace-element-free detergent CITRANOX®, HCl (10%), HNO<sub>3</sub> (10%) and triple rinsed with deionized (DI) water. The samplers and samples were protected in acid-washed double plastic bags during transport.

### 5.3.2 Ultrafiltration

Trace elements were separated in two size fractions (<0.45 µm and <5 nm). To obtain the <5 nm size fraction, ultrafiltration of samples preserved in gas-tight syringes was carried out in an N<sub>2</sub> pre-purged glove box to minimize the potential for oxidation of reduced species (Saeed *et al.*, 2018), using an Amicon stirred-cell ultrafiltration system (Amicon® model 8400) equipped with 100 kDa (molecular weight cut-off (MWCO)) regenerated cellulose ultrafiltration discs (Millipore Corporation, Billerica, MA, USA) under zero-grade N<sub>2</sub> (200 Pa). The ultrafiltration cell was rinsed with DI water to remove any secondary filtration sites on the filter membrane, and minimize contamination between samples. The filtrate was acidified to 2% final acid concentration using distilled ultrapure HNO<sub>3</sub> for ICP-MS. The colloidal fraction (C<sub>x</sub>) was calculated using Eq. 5-1.

$$C_x = C_{<0.45 \mu m} - C_{<5 nm} \quad (5-1)$$

where, C<sub><0.45 µm</sub>, and C<sub><5 nm</sub> refer to concentrations in the two size fractions obtained by filtration at 0.45 µm and 100 kDa (~ 5 nm), respectively.



### 5.3.3 Assessing potential metal bioavailability with DGT

The DGT-labile concentration of trace metals was determined using DGT solution probes with a diffusive gel thickness of 0.8 mm and Chelex-100 metal-binding resin layer. Chelex-100 has a strong affinity for free metal ions, inorganic complexes, and metal-organic complexes, which exhibit relatively fast dissociation kinetics (Zhang & Davison, 1995). The probes were deployed in triplicate, at identical depths to the collected water samples (Saeed *et al.*, 2018).

DGT's were retrieved from the lake after one week, rinsed with DI water, and stored in plastic double bags for subsequent analysis. The resin gels were retrieved from the DGT housings and eluted in 1 mL of 1 M HNO<sub>3</sub> for at least 24 h on a shaker plate in a class-100 clean room. The concentrations of the target analyte ( $C_{DGT}$ ) in the lake water were calculated after Davison and Zhang (Davison & Zhang, 2012) and are reported as representative of the end date of each respective measurement period. For quality control purposes, a set of three chelex probes was prepared, transported to and from the field site and analysed under the same conditions as that of deployed DGTs. Presented  $C_{DGT}$  values are blank corrected using these values, where applicable.

The diffusive boundary layer (DBL) effect was not determined in this study. However, previous analysis of phosphorus concentrations in Lake Ngapouri using ferrihydrite DGT probes showed a close agreement between concentrations measured by DGT and dissolved reactive phosphorus, indicating that diffusive boundary layer effects were minimized by the longer deployments (Saeed *et al.*, 2018). Following analysis by ICP-MS, trace metals were ranked (0-9) based on their median percentage associations in colloidal and DGT-labile fractions (Table 5.1). A higher median percentage association, equated to a higher rank on the relative scale.

**Table 5.1: Trace metal ranking based on the median colloidal and DGT-labile concentrations in surface (2.5-10 m) and deep waters (15 and 20 m) across the hydrologic year.**

<b>Colloid median (% range)</b>	<b>Colloid scale</b>	<b>C<sub>DGT</sub> median (% range)</b>	<b>DGT-labile scale</b>
0-10	0	0-10	0
11-20	1	11-20	1
21-30	2	21-30	2
31-40	3	31-40	3
41-50	4	41-50	4
51-60	5	51-60	5
61-70	6	61-70	6
71-80	7	71-80	7
81-90	8	81-90	8
91-100	9	91-100	9

### **5.3.4 Trace metal, Chl-a and nutrient analysis**

We selected trace elements we considered representative of different chemical characteristics and behaviour (1) easily hydrolysable and mineral forming species such as Fe and Mn, (2) other transition metals such as Cu, Ni, Zn and Cr. The concentration of trace metals (Fe, Mn, Cr, Cu, Ni, Co, Cd, and Zn) in both size fractions and the DGT eluents were determined using a Perkin Elmer (Elan, Waltham MA) quadrupole ICP-MS. The instrument was previously reported to have adequate sensitivity for direct metal analysis to low ppb levels (Hartland *et al.*, 2019). The instrument was calibrated using certified reference materials SLR-6 (Sigma Aldrich, Auckland, Aotearoa, New Zealand) and reported values are blank-corrected where applicable. We refer readers to Saeed *et al.*, 2018 for detailed description of trace element analyses (Saeed *et al.*, 2018). Chl-a was extracted using acetone after Lorenzen (1966) (supplementary information for method details). The relationship between fluorescence and Chl-a concentration was used to convert the fluorescence signal of the CTD to Chl-a value.

### 5.3.5 Equilibrium speciation modelling

PHREEQC is an open-source modeling code that contains a widely accepted database of thermodynamic constants for the solution and solid-phase geochemical constituents commonly found in natural systems. The monitoring data from Lake Ngapouri was balanced for charge difference with either  $\text{Na}^+$  or  $\text{HCO}_3^-$  prior to speciation in PHREEQC (Parkhurst & Appelo 2003). The charge-balanced element concentration data, pH, and temperature values of each sample were then used to calculate the saturation indices of mineral phases of Fe, Mn, and Al in the lake water column. Components included in the speciation model were F, Cl, S (6), S (-2), N (-3), N (+5), N(+3), Na, K, Mg, Ca, Fe, Mn, Ni, Cu, Zn, P, Al,  $\text{HCO}_3^-$ , As, B, Ba, and Si, where the numbers in parentheses refer to the elemental oxidation state. The model was run for individual samples, and the resulting saturation indices (SI) were used to drive mineral dissolution or precipitation reactions on the following basis:

SI < 0; the mineral dissolves to reach equilibrium,

SI > 0; the mineral can be present as a solid precipitate, and

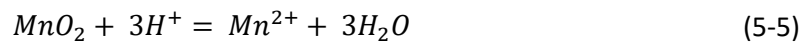
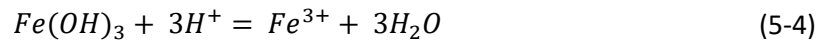
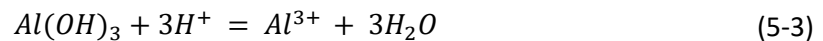
SI = 0; the mineral is unlikely to be in purely dissolved or solid form, but can exist in equilibrium with these species.

In order to constrain the redox equilibrium of the important Mn- and Fe-bearing minerals, solution electron activity was calculated in PHREEQC prior to the mineral equilibration step. Electron activity (pe) was calculated using  $\text{O}_2/\text{H}_2\text{O}$ ,  $\text{Fe}^{3+}/\text{Fe}^{2+}$  and  $\text{SO}_4^{2-}/\text{H}_2\text{S}$  redox couples. The mineral equilibrium was then calculated following the Gibbs phase rule. Although  $\text{HS}^-$  and  $\text{H}_2\text{S}$  were not measured directly, we followed the approach used by Hartland *et al.*, (2015), whereby S loss in the hypolimnion was considered as an indicator of dissimilatory S reduction. It was previously shown that the hypolimnion of Lake Ngapouri approximates a closed system (Hartland *et al.*, 2015), and that the stoichiometry of  $\text{SO}_4^{2-}$  and  $\text{HCO}_3^-$  was consistent with the overall reaction:



The solution concentrations of Fe, Mn, and Al were thus adjusted for mineral stability (as defined by SI values), but only allowing precipitation to occur. These simulations were then used in the calculation of the concentration of suspended mineral phases, which the solution was likely to be in contact with. This exercise therefore allowed for the exploration of potential adsorption and complexation reactions between the aforementioned mineral surfaces and trace elements in the samples. It was also necessary because inorganic components (*e.g.*, Fe, Mn hydroxides) in the water samples are ionized during elemental analysis, and therefore information on the mineralogy of colloidal/particulate matter is necessarily lost.

For surface-complexation simulations in Visual MINTEQ, we assumed that solution activities of  $Al^{3+}$ ,  $Fe^{3+}$  and Mn(IV) are controlled by the solubilities of aluminium hydroxide/gibbsite ( $Al(OH)_3$ ), amorphous iron (III) hydroxide ( $Fe(OH)_{3(a)}$ ) and manganese dioxide ( $MnO_2$ ) according to the reactions 5-3 to 5-5.



In addition to the calculated concentrations of  $Fe(OH)_{3(a)}$ ,  $MnO_2$ , and  $Al(OH)_3$  in suspension (based on PHREEQC equilibria), modelling in visual MINTEQ was further constrained by the incorporation of physical parameters, *e.g.*, DO and pH (derived from CTD measurements), trace elements (ICP-MS analysis), and colloidal size dimensions (Atomic Force Microscopy data sourced from Saeed *et al.*, (2018)). The particle geometry for surface complexation/adsorption modelling was assumed to be spherical, although the use of a planar geometry gave similar results. Visual MINTEQ (Gustafsson, 2007) was used to calculate (i) the activities of aquatic components, and (ii) the percentage distribution between dissolved and adsorbed species. Complexation and surface adsorption in the lake water column was primarily modelled for  $Fe(OH)_3$ ,  $MnO_2$ , and  $Al(OH)_3$  and the percent distribution of trace elements between dissolved and adsorbed species. Furthermore, the complexation

and surface adsorption of trace metals was modelled using NICA-Donnan model (Gustafsson, 2013), in which all DOM was considered to be 'fulvic' for modelling purposes.

## 5.4 Results

### 5.4.1 Thermal and redox stratification

The physical properties of Lake Ngapouri in 2015-2016 are presented in depth-time contour plots (Figure 5.1). The white vertical lines in Figure 5.1a show the actual sampling times, while contours show interpolated data between those sampling events.

Surface water temperature ranged from about 9 to 23°C (Figure 5.1a). Thermal stratification commenced during austral spring and persisted for about ten months until autumn. Over this time a stable metalimnion developed, which was centered around 5m in late summer and was broader and deeper before and after this time. The entire water column mixed in July 2016, denoted by the absence of a vertical gradient of temperature, coincident with cooler air temperatures and stronger winds (data collected from CliFlo, NIWA).

The distribution of dissolved oxygen showed two distinct periods (Figure 5.1b). First, a uniform concentration close to saturation throughout the water column over winter (Figure 5.1b). Second, oxygen-depletion in the hypolimnion. Summer time concentrations were close to zero in the deeper water (Figure 5.1b). During summer, the surface-water DO concentrations at times exceeded saturation (Ohnstad *et al.*, 1978), with values up to 0.55 mM O<sub>2</sub> (Figure 5.1b). Thus, stratification created three distinct vertical zones of varying temperature and oxygen concentrations: an oxic epilimnetic layer of nearly uniform temperature, a transitional metalimnetic layer characterised by a rapid change in temperature and dissolved oxygen, and a hypolimnetic layer that, when essentially isolated from surface waters by the prevailing temperature stratification, transitioned from suboxic to anoxic, and remained anoxic for the remainder of the stratified period.

Figure 5.1c shows the Chl-a distribution in the lake water; the length of the white vertical lines represent the transparency of the lake measured as Secchi depth. High Chl-a (> 10 µg L<sup>-1</sup>) occurred during three sampling periods: (i) near-surface (~ 5 m) in September 2015, (ii) 7-9 m coincident with the metalimnion depth in January-March 2016, and (iii) surface water in

October 2016. Surface water pH (Figure 5.1d) was circumneutral during the study period except in October 2016, coincident with the chl-a peak, when pH values were hyper-alkaline (9.2). The pH of the hypolimnion, in contrast, decreased during the summer stratified period to a minimum of 6.4 in May.

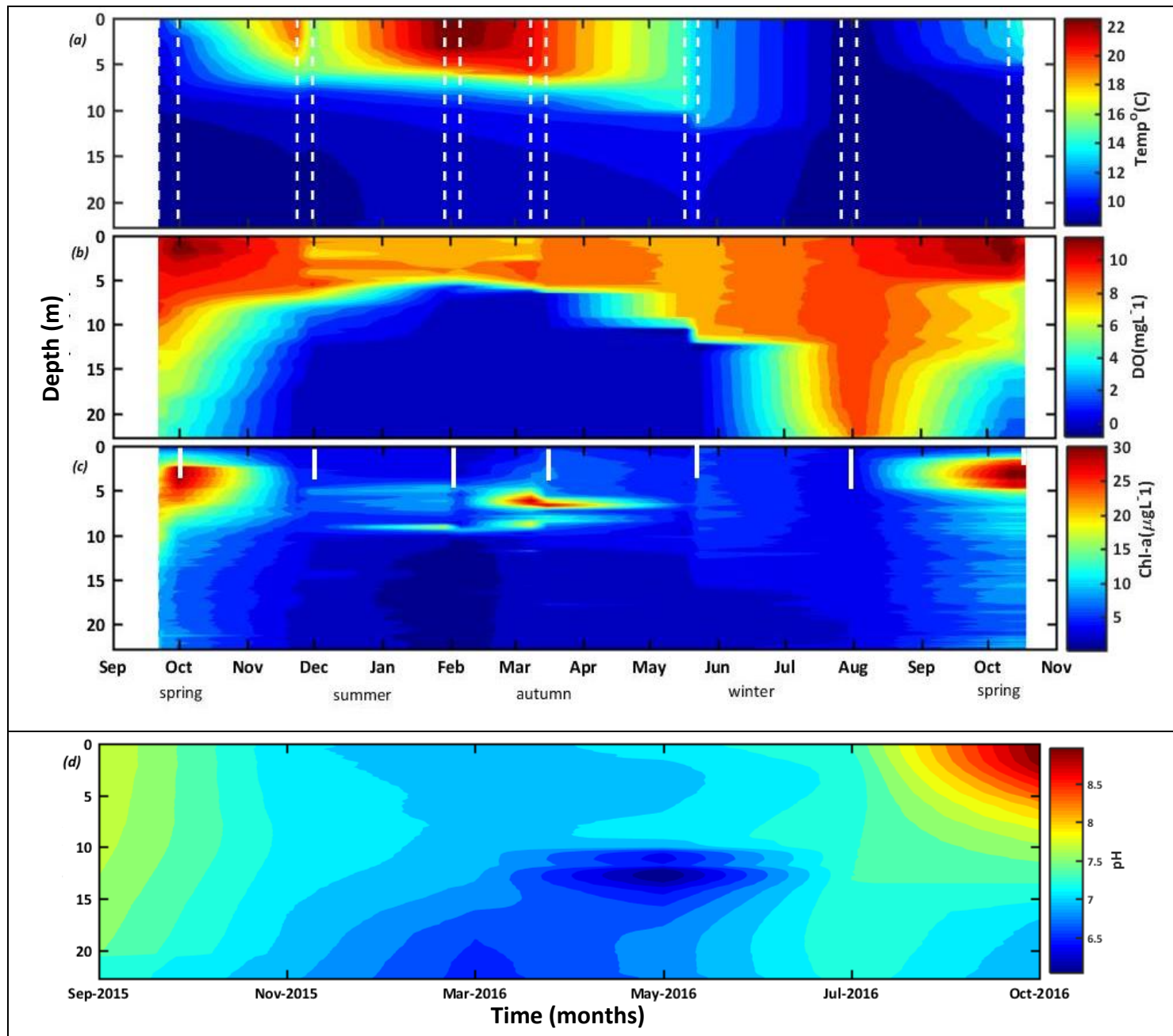


Figure 5.1: Time vs Depth contour plots of physiochemical variables in Lake Ngapouri. (a) Temperature (°C), (b) dissolved oxygen (mg L<sup>-1</sup>), (c) Chl-a (µg L<sup>-1</sup>), (d) pH

## 5.4.2 Trace element concentrations: vertical and seasonal profiles

### 5.4.2.1 Iron, manganese, and aluminium

Figure 5.2 shows data from three major mineral forming elements, Fe, Mn, and Al, in dissolved, colloidal, and DGT-labile fractions. Comparison of trace element distributions across the two size fractions ( $<0.45\ \mu\text{m}$ , and colloidal) with  $C_{\text{DGT}}$  showed that the Fe and Mn dynamics were strongly dictated by thermal stratification and redox processes in the hypolimnion (Figure 5.2). Fe and Mn concentrations decreased across the series  $<0.45\ \mu\text{m} \rightarrow \text{colloidal} \rightarrow C_{\text{DGT}}$  although more Fe than Mn was generally present in the colloidal fraction (Figure 5.2, Table 5.2).

Fe concentration increased in all three fractions near the benthic-nepheloid layer in spring and summer (Figure 5.2a-c). The colloidal Fe fraction (Figure 5.2b) had a similar distribution to the  $<0.45\ \mu\text{m}$  fraction (median colloidal association of 97%, Table 5.2), with the DGT-labile fraction lagging the dissolved and colloidal fractions up until mid-summer (Figure 5.2c). After summer, when the lake was mixed, the total concentration of Fe was uniformly low in all three fractions (Figure 5.2a-c).

The increase in Mn in the  $<0.45\ \mu\text{m}$  and  $C_{\text{DGT}}$  fractions, preceded Fe and closely followed the loss of dissolved oxygen (Figure 5.1b). The dissolved Mn fraction exhibited a similar pattern to dissolved Fe in the hypolimnion that appeared to slightly precede Fe (Figure 5.2a and d). A well-defined peak in Mn occurred in the metalimnion, with a maximum concentration of  $22.8\ \mu\text{mol L}^{-1}$  in May, with  $>50\%$  of Mn in-association with colloids (Figure 5.2e, Table 5.2). Otherwise, the distribution of Mn colloids was mostly patchy through time and with depth, constituting only a small fraction of the total Mn (Figure 5.2c). For the most part, Mn was DGT-labile, being ranked the most DGT-labile metal measured in this study (Figure 5.2c, Table 5.2).

Aluminium (Al) in the  $<0.45\ \mu\text{m}$  fraction was almost featureless as a function of depth, thermal stratification, and redox conditions, with the exception of transient peaks in Al at a depth of 20 m in November 2015 (Figure 5.2g). The colloidal fraction ( $\text{Al}_c$ ) was present in low, but resolvable concentrations, and was partially DGT-labile (Figure 5.2h-i). Colloidal Al ( $\text{Al}_c$ ) generally followed the same spatial pattern as  $\text{Al } C_{\text{DGT}}$ , the  $C_{\text{DGT}}$  concentrations being  $\sim 4$  times lower than  $\text{Al}_c$  values.



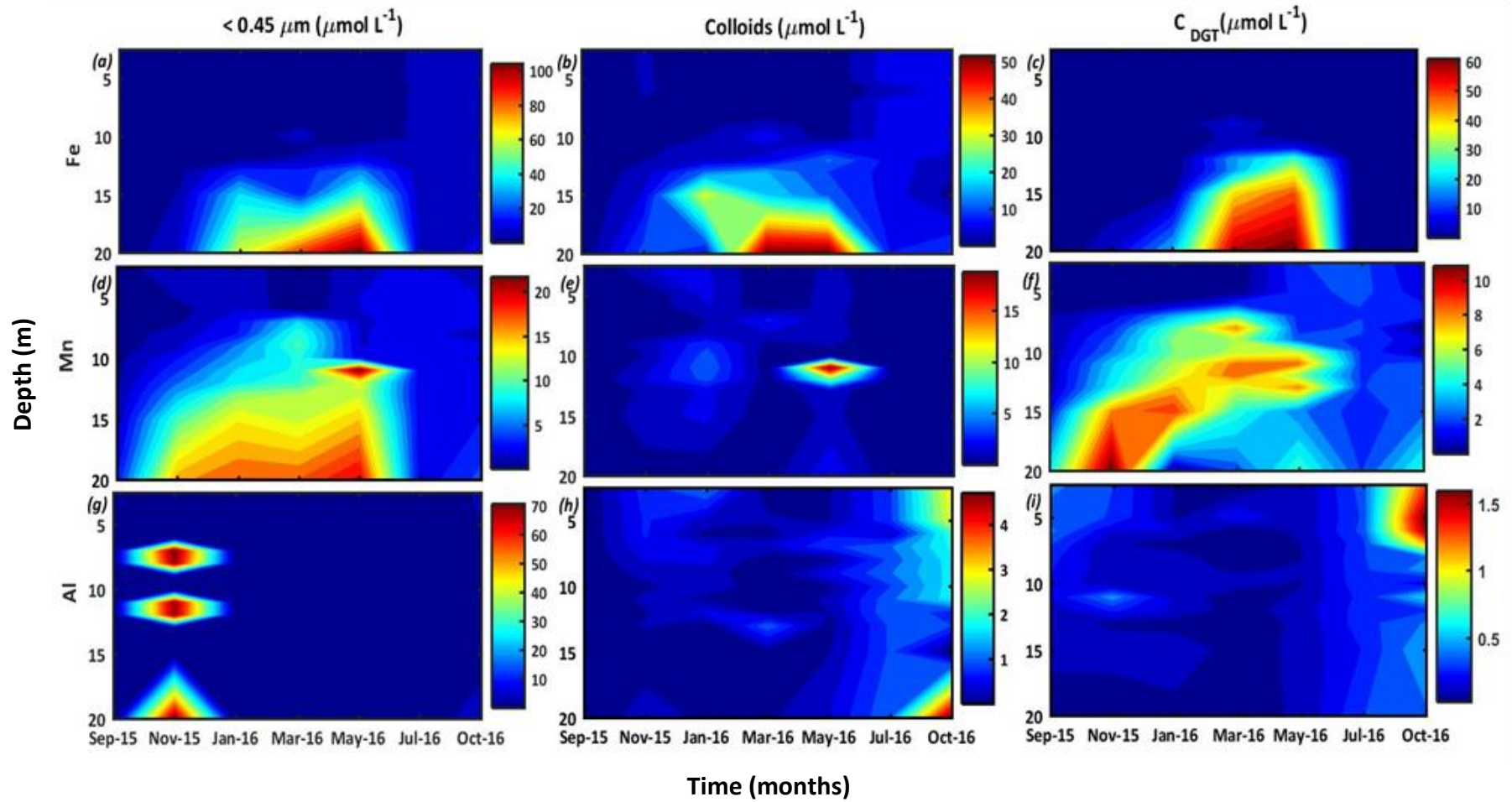


Figure 5.2: Time-depth distributions of three major mineral-forming trace elements (Fe (a-c), Mn (d-f), and Al (g-i)) in Lake Ngapouri.

#### 5.4.2.2 Cadmium, chromium, and cobalt

Three trace metals, Cd, Cr, and Co, exhibited seasonal redox-driven variability to varying degrees and hence are presented together. Figure 5.3 shows their vertical distributions in the three fractions. The DGT-labile concentrations were around one order of magnitude lower than the  $<0.45\ \mu\text{m}$  fraction for all three metals.

The concentrations of dissolved Cd increased slightly throughout the water column in January 2016 (Figure 5.3a), but colloidal Cd was more variable, increasing slightly in concentration during November 2015 (Figure 5.3b) in the hypolimnion. This increase was consistent with increases observed in the DGT-labile fraction at the same time (Figure 5.3c). During winter, there was no significant increase in the concentration of Cd in either size fraction, but DGT-labile Cd was elevated during winter, coinciding with full lake oxygenation.

A fraction of chromium (Cr) was present in the nominally-dissolved fraction ( $<5\ \text{nm}$ ) throughout the water column (Table 5.2a and 5.2b). Cr showed some seasonal variability in all three fractions and was mostly present (up to 95%) as colloids ( $<0.45\ \mu\text{m}$  fraction) in the upper 10 m (Figure 5.3d-f), ranking '9' on the colloid-association scale (Table 5.1, 5.2a). Importantly, Cr associated with colloids was not DGT-labile (ranked 0, DGT-labile scale, Table 5.2a). Conversely, in the hypolimnion, Cr did not show an appreciable colloidal association (ranked 0 on the colloidal scale), but again Cr was weakly DGT-labile (Table 5.2b).

Concentrations of cobalt (Co) were about three orders of magnitude lower than Mn in the water column but had a similar seasonal distribution (compare Figure 5.2d-f to Figure 5.3g-i). Concentrations of dissolved Co increased in the hypolimnion and metalimnion between January and May 2016 (Figure 5.3g), achieving a maximum colloidal association (42%, Table 5.2a) in Jan-16 in the upper 10 m, coincident with higher colloidal Mn. Both Mn and Co were scarcely present as colloids and ranked between 0 and 2 on the colloidal scale (Table 5.2).

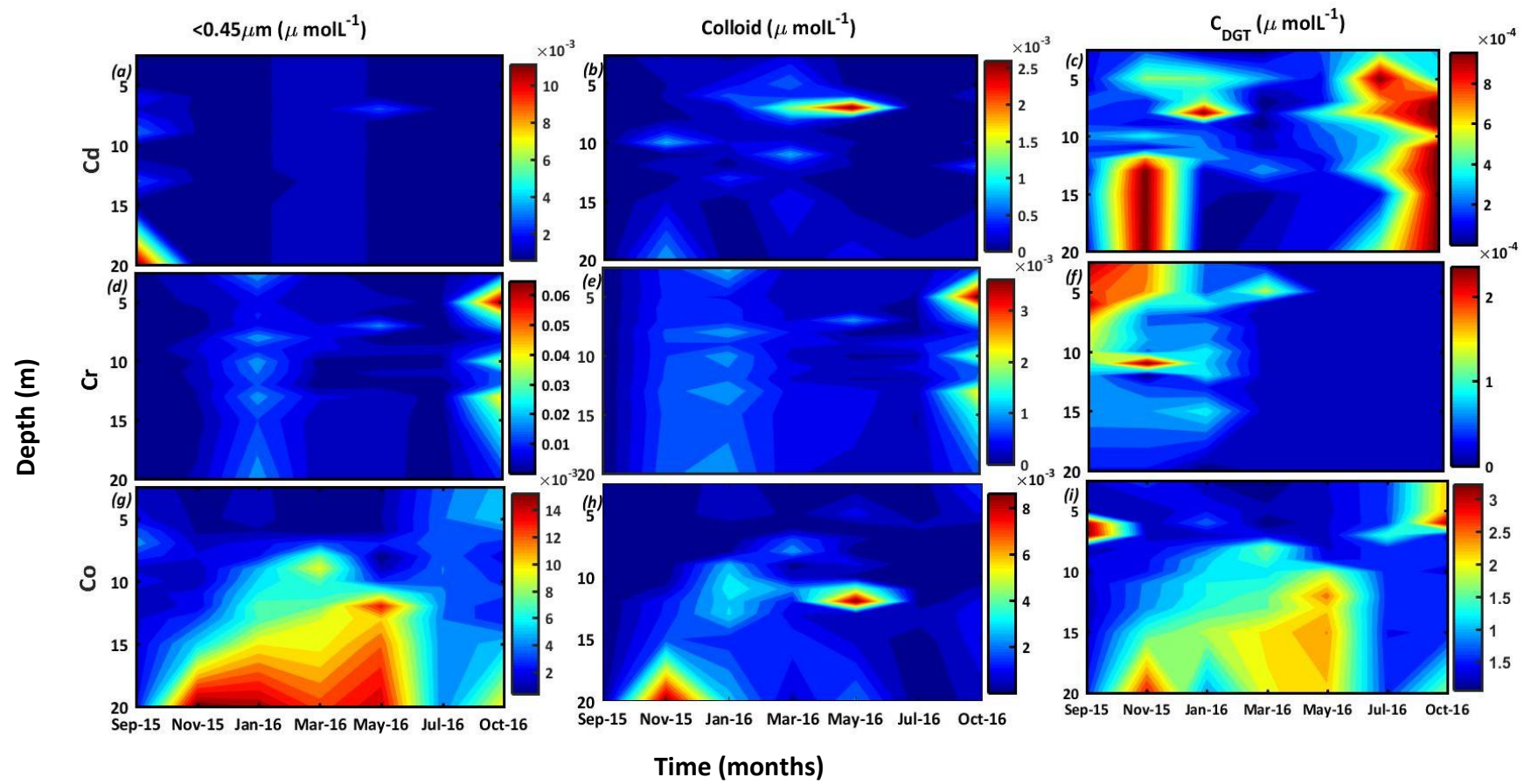


Figure 5.3: Time-depth distributions of Cd (a-c), Cr (d-f), and Co (g-i) in Lake Ngapouri.

#### **5.4.2.3 Zinc, nickel, and copper**

Concentrations of divalent transition metals, Zn, Ni, and Cu, were highly variable through time and with depth, and were decoupled from seasonal transitions evident for Fe, Mn, and Co (Figure 5.4), and hence are presented together. The exception here was Zn, which decreased in all three size fractions following mixing in July 2016.

Overall, Zn was variable over time and space, but was mainly present in association with colloids (ranked 8 on the colloidal scale), exhibiting low lability (DGT rank 0). Elevated colloidal Zn was observed in the hypolimnion during March 2016, but was not correlated with Cu and Ni.

Copper (Cu) and Nickel (Ni) were generally partitioned between the <5 nm and colloidal fractions, with a small fraction being DGT-labile in the upper 10 m (Figure 5.4d-i). Zn, Ni, and Cu bioavailability as measured by DGT was greatest during July, when the lake following mixing (Table 5.2 a-b). For Cu and Ni, patches of increased concentrations were observed in surface water during late summer in association with colloids.

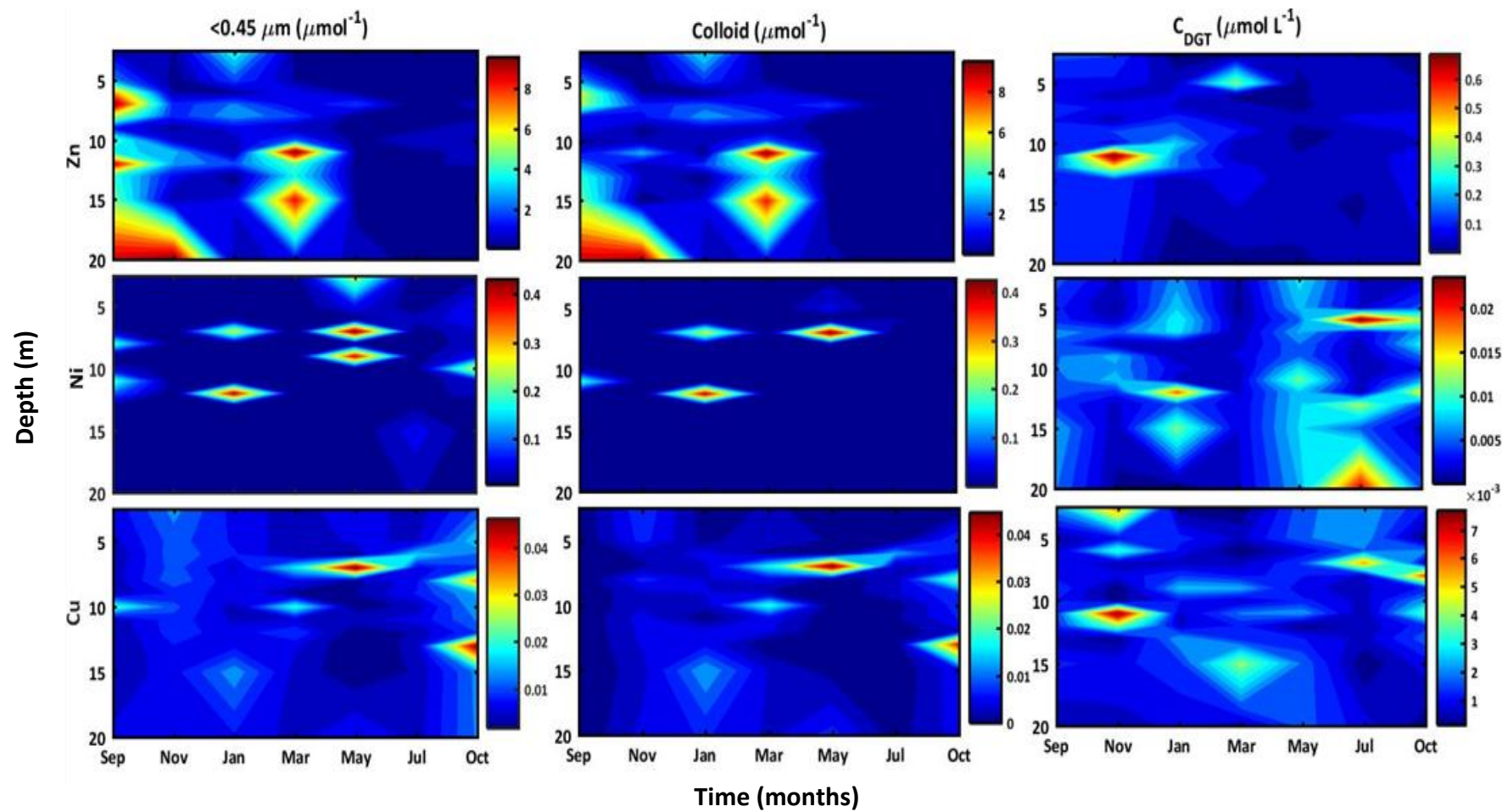


Figure 5.4: Time-depth distributions of Zn (a-c), Ni (d-f), and Cu (g-i) in Lake Ngapouri.

### 5.4.3 Precipitation and dissolution of mineral colloids: equilibrium speciation modelling

#### 5.4.3.1 Mineral solubility modelling in PHREEQC

The PHREEQC-modelled stability of mineral precipitates for the three major mineral-forming metals, Fe, Mn, and Al, are presented in Figure 5.5. This exercise revealed that iron was likely to be present as Fe(II) species, or iron monosulphide FeS (Figure 5.5c), in the hypolimnion, and amorphous Fe(OH)<sub>3</sub> in the epilimnion. Mn was predicted to be distributed between an oxide (MnO<sub>2</sub>) in the epilimnion, and MnHPO<sub>4</sub> in the hypolimnion, coincident with benthic P releases during peak stratification.

Fe(OH)<sub>3(a)</sub> most likely predominated under oxic conditions, in particular following turnover in July 2016 (Figure 5.5a), leading to the rapid addition of reactive Fe(OH)<sub>3</sub> surfaces to the water column. Concentrations of MnS were predicted to be near zero, and considerably lower than FeS concentrations (Figure 5.5c). Our modelling also indicated a uniform distribution of AlO(OH) precipitates except in November when the accumulation of AlO(OH) was predicted in the thermocline and hypolimnion (Figure 5.2g). Further, PHREEQC predicted the formation of CdS in the hypolimnion in November, coinciding with ~48% of the dissolved Cd load being present as colloids (Table 5.2b).

PHREEQC predicted the formation of MnHPO<sub>4(s)</sub> in the hypolimnion during the summer-stratified period also coincident with depletion in DGT-labile Mn and P. Similarly to iron, MnO<sub>2</sub> was predicted to be the dominant phase in the lake's surface waters throughout the study period and throughout the water column in winter (July).



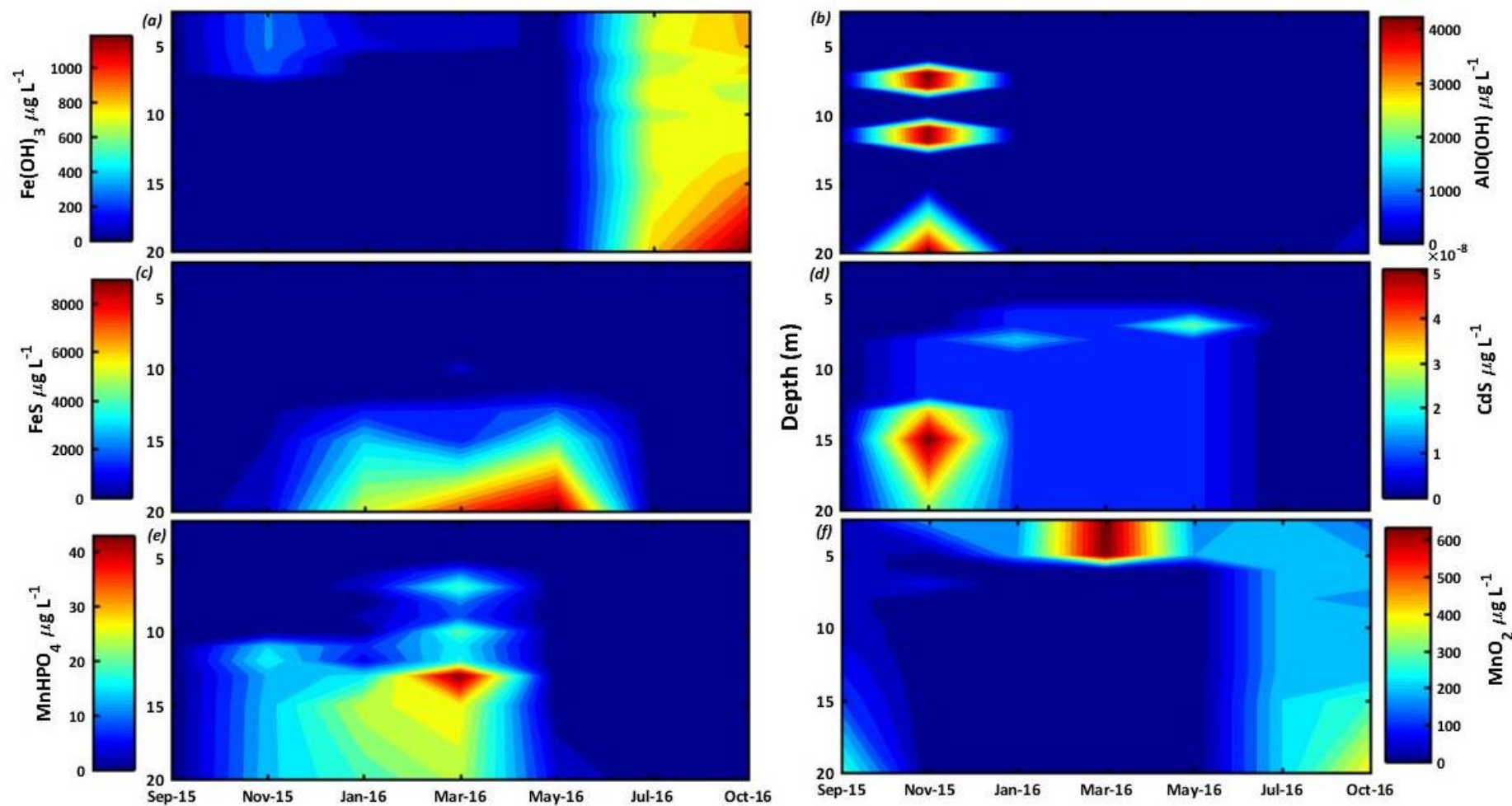


Figure 5.5: Time-depth distributions of modelled colloidal minerals in the water column of Lake Ngapouri. (a) iron(III) oxy-hydroxide ( $\text{Fe(OH)}_3$ ), (b) boehmite<sub>(a)</sub> ( $\text{AlO(OH)}$ ), (c) iron(II) sulphide<sub>(a)</sub> ( $\text{FeS}$ ), (d) cadmium sulphide ( $\text{CdS}$ ), (e) manganese hydrogen phosphate ( $\text{MnHPO}_4$ ), (f) pyrolusite ( $\text{MnO}_2$ ). The values are presented in  $\mu\text{g L}^{-1}$ , representing the simulated concentration of suspended mineral solids in the water column.

**Table 5.2: Percentage association of trace elements with colloids and solutes in <0.45 µm fraction (a) average surface water 2.5-5 m and (b) average hypolimnetic water from 15-20 m**

2a	Fe (% <0.45 µm)			Mn (% <0.45 µm)			Al (% <0.45 µm)			Cr (% <0.45 µm)			Cd (% <0.45 µm)			Co (% <0.45 µm)			Cu (% <0.45 µm)			Zn (% <0.45 µm)			Ni (% <0.45 µm)		
	ND	Col.	C <sub>DGT</sub>	ND	Col.	C <sub>DGT</sub>	ND	Col.	C <sub>DGT</sub>	ND	Col.	C <sub>DGT</sub>	ND	Col.	C <sub>DGT</sub>	ND	Col.	C <sub>DGT</sub>	ND	Col.	C <sub>DGT</sub>	ND	Col.	C <sub>DGT</sub>	ND	Col.	C <sub>DGT</sub>
Sep	100	0	22	100	0	96	100	0	100	5	95	1	30	70	11	100	0	18	100	0	24	100	0	7	100	0	41
Nov	1	99	1	15	85	24	21	79	34	9	91	3	12	88	35	59	41	28	36	64	29	5	95	31	92	8	15
Jan	1	99	1	1	99	5	10	90	11	28	72	2	18	82	26	62	38	17	87	13	11	11	89	1	33	67	31
Mar	8	92	23	43	57	63	48	52	51	100	0	79	0	100	11	100	0	32	79	27	82	26	74	44	78	22	15
May	3	97	8	39	61	94	29	71	39	10	90	1	18	82	16	47	53	17	94	6	27	58	42	10	41	59	19
Jul	2	98	1	91	9	100	38	62	25	20	80	2	20	80	70	96	4	17	91	9	43	14	86	13	77	23	19
Oct	8	92	2	72	28	57	21	79	40	5	95	0	2	98	34	75	25	43	100	0	5	26	74	6	24	76	7
Median	0	97	2	43	57	63	29	71	39	10	90	2	18	82	26	75	25	18	91	9	27	26	74	10	77	23	19
CR		9			5			7			8			8			3			0			7			2	
LR			0			6			3			0			2			1			2			0			1

2b	Fe (% <0.45 µm)			Mn (% <0.45 µm)			Al (% <0.45 µm)			Cr (% <0.45 µm)			Cd (% <0.45 µm)			Co (% <0.45 µm)			Cu (% <0.45 µm)			Zn (% <0.45 µm)			Ni (% <0.45 µm)		
	ND	Col.	C <sub>DGT</sub>	ND	Col.	C <sub>DGT</sub>	ND	Col.	C <sub>DGT</sub>	ND	Col.	C <sub>DGT</sub>	ND	Col.	C <sub>DGT</sub>	ND	Col.	C <sub>DGT</sub>	ND	Col.	C <sub>DGT</sub>	ND	Col.	C <sub>DGT</sub>	ND	Col.	C <sub>DGT</sub>
Nov	0	100	35	93	7	76	0	100	0	6	94	0	52	48	100	67	33	14	42	58	12	32	68	2	89	11	12
Jan	62	38	22	92	8	31	40	60	32	51	49	3	8	92	3	84	16	11	9	91	11	28	72	3	86	14	45
Mar	32	68	73	98	2	24	69	31	26	11	89	0	24	100	4	93	7	18	100	0	52	1	99	1	68	32	22
Median	32	68	35	93	7	31	40	60	26	11	89	0	24	92	4	84	16	14	42	81	12	28	72	2	86	14	22
CR		6			0			5			8			9			1			8			7			1	
LR			3			3			2			0			0			1			1			0			2

CR = Colloidal rank    LR = Labile rank    ND= <5 nm    Col. = Colloid ( <0.45 µm – <5 nm)

Table 5.1 on colloidal and labile rank calculations



#### 5.4.4 Surface complexation modelling of micronutrient binding to mineral colloids

The percent adsorption of trace elements to mineral precipitates (hydrous ferric oxide (HFO), hydrous manganese oxide (HMO), and gibbsite  $\text{Al}(\text{OH})_3$ ) was modelled with Visual MINTEQ for the upper 10 m of the lake water column (Figure 5.6). The percentage of each trace element measured by DGT, which we interpret as a proxy for free ion activity, is also shown in Figure 5.6.

VMINTEQ outputs did not show any adsorption of Co to HFO or gibbsite (Figure 5.6a). However, HMO was predicted to be of importance for Co adsorption. As the degree of Co-HMO adsorption increased, the lability of Co to DGT decreased in an inverse manner (Figure 5.6a). Generally, Co was less DGT-labile during the summer-stratified period in the upper water column than during winter for the same depth. The DGT-labile Co fraction was higher in May and immediately decreased at the time of lake turnover.

Most Cu measured in the lake was in the nominally dissolved (*i.e.*, <5 nm) fraction (Figure 5.4g-f). By contrast, VMINTEQ modelling suggested that HFO influenced Cu lability to DGT by the highest degree, which is consistent with the lower DGT-labile Cu concentrations measured at times of higher simulated Cu adsorption to HFO. The inclusion of DOM into the VMINTEQ model (NICA-Donnan) did not change the % association between Cu and Ni to mineral phases.

The MINTEQ modelling also indicated that a certain fraction of Zn and Ni partitioned into DOM, this fraction remained consistent when mineral phases were added, but being a relatively minor component (< 10%), within the modelled species distribution.

Measurements from lake water show that Zn was mainly present in association with colloids (Table 5.2) and that the DGT-labile fraction did not exhibit any clear trend that could be correlated with the surface-complexation model. Ni was generally less DGT-labile when more was present in the colloidal fraction (Table 5.2 and Figure 5.6d), and also was not predicted by VMINTEQ to be associated with mineral phases (Figure 5.6d).

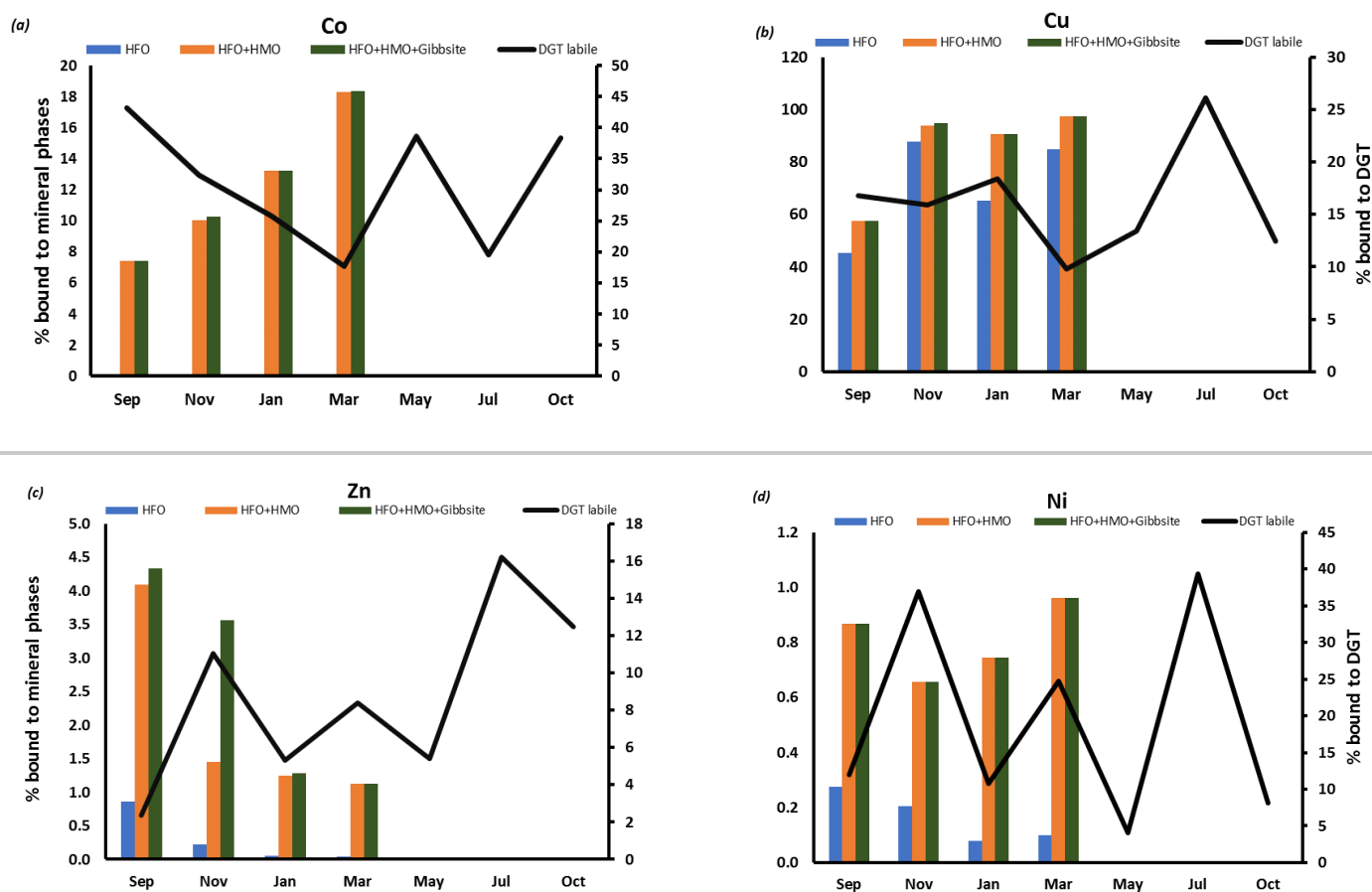


Figure 5.6: Surface complexation modelling of the interaction between Co, Cu, Zn, and Ni and suspended mineral particles in the lake surface water previously simulated with PHREEQC. The percent of  $<0.45 \mu\text{m}$  available for DGT uptake (DGT-labile) is shown on the secondary Y-axis. Plots show (a) Co, (b) Cu, (c) Zn, and (d) Ni, respectively

## 5.5 Discussion

The findings of this study clearly show that trace metal micronutrients in lake systems are subject to a wide range of geochemical processes and interactions that drive substantial variations in bioavailability (as measured by DGT).

The degree of colloidal association for a given metal was a strong predictor of trace metal (*i.e.*, Fe, Cr, Cu, Cd, Zn) limitation (*i.e.*, DGT-lability) in oxic lake surface water. This colloid-limitation effect was most prominent for Fe and Cr. Manganese was dissolved to a higher degree than Fe under oxic conditions, and was found to be the most DGT-labile metal in surface water (Table 5.2a). Conversely, colloidal association in the anoxic hypolimnion was not a strong predictor of Mn and Co limitation. Here, Cd and Cr were found to be the most colloidal metals and also the least DGT-labile. Hence, metal-colloid association can limit metal bioavailability under oxic conditions, but less so under anoxic conditions.

As a general rule, the lability of a metal will be retarded more by organic complexes than by surface adsorption on inorganic mineral phases (Morel & Morel-Laurens, 1983). Within the inorganic ion pool, the fraction associated with  $\text{OH}^-$ ,  $\text{Cl}^-$  and  $\text{CO}_3^{2-}$  is considered readily available due to fast dissociation kinetics as compared to metal in organic complexes (Eigen & Wilkins, 1965; Hudson, 1998). The deviation between an elements' concentration and its bioavailability (*i.e.*, total vs free ion activity) has clear ecological implications because the concept of 'limiting' nutrients in a sense is founded on the presumption that nutrients (where present) are fully available and exchangeable. If this assumption was applied literally to trace metals, the actual available metal would be overestimated by an order of magnitude or more. Thus, the role of adsorption, complexation, and precipitation (into solid phases) should be considered when assessing the degree to which an ecosystem is 'limited' with respect to a given micronutrient. For instance, our results show that a lake that contains Co at non-limiting concentrations but simultaneously contains Mn at ppm levels is likely (if oxygenated) to be Co-limiting. The following discussion considers the driving factors behind trace element speciation and the implications of these processes for understanding micronutrient bioavailability in complex natural systems like lakes.

Cobalt is particularly interesting due to strong controls by redox-driven transformations of Mn. Our data suggests that Co was mainly present in the <5 nm fraction (Table 5.2) suggesting that when detectable, the metal was not present in association with colloids

above a few nm in diameter. The dissolved concentration of Co showed seasonal variability in the water column and a similar structure to Mn and Fe, indicating that the processes that control the cycling of Co are similar, and/or linked to that of Fe and/or Mn, likely through adsorption or co-precipitation reactions.

Elemental abundances showed a strong relation between Mn/Co ( $r^2 = 0.5$ ) and Fe/Co ( $r^2 = 0.6$ ) in the surface water, but the wider literature suggest a role for Mn, given chemical and microscopic evidence for Co association with Mn particles (Lienemann *et al.*, 1997; Van Cappellen *et al.*, 1998; Kay *et al.*, 2001; Saratovsky *et al.*, 2006) and on this basis we interpret the changes in Co in terms of this known coupling of Co with Mn.

Increases in Co concentration originated in the anaerobic manganese reduction zone (AMR) (Bratina *et al.*, 1998) of the hypolimnion in November 2015 when the concentration of dissolved oxygen dropped to  $0.15 \text{ mg L}^{-1}$  and the concentration of  $\text{Mn}^{2+}$  simultaneously increased (DGT labile fraction; Figure 5.2). PHREEQC modelling predicted reduction of  $\text{MnO}_2$  to  $\text{Mn}^{2+}$ , coincident and consistent with the observed lowering of pH at this depth interval, i.e. alkalinity generation (Figure 5.1d, Table 5.3). The coupling of Mn and Co is also clear from their clear covariation over depth and time.

Adsorption of Co onto Mn-oxide surfaces involves oxidation from Co (II) to Co (III), followed by Co (III) incorporation into the Mn-oxide crystal lattice (Murray & Dillard, 1979). The large surface area and charge distribution of Mn-oxides also play a role leading to rapid transformations between Co and Mn (Stumm & Morgan, 1970). Indeed, adsorption experiments conducted in a meromictic lake have shown that Mn-enriched particles bind more Co than Mn-depleted particles (Balistrieri *et al.*, 1994). Stockdale *et al.*, (2010) also showed that Co cycling is closely linked with Mn in anaerobic marine sediments (Stockdale *et al.*, 2010). Indeed, the identification of the same signature in Lake Ngapouri is highly relevant for any process involving Co (or Mn) availability. We speculate that within the operationally dissolved fraction ( $<0.45 \text{ } \mu\text{m}$ ) Co was probably associated with Mn-oxides in lake surface water (Table 5.3, Eq. vi).

**Table 5.3: Suggested pathways for micronutrient cycling associated with redox reactions in a typical monomictic lake.**

Element	Zone	Reaction name	Reaction	Bioavailability as measured by DGT lability	
Mn	H	MnO <sub>2</sub> reduction	$MnO_2 + 4H^+ \rightarrow Mn^{2+} + 2H_2O$	↑	i
Fe	H	Fe <sup>3+</sup> reduction	$2H^+ + 2Fe(OOH)_s \rightarrow 2Fe^{2+} + 2H_2O$	↑	ii
Mn	H	MnHPO <sub>4</sub> precipitation	$Mn^{2+} + HPO_4^{2-} \rightarrow MnHPO_4$	↓	iii
Fe	H	FeS/FeS <sub>2</sub> formation	$Fe^{2+} + 2H_2S \rightarrow FeS_2 + 4H^+$	↓	iv
Mn	E/WL	MnO <sub>2</sub> precipitation	$Mn^{2+} + 2H_2O \rightarrow MnO_2 + 4H^+$	↓	v
Co	E/WL	Adsorption to MnO <sub>2</sub>	$MnO_2 \rightleftharpoons Co$	↓	vi
Fe	E/WL	Fe <sup>2+</sup> oxidation	$4Fe^{2+} + 6H_2O + 3O_2 \rightarrow 4Fe(OH)_3$	↓	vii
Organic complexes	WL	Organic complexation	$M^+ + L^- \rightarrow ML$	↓	viii

Where H = hypolimnion (15 m to the sediment), WL = whole lake, ↓ = bioavailability of the nutrient decreases as a result of the reaction, ↑ = bioavailability of the nutrient increases as a result of the reaction.

Our study also documents the rapid removal of redox-sensitive metals by lake aeration (mixing in this instance). Hence, a paradigm of oxic (less-available) / reduced (more-available) holds for Fe, Mn, Co and Cd (Table 5.3, Figure 5.3c). The increased but not complete lability of Fe, Mn, Co and Cd, under reducing conditions points to the formation of a controlling mineral phases (likely sulfides, *e.g.*, CdS Figure 5.5d). Interestingly, CdS and FeS formation in the hypolimnion did not strongly impact the lability of these metals, since Cd was simultaneously the most colloidal and most labile metal in the anoxic hypolimnion (Table 5.2).

Processes of mineral formation in the lake hypolimnion (*e.g.*, FeS) are further corroborated by observed pH shifts. While the pH of the water column was circumneutral to neutral during the study period, a slight pH decrease in the hypolimnion during the summer can be explained by quenching of OH<sup>-</sup> ions from the water column, by sulphide formation (Table 5.3, Eq. iv).

It is also important to note that localised decreases in Mn lability in the hypolimnion were consistent with simulated  $\text{MnHPO}_{4(s)}$  precipitation (Figure 5.2f, Figure 5.5e). This finding highlights a mechanism of phosphate ( $\text{PO}_4^{3-}$ ) limitation not previously considered by this body of research (Saeed *et al.*, 2018), but which is consistent with experimental studies (McKenzie, 1979; Slavek & Pickering, 1985), including experiments targeting orthophosphate adsorption to Mn oxide (Kawashima *et al.*, 1986; Tonkin *et al.*, 2004). Hence, Mn and Fe oxide formation and reductive dissolution could have wide-reaching effects on micronutrient bioavailability in lacustrine environments.

### **5.5.1 Particulate organic matter and dissolved organic ligands limit metal bioavailability**

In contrast to the clear redox zonation control on Fe, Mn, Co, and Cd, other transition metals (Cu, Zn, and Ni) exhibited a more chaotic pattern over time and space. The cycling of Ni, Cu and Zn was likely influenced by adsorption to organic phases, *e.g.*, dissolved organic matter, sinking particles and/or phytoplankton (Balistrieri *et al.*, 1994; Zwolsman *et al.*, 1997). Indeed, the noisy nature of the data is consistent with the known affinity of these metals for binding with suspended and sinking particles (Duinker, 2009; Baken *et al.*, 2011). The DGT-labile fraction of Ni, Zn, and Cu was an order of magnitude smaller than the  $<0.45\ \mu\text{m}$  fraction which also reinforces the likely importance of complexation in stabilising these metals (Hudson, 1998; Tyler, 2004).

In aquatic environments, both  $\text{Cr}^{3+}$  and  $\text{Cr}^{6+}$  can be present, however,  $\text{Cr}^{3+}$  is prevalent under anoxic, low pH conditions (Li & Xue, 2001). Indeed, depth profiles of Cr show some effect of seasonality as well as the overall loss of Cr from the hypolimnion during the sub-oxic to anoxic summer period, suggesting that  $\text{Cr}^{6+}$  was probably reduced to  $\text{Cr}^{3+}$ , the more particle-reactive form. On the balance of available data, it is hard to evaluate Cr speciation any further and it should be noted that Chelex-100 resin does not accumulate  $\text{Cr}^{6+}$  species.

### 5.5.2 Implications for phytoplankton phenology and micronutrient dosing studies

One or more micronutrients are often added in experimental incubations to determine the organism-specific bioavailability of micronutrients (Kuiper, 1981; Saito *et al.*, 2002; Willis *et al.*, 2004; Njiru *et al.*, 2008). Such experimental designs provide limited understanding of the effects of competing ions, mineral formation and dissociation kinetics in the water body. The present study provides a context for future micronutrient limitation studies and lake management strategies particularly regarding the role of mineral formation in modulating trace metal cycling and availability.

Various biological processes such as exudation, excretion and mineralization, as well as geochemical processes, including adsorption and complexation can affect the dynamics of trace metals. These geochemical processes may serve to increase an element's lability, or conversely restrict their mobility through the membranes of certain groups of phytoplankton (Rout & Sahoo, 2015). In this context, it is clear that colloids can serve as a vector for trace metals, or inhibit their bioavailability.

We therefore propose that future micronutrient dosing studies should incorporate a chemical speciation/bioavailability assessment, for example by deploying DGT in tandem. In summary, while multi-factorial dosing studies have unparalleled power in elucidating specific nutrient effects on the growth of phytoplankton, the power of these studies is likely to be limited, if the specific geochemical speciation and activity of nutrients are not explicitly considered.

## 5.6 Conclusion

This study shows that the degree of colloidal influence over metal bioavailability in lakes varies amongst different metals. Fe, Mn, Co and Cd, were strongly driven by redox conditions. That said, the degree of limitation in metal availability was a function of their particular speciation. In general, colloid association is a predictor of lower lability under oxic conditions in lake surface water (*e.g.*, Fe, Mn, Cr, Al, Cd), but colloids present in anaerobic compartments, like hypolimnion, (*e.g.*, FeS, CdS) can be much more labile. We conclude that the geochemical speciation and adsorption characteristics of metals are

likely to have a strong control over their bioavailability as micronutrients and these factors should be considered in dosing experiments and lake management strategies.

## 5.1 Acknowledgments

We thank the Ministry of Business, Innovation and Employment for providing funding via the contract for Enhancing the Health and Resilience of New Zealand Lakes (UOWX1503). We are thankful to Andrew Pearson for assistance during field campaigns and Dorisel Torres-Rojas for useful comments that improved the quality of this manuscript. We further thank the technical staff at School of Science, University of Waikato, for field assistance and laboratory analysis. The authors declare no conflict of interest.

## 5.7 Author contribution

Huma Saeed prepared DGT's, collected and analysed water samples, analysed data and wrote the manuscript. David Hamilton co-supervised the study and helped with refining the manuscript. Niklas Lehto trained Huma Saeed in the preparation of DGT devices and provided feedback on the manuscript. Adam Hartland provided primary supervision, secured funding for the project, helped with data modelling and manuscript writing.

## 5.8 References

- Achterberg, E. P., & Braungardt, C. (1999). Stripping voltammetry for the determination of trace metal speciation and *In-situ* measurements of trace metal distributions in marine waters. *Analytica chimica acta*, 400(1-3), 381-397.
- Adams, S., Honeysett, J., Tiller, K., & Norrish, K. (1969). Factors controlling the increase of cobalt in plants following the addition of a cobalt fertilizer. *Soil Research*, 7(1), 29-42.
- Allan, I. J., Knutsson, J., Guigues, N., Mills, G. A., Fouillac, A.-M., & Greenwood, R. (2008). Chemcatcher® and DGT passive sampling devices for regulatory monitoring of trace metals in surface water. *Journal of Environmental monitoring*, 10(7), 821-829.
- Baeyens, W., Bowie, A. R., Buesseler, K., Elskens, M., Gao, Y., Lamborg, C., Leermakers, M., Remenyi, T., & Zhang, H. (2011). Size-fractionated labile trace elements in the Northwest Pacific and Southern Oceans. *Marine Chemistry*, 126(1-4), 108-113.
- Baken, S., Degryse, F., Verheyen, L., Merckx, R., & Smolders, E. (2011). Metal Complexation Properties of Freshwater Dissolved Organic Matter Are Explained by Its Aromaticity and by Anthropogenic Ligands. *Environmental Science & Technology*, 45(7), 2584-2590.



- Balistrieri, L. S., Murray, J. W., & Paul, B. (1994). The geochemical cycling of trace-elements in a biogenic meromictic lake. *Geochimica Et Cosmochimica Acta*, 58(19), 3993-4008.
- Bennett, W. W., Arsic, M., Panther, J. G., Welsh, D. T., & Teasdale, P. R. (2016). Binding Layer Properties. In W. Davison (Ed.), *Diffusive Gradients in Thin-Films for Environmental Measurements* (pp. 66-92). Cambridge: Cambridge University Press.
- Bratina, B. J., Stevenson, B. S., Green, W. J., & Schmidt, T. M. (1998). Manganese reduction by microbes from oxic regions of the Lake Vanda (Antarctica) water column. *Applied and environmental microbiology*, 64(10), 3791-3797.
- Camacho González, A. (2006). On the occurrence and ecological features of deep chlorophyll maxima (DCM) in Spanish stratified lakes. *Limnetica*, 25(1-2), 453-478.
- Churchman, G. J., & Lowe, D. J. (2012). Alteration, formation, and occurrence of minerals in soils. In *Handbook of Soil Sciences: Properties and Processes* (pp. 1-72). CRC Press.
- Cindrić, A.-M., Marcinek, S., Garnier, C., Salaün, P., Cukrov, N., Oursel, B., Lenoble, V., & Omanović, D. (2020). Evaluation of diffusive gradients in thin films (DGT) technique for speciation of trace metals in estuarine waters - A multimethodological approach. *Science of The Total Environment*, 721, 137784.
- Davison, W. (1993). Iron and manganese in lakes. *Earth-Science Reviews*, 34(2), 119-163.
- Davison, W., & Zhang, H. (2012). Progress in understanding the use of diffusive gradients in thin films (DGT)—back to basics. *Environmental Chemistry*, 9(1), 1-13.
- Duinker, J. C. (2009). Partition of Fe, Mn, Al, K, Mg, Cu and Zn between Particulate Organic Matter and Minerals, and its Dependence on Total Concentrations of Suspended Matter. In *Holocene Marine Sedimentation in the North Sea Basin* (pp. 451-459).
- Eigen, M., & Wilkins, R. G. (1965). The kinetics and mechanism of formation of metal complexes. In *Mechanisms of Inorganic Reactions* (Chapter 3, pp. 55-80). American Chemical Society.
- Evans, J. C., & Prepas, E. E. (1997). Relative importance of iron and molybdenum in restricting phytoplankton biomass in high phosphorus saline lakes. *Limnology and Oceanography*, 42(3), 461-472.
- Facey, J. A., Apte, S. C., & Mitrovic, S. M. (2019). A Review of the effect of trace metals on freshwater cyanobacterial growth and toxin production. *Toxins*, 11(11), 643.
- Flemming, C. A., & Trevors, J. T. (1989). Copper toxicity and chemistry in the environment: a review. *Water, Air, and Soil Pollution*, 44(1), 143-158.
- Gao, Y., Zhou, C., Gaulier, C., Bratkic, A., Galceran, J., Puy, J., Zhang, H., Leermakers, M., & Baeyens, W. (2019). Labile trace metal concentration measurements in marine environments: From coastal to open ocean areas. *TrAC Trends in Analytical Chemistry*, 116, 92-101.
- Gustafsson, J. P. (2007). *Visual MINTEQ ver. 3.1* [software]. <https://vminteq.lwr.kth.se/>.

- Gustafsson, J. (2013). Visual MINTEQ, Version 3.1 Division of Land and Water Resources. Royal Institute of Technology, Stockholm, Sweden <http://www2.lwr.kth.se/English/Oursoftware/vminteq/download.html>.
- Hartland, A., Andersen, M. S., & Hamilton, D. P. (2015). Phosphorus and arsenic distributions in a seasonally stratified, iron-and manganese-rich lake: microbiological and geochemical controls. *Environmental Chemistry*, 12(6), 708-722.
- Hartland, A., Zitoun, R., Middag, R., Sander, S., Laferriere, A., Saeed, H., De Luca, S., & Ross, P. M. (2019). Aqueous copper bioavailability linked to shipwreck-contaminated reef sediments. *Scientific Reports*, 9(1), 9573.
- Hay, R. W. (1984). *Bio-inorganic chemistry*. Ellis Horwood Chichester.
- Healey, F. P. (1979). Short - term responses of nutrient - deficient algae to nutrient addition 1. *Journal of Phycology*, 15(3), 289-299.
- Holm, R. H., Kennepohl, P., & Solomon, E. I. (1996). Structural and Functional Aspects of Metal Sites in Biology. *Chemical Reviews*, 96(7), 2239-2314.
- Hongve, D. (1997). Cycling of iron, manganese, and phosphate in a meromictic lake. *Limnology and Oceanography*, 42(4), 635-647.
- Horne, A. J. a. C. R. G. (1994). *Limnology* McGraw-Hill.
- Hudson, R. J. (1998). Which aqueous species control the rates of trace metal uptake by aquatic biota? Observations and predictions of non-equilibrium effects. *Science of the Total Environment*, 219(2-3), 95-115.
- Hudson, R. J. M., & Morel, F. M. M. (1990). Iron transport in marine phytoplankton: Kinetics of cellular and medium coordination reactions. *Limnology and Oceanography*, 35(5), 1002-1020.
- Juneja, A., Ceballos, R. M., & Murthy, G. S. (2013). Effects of environmental factors and nutrient availability on the biochemical composition of algae for biofuels production: a review. *Energies*, 6(9), 4607-4638.
- Kabata-Pendias, A. (2010). *Trace elements in soils and plants: Fourth edition*.
- Kawashima, M., Tainaka, Y., Hori, T., Koyama, M., & Takamatsu, T. (1986). Phosphate adsorption onto hydrous manganese(IV) oxide in the presence of divalent cations. *Water Research*, 20(4), 471-475.
- Kay, J. T., Conklin, M. H., Fuller, C. C., & O'Day, P. A. (2001). Processes of nickel and cobalt uptake by a manganese oxide forming sediment in Pinal Creek, Globe Mining District, Arizona. *Environmental science & technology*, 35(24), 4719-4725.
- Kimball, B. A., Callender, E., & Axtmann, E. V. (1995). Effects of colloids on metal transport in a river receiving acid mine drainage, upper Arkansas River, Colorado, U.S.A. *Applied Geochemistry*, 10(3), 285-306.

- Korb, R. E., & Whitehouse, M. (2004). Contrasting primary production regimes around South Georgia, Southern Ocean: large blooms versus high nutrient, low chlorophyll waters. *Deep Sea Research Part I: Oceanographic Research Papers*, 51(5), 721-738.
- Kouba, A., Buřič, M., & Kozák, P. (2010). Bioaccumulation and effects of heavy metals in crayfish: a review. *Water, Air, & Soil Pollution*, 211(1-4), 5-16.
- Kuiper, J. (1981). Fate and effects of cadmium in marine plankton communities in experimental enclosures. *Mar. Ecol. Prog. Ser.*, 6, 161-174.
- Li, Y., & Xue, H. (2001). Determination of Cr(III) and Cr(VI) species in natural waters by catalytic cathodic stripping voltammetry. *Analytica Chimica Acta*, 448(1), 121-134.
- Lienemann, C.-P., Taillefert, M., Perret, D., & Gaillard, J.-F. (1997). Association of cobalt and manganese in aquatic systems: Chemical and microscopic evidence. *Geochimica et Cosmochimica Acta*, 61(7), 1437-1446.
- Lorenzen, C. J. (1966). A method for the continuous measurement of in vivo chlorophyll concentration. *Deep Sea Research and Oceanographic Abstracts*, 13(2), 223-227.
- McKenzie, R. M. (1979). Proton release during adsorption of heavy metal ions by a hydrous manganese dioxide. *Geochimica et Cosmochimica Acta*, 43(11), 1855-1857.
- Mildvan, A. S. (1970). 9 Metals in Enzyme Catalysis. In P. D. Boyer (Ed.), *The Enzymes* (pp. 445-536). Academic Press.
- Montero, N., Belzunce-Segarra, M., Gonzalez, J.-L., Larreta, J., & Franco, J. (2012). Evaluation of diffusive gradients in thin-films (DGTs) as a monitoring tool for the assessment of the chemical status of transitional waters within the Water Framework Directive. *Marine pollution bulletin*, 64(1), 31-39.
- Morel, F., & Morel-Laurens, N. (1983). Trace metals and plankton in the oceans: facts and speculations. In *Trace metals in sea water* (pp. 841-869). Springer.
- Morel, F. M. M., Hudson, R. J. M., & Price, N. M. (1991). Limitation of productivity by trace metals in the sea. *Limnology and Oceanography*, 36(8), 1742-1755.
- Murray, J. W., & Dillard, J. G. (1979). The oxidation of cobalt (II) adsorbed on manganese dioxide. *Geochimica et Cosmochimica Acta*, 43(5), 781-787.
- Njiru, M., Kazungu, J., Ngugi, C., Gichuki, J., & Muhoozi, L. (2008). An overview of the current status of Lake Victoria fishery: Opportunities, challenges and management strategies. *Lakes & Reservoirs: Research & Management*, 13(1), 1-12.
- North, R., Guildford, S., Smith, R., Havens, S., & Twiss, M. (2007). Evidence for phosphorus, nitrogen, and iron colimitation of phytoplankton communities in Lake Erie. *Limnology and Oceanography*, 52(1), 315-328.
- Ohnstad, M., Golterman, H. L., & Clymo, R. S. (1978). *Methods for Physical and Chemical Analysis of Fresh Waters*. Blackwell.

- Paerl, H. W., Xu, H., Hall, N. S., Rossignol, K. L., Joyner, A. R., Zhu, G., & Qin, B. (2015). Nutrient limitation dynamics examined on a multi-annual scale in Lake Taihu, China: implications for controlling eutrophication and harmful algal blooms. *Journal of Freshwater Ecology*, 30(1), 5-24.
- Peers, G., Quesnel, S.-A., & Price, N. M. (2005). Copper requirements for iron acquisition and growth of coastal and oceanic diatoms. *Limnology and Oceanography*, 50(4), 1149-1158.
- Pilon, M., Abdel-Ghany, S. E., Cohu, C. M., Gogolin, K. A., & Ye, H. (2006). Copper cofactor delivery in plant cells. *Current Opinion in Plant Biology*, 9(3), 256-263.
- Pokrovsky, O. S., Shirokova, L. S., Zabelina, S. A., Vorobieva, T. Y., Moreva, O. Y., Klimov, S. I., Chupakov, A. V., Shorina, N. V., Kokryatskaya, N. M., Audry, S., Viers, J., Zoutien, C., & Freydier, R. (2012). Size Fractionation of Trace Elements in a Seasonally Stratified Boreal Lake: Control of Organic Matter and Iron Colloids. *Aquatic Geochemistry*, 18(2), 115-139.
- Preisendorfer, R. W. (1986). Secchi disk science: Visual optics of natural waters1. 31(5), 909-926.
- Rainbow, P. S. (2018). Biology of Trace Metals. In P. S. Rainbow (Ed.), *Trace Metals in the Environment and Living Organisms: The British Isles as a Case Study* (pp. 68-123). Cambridge: Cambridge University Press.
- Rout, G. R., & Sahoo, S. (2015). Role of iron in plant growth and metabolism. *Reviews in Agricultural Science*, 3, 1-24.
- Saeed, H., Hartland, A., Lehto, N. J., Baalousha, M., Sikder, M., Sandwell, D., Mucalo, M., & Hamilton, D. P. (2018). Regulation of phosphorus bioavailability by iron nanoparticles in a monomictic lake. *Scientific Reports*, 8(1), 17736.
- Saito, M. A., Moffett, J. W., Chisholm, S. W., & Waterbury, J. B. (2002). Cobalt limitation and uptake in *Prochlorococcus*. *Limnology and Oceanography*, 47(6), 1629-1636.
- Saratovsky, I., Wightman, P. G., Pastén, P. A., Gaillard, J.-F., & Poeppelmeier, K. R. (2006). Manganese oxides: parallels between abiotic and biotic structures. *Journal of the American Chemical Society*, 128(34), 11188-11198.
- Sigg, L., Black, F., Buffle, J., Cao, J., Cleven, R., Davison, W., Galceran, J., Gunkel, P., Kalis, E., & Kistler, D. (2006). Comparison of analytical techniques for dynamic trace metal speciation in natural freshwaters. *Environmental science & technology*, 40(6), 1934-1941.
- Slavek, J., & Pickering, W. (1985). Chemical leaching of metal ions sorbed on hydrous manganese oxide. *Chemical Geology*, 51(3-4), 213-223.
- Solomon, E. I., & Hadt, R. G. (2011). Recent advances in understanding blue copper proteins. *Coordination Chemistry Reviews*, 255(7), 774-789.

- Stockdale, A., Davison, W., Zhang, H., & Hamilton-Taylor, J. (2010). The Association of Cobalt with Iron and Manganese (Oxyhydr)oxides in Marine Sediment. *Aquatic Geochemistry*, 16(4), 575-585.
- Stumm, W., & Morgan, J. J. (1970). *Aquatic chemistry; an introduction emphasizing chemical equilibria in natural waters*.
- Tonkin, J. W., Balistrieri, L. S., & Murray, J. W. (2004). Modeling sorption of divalent metal cations on hydrous manganese oxide using the diffuse double layer model. *Applied Geochemistry*, 19(1), 29-53.
- Tyler, G. (2004). Vertical distribution of major, minor, and rare elements in a Haplic Podzol. *Geoderma*, 119(3), 277-290.
- Valerie, M. F., Kenneth, W. B., David, A. H., & Mark, A. B. (2003). Iron and zinc effects on silicic acid and nitrate uptake kinetics in three high-nutrient, low-chlorophyll (HNLC) regions. *Marine Ecology Progress Series*, 252, 15-33.
- Van Cappellen, P., Viollier, E., Roychoudhury, A., Clark, L., Ingall, E., Lowe, K., & Dichristina, T. (1998). Biogeochemical cycles of manganese and iron at the oxic- anoxic transition of a stratified marine basin (Orca Basin, Gulf of Mexico). *Environmental science & technology*, 32(19), 2931-2939.
- Venables, H., & Moore, C. M. (2010). Phytoplankton and light limitation in the Southern Ocean: Learning from high - nutrient, high - chlorophyll areas. *Journal of Geophysical Research: Oceans*, 115(C2).
- Vrede, T., & Tranvik, L. J. (2006). Iron Constraints on Planktonic Primary Production in Oligotrophic Lakes. *Ecosystems*, 9(7), 1094-1105.
- Welschmeyer, N. A. (1994). Fluorometric analysis of chlorophyll a in the presence of chlorophyll b and pheopigments. *Limnology and Oceanography*, 39(8), 1985-1992.
- Willis, K. J., Van Den Brink, P. J., & Green, J. D. (2004). Seasonal variation in plankton community responses of mesocosms dosed with pentachlorophenol. *Ecotoxicology*, 13(7), 707-720.
- Wong, P. T., Burnison, G., & Chau, Y. (1979). Cadmium toxicity to freshwater algae. *Bull. Environ. Contam. Toxicol.:(United States)*, 23(4/5).
- Worms, I. A. M., Chmiel, H. E., Traber, J., Tofield-Pasche, N., & Slaveykova, V. I. (2019). Dissolved Organic Matter and Associated Trace Metal Dynamics from River to Lake, Under Ice-Covered and Ice-Free Conditions. *Environmental Science & Technology*, 53(24), 14134-14143.
- Welschmeyer, N. A. (1994). Fluorometric analysis of chlorophyll a in the presence of chlorophyll b and pheopigments. *Limnology and Oceanography*, 39(8), 1985-1992. <https://doi.org/https://doi.org/10.4319/lo.1994.39.8.1985>
- Wong, P. T., Burnison, G., & Chau, Y. (1979). Cadmium toxicity to freshwater algae. *Bull. Environ. Contam. Toxicol.:(United States)*, 23(4/5).

- Zhao, S., Yin, L., Chang, F., Olsen, S., Søndergaard, M., Jeppesen, E., & Li, W. (2016). Response of *Vallisneria spinulosa* (Hydrocharitaceae) to contrasting nitrogen loadings in controlled lake mesocosms. *Hydrobiologia*, 766(1), 215-223. <https://doi.org/10.1007/s10750-015-2456-1>
- Zhang, H., & Davison, W. (1995). Performance characteristics of diffusion gradients in thin films for the in situ measurement of trace metals in aqueous solution. *Analytical chemistry*, 67(19), 3391-3400.
- Zwolsman, J. J., Van Eck, B. T., & Van Der Weijden, C. H. (1997). Geochemistry of dissolved trace metals (cadmium, copper, zinc) in the Scheldt estuary, southwestern Netherlands: impact of seasonal variability. *Geochimica et Cosmochimica Acta*, 61(8), 1635-1652.

## 5.2 Supplementary information

### 5.2.1 Fluorometric estimation of Chl-a

Chl-a was extracted by transferring the frozen filter membranes to clean tubes containing five mL buffered in very-dim light. The filter membranes were ground using an IKA® T10 basic Ultra-Turrax homogenizer (Thermo Fisher Scientific, Auckland, New Zealand). Five mL buffered acetone was used to wash any residue off the grinding tip. The samples were allowed to steep for 24 hrs to ensure a complete extraction and were then centrifuged for 10 minutes at 3300 rpm. The samples were allowed to stand for 30 minutes before reading and then transferred to glass cuvettes pre-checked for scratches. The method considers Chl-a and phaeophyton as the two fluorescent pigments in the extract and involves correction for phaeopigment was achieved by adding 0.1N HCl (second blank).

Buffered acetone (5 mL) was read as the first instrument blank and 150 µL of 0.1 N HCl was added and read as the second blank. Five mL of the sample was decanted off and read at the same settings as the blank. This initial reading  $R_1$  is the fluorescence of Chl-a and Phaeopigment. HCl, 150 µL was added to the sample, allowed to stand for 90 seconds, and read again ( $R_2$ ). Chl- a concentration was calculated using the following equation

$$Chl - a (\mu g L^{-1}) = F_s [ (r / (r - 1)) (R_1 - R_2) ] [(V_e * d_f / V_f)] \quad (5-6)$$

Where  $F_s$  is the response factor of the fluorometer,  $r$  is the acidification constant,  $V_e$  is the extraction volume,  $d_f$  is the dilution factor and  $V_f$  the volume of the water filtered. The relationship between fluorescence and Chl-a concentration was used to convert fluorescence signal of the CTD to Chl-a value.

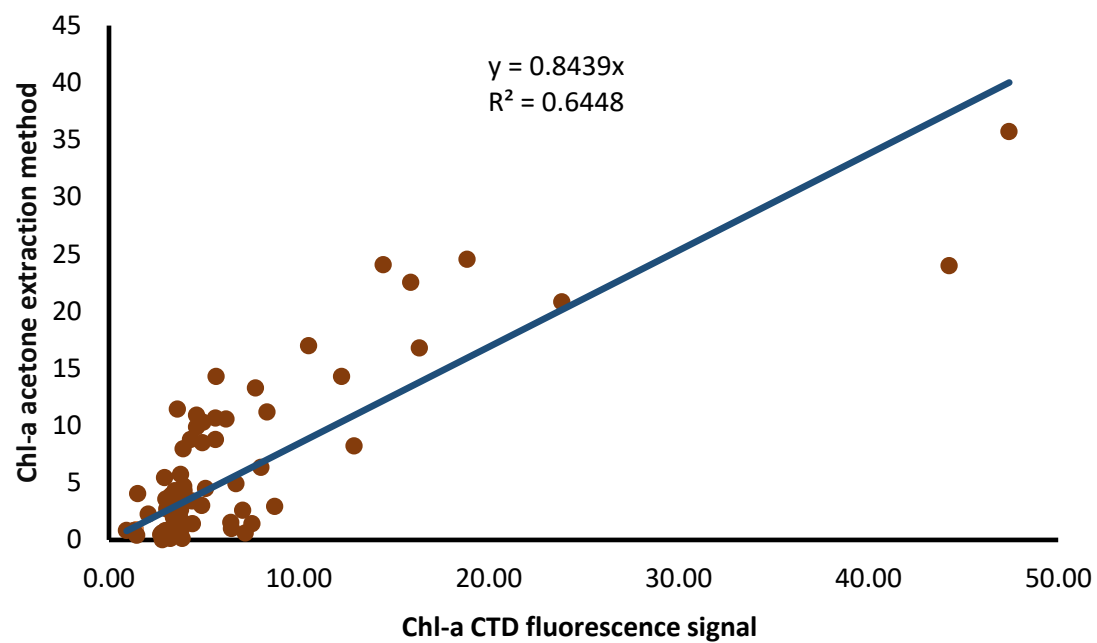


Figure S1: The CTD fluorescence signal corrected for Chl-a concentration



## Chapter 6

### Summary and suggested future work

---

#### 6.1 Conclusion

Colloidal associations in the cycling of macronutrients and micronutrients have been shown here to be an important facet in the 'nutrient limitation' paradigm. The research presented in this thesis examined the physicochemical characteristics of Lake Ngapouri, focussing on the size distribution of phosphorus and trace metals, including trace elements recognized as important micronutrients. The study also evaluated the evolution of inorganic mineral phases under varying redox conditions, with a view to understanding if these mineral phases control the lability of micronutrients.

This section summarises the main findings of the study.

1. Results from bi-monthly sampling expeditions over the course of a year, show Lake Ngapouri as a dynamic system in which the concentration of dissolved oxygen (DO) governs the speciation and abundance of colloidal phases. This in turn is a significant determinant of nutrient mobility (and DGT lability) in the lake system. The aim of Chapters Three and Five was to determine the size distribution of the nutrients studied, visualize the Spatio-temporal distribution of the nutrients, and determine which colloids were important in affecting nutrient lability.
2. Temperature and DO concentration exhibited two distinct cycles in Lake Ngapouri, 1) isothermal conditions with uniform DO, and 2) a marked temperature and DO gradient from 5 to 13 m depth during summer stratification. Above the thermocline, the water had a high and uniform temperature and DO concentration. The water compartment below the thermocline (*i.e.*, hypolimnion) was colder than the above two chambers and progressively developed anoxia during the course of the summer.
3. The seasonal profiles of phosphorus, iron, manganese, and cobalt exhibited similar overall trends, with concentrations building from the sediment as the lake basin became progressively anoxic. The increase in Fe concentration was coincident with the rise in P (Chapter 3), suggesting

that both were mechanistically related. Generally, the concentration of nutrients was higher in summer in the hypolimnion than during the winter (under isothermal conditions). However, Fe-bearing colloids were produced when the lake turned over and these likely scavenged available P, resulting in a loss of both Fe and P from the water column possibly due to sedimentation. We suggest that freshly precipitated Fe colloids (detected in the hypolimnion and metalimnion) were sufficiently small to allow 'solute-like' behavior, thereby enabling the Fe colloids to diffuse through the DGT solution probes hydrogel layers.

4. In Chapter Five, micronutrients were broadly categorized into two categories: 1) redox-controlled elements comprising Fe, Mn, and Co, and 2) elements governed by heterogeneous, largely organic, particles (Cr, Ni, Cu, and Zn). Based on the redox behavior, studied elements were grouped into two categories. For Category 1 elements (*e.g.*, Mn and Co), the total, colloidal and DGT-labile concentrations exhibited similar spatial and temporal patterns, reflecting the Lake's redox state. We suggest that Co is most closely related to Mn, whereas Fe is more important for P and S. Other trace metals such as Cr, Zn, and Ni, in category two, did not show an appreciable relation with the redox state and were probably more related to complexation with organic phases.
5. Results from Chapter 4, demonstrate that dissolved organic matter (DOM) fluorescence was comprised of two humic-like and one protein-like fluorophore in the lake water column. Out of these three components, low molecular weight protein-like materials predominated and were more actively cycled in the lake than the humic-like fluorophores. While these results cannot be directly linked to the consumption of specific electron acceptors, a clear trend toward faster consumption of protein-like DOM was observed in the hypolimnion. This has implications for how DOM is both generated, metabolized, and stored within lake basins.

## 6.2 Suggested future work

This study's contributions are both academic and practical with relevance to any aquatic system with similar physicochemical characteristics. However, there are many more questions about elemental cycling in lake systems that warrant further research.

The rise in the concentration of Category 1 (Fe, Mn, and Co) elements from the anaerobic sediments of Lake Ngapouri suggests that these elements were probably released back to the overlying water due to reduction reactions within the sediments. Therefore, it could be useful to incubate sediment cores with overlying water under laboratory conditions where free oxygen is excluded. Such an approach would enable the real-time monitoring of the generation and dissolution of colloids of which the bioavailable fraction could be continuously monitored using diffusive gradients in thin films. In addition, prominent phytoplankton species indigenous to the lake system could be introduced to the experimental enclosure to estimate the effect of phytoplankton on elemental cycling.

SUVA<sub>254</sub> is extensively used as a proxy for dissolved organic matter aromaticity in studies attempting to characterize the DOM pool. However, the present study identifies interferences from Fe<sup>2+</sup> and Fe<sup>3+</sup> species on the SUVA<sub>254</sub> signal at the concentrations reported in this thesis. Future studies would benefit from a systematic evaluation of the effect of various Fe species concentrations on the SUVA signal, with relevance to the characterization of DOM by this method.